StG
987

UniServices

Auckland UniServices Limited

Our Ref: 4771.00

THE SEISMIC RESPONSE OF VOLCANIC SITES

AUCKLAND UNISERVICES LIMITED

a wholly owned company of

THE UNIVERSITY OF AUCKLAND

Report prepared for:
Earthquake Commission
PO Box 311
WELLINGTON

Date: June 1996

Consultants:
Mr S Marks and Dr T Larkin
Department of Civil
and Resource Engineering
University of Auckland

Reports from Auckland UniServices Limited should only be used for the purposes for which they were commissioned. If it is proposed to use a report prepared by Auckland UniServices for a different purpose or in a different contest from that intended at the time of commissioning the work, then UniServices should be consulted to verify whether the report is being correctly interpreted. In particular it is requested that, where quoted, conclusions given in UniServices Reports should be stated in full.

Abstract

This report presents both an analytical and experimental investigation of the seismic response of volcanic soil sites. This important area of investigation has very little published research data. Volcanic soils are commonly found in the Auckland and central North Island areas of New Zealand.

A numerical two dimensional effective stress method of analysis was developed that allowed the inclusion of the in-plane geometry of a site when determining its site response and liquefaction potential. Liquefaction of volcanic sands was observed during the 1987 Edgecumbe earthquake, and the effective stress analysis provides a means of gaining an insight into this behaviour.

A cyclic triaxial testing programme on a central North Island pumiceous sand was undertaken to evaluate its dynamic properties. These results indicated that the pumice sand behaved similarly to other sands when subjected to the relatively low stress dynamic motions. The induced stresses were found to be of insufficient magnitude to induce grain crushing. This testing programme allowed an indepth investigation of two numerical pore pressure models to be carried out. These results showed that the models were capable of simulating the dynamic behaviour of the volcanic sand with reasonable accuracy.

The influence of permeability on the liquefaction process was investigated using a one dimensional effective stress solution. It was found that the relatively high permeabilities of volcanic sands significantly reduced the liquefaction response due to excess pore water drainage.

Low strain analyses suggested that the influence of the boundaries in the two dimensional solution was to stiffen the overall properties of the basin when the aspect ratio is decreased. High magnitude (non linear) analyses showed a more complex behaviour in which there were no clear trends as to the influence of basin geometry. Effective stress analyses showed that the lateral boundaries can also have a significant effect on the liquefaction response of a site.

Acknowledgments

The financial assistance of the New Zealand Earthquake Commission grant number 93/150 is gratefully acknowledged.

Mr Graeme Duske is also acknowledged for his assistance in using the MTS materials testing system machine

Contents

List of Symbols

The following is a list of symbols used in this study. All are in S.I. units.

α	Shape factor for pore pressure generation curves
ε_{vd}	Volumetric strain
γ	Unit weight
γ	Shear strain
ρ	Mass density
σ'_v	Vertical effective stress
σ'_m	Mean effective stress
τ	Shear stress
τ_{av}	Average shear stress
a_{max}	Maximum surface acceleration
B_1	Volumetric strain parameter
B_2	Volumetric strain parameter
C	Permeability constant in Hazen's equation
CPT	Cone penetrometer test
D_r	Relative density
D_{10}	Effective 10% grain diameter
D_{50}	Mean grain size
E_r	Rebound modulus
g	Acceleration due to gravity
G	Shear modulus
G	Secant shear modulus
G_{max}	Maximum (low strain) tangent shear modulus
h	Depth of liquefaction zone
H	Depth of soil column
H_1	Strain hardening parameter

H_2	Strain hardening parameter
I_{mm}	Modified Mercalli Intensity
k	Stiffness
k	Coefficient of permeability
k_2	Rebound modulus parameter
k_2	Sand coefficient
K_s	Stress ratio correction factor for overburden pressure
m	Rebound modulus parameter
m_v	Coefficient of volume compressibility
n	Rebound modulus parameter
N	Number of equivalent stress cycles
N_l	Number of equivalent stress cycles to induce liquefaction at constant stress
$(N_1)_{60}$	Normalised SPT blow count
Q_c	Normalised CPT resistance
r_d	Stress reduction factor for Seed's simplified method
R	Coulomb resistance
t_I	Intensity time
t_L	Time of liquefaction
SPT	Standard penetration test
T	Period
u	Pore pressure
u	Horizontal particle displacement
V_s	Shear wave velocity
z	Depth

Chapter One

Introduction

1.1 INTRODUCTION

A recent study by Holzer (1994) stated that approximately 98% of the US$ 5.9 billion in property damage from the 1989 Loma Prieta earthquake was caused directly by ground shaking. Amplified ground shaking from site response effects was responsible for approximately two thirds (US$4.1 billion) of that property damage. The other 2% of damage was attributed to permanent ground deformation. From this data it is clear that ground shaking and local motion amplification must be understood if realistic structural design loads and attempts at hazard mitigation are to be achieved.

Both site response amplification and liquefaction behaviour may be included under the general heading of site effects. Many recent earthquakes, in addition to Loma Prieta, have produced graphic evidence of the problems that site effects can cause. The earthquake events of Kobe (1995), Northridge (1994), Armenia (1988) and Mexico City (1985) all exhibited significant ground motion amplification and site response effects. Significant liquefaction and liquefaction induced damage was observed during the Kobe (1995), Hokkaido (1993) and Edgecumbe (1987) earthquakes. These recent events have prompted a renewed research interest in the field of numerical and experimental site response in the 1990's, which continues today.

Many cities and industrial areas are concentrated in alluvial valleys, often near the coast, such as Wellington and the Edgecumbe area in New Zealand, and the Hanshin district in Japan. Much of the soil in these areas is soft alluvium that has been deposited to form the infill valleys. Foreshore reclamation is also a feature of many coastal cities, which has been shown to be very susceptible to liquefaction and lateral spreading in past events. The infrastructure of an entire region, including underground services, port facilities and major arterial transport routes can be severely damaged in these areas. For the numerical earthquake analyses of these types of valleys a two dimensional analysis method is desirable, which accounts for the lateral geometry of a valley structure.

The nature of the soil within many valleys depends on the composition of the surrounding mountains and the proximity of the valley to significant volcanic areas. Vast areas of the central North Island of New Zealand have significant deposits of volcanically derived soils, both from aerial deposition during an eruption (ash) and from alluvial deposition onto flood plains. The Edgecumbe earthquake showed that the volcanically derived sands in the area are susceptible to liquefaction, and other failures in the past have also suggested that volcanic soils can pose special problems in geotechnical design. The literature provides very little information on the seismic responses of volcanically derived residual soils, and therefore there is a need for New Zealand research in this area.

This study investigates the two dimensional response of volcanically derived soils using a non linear soil response program. This model accounts for the in-plane geometry of the site, which has been found to be significant in many previous studies in the literature. A pore pressure model was incorporated into the computer program to account for liquefaction behaviour, which can be significant for sandy soil deposits. The two dimensional program allowed valley deposits to be more accurately modelled than the more standard one dimensional approximation that only accounts for the vertical dimension.

Numerical site response and liquefaction methods have been developed in an attempt to model the response of a soil deposit to incoming seismic motion. To accurately model this system however, a reasonable understanding of the behaviour of the different soils within the deposit is required. There is a significant data base available concerning the behaviour of sedimentary sands and clays, but very little on the volcanic residual soils found in significant parts of New Zealand. An experimental programme was therefore undertaken to investigate the dynamic and liquefaction response of a volcanic sand from near the Waikato river in the upper central North Island. This sand originates from the Taupo Volcanic Zone (TVZ) in the central North Island. These results were then used in the numerical modelling of idealised valley structures to investigate some of the behaviour that is characteristic of two dimensional valleys.

In summary the main focus of this report is to further the understanding of the seismic response of New Zealand volcanic soil deposits.

1.2 SCOPE OF THIS REPORT

Chapter two outlines some of the work available in the literature that has previously been done in the area of site response and numerical liquefaction evaluation. This literature review discusses the development of the one, two and three dimensional site response analyses with the various constitutive relationships of each method included. The effective stress analyses and associated liquefaction models available are also briefly reviewed.

The theoretical considerations behind the one and two dimensional total stress analysis programs are presented in detail in chapter four. All aspects of the various models and mechanisms included are derived and explained, including the constitutive relationships. Chapter five describes two liquefaction models in detail and how they were incorporated into the two dimensional analysis described in chapter four.

The nature of volcanic soil properties under both static and dynamic conditions are reviewed in chapter six. The rest of the chapter is devoted to the results of the experimental programme that was undertaken on a sand of volcanic origin. Experimental results are presented on the static properties of the sand, such as void ratio, relative density and particle size distribution. The bulk of the chapter is then devoted to the experimental determination of the dynamic properties, such as the liquefaction response, the low strain shear modulus and the non linear nature of the constitutive relationship.

Many aspects of the seismic response of two dimensional volcanic cohesive soil deposits are described in chapter seven. The influence of geometry and earthquake magnitude are evaluated in detail using single frequency harmonic input motions, as well as recorded earthquake motions. Some comparisons to closed form solutions are also made.

Chapter eight investigates the liquefaction and effective stress response of the volcanic sand described in chapter six. The two dimensional numerical effective stress programs developed at the University of Auckland are used. The influence of the high permeabilities of the volcanic sand that were found during the experimental programme are also investigated The focus of this chapter is to evaluate the main features of the seismic response of volcanic sandy sites.

Finally, conclusion are drawn in chapter nine, along with recommendations for further work.

Chapter Two

Literature Review

2.1 INTRODUCTION

The study of site response has regained impetus in the past few years as recent earthquake events have highlighted site amplifications. Liquefaction modelling is a specialised extension of the general site response area and has also received renewed attention. The solution of site response problems has involved a number of approaches. The main distinctions are between linear and non linear solutions, and total or effective stress. Linear solutions assume the constitutive relationship of the soil to be linear elastic, which has been found in experimental work to be a large assumption for many soils. Non linear solutions of varying forms have been developed to account for this inelastic behaviour. The term "total stress" applies to analyses which do not account for the generation of pore pressures in sandy soils, and hence effective stress analyses are required to determine the liquefaction potential of such sites.

Numerous numerical and analytical site response and liquefaction analysis methods have been developed over the past 30 years. Most effort has centred on linear studies, although significant research has occurred in some aspects of non linear solutions. This chapter is not a complete review of the vast area of seismic site response, but attempts to document and review some of the world wide research that is most relevant to this study.

2.2 ONE DIMENSIONAL ANALYSES

The one dimensional analysis is the simplest method of solving site response problems, and hence were the first developed. The basic methodology of the one dimensional analysis is to take a vertical slice of the soil column under investigation, and consider the vertically propagating shear waves generated from a distant earthquake. One dimensional analyses assume that lateral conditions have no influence on the response of the soil column, an assumption that has been found to be valid in some situations (Marsh 1992). These analyses are the most commonly performed in engineering practice today, although are still relatively rarely used in the New Zealand context.

TOTAL STRESS

The first one dimensional analyses were linear and total stress (Kanai 1950), and hence were not a true representation of the well established non linear properties of most soils. Idriss and Seed (1968) also solved the visco-elastic one dimensional problem, for both constant shear moduli and moduli varying with depth. The constant moduli case was solved directly, and more complex strata were solved using a lumped mass system with connecting springs and viscous damping. As this model did not represent the inherent non linear soil properties, a further development was made by Idriss and Seed which was termed the equivalent linear method. The same lumped mass system was used, with an average (strain dependent) value of shear modulus incorporated instead of the low strain value. A iterative procedure generates the correct average shear modulus value in accordance with the induced level of strain.

A frequency domain solution was formed by calculating the transfer function in the frequency domain and employing fast fourier transforms and an iterative strain compatible equivalent liner scheme. This system was incorporated into the computer program SHAKE (Schnabel et al. 1972, and updated in 1988) along with an improved solution scheme performed in the frequency domain. Even today SHAKE remains the most widely used computer program in site response analyses.

Truly non linear analysis methods developed with the advent of greater computing power, allowing time domain solutions to be performed in a realistic time frame. Larkin (1975) used an array of elasto-plastic (Iwan) elements for the constitutive relationship and incorporated this, along with a finite difference solution of the wave equation, into the computer program DENSOR (Larkin 1978).

Other fully non linear solutions were developed by Joyner and Chen (1975) using similar nested Iwan elements for the constitutive relationship, and incorporating the lumped mass approach. Streeter et al. (1974) used the method of characteristics to analyses both viscoelastic and fully non linear soils, incorporating the Ramberg-Osgood (1943) expression for the non linear model.

EFFECTIVE STRESS

Effective stress analyses allow for the generation of excess pore pressure in sandy soils and attempts to model this behaviour in addition to the general site response of the site. The computer programs MASH and APOLLO (Martin P.P. 1975, Martin and Seed 1979) were developed at Berkeley, California. MASH computes the dynamic response and APOLLO calculates the associated pore pressure response for sandy soils. It is possible to iterate back and forth between the two programs to allow for pore pressure softening. APOLLO calculates pore pressures by using an analytical expression (Seed et al. 1975), derived from empirical pore pressure buildup curves.

Finn et al. (1977) developed a truly non linear effective stress analysis computer program DESRA (later revised as DESRA-2). This is a fully coupled program. Pore pressures are calculated using the Martin et al. (1975) model and associated rebound modulus and volumetric strain expressions. Dissipation is also incorporated into the analysis. DESRA-2 includes a transmitting boundary at the base to allow for radiation damping. The soil profile is discretised and represented using finite difference techniques.

CHARSOIL (Liou et al. 1977) is an advancement on the work of Streeter et al. (1974) incorporating a pore pressure model based on an assumed relationship between shear modulus and constrained modulus. Dikmen and Ghaboussi (1984) have also produced an effective stress method of analysis, LASS-IV.

Ishihara and Towhata (1982) use a lumped mass non linear system and a pore pressure model based on following the stress path history of the analysis. Yanagisawa et al. (1987) incorporate this pore pressure model into a finite element program.

Th endochronic model proposed by Valanis (1971) utilises the length of the strain path (termed "intrinsic time") to determine the deviatoric and hydrostatic response of cohesionless soils. This can then be extended to determine the generation of pore pressure from the volumetric strains calculated from the endochronic model. A number of researchers have investigated this, including Bhatia and Nanthikesan (1987), Bazant et al. (1983) and Finn and Bhatia (1981).

Prevost (1988) developed the one dimensional finite element liquefaction analysis program DYNA1D, which has a constitutive relationship based on three dimensional multi-surface plasticity theory. The two phase coupled field equations proposed by Biot (1962) are used for the generation of pore pressures.

Byrne and Yan (1990) presented an analysis program 1D-LIQ which is a one dimensional coupled analysis incorporating Byrne's expressions for both volumetric strain (chapter five) and a simplified rebound modulus into the framework of the Martin et al model.

The computer program used in this study, NESSA (Larkin 1978b), incorporates the Martin et al. pore pressure model, but modified to include a simpler expression for the volumetric strain. This program is an extension of the non linear total stress program DENSOR. The theory for this program is given in chapters four and five.

2.3 TWO DIMENSIONAL ANALYSES

The two dimensional analysis adds a lateral dimension to the solution scheme, allowing for lateral boundaries, heterogeneities and variable soil depths to be more accurately modelled. For two dimensional analyses a cross section is taken of the problem, with the assumption that the cross section remains constant in the third dimension. Both in-plane and out of plane analyses are also possible with a two dimensional analysis.

Geometrical considerations tend to make two dimensional analyses most applicable to in-filled valleys and gravity dams and embankments. This review shall focus on the valley applications as it is the form of the two dimensional analysis used in this study.

TOTAL STRESS

The majority of studies reported to date have considered two dimensional (plane strain) elastic wave scattering problems idealised as circular or elliptical valleys within a homogeneous half-space. These solutions have been achieved using a wide array of analytical and numerical schemes. The elastic two dimensional problem for incident shear waves was solved by Aki and Larner (1970). It was a semi numerical and semi analytical scheme, with the solution found from the linear combination of the response of the system to discrete wave number representations. This solution has been utilised by other researchers and has served as a benchmark for other solution schemes. Bouchon (1973) and Bard and Bouchon (1980,1985) extended this into the time domain to investigate the response of relatively steeply embanked alluvial basins.

Exact closed form solutions are available for the case of SH waves incident of a semi-cylindrical (Trifunac 1971) and semi-elliptical (Wong and Trifunac 1974) sediment filled valleys. Again these two solutions have been used for testing numerical methods applicable to more general geometries (Aki 1988).

A great variety of boundary element methods exist (BEM), which have become very popular for the analysis of site response problems. It is well suited to deal with wave propagation problems as the solution reduces the dimensionality of the problem by one. Wong and Jennings (1975) formulated integral equations for the solution of incident SH wave scattering for irregular shaped canyon topographies. BEM's have also been incorporated into finite element analyses by Shah et al. (1982) and finite difference analyses by Cole et al. (1988).

Direct Boundary Element formulations have been applied to solve the scattering of elastic waves by alluvial deposits (Sanchez-Sesma and Esquviel 1979) for different types of waves and scattering patterns. Fishman and Ahmad (1995) have performed extensive numerical studies using a direct BEM method for semi elliptical valleys, analysing the influence of key parameters on the response of the valley.

An indirect Boundary Element Method has been employed by Pedersen et al. (1995) to model elastic three dimensional wave scattering in a two dimensional valley. This accounts for waves arriving from outside the 2D plane of the analysis, which is termed "2.5D scattering" in the literature. The analysis is still two dimensional however.

Benites and Haines (1991) presented a hybrid method for a viscoelastic solution which uses a Riccati equation approach to compute the wave field response within a heterogeneous soil valley, and the Boundary Integral Technique to model the wave paths across the boundary of soil and the underlying media. The solution is performed in the frequency domain. The soil valley may be of arbitrary shape and material composition, which is an improvement on the common semi-circular and semi-elliptical geometries. Comparisons of this and the non linear two dimensional solution used in this study are presented in Marsh et al. (1995).

Other elastic solutions include Ray methods (Hong and Helmberger 1977), which calculate all possible ray paths for incoming waves, scale them, and then sum these rays to achieve a time domain solution. This has been extended by Nowack and Aki (1984) into a method known as the Gaussian beam method. Both solutions have been used to calculate the ground motion of sediment filled basins, with good results reported. Ray methods can not however deal with cases in which surface waves play a major role in the analysis.

Two dimensional non linear solutions of sedimentary valleys have undergone significantly less development than their elastic counterparts. Two dimensional non linear solutions are also less prevalent than one dimensional versions. This is primarily due to the reduced efficiency of the numerical schemes required to solve non linear solutions, particularly in the time domain. The advent of more accessible faster computers however has made such analyses possible to achieve with realistic computer cost.

Idriss and Seed (1974) developed a finite element solution for a two dimensional mesh that incorporated the equivalent linear method of approximating non linear soil properties. Once again this required an iterative procedure to determine the appropriate levels of the strain dependent shear modulus and damping ratio. Lysmer et al. (1974) used the equivalent linear system in the program LUSH, which was directed towards two dimensional soil structure interaction problems. Quad4M (Hudson et al. 1994) is a time domain equivalent of LUSH, which incorporates Raleigh material damping and an equivalent linear system.

Streeter et al. (1974) extended their truly non linear one dimensional solution to incorporate the second dimension by representing the continuum with a latticework of one dimensional elements. Recently Yu et al. (1993) studied the non linear response of layered sedimentary valleys by incorporating a hyperbolic function to model the constitutive relationship. Papageorgiou (1994) presented a two dimensional equivalent linear finite element program with a boundary element transmitting boundary

Joyner (1975) extended his previous one dimensional work into a two dimensional non linear finite difference solution scheme. The solution is performed in the time domain and can account for shear, compressional and surface waves. Marsh (1992) used this program in a number of validation exercises and found good agreement with both existing (linear) solutions and reported case studies. This program was also the basis of this study, with effective stress models being programmed into the existing code.

EFFECTIVE STRESS

Siddharthan and Finn (1982) produced the non linear computer program TARA-2 which was a two dimensional version of the program DESRA-2, incorporating the same pore pressure generation model. This was subsequently updated to TARA-3 (Finn et al. 1986) and has had considerable validation from both case studies and centrifuge comparisons (Finn 1988). A hyperbolic model is used to simulate non linear soil properties and the solution is incremental in the time domain. The two dimensional geometry allows not only cross sectional valley structures to be analysed, but also earth structures such as dams and embankments. This program has been primarily used in the effective stress study of earth dams, although some valley structures have also been analysed. Pore pressure redistribution is not accounted for, so the analysis is entirely undrained.

Ohtsuka and Itoh (1987) presented a non linear (elasto-plastic) effective stress solution incorporated within a combination implicit-explicit finite element formulation. Pore pressures are calculated using a first and second order approximation procedure, which assumes undrained conditions throughout the analysis. Soil structure interaction routines are also included which assume the structure rigid, and a three degree of freedom system with bi-linear springs.

A two dimensional non linear finite element solution (DYSAC2), (Muraleetharan et al. 1994), has been primarily used and validated in the analysis of saturated earth/clay structures, although is again applicable to alluvial valleys. The constitutive behaviour is based on boundary surface plasticity theory, within the framework of critical state soil mechanics, and is combined with a pore pressure redistribution model.. O'Halloran (1986) used the code of Joyner (1975) and incorporated an empirical stress history based pore pressure model for the study of earth embankments. This pore pressure model is outlined in chapter 4, as it is used in a valley comparison analysis later in this study.

2.4 THREE DIMENSIONAL ANALYSES

Considerably fewer studies have occurred in the development of three dimensional solutions to date, although efforts have been made in this area. The major limiting factor is the considerable computational cost in terms of memory and/or computer time. As a result, most simulations are characterised by either very constricting assumptions as to the geometry of the problem, or are limited to low frequencies. Due to the mathematical simplifications of visco elastic models, most effort has been focused on these types of solutions.

The pioneering work of Lee (1978,1984) developed a closed form solution for the three dimensional response of hemispherical basins, making use of wave function expansions.

Boundary Element formulations (BEM) have also been used to solve the three dimensional problem. Sanchez-Sesma (1983) and Sanchez-Sesma et al. (1984) combined wave function expansions with the direct BEM to solve a few problems. Luco et al. (1990) used an indirect BEM to obtain the three dimensional response of an infinitely long canyon of arbitrary cross section.

Mossessan and Dravinski (1989,1990) investigated the steady state and transient response of three dimensional valleys, including the scattering of elastic waves from surface topographies. Comparisons are made with elastic two dimensional solutions. Other researchers (Lee and

Langston (1983), Frankel and Vidale (1992)), have also investigated the elastic three dimensional response of circular valleys and the Santa Clara Valley in California respectively.

Chapter Three

Liquefaction

3.1 DEFINITION OF LIQUEFACTION

Liquefaction is a general term used by many engineers and lay people for the phenomenon of significant strength loss of saturated soils during earthquake loading. This strength loss is primarily due to the generation of excess pore pressures within the saturated soil deposit. An increase in excess pore pressures leads to a reduction in the effective confining stress of the soil, with a resulting influence on the strength properties. Saturated cohesionless soils, particularly sands and silts, are most prone to the mechanisms stated above, and hence are the soils of concern in respect to liquefaction. Liquefaction induced ground damage includes flow and bearing capacity failures, lateral spreading, settlements and ground oscillation.

The term "liquefaction" covers a relatively broad range of different and complex mechanisms and phenomenon that require stricter definition. Loose saturated sands subjected to shear loadings may develop high pore pressures (due to the internal compaction of the particles) and lose virtually all resistance to deformation, regardless of the magnitude. Such an event may be triggered by static loading alone. In the terminology of Seed (1979), this situation of a loose sand with virtually no resistance to deformation is termed liquefaction. This is a strict definition that is different from the general usage of the term. This is potentially the most damaging of all the "liquefaction" type phenomenon.

Earthquake and vibrational loading is of a different form to the above case and applies a series of relatively low magnitude cyclic shear stress loadings to the soil mass. Under this loading system, medium and relatively dense sands that would dilate under static loading may develop high excess pore pressures as well. If these pore pressures reach the level of the confining pressure, the sand is defined as having a "cyclic pore pressure ratio of 100%" (Seed 1979). Significant deformations may also occur in this particular mechanism of "liquefaction", but are unlikely to be unlimited. The levels of deformation (induced strains) experienced during the cyclic loading are primarily a function of the density of the sand; a dense sand will experience lower deformations than a loose one. Seed's term "limited strain potential" or Casagrade's "cyclic mobility" are used to describe this mechanism where unlimited strains are unlikely to occur, as is the case in most earthquake loading situations.

Vibrational loadings usually induce lower stress levels than earthquake loading, but for longer duration. Carter and Seed (1988) list many sources of such low level excitation that have been found to initiate some forms of "liquefaction". This study is primarily concerned with the seismic loading of soils and vibrational loading is therefore only included as an aside and reference.

3.2 EARTHQUAKE INDUCED CYCLIC LOADING

Earthquake loading induces cyclic shear stresses and strains on soil deposits primarily from vertically propagating shear waves, although other wave forms do occur. This cyclic loading is usually non uniform and somewhat random in pattern and magnitude, but clearly cyclic in nature. A typical recorded cyclic shear stress loading sequence is shown in figure 3.1(a). For a level soil deposit (with no initial static shear stresses), the loading system is shown in figure 3.1(b).

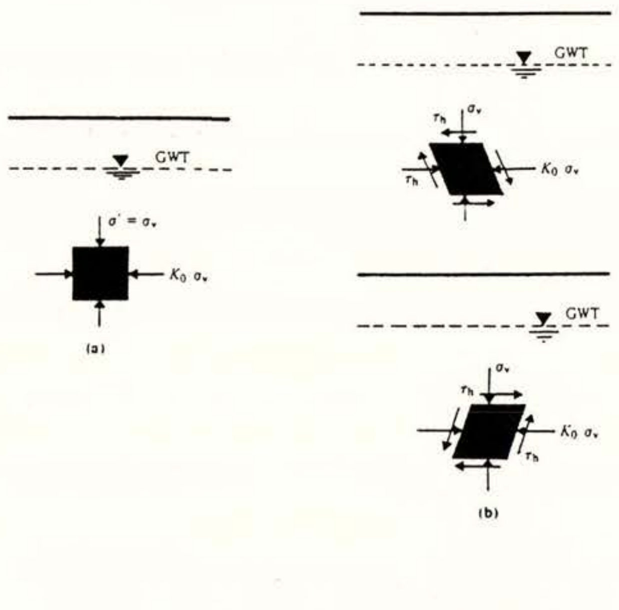

Fig. 3.1 Cyclic stresses from earthquake loading on a soil element (from Seed 1979)

This system of cyclic shear loading is experienced by all soil deposits, but only saturated cohesionless soils exhibit significantly elevated pore pressures. The tendency for sands to compact under cyclic loading is the primary cause of pore pressure generation. Due to relatively undrained behaviour of many sands under short term cyclic loading, this tendency for volume reduction pressurises the pore water and leads to various extents of liquefaction. A full description of this mechanism is given in chapter five.

As elevated excess pore pressures approach the level of the confining stress of a soil element, the associated reduction in effective stress acting on the sand skeleton leads to a loss of strength properties. It is well established that the shear modulus of a sand is proportional to the square root of the mean effective stress. This leads to a declining modulus, strength properties and significant deformations. There is however significant differences in the response of loose and dense sands to the same loading. A loose sand may experience deformations in excess 20%, whereas a dense sand will not experience such extreme deformations. The experimental results of undrained cyclic torsional shear tests on the same uniform medium sand in both a dense and loose state are shown in figure 3.2

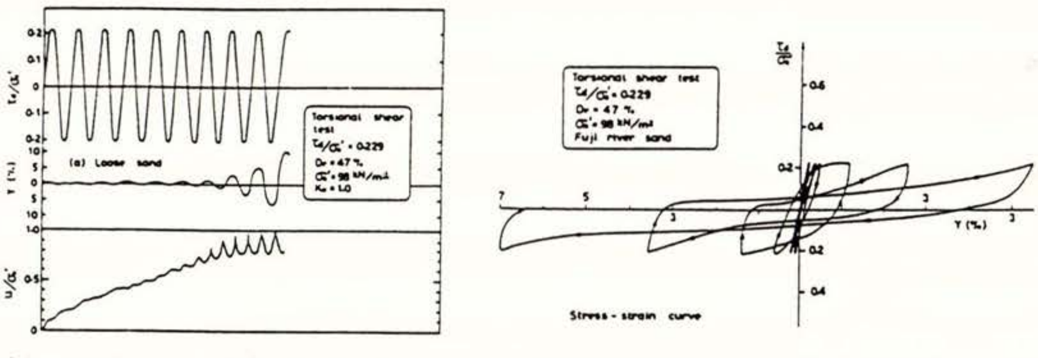

(a) Loose sand (D_r = 47%)

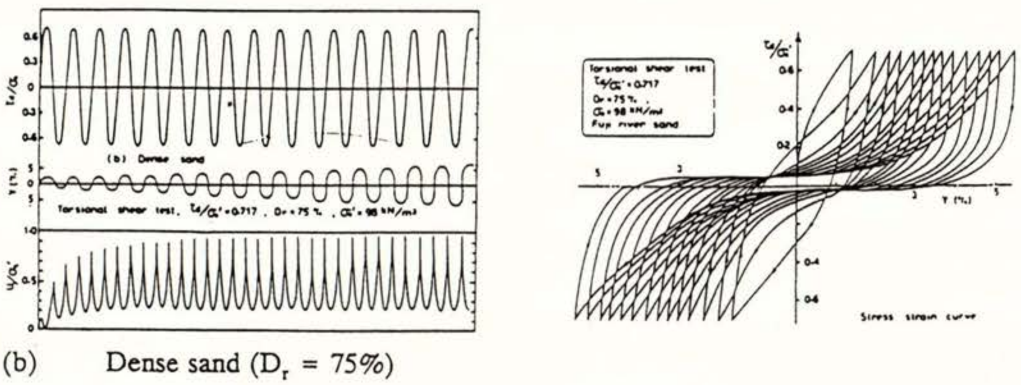

(b) Dense sand (D_r = 75%)

Fig. 3.2 Cyclic torsional testing on Fuji river sand for loose and dense states (Ishihara 1985)

It can bee seen from this figure that once a loose sand has reached initial liquefaction, the pore pressures (u) remain very high during subsequent loading cycles, and consequently the effective stress and strength parameters remain low. For the dense sand however, u only approaches the level of confining pressure twice during a full loading cycle. Due to the dilatant tendencies of dense sands, during the remainder of the load cycle the confining stresses remain significant, thus mobilising much of the strength of the sand. As a result, induced deformations are less significant, although greater than in dry sands. This behaviour leads to the term "limited strain potential", or the alternative "cyclic mobility".

Excess pore pressures tend to dissipate as they are generated, the rate of dissipation being governed by the permeability. Due to the pressure gradients generated within a soil column, excess pore water dissipates vertically toward the surface, or if impermeable layers are present, laterally. The resulting upward flow of water may have devastating effects on soils above the liquefied zone. Surface layers may experience symptoms of liquefaction such as sand boils, a "quick" condition where surface layers lose all strength and bearing capacity (as suspected in some of the Niigata failures), or general water seepage damage. Surface manifestations may not appear until a significant time after shaking has ceased, depending on the depth of the liquefied zone, the permeability and the drainage paths. The liquefaction risk is therefore not just from the surface layers, but from any subsurface loose saturated sandy layers that may be present.

Associated with the dissipation of excess pore pressures are settlements of the affected and surrounding layers of soil. This can be attributed to the tendency for sands to densify under cyclic loading, and once the excess pore water has dissipated, the sand deposit will decrease in volume. Sands of medium to low permeability may take a number of hours or days to exhibit such behaviour. Settlements are usually uneven, which results in differential settlements, leading to damage of both underground utilities and surface structures.

In summary the potential hazards from earthquake induced loading are large deformations, post liquefaction settlements and surface manifestations resulting from the dissipation of the excess pore water.

3.3 EVALUATION OF LIQUEFACTION POTENTIAL

From experimental and particularly field data, it has been found there is a range of saturated sands that are most susceptible to liquefaction. This experience has been summarised in the grading curves produced by Tsuchida and Hayashi (1971) which show the ranges of the most critical sand gradings that are susceptible to liquefaction (figure 3.3)

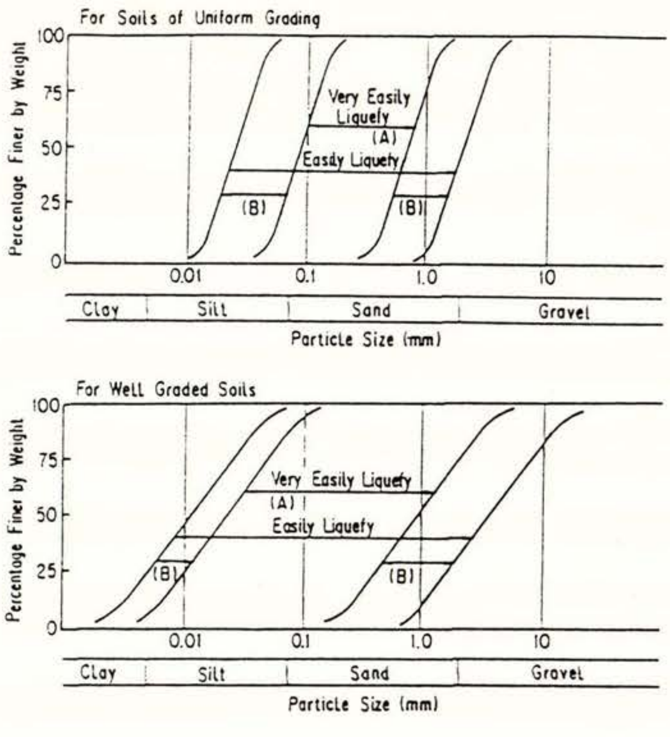

Fig. 3.3 Grading curves for sands most susceptible to liquefaction (from Tsuchida and Hayashi 1971)

The two main factors in the susceptibility of soils to liquefaction is their tendency to densify under cyclic loading and the permeability, which governs the rate at which the pore pressures dissipate. Gravels for example will generate high pore pressures, but tend to dissipate them very quickly, which in combination makes gravels less susceptible. For fine soils, the permeability is very high, but there is little tendency to densify under loading and hence these soils are also relatively immune to liquefaction.

LEVEL GROUND LIQUEFACTION

Liquefaction damage to level ground soil deposits include ground settlements, formation of sand boils, foundation and bearing capacity failures. There are a number of approaches that may be taken in the evaluation of liquefaction potential for a particular site and some of them shall be outlined below.

The most widely used is an empirical approach that draws upon the data and experience of past events. By noting which sites did and did not experience liquefaction effects, and relating the properties of these different sites, it is possible to evaluate the liquefaction potential for a future site by correlating its properties to the historical data base.

Another approach is to use uncoupled numerical modelling to predict the response of a site to both the propagation of earthquake motion and the resulting pore pressure generation, or a combination of numerical and empirical techniques may be used.

The basic concept of the above methods is to compare the liquefaction resistance of a soil deposit to the excitation levels likely to be induced by an earthquake. This then allows a factor of safety against liquefaction to be determined. There are two basic methods of comparison that may be used: the shear stress and the shear strain approach. The shear stress approach is the most common form and compares the levels of shear stress required to cause liquefaction with those induced in the deposit from earthquake loading. The shear strain approach compares induced shear strains instead of shear stresses and is gaining recognition as a useable tool. Both are outlined below. Each method may require experimental cyclic loading of test samples, or can be used in conjunction with some components of the empirical approach. Experimental techniques are explained in section 3.4.

Other significant liquefaction potential evaluation techniques include an energy dissipation method (outlined in Berrill 1995), which is based on the suggestion that pore pressure increase is proportional to the density of seismic energy released by the earthquake event.

3.3.1 Shear Stress Approach

The shear stresses induced within a soil deposit from an earthquake may be determined from either a total stress ground response analysis or by the simplified expression proposed by Seed and Idriss (1971)

$$\tau_{av} \approx 0.65\frac{\gamma h}{g}a_{max}r_d \qquad 3.1$$

where τ_{av} is the average induced shear stress

γ is the unit weight of the soil

h is the depth of the element under consideration

a_{max} is the maximum ground surface acceleration

r_d is the stress reduction factor (which is a function of depth)

This expression is derived from a rigid body, and the assumption that irregular stress history cycles can be replaced with an equivalent number of uniform stress cycles. The magnitude of these equivalent cycles is assumed as 0.65 of the peak stress value.

The second component of this analysis method is to determine the levels of stress required to cause liquefaction of the actual in situ sand, called the liquefaction resistance. This is then compared to the induced value from the earthquake to determine a factor of safety. One method of determining the liquefaction resistance is to perform cyclic laboratory testing, which is outlined in section 3.4. The alternative to sampling is to empirically relate the measured in situ properties to performance data from previous earthquakes. This has been investigated by many researchers who have used the standard penetration test (SPT) and to a lesser extent the cone penetration test (CPT) as the main index for determining liquefaction resistances. The penetration tests were chosen as the index test based on observations that the main factors influencing liquefaction (density, soil fabric, particle size) also generally influence penetration. There is also a wealth of SPT data from sites that have experienced past earthquake events.

Shear stress may be normalised by the vertical effective confining stress to give a non dimensional term known as the stress ratio (τ/σ_v'). Based on past events, Seed et al. (1984) produced figure 3.4 relating the stress ratio required to initiate liquefaction from a magnitude 7.5 earthquake to the normalised SPT blow count $(N_1)_{60}$. From this figure, empirical liquefaction resistance may be determined based on blow counts. It can be seen from this data that the content of smaller particles (silt content) has the effect of increasing the liquefaction resistance of a sand.

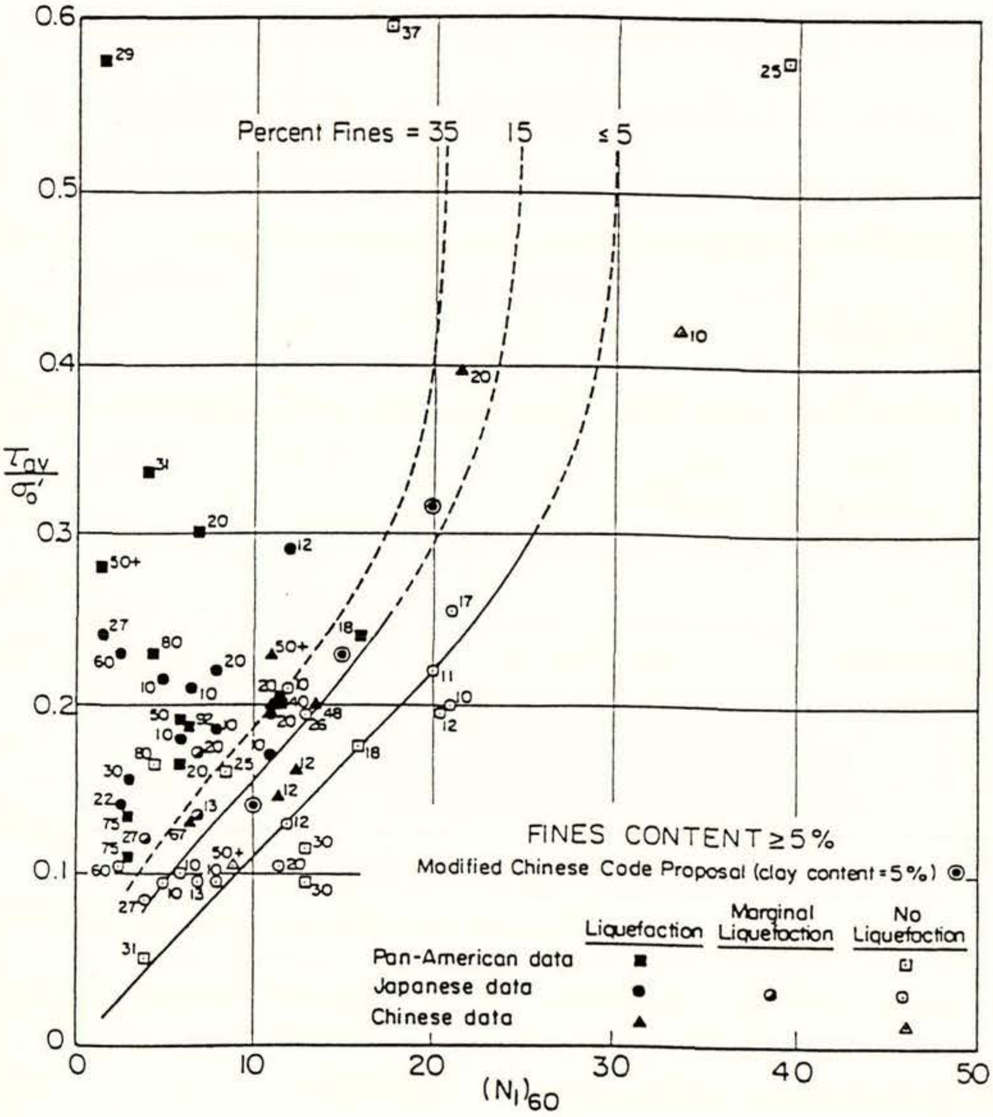

Fig. 3.4 Relationship between SPT and stress ratio for liquefaction (from Seed et al. 1984)

The CPT has several advantages over the SPT in liquefaction engineering as outlined by Berrill (1995). These include providing a continuous rather than discrete profile of the soil strata and causing less in situ sample disturbance from bore drilling. There are also problems with energy input standardisation for the SPT. Robertson and Campanella (1985) have proposed a similar correlation of stress ratio resistance for a magnitude 7.5 earthquake with cone tip resistance. There is much less historical data available for the CPT, and correlations with the SPT in addition to the CPT data base were used in the preparation of this relationship. The resulting correlation is shown in figure 3.5. Some limited experience in the Edgecumbe area (Marks 1992) has shown that the correlations between the SPT and CPT from Robertson and Campanella (1985), on which much of figure 3.5 is based, may not be valid for some New Zealand soils.

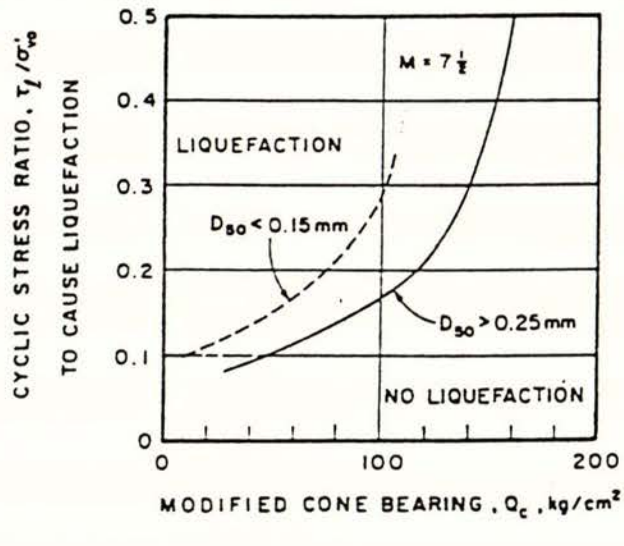

Fig. 3.5 Relationship between CPT and stress ratio required to initiate liquefaction (from Robertson and Campanella 1985)

The relationships of figures 3.4. and 3.5 have been collected and correlated for a magnitude 7.5 earthquake. This data may be extended to other magnitude events based on the observation that from a liquefaction point of view, the main difference between different magnitude earthquakes is the number of equivalent stress cycles they induce. Statistical analysis by Seed et al. (1975) has shown that the number of equivalent stress cycles at constant stress induced by different magnitude earthquakes have typical values shown in table 3.1

Table 3.1 Magnitude Correction Factors

Earthquake Magnitude (M)	Number of equivalent stress cycles	Correction Factor (C_M)
8.5	26	0.89
7.5	15	1.0
6.75	10	1.13
6.0	5-6	1.32
5.25	2-3	1.5

Relationships between cyclic stresses and number of cycles to liquefaction gained from large scale simple cyclic shear tests on sands have been presented by De Alba et al. (1976). When normalised by the shear stress required to cause liquefaction in one cycle (τ_1), the results take the form shown in figure 3.6

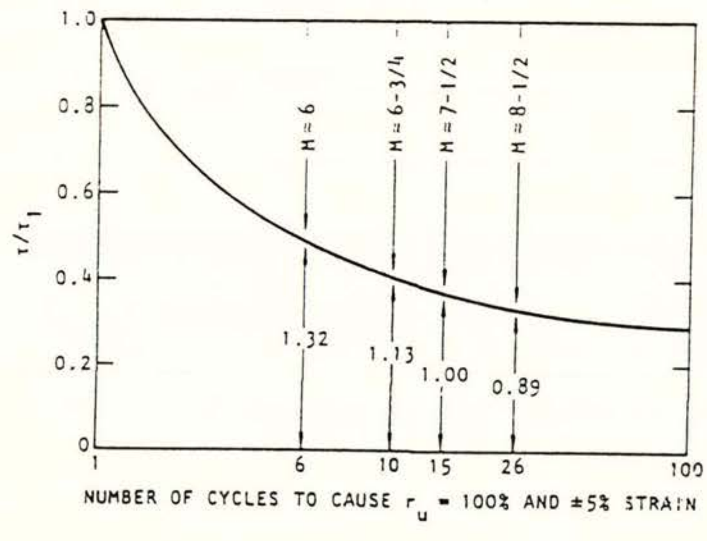

Fig. 3.6 Relationship between normalised shear stress and number of cycles to initiate liquefaction

The data collapses to a single line which is constant for any density. From this, the ratio of stresses required to cause liquefaction for any number of equivalent loading cycles may be determined. Using the magnitude 7.5 earthquake as unity (15 equivalent loading cycles), the stress ratios required to cause liquefaction for other equivalent loading cycles (and hence magnitudes) may be determined from the Magnitude Correction Factor (C_M) taken from figure 3.6 and shown in table 3.1.

From figures 3.4 or 3.5 and the correlations in table 3.1, it is possible to generate a liquefaction resistance curve for any sand based on the blow count alone. Liquefaction resistance curves are expressed as a stress ratio versus number of cycles to liquefaction on a semi log scale. It must be stated that this curve will not be an exact representation of the properties of the soil under investigation as this method is completely empirical.

The stress ratio required to cause liquefaction is not uniquely related to the number of equivalent loading cycles however, but it is also a function of the confining pressure, initial static shear stresses and overconsolidation ratio.

Based on data from 18 different sands, Harder (1988) produced a correction factor K_σ to be applied to the empirically determined resistance stress ratio for different confining pressures. K_σ is defined as the stress ratio required to cause liquefaction at any confining pressure divided by the stress ratio required to initiate liquefaction in the same number of cycles at a confining pressure of 100 kPa. The data and proposed correction factors are shown in figure 3.7. From this figure it can be seen that the stress ratio to initiate liquefaction decreases with increasing confining pressure, although there is a wide scatter of data that the correction factor has been fitted to.

A number of researchers have investigated the effect of initial static shear stresses on the resistance of a sand to liquefaction. For level ground conditions (as investigated in this study), no initial static shear stresses are present. This is not the case for sloping ground surfaces or in areas near the edges of surface structures. Rollins and Seed (1990) summarised the state of knowledge which indicates that for increasing static shear stresses there is a lower resistance to liquefaction for loose sands and a higher resistance for dense sands.

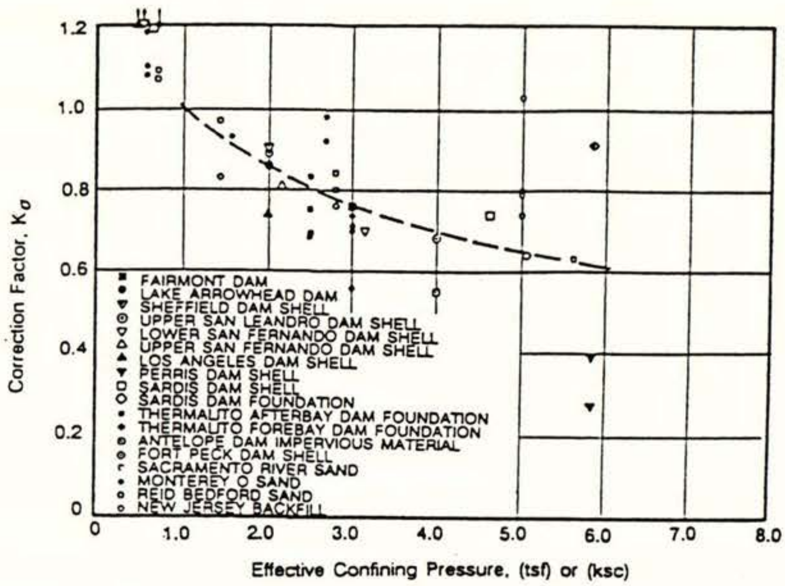

Fig. 3.7 Correction factor K_σ for different confining pressures (from Harder 1988)

Rollins and Seed (1990) have again summarised the available experimental and analytical data for the effect of overconsolidation ratio on liquefaction resistance. This indicates the stress ratio required to cause liquefaction increases for increasing overconsolidation ratio, and for high levels of overconsolidation the stress ratio may as much as double.

Settlements, shear strains and surface manifestations as indicated previously can cause very significant damage to surface structures. Settlements and surface manifestations are caused by the dissipation of high excess pore pressures towards the surface, whereas excess shear strains are developed due to a loss of strength and stiffness resulting from the high generated pore pressures.

Experimental data for settlements of sands under cyclic loading has been reviewed by Tokimatsu and Seed (1987) who found settlements are a function of cyclic shear strain and relative density, but are independent of overburden pressure. From this data, empirical curves were developed correlating the stress ratio and normalised SPT blow counts to volumetric strains (settlement). Figure 3.8 shows these empirical relationships for a magnitude 7 earthquake. Case studies of actual settlements indicate these predictions are in the order of those observed in the field, but may be somewhat conservative in some cases (Martin et al. 1991)

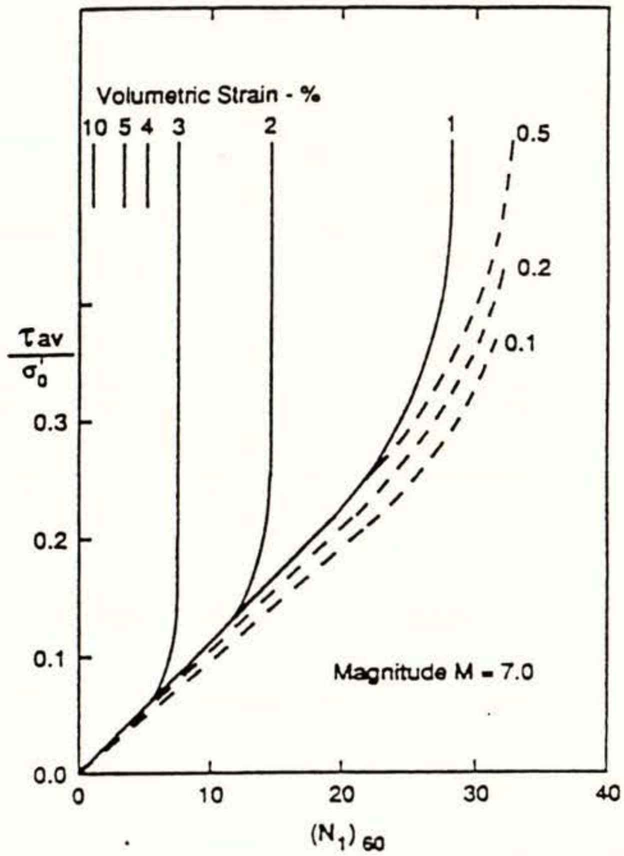

Fig. 3.8 Empirical volumetric strain relationships (from Tokimatsu and Seed 1987)

The extent of shear strains developed by a sand due to stiffness loss is primarily a function of the relative density of the soil. Loose sands may experience very large strains while dense sands, because of their dilatancy properties at relatively high shear strains, exhibit some strain resistance (limited strain potential). It is important to note that high pore pressures developed in a dense sand will generally result in lower levels of damage than in a loose sand. Based on collected empirical and experimental data, Seed et al. (1984) produced a tentative relationship to determine the magnitude of shear strains that may be developed, which is dependent on the normalised SPT blow count and the magnitude of the stress ratio induced. This relationship is shown in figure 3.9.

From this data, three approximate ranges of potential damage levels have been identified based on SPT blow count, as shown in the top diagram of figure 3.9. This difference in ground damage potential for different sand properties should be noted in evaluating the significance of any liquefaction risk that may exist for a site.

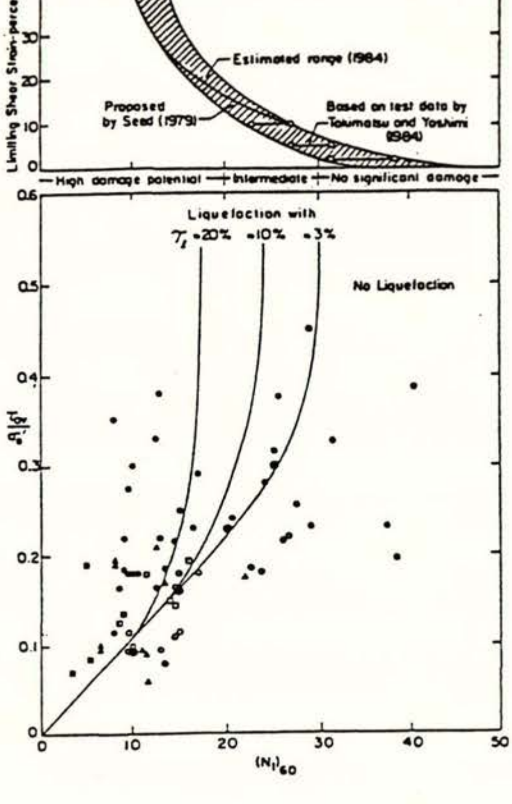

Fig. 3.9 Tentative relationship for prediction of induced strains during liquefaction (from Seed et al. 1984)

Surface manifestations of liquefaction such as sand boils, ground fissures and lateral spreading have been investigated by Ishihara (1985) and Scott and Zuckerman (1973). Scott and Zuckerman studied the formation of sand boils and concluded that a layer of finer particles overlying a liquefied layer is most susceptible to this phenomenon. They also observed, along with many other researchers, that dense sand layers overlaying a loose liquefiable layer may be subjected to a phenomenon known as secondary liquefaction, where the dense layer is affected by both the upward propagation of pore water and the loss of support for the dense layer. Empirical relationships based on case studies and field data from Japan have been produced by Ishihara (1985) to account for this.

The shear stress approach outlined above is the most developed and widely used method available today to determine the liquefaction potential of a site. The primary reason for this is the fact that induced cyclic shear stresses are closely related to ground surface accelerations (equation 3.1). Ground surface accelerations may be estimated for a predicted or design event and the potential for liquefaction evaluated on this basis. Experimental evidence (section 3.4) suggests that shear stress is not the fundamental governing parameter in the mechanics of pore pressure generation and liquefaction, but this method has been refined to the point of giving relatively confident prediction results.

3.3.2 Shear Strain Approach

The shear strain approach to evaluating liquefaction potential is based on the experimental observation that shear strain is the fundamental parameter governing pore pressure buildup. A factor of safety against liquefaction based on induced and resisted shear strains instead of shear stresses is therefore used. From equation 3.1, Dobry et al. (1981b) derived equation 3.2 to determined the shear strains induced by an earthquake of a known surface acceleration.

$$\gamma_e = \frac{\tau_e}{G} = 0.65 \frac{a_{max}}{g} \frac{\gamma h r_d}{G_{max}\left(\dfrac{G}{G_{max}}\right)_{\gamma_e}} \qquad 3.2$$

where γ_e is the equivalent uniform strain amplitude

G is the equivalent shear modulus of the soil

G_{max} is the maximum shear modulus of the soil

As previously, this replaces an irregular strain time history with an equivalent number of uniform cyclic shear cycles (but different in number for different magnitude events than equivalent shear stress cycles shown in table 3.1). The main difficulty with this expression is the ratio $(G/Gmax)_{\gamma e}$. This ratio decreases as pore pressure increases, but these pore pressure changes can not be accurately determined using this relationship alone. Shear strain is also heavily dependent on the values of shear modulus. Added difficulty may be experienced in accurately determining G_{max}.

Very little data is available in the form of figures 3.4 or 3.5 relating shear strain levels to cause liquefaction and blow count or a similar indicators. As a result the only viable option is to perform strain controlled laboratory liquefaction testing on specified samples of interest.

Laboratory testing has shown there to be a level of applied shear strain at which there is no volumetric reduction is dry sands subjected to cyclic loading, and by extension, limited pore pressure generation in saturated sands. Data from the NRC (1985) and attributed to Dobry for strain controlled cyclic triaxial testing is shown in figure 3.10, and indicates a value of threshold strain around 10^{-2}%. Dobry et al. (1981b) have collected data that suggests the value of threshold strain is similar for most sands and is independent of relative density, confining pressure and initial consolidation shear stresses. The only parameter identified as having a significant effect on threshold strain is the over consolidation ratio.

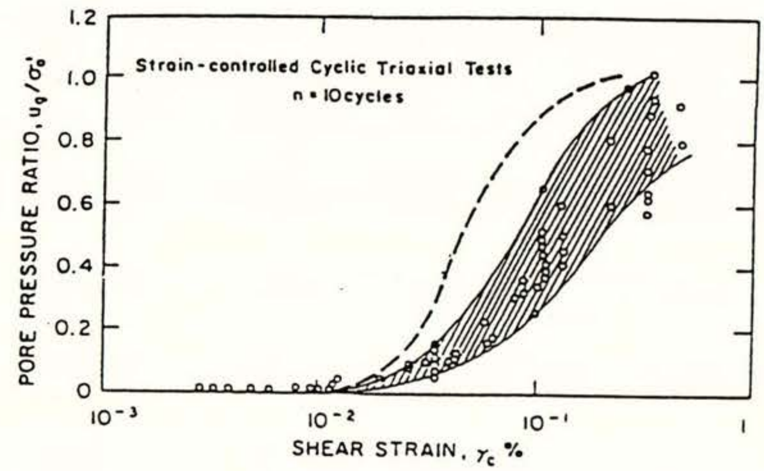

Fig. 3.10 Threshold shear strain data (from NRC 1985)

The threshold strain may be used as a means of determining the liquefaction resistance of a sand in situ by correlating threshold strain with resulting surface accelerations and shear wave velocities. Dobry et al. (1981a) have presented correlations of this form. They are very conservative however because shear strains exceeding the threshold strain may not be sufficient to generate significantly high pore pressures, as the threshold strain is the strain level at which effectively no pore pressure generation has been observed.

The biggest draw back with the shear strain approach is the significant uncertainty in the evaluation of induced shear strains from the earthquake loading. There are also few correlations for determining the in situ strain resistance of sands to liquefaction, hence requiring relatively expensive testing. The major advantage is in the fact that shear strain is the governing parameter of pore pressure generation, and therefore any analysis based on shear strain has a physical basis and motivation

SLOPING GROUND AND EMBANKMENTS

The main difference between these cases and the level ground condition is that a magnitude of shear strength is required to resist failure. As a result, any liquefaction analysis must involve investigation of the potential for shear strength loss as a result of elevated pore pressures. As this study is concerned with level ground conditions only, the reader is referred to Berrill (1995) or Ishihara (1993) for an overview of the cases of shear strength resistance.

3.4 LABORATORY DETERMINATION OF LIQUEFACTION POTENTIAL

Laboratory cyclic testing of soils has received much attention over the years by many researchers. The main testing equipment that have been developed to investigate liquefaction are the cyclic simple shear test, cyclic triaxial test and the cyclic torsional test. The cyclic simple shear test simulates the in situ stress conditions most closely but most laboratories use the cyclic triaxial test as it requires less specialised hardware than other tests. Experimental results presented in this study are from cyclic triaxial testing. The basis of the testing methodology shall be outlined below, but initially the cyclic simple shear test is briefly discussed. The recent addition of centrifuge testing is also investigated.

3.4.1 Cyclic Simple Shear Test

The first simple cyclic shear tests were reported by Peacock and Seed (1968) using a Roscoe type simple shear device. The other most common simple shear device was developed by the Norwegian Geotechnical Institute (NGI). The shake table may also be used to generate a similar type of test. These tests were developed in an attempt to eliminate some of the deficiencies of the triaxial test. Unlike the cyclic triaxial test, this device duplicates the simple shear or plane strain conditions that are induced within soil deposits.

The main disadvantage of the simple shear test is the stress concentrations and non uniform strain distributions that can develop due to boundary conditions, Many researchers, including Finn and Vaid (1977) and De Alba et al. (1976), have concluded that it is impossible to construct a device in which the ideal boundary conditions may be applied. "Practical" boundary conditions may be devised however by using a sample of large area, allowing the bulk of the sample to experience essentially uniform strain conditions. Large samples require large driving forces however, and the cost of such equipment can be great. Figure 3.11 shows the ideal stress conditions induced within a simple shear test

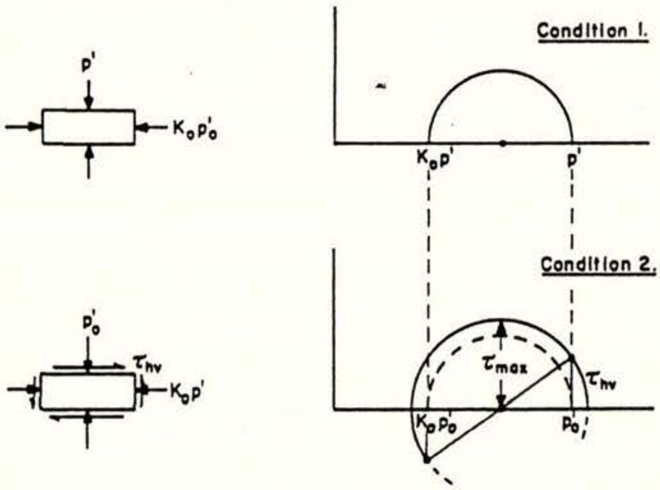

Fig. 3.11 Induced cyclic shear stresses in an ideal simple shear test

The shear stress τ_{xy} is normalised by the vertical effective stress σ_y' to calculate the stress ratio τ/σ_v', which is then used in the common liquefaction strength curves. This is the stress ratio that is also used in the empirical method of Seed and Idriss (section 3.3.1).

3.4.2 Cyclic Triaxial Test

Seed and Lee (1966) were the first to extend the standard triaxial test into the area of cyclic testing of soils for liquefaction analyses, and it is now the most commonly used cyclic soil test. The basic methodology of the test is as follows:

A cylindrical triaxial sample is initially consolidated under a cell pressure σ_3. In principle (figure 3.12(a)) the sample is then subjected to cyclic axial deviator stress of $\pm\ \sigma_d/2$ and a simultaneous reduction in cell pressure by an equal amount. The normal stress on the 45° plane through the sample is unchanged, but a shearing stress is developed on that plane. Upon load reversal, the shearing stress is reversed on that plane whilst the normal stress remains unchanged, generally leading to a pore pressure increase. The cyclic stress conditions of this 45° plane are intended to simulate those on a horizontal plane in the field. For convenience, the test is normally performed by maintaining a constant cell pressure and cycling the axial stress at $\pm\sigma_d$, as shown in figure 3.12(b).

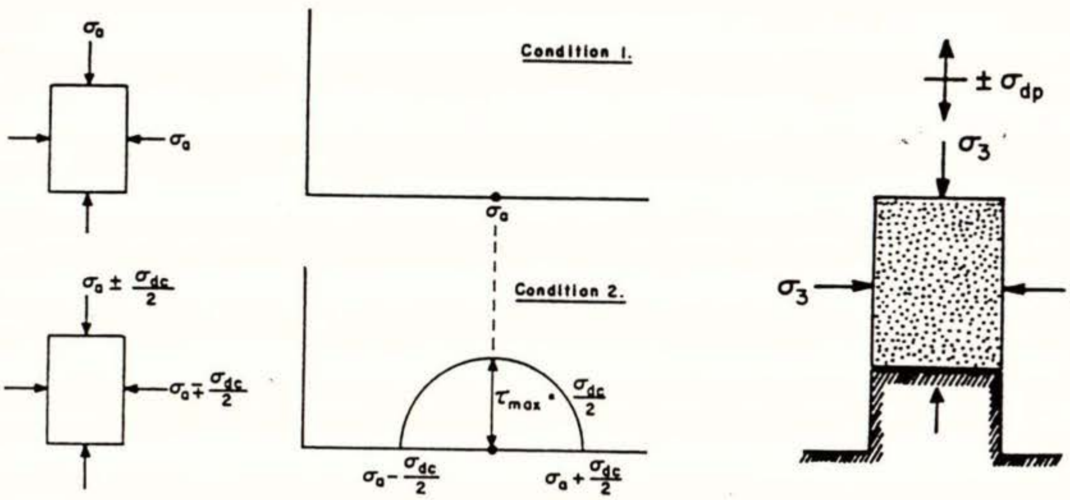

Fig. 3.12 Stress conditions in cyclic triaxial testing: a) ideal, b) constant cell pressure

This technique results in essentially the same stress conditions in the sample as long as it is fully saturated and undrained (Seed and Lee, 1966). The stress ratio used to express the results is $\sigma_d/2\sigma_3$, which is the ratio of maximum shear stress to the ambient confining pressure, rather than the shear stress on a horizontal plane to the initial effective overburden pressure, as in the cyclic simple shear test. As these are two different stress ratios, the pore pressure response will not be the same for each test and a correction factor c_r is required, as shown below

Many researchers have investigated the form of the correction factor c_r, with ranges of 0.55 to 1.0 being proposed, although most agree on a range of 0.6 to 0.7. High quality testing from Berkeley has produced correlations between the two tests for stress ratios required to initiate liquefaction in 10 loading cycles, as shown in **figure** 3.13.

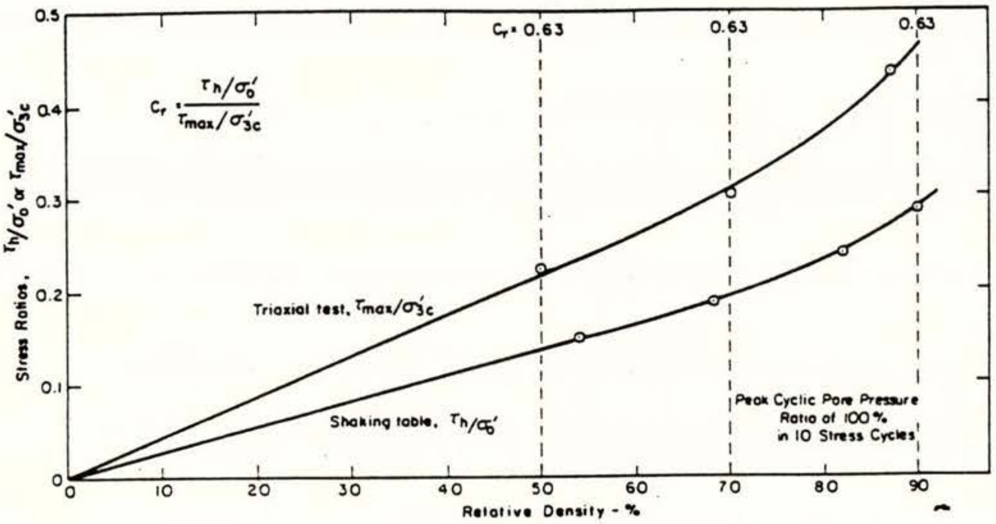

Fig. 3.13 Comparison of shaking table and triaxial test results (from Seed 1979)

From these results the value of c_r is relatively constant at 0.63 for a range of densities. There is no theoretical relationship between the induced stress ratios of the two tests, and therefore the correlation is purely an experimental observation. For use in numerical or empirical liquefaction analyses, results generated from cyclic triaxial testing must therefore be multiplied by this correction factor.

Stress controlled cyclic testing are more commonly used than strain control due to the prevalence of the shear stress approach in liquefaction analysis (section 3.3.1). More correctly the tests are load controlled with a calculation of the stress state made later. This system leads to non uniformities between the compression and extension phase of the loading cycle and generates non symmetrical hysteresis loops. Necking of samples due to high stress concentrations in the extension phase is common, and renders the results of little use.

As discussed earlier, excess pore pressure generation is a function of shear strain. For cyclic stress controlled testing, the stress levels may be viewed as those required to produce the corresponding magnitude of cyclic strain. It is found that cyclic stresses are strongly a function of density, method of sample preparation, confining stress, type of sand and its initial structure/fabric (Castro 1987, Ladd et al. 1989)). In other words, these factors determine the magnitude of cyclic stress that one needs to apply to produce a value of cyclic strain. Because cyclic stress is a function of a number of factors in the context of liquefaction testing, great care is required to achieve repeatable results, and results that are comparable with those at other laboratories. A number of testing studies have been undertaken in an attempt to investigate the repeatability aspect (Silver et al. (1976), Mulilis et al. (1977), Toki et al. (1976), and most recently Miura et al. (1994)). These studies have clearly shown that the method of sample preparation and testing procedure must be clearly specified and followed to achieve consistent results. The ASTM (1991) produced a standardised testing procedure in an attempt to achieve some consistency in the experimental results.

Strain controlled cyclic triaxial testing is a more robust alternative to the stress controlled test, as pore pressure generation is a function of the magnitude of the induced shear strains. As a result this liquefaction test is a lot less sensitive to the factors that influence the stress controlled test (Ladd et al. (1989)). The difficulties associated with this shear strain approach (as explained in section 3.3.2) is the lack of well researched methods that can make use of the experimental data for the investigation of liquefaction potential.

3.4.3 Centrifuge Testing

The centrifuge has received a great deal of research effort in recent years. Although very expensive to develop and use, there are a number of centrifuges around the world that are available for soil testing. A wide variety of both static and dynamic scale problems may be studied using a centrifuge. The main asset of the centrifuge is the increased gravity force it generates on model structures. This allows small scale models to experience confining pressures that are analogous to those the full scale structure would experience. The greatest application is in cohesionless soils where strength and modulus properties are a function of the confining pressures. Relevant to this report are studies of liquefaction behaviour that have been reported in the literature (Finn 1985, 1988, Whitman and Arulanandan 1985) and allow comparison of experimental results with numerical models. The reader is referred to Scott (1994) for an indepth review of the development of the centrifuge and its applications.

Chapter Four

Site Response Theory

4.1 INTRODUCTION

This study makes use of both one and two dimensional stress site response programs, and the theory behind both versions is discussed in this chapter. Initially the two dimensional program first developed by Joyner (1975) is discussed, with the one dimensional system (Larkin 1978a) following.

The two dimensional program was split by Joyner into two separate solution schemes: the in plane PSV, and out of plane SH solutions. This was done on the observation that in plane and out of plane motions were relatively independent of each other, and hence could be uncoupled. The advantage of this was an increase in computational efficiency. For this study the in plane scheme was required for extension into an effective stress solution, and therefore only the theory of this solution shall be detailed below. The pore pressure model and its implementation is detailed in chapter five. Therefore this chapter may be considered as the theory of the total stress programs. The transmitting boundary and non linear constitutive models are also presented. The two dimensional theory is largely reproduced from Marsh (1992).

4.2 TWO DIMENSIONAL IN-PLANE TOTAL STRESS SOLUTION

4.2.1 Basic Computational Scheme

To undertake a two dimensional site response analysis it is assumed that over a substantial length of the site the cross-section is reasonably constant in shape. This two dimensional cross-section is then discretized spatially and a grid of nodes and elements is used as the basis of all calculations. The soil mass is therefore divided into prismatic elements of infinite length and the analysis is carried out per metre run. The mass of each element is divided equally amongst the adjoining nodes, and the shape of these elements can be irregular quadrilaterals or triangles. A typical two dimensional mesh is displayed in figure 4.1. The numbering convention for the components of motion is also shown.

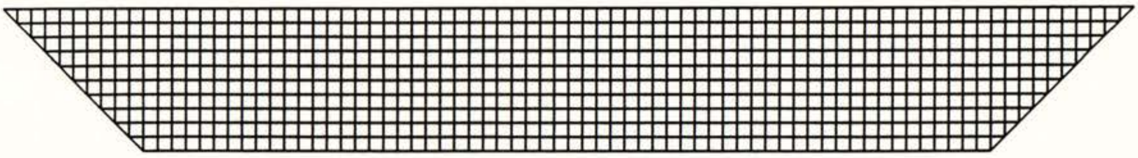

Fig. 4.1 Typical Two Dimensional Mesh Configuration

The solution is based on a finite difference approximation for the scattering of seismic waves within the solution space. Velocities are calculated in the two dimensional mesh of points for the three components of motion, and the key to the analysis is that all components of motion are independent of the x_2 coordinate. This is the fundamental property of a two dimensional analysis.

$$\frac{\partial V_i}{\partial x_2} = 0 \quad , i = 1,2,3 \qquad 4.1$$

Displacements of the grid points are considered small, and so a first order finite difference scheme is sufficient in approximating the velocity gradients throughout the mesh. The soil mass is underlain by a semi-infinite elastic medium representing the bedrock. The properties required to model the two media are discussed later.

The behaviour of the soil mass is described in terms of the three components of particle velocity V_i and the nine components of total stress and strain S_{ij} and E_{ij}. These total stresses and strains are divided into both mean and deviatoric components. The mean stress and strain, σ_m and e_m, and the deviatoric stresses and strains, σ_{ij} and e_{ij}, are defined in terms of the total stresses and strains

$$\begin{aligned} \sigma_m &= \tfrac{1}{3}\left(S_{11} + S_{22} + S_{33}\right) \\ e_m &= \tfrac{1}{3}\left(E_{11} + E_{22} + E_{33}\right) \end{aligned} \qquad 4.2$$

and

$$\sigma_{ij} = S_{ij} - \sigma_m \delta_{ij}$$
$$e_{ij} = E_{ij} - e_m \delta_{ij} \qquad 4.3$$

where δ_{ij} is the Kronecker delta such that

$$\delta_{ij} = 1 \quad \textit{for} \;\; i = j$$
$$= 0 \quad \textit{for} \;\; i \neq j \qquad 4.4$$

Therefore with the normal components of stress and strain, for example with the 11 component

$$S_{11} = \sigma_m + \sigma_{11} \qquad 4.5$$

and with the shear components of stress and strain, for example with the 13 component

$$S_{13} = \sigma_{13} \qquad 4.6$$

It is evident that the mean strain is one third of the total volumetric strain. The constitutive relationships for the mean and deviatoric stresses and strains are detailed in section 4.2.2.

Based on these quantities the solution procedure is as follows:

At each node the velocities V_i are known at time t, and the mean stress, σ_m, and deviatoric stresses, σ_{ij}, in each element are known at time t - Δt/2.

From V_i the increments in total strain ΔE_{ij} are calculated for each element. They are found from the velocity gradients across the elements

$$\Delta E_{ij} = \frac{1}{2}\left(\frac{\partial V_i}{\partial x_j} + \frac{\partial V_j}{\partial x_i}\right)\Delta t \qquad 4.7$$

where the partial quantities are calculated by means of a linear finite difference scheme. With all variables independent of the x_2 coordinate, the only variation in the total stress increments is with respect to the x_1 and x_3 coordinates, namely throughout the two dimensional mesh. Therefore for the triangle pictured

$$\frac{\partial V_i}{\partial x_1} = \frac{1}{\Delta x}\left(V_i(3) - V_i(1)\right)$$
$$\frac{\partial V_i}{\partial x_3} = \frac{1}{\Delta x}\left(V_i(3) - V_i(2)\right) \qquad 4.8$$

A similar result is obtained for a square by splitting the square into two triangles and averaging the result. With these velocity gradients the increments in total strain can be calculated.

The increments in mean strain Δe_m and deviatoric strain Δe_{ij} are computed from the increments in total strain as described earlier for each element.

Using the relevant constitutive relationships the increments in mean stress $\Delta\sigma_m$ and deviatoric stress $\Delta\sigma_{ij}$ in each element are found from the corresponding increments in mean and deviatoric strains. These constitutive relationships are described in detail in section 4.2.2

These increments in stress are added to the existing values to find the updated values for each element of the mean stress σ_m and deviatoric stresses σ_{ij}.

From the new values of mean and deviatoric stresses the updated values of total stress are found.

The updated total stresses in each element are then used to find the forces acting at each node in the mesh. Cauchy's line integral formula is used to calculate the force acting on each segment of an element due to the internal stresses of that element. This force is divided equally between the two nodes at either end of the segment. The total force acting at a particular node due to internal stresses is found by adding the forces from all the segments attached to that node. The total force F_i on an internal node is the sum of these forces and the force due to gravity. Nodes along the boundary between the soil medium and the underlying bedrock are subject to an additional force due to the seismic disturbances in the bedrock. These additional forces are described in section 4.2.3.For every node the new total forces acting are now known.

From these forces the updated particle velocities can be calculated. Newton's second law is applied at every node and so

$$V_i(t+\Delta t) = V_i(t) + \frac{F_i \Delta t}{m_i} \qquad 4.9$$

where m_i is the total mass acting at that node.

The new values of V_i are then used to start the next time step. The site response analysis problem is thus solved across the two dimensional mesh step by step in time.

Joyner (1975) compared his results with those published by Boore, Larner and Aki (1971) for the solution of a linear elastic problem by a finite difference method and found satisfactory agreement.

4.2.2 Constitutive Relationships

The constitutive relationships define the essential dependence of the stress increments on the strain increments. The relationship between the increments in mean stress and strain is presumed elastic with

$$\Delta e_m = \frac{\Delta \sigma_m}{3K} \qquad 4.10$$

where K is the bulk modulus of the soil and is therefore assumed constant. This means that there is no energy loss in compressional deformation within the nonlinear soil medium.

The relationships between the increments in deviatoric stress and strain used in the analysis follow those of Iwan (1967) with some minor modifications. Iwan extended the theory of incremental plasticity in three dimensional stress space by utilising a family of yield surfaces, instead of a single yield surface. All nine components of stress and strain are taken into account. For each yield surface the formulation is the same as the classical approach. An initial yield surface specifies the stress state for which yielding first occurs, a work-hardening rule specifies how the yield surface is changed during plastic flow, and a flow rule relates the plastic strain increment to the state of stress and the stress increment. In one dimension the system may be considered as a series of linear springs and Coulomb friction sliders in parallel, each unit having a stiffness G_i until the yield stress Y_i is reached. Each of these units obeys a linear kinematic work-hardening rule individually, but their combined action when arranged in series gives rise to a nonlinear work-hardening rule for the material as a whole. The yield stress Y_1 of the first unit is generally set to zero and the stiffness to the low strain shear modulus G_0. Under cyclic loading piecewise-linear hysteresis loops are therefore produced with this system as shown in figure 4.2. 10 yield surfaces are used in the nonlinear soil model in all the work presented in this study.

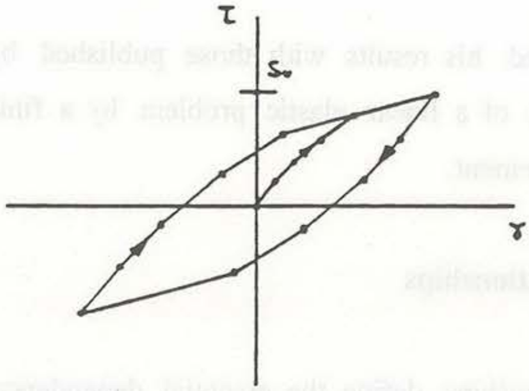

Fig. 4.2 Typical Piecewise-Linear Hysteresis Loops

Thus in three dimensional stress space there is a family of nested yield surfaces, each of which follows the classical approach of plasticity, but whose collective action results in a model capable of following the nonlinear yielding behaviour of continuous systems. Some examples of the behaviour of Iwan's model are displayed in figure 4.3. Diagram (a) represents the distribution of yield surfaces for the virgin material. Diagrams (b) and (c) show a possible loading and unloading curve for the system with kinematic work-hardening. Even though unloading occurs down the initial loading curve a different stress state is produced than is initially seen. The agreement of the system with Masing's criteria is also clear. The shape of the unloading and reloading curves are the same as the initial loading curve except that they are scaled by a factor of two, and the shear modulus upon each loading reversal is the same as the initial tangent modulus of the initial loading curve. Diagram (d) is an example of monotonic loading and shows how the three dimensional stress model can be related to a one dimensional formulation.

As stated earlier the deviatoric stress components in three dimensional stress space are

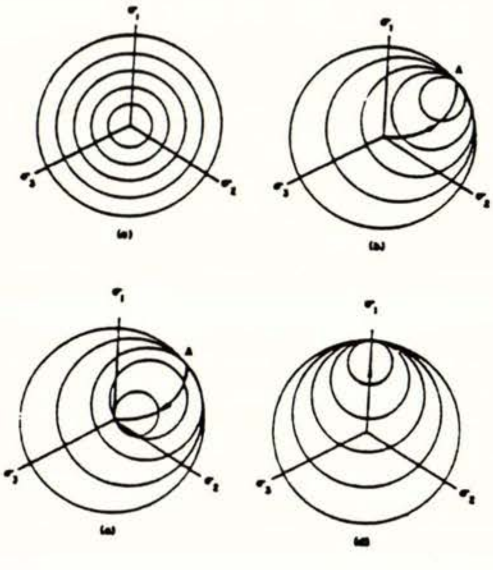

Fig. 4.3 Examples of 3D Yield Surface Behaviour

modelled by the nine components of the stress tensor σ_{ij}. The components of deviatoric strain are also represented by a tensor e_{ij}, and the more commonly used engineering strain vector γ_{xy} is equal to twice this value of tensorial strain.

$$\gamma_{xy} = 2\, e_{ij} \qquad 4.11$$

The deviatoric strain e_{ij} consists of an elastic component e_{Eij} and a plastic component e_{Pij}. The elastic component of the increment in deviatoric strain is given by

$$e_{Eij} = \frac{\sigma_{ij}}{2G_o} \qquad 4.12$$

Iwan (1967) and Joyner (1975) originally formulated the constitutive relationships so that there was a plastic component of the increment in deviatoric strain associated with each yield surface that was yielding, e_{Pnij}. These components were then summed to obtain the total plastic component of the increment in deviatoric strain e_{Pij}. A modification was proposed by Larkin (1985) to this scheme. The plastic component of deviatoric strain is now associated only with the outermost yielding surface, with the yield hardening constants adjusted accordingly. The alteration to the constitutive relationships and the adjustments necessary with the hardening constants will be described later in this section. This approximation is an exact representation of the original scheme unless more than one yield surface is engaged within any one time step. If this is the case then the stiffness of the lower yield surface is used, resulting in an overestimation of the stiffness of the system and the plastic increment in deviatoric stress. Comparisons have been made between the two schemes, and using 10 yield surfaces and a small time step results have been extremely good and have produced computational savings of between 10 and 15 %.

The constitutive relationships relating plastic components of deviatoric stress and strain are as follows:

A family of circular yield surfaces are postulated in three dimensional stress space when viewed down the space diagonal, with each surface represented by the yield function,

$$F_n\,(\sigma_{ij} - \alpha_{nij}) = k_n^2 \qquad 4.13$$

where k_n is a characteristic of the n^{th} yield surface and α_{nij} is the origin of that yield surface in stress space. Regarding k_n as a constant for the circular yield surfaces, differentiating equation 4.13 leads to

$$\frac{\partial F_n}{\partial \sigma_{ij}} = -\frac{\partial F_n}{\partial \alpha_{nij}} \qquad 4.14$$

Prager type linear kinematic work hardening is assumed, thus for any yield surface,

$$d\alpha_{nij} = C_n de_{Pnij} \qquad 4.15$$

where C_n is a hardening constant associated with the n^{th} yield surface.

From Drucker (1956) for work hardening materials the associated flow rule which ensures that the plastic strain increments are normal to the yield surface is

$$de_{Pnij} = L_n h_n \frac{\partial F_n}{\partial \sigma_{ij}} \qquad 4.16$$

where

$$L_n = 0 \quad if \; F_n < k_n^2 \; or \; \frac{\partial F_n}{\partial \sigma_{ij}} d\sigma_{ij} < 0$$

$$L_n = 1 \quad if \; F_n = k_n^2 \; and \; \frac{\partial F_n}{\partial \sigma_{ij}} d\sigma_{ij} \geq 0 \qquad 4.17$$

and h_n will be derived later. The above equation gives the plastic component of the deviatoric strain associated with each yield surface, with the value of L_n being determined depending on whether that yield surface is yielding or not. All n yielding components are then summed. With Larkin's approximation the plastic increment of deviatoric strain is only associated with the outermost yielding surface, and so once this surface has been determined the plastic increment of deviatoric strain is

$$de_{Pij} = h_t \frac{\partial F_t}{\partial \sigma_{ij}} \qquad 4.18$$

where t is the outermost yielding surface.

To derive the constants h_n, first Prager's consistency equation stipulates that loading from one plastic state must lead to another plastic state,

$$F_n \left(\sigma_{ij}, e_{Pnij}, k_n \right) = 0 \qquad 4.19$$

If k_n are constant then the only variables are σ_{ij} and e_{Pnij}, and therefore for a small change in the yield function

$$dF_n = \frac{\partial F_n}{\partial \sigma_{ij}} d\sigma_{ij} + \frac{\partial F_n}{\partial e_{Pnij}} de_{Pnij} = 0 \qquad 4.20$$

Combining this with the flow rule in equation 4.16 gives

$$h_n = - \frac{\dfrac{\partial F_n}{\partial \sigma_{kl}} d\sigma_{kl}}{\dfrac{\partial F_n}{\partial e_{Pnij}} \dfrac{\partial F_n}{\partial \sigma_{ij}}} \qquad 4.21$$

From the linear work hardening rule in equation 4.15, and the derivative of the initial circular yield function in terms of σ_{ij} and α_{ij} in equation 4.14

$$\begin{aligned} \frac{\partial F_n}{\partial e_{Pnij}} &= \frac{\partial F_n}{\partial \alpha_{nij}} \frac{\partial \alpha_{nij}}{\partial e_{Pnij}} \\ &= -\frac{\partial F_n}{\partial \sigma_{ij}} C_n \end{aligned} \qquad 4.22$$

Therefore

$$h_n = \frac{1}{C_n} \frac{\dfrac{\partial F_n}{\partial \sigma_{rs}} d\sigma_{rs}}{\dfrac{\partial F_n}{\partial \sigma_{kl}} \dfrac{\partial F_n}{\partial \sigma_{kl}}} \qquad 4.23$$

where kl denotes summation over all ij components. For the case of Larkin's approximation the method is similar, resulting in an expression for the constant related to the outermost yielding surface

$$h_t = \frac{1}{H_t} \frac{\dfrac{\partial F_t}{\partial \sigma_{rs}} d\sigma_{rs}}{\dfrac{\partial F_t}{\partial \sigma_{kl}} \dfrac{\partial F_t}{\partial \sigma_{kl}}} \qquad 4.24$$

The modified yield hardening constants H_t correspond to the values C_n mentioned earlier in the linear kinematic work-hardening equation, but due to the differences in the two methods they are calculated in a separate manner as will be described later in this section.

Therefore adding the elastic and plastic components of the increment in deviatoric strain,

$$\Delta e_{ij} = \Delta e_{Eij} + \Delta e_{Pij} \qquad 4.25$$

and with the original constitutive relationships

$$\Delta e_{ij} = \frac{\Delta\sigma_{ij}}{2G_o} + \sum_n \Delta e_{Pnij}$$
$$= \frac{\Delta\sigma_{ij}}{2G_o} + \sum_n L_n h_n \frac{\partial F_n}{\partial\sigma_{ij}} \qquad 4.26$$

and with Larkin's approximation

$$\Delta e_{ij} = \frac{\Delta\sigma_{ij}}{2G_o} + h_t \frac{\partial F_t}{\partial\sigma_{ij}} \qquad 4.27$$

with h_n and h_t as previously. The complete description of the increment in deviatoric strain with the approximation used in this study is then

$$\Delta e_{ij} = \frac{\Delta\sigma_{ij}}{2G_o} + \frac{1}{H_t} \frac{\dfrac{\partial F_t}{\partial\sigma_{ij}} \dfrac{\partial F_t}{\partial\sigma_{rs}}}{\dfrac{\partial F_t}{\partial\sigma_{kl}} \dfrac{\partial F_t}{\partial\sigma_{kl}}} \Delta\sigma_{rs} \qquad 4.28$$

For each ij component there are rs contributing terms forming the plastic component of the deviatoric strain. However of the nine components of the stress tensor only three are independent for the PSV solution. From the symmetry of the tensors

$$\sigma_{rs} = \sigma_{sr} \qquad 4.29$$

and from the definition of deviatoric stresses earlier

$$\sigma_{11} + \sigma_{22} + \sigma_{33} = 0 \qquad 4.30$$

Therefore for every ij component the increment in deviatoric strain is,

$$\Delta e_{ij} = \frac{\Delta\sigma_{ij}}{2G_o} + P_{ij11}\Delta\sigma_{11} + P_{ij13}\Delta\sigma_{13} + P_{ij33}\Delta\sigma_{33} \qquad 4.31$$

where

$$P_{ij11} = \frac{\dfrac{\partial F_t}{\partial \sigma_{ij}}\left(\dfrac{\partial F_t}{\partial \sigma_{11}} - \dfrac{\partial F_t}{\partial \sigma_{22}}\right)}{H_t \dfrac{\partial F_t}{\partial \sigma_{kl}}\dfrac{\partial F_t}{\partial \sigma_{kl}}} \qquad 4.32$$

$$P_{ij13} = \frac{\dfrac{\partial F_t}{\partial \sigma_{ij}}\left(\dfrac{\partial F_t}{\partial \sigma_{13}} + \dfrac{\partial F_t}{\partial \sigma_{31}}\right)}{H_t \dfrac{\partial F_t}{\partial \sigma_{kl}}\dfrac{\partial F_t}{\partial \sigma_{kl}}} \qquad 4.33$$

$$P_{ij33} = \frac{\dfrac{\partial F_t}{\partial \sigma_{ij}}\left(\dfrac{\partial F_t}{\partial \sigma_{33}} - \dfrac{\partial F_t}{\partial \sigma_{22}}\right)}{H_t \dfrac{\partial F_t}{\partial \sigma_{kl}}\dfrac{\partial F_t}{\partial \sigma_{kl}}} \qquad 4.34$$

Therefore three simultaneous equations exist relating the independent components of the increments in deviatoric stress and strain. Gaussian elimination is used to obtain the deviatoric stress increments. Both the increments in mean and deviatoric stress have now been calculated, and these are added to the existing values of mean and deviatoric stress from the previous time step. The new values of mean and deviatoric stress are combined to obtain the new values of total stress for each element, and these are then used to calculate the forces acting at every node.

Determination of outermost yielding surface

The Von Mises yield condition is used such that

$$F_n = \tfrac{1}{2}(\sigma_{ij} - \alpha_{nij})(\sigma_{ij} - \alpha_{nij}) \qquad 4.35$$

and

$$\frac{\partial F_n}{\partial \sigma_{ij}} = \sigma_{ij} - \alpha_{nij} \qquad 4.36$$

Comparing this yield condition with that postulated for the family of circular yield surfaces earlier in equation 4.13

$$k_n = \frac{\sigma_{ij} - \alpha_{nij}}{\sqrt{2}} \qquad 4.37$$

and so therefore the values of k_n are equivalent to the initial yield stress in simple shear.

As shown earlier for the determination of L_n in Joyner's routine, to ascertain the outermost yielding surface the value of F_n and the sign of $(\partial F_n/\partial\sigma_{ij})\Delta\sigma_{ij}$ must be found for every yield surface up to the outermost one at each time step. F_n is known, but $\Delta\sigma_{ij}$ is an unknown still to be solved by Gaussian elimination in the current time step. The approximation of using the sign of $(\partial F_n/\partial\sigma_{ij})\Delta\sigma_{ij}$ inherited from the previous time step is used, and the adequacy of this approximation has been checked by Joyner (1975). The outermost yielding surface is therefore determined for every element, and these values are used for the subscript t when calculating the factors H_t and $\partial F_t/\partial\sigma_{ij}$ to obtain the coefficients P_{ijrs}.

Calculation of Partial Derivatives

If during a given time step yielding takes place on the n^{th} surface then the values of the centre of that yield surface α_{nij} change due to the kinematic work-hardening. To ensure that the stress point remains exactly on a yielding surface, the linear work-hardening rule in equation 4.15 is not used in calculating the values of the partial derivatives. Instead consider figure 4.4 below in stress space, where the primed quantities are computed in the current time step, and the unprimed values are inherited from the previous time step,

From geometry it can be seen that

$$\frac{\sigma'_{ij} - \alpha_{nij}}{\left((\sigma'_{kl} - \alpha_{nkl})(\sigma'_{kl} - \alpha_{nkl})\right)^{\frac{1}{2}}} = \frac{\sigma'_{ij} - \alpha'_{nij}}{\sqrt{2}k_n} \qquad 4.38$$

Therefore

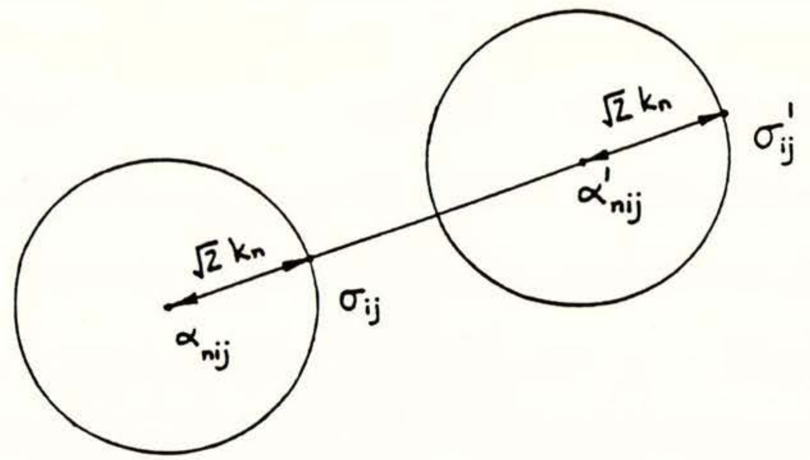

Fig. 4.4 Kinematic Work Hardening in Stress Space

$$\alpha'_{nij} = \sigma'_{ij} - \frac{k_n(\sigma'_{ij} - \alpha_{nij})}{\left(\frac{1}{2}(\sigma'_{kl} - \alpha_{nkl})(\sigma'_{kl} - \alpha_{nkl})\right)^{\frac{1}{2}}} \qquad 4.39$$

From equation 4.36

$$\frac{\partial F_n}{\partial \sigma_{ij}} = \sigma_{ij} - \alpha_{nij} = \sigma'_{ij} - \alpha'_{nij} \qquad 4.40$$

Thus for the outermost yielding surface t

$$\frac{\partial F_t}{\partial \sigma_{ij}} = \frac{k_t\,(\sigma'_{ij} - \alpha_{tij})}{\left(\frac{1}{2}(\sigma'_{kl} - \alpha_{tkl})(\sigma'_{kl} - \alpha_{tkl})\right)^{\frac{1}{2}}} \qquad 4.41$$

and the partial derivatives forming part of the coefficients P_{ijrs} can be calculated. The new values of the centre of the current yield surface in stress space are also calculated with equation 4.39 for use in the following time step.

Determination of the Yield Stresses and Yield Hardening Constants

Iwan (1967) showed that the behaviour of the three dimensional stress system in simple shear is equivalent to the one dimensional model. The distribution of the yield surfaces can be determined from the distribution of the yielding elements in the one dimensional model. An initial loading curve from a state of zero deviatoric stress and strain is assumed, either based on an empirical relationship or on laboratory experiments.

The parameter k_n represents the yield stress in simple shear for the n^{th} yield surface, and a set of values for k_n are chosen to cover the range of stresses likely to be encountered. From the assumed loading curve a set of corresponding shear strain values e_n are calculated. These values k_n and e_n determine the yield hardening constants C_n and H_n used in the deviatoric constitutive relationships. 10 yield surfaces are used in the nonlinear soil model in all the analyses presented in this study. A theoretically unobtainable 11^{th} yield surface is also defined at a level of stress greater than k_{10} and larger than any stress that is expected to occur.

All calculations are carried out in terms of normalised stresses and strains. The stresses are normalised by dividing by the maximum shear strength S_u, and the strains by multiplying by $2G_o/S_u$. The normalised stress-strain relationships have a high stress limit of 1.0 and an initial slope at the origin of 1.0. In the work presented in this study the values of k_n are spread evenly from 0 to 0.9 for k_0 to k_9, with k_{10} of 0.99 and k_{11} of 0.9999.

For the three dimensional system in simple shear the non-vanishing components of stress are σ_{13} and σ_{31}. The earlier equation for Δe_{ij} reduces to

$$\Delta e_{13} = \frac{\Delta \sigma_{13}}{2G_o} + P_{ij13}\, \Delta \sigma_{13} \qquad 4.42$$

Considering the formulations for the partial derivatives derived earlier and recognising only the non-vanishing terms in the summative kl terms, the above equation reduces further to

$$\Delta e_{13} = \left(\frac{1}{2G_o} + \sum_{n=1}^{j} \frac{1}{C_n} \right) \Delta \sigma_{13} \qquad 4.43$$

for Joyner's original routine, and

$$\Delta e_{13} = \left(\frac{1}{2G_o} + \frac{1}{H_t} \right) \Delta \sigma_{13} \qquad 4.44$$

for the approximate hardening method. Reversing the relationship in equation 4.44 gives a recursion relation for evaluating the set of hardening constants H_t.

$$\frac{1}{H_t} = \frac{e_{j+1} - e_j}{k_{j+1} - k_j} - \frac{1}{2G_o} \qquad 4.45$$

All the details concerning the evaluating of the coefficients P_{ijrs} have now been described, and the simultaneous equations relating the increments in deviatoric stress and strain can be solved to obtain the increment in deviatoric stress.

4.2.3 Transmitting Boundary Conditions

In this section the additional forces acting on a boundary node due to the seismic disturbances in the elastic underlying medium are described. The method used to approximate these forces is that developed by Joyner (1975) in the original program. Energy is allowed to radiate back into the elastic half-space from the boundary if the impedance contrast between the soil and the bedrock is finite.

At every boundary node an input velocity V_F is applied which would be the velocity at the boundary if the boundary were a free surface. This source V_F is then approximated by a combination of plane P and S waves normally incident on the boundary, and the actual motion V_i at the boundary is obtained by solving for all the forces acting there.

The coordinate system is rotated to be normal to the individual segment of the boundary. Therefore

$$V'_{Fi} = \beta_{ij} V_{Fj} \qquad 4.46$$

where β_{ij} is the rotation matrix, and $'$ denotes the rotated coordinate system. The axis of rotation is the x_2 axis, giving the components of the rotation matrix

$$\beta_{ij} = \begin{pmatrix} \cos\theta & 0 & -\sin\theta \\ 0 & 1.0 & 0 \\ \sin\theta & 0 & \cos\theta \end{pmatrix} \tag{4.47}$$

where θ is the angle of rotation of the coordinate system.

The motion V_i' at the boundary node is considered to be the sum of incident and reflected compression and shear waves, with

$$\begin{aligned} V_3' &= V_{PI}' + V_{PR}' \\ V_1' &= V_{SVI}' + V_{SVR}' \\ V_2' &= V_{SHI}' + V_{SHR}' \end{aligned} \tag{4.48}$$

Because V_{Fi}' is defined as being on a free surface we have perfect reflection there, and so for the components normal to the segment

$$\begin{aligned} V_{F3}' &= 2\,V_{PI}' \\ V_{F1}' &= 2\,V_{SVI}' \\ V_{F2}' &= 2\,V_{SHI}' \end{aligned} \tag{4.49}$$

With the approximation of plane waves normally incident from the underlying medium, the displacements in the x_3' direction from the wave equation are

$$\begin{aligned} U_{PI}' &= f(x_3' - v_p t) \\ U_{PR}' &= f(x_3' + v_p t) \end{aligned} \tag{4.50}$$

with v_p the compression wave velocity in the underlying medium. From equation 4.7 relating total strain to velocity gradients

$$E_{PI33}' = \frac{\partial U_{PI}'}{\partial x_3'} = \frac{\partial U_{PI}'}{\partial t}\frac{\partial t}{\partial x_3'} = -\frac{V_{PI}'}{v_p} \tag{4.51}$$

and similarly

$$E'_{PR33} = \frac{V'_{PR}}{v_p} \qquad 4.52$$

Assuming an elastic underlying bedrock

$$\begin{aligned} S_{ij} &= (\lambda\,\delta_{ij} + 2G)E_{ij} \\ \therefore\ S_{33} &= (\lambda + 2G)E_{33} \qquad 4.53 \\ &= \rho\, v_p^2\, E_{33} \end{aligned}$$

Therefore

$$\begin{aligned} S'_{P33} &= S'_{PI33} + S'_{PR33} \\ &= \rho v_p(-v'_{PI} + v'_{PR}) \qquad 4.54 \\ &= \rho v_p(v'_3 - v'_{F3}) \end{aligned}$$

For the case of SH and SV waves all the components of stress are in shear, thus,

$$\begin{aligned} S_{ij} &= 2GE_{ij} \qquad for\ \ i \neq j \\ &= \rho v_s^2 E_{ij} \qquad 4.55 \end{aligned}$$

where v_s is the shear wave velocity in the underlying medium.

The total strain components are found as for the case of the compression waves, with the components in shear

$$\begin{aligned} E'_{SVI13} = E'_{SVI31} &= \frac{1}{2}\frac{\partial U'_{SVI}}{\partial x_3} = -\frac{1}{2}\frac{V'_{SVI}}{v_s} \\ E'_{SVR13} = E'_{SVR31} &= \frac{1}{2}\frac{V'_{SVR}}{v_s} \qquad 4.56 \end{aligned}$$

Following a similar method to before

$$S'_{SV13} = S'_{SV31} = \rho v_s(-V'_{SVI} + V'_{SVR}) \qquad 4.57$$

$$= \rho v_s(V'_1 - V_{F1})$$

Similarly

$$S'_{SH23} = S'_{SH32} = \rho v_s(V'_2 - V'_{F2}) \qquad 4.58$$

All other stress components are zero.

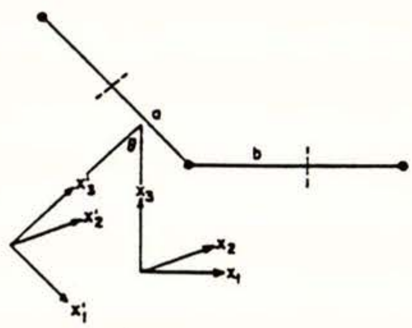

Fig. 4.5 Boundary Segment Configuration

Half the force acting on segment **a** in figure 4.5 is applied to each of the nodes connected to that segment, where ΔS_a is the length of the segment.

$$F'_{a3} = -\frac{1}{2}\rho v_p(V'_3 - V'_{F3})\Delta S_a$$

$$F'_{a1} = -\frac{1}{2}\rho v_s(V'_1 - V'_{F1})\Delta S_a \qquad 4.59$$

$$F'_{a2} = -\frac{1}{2}\rho v_s(V'_2 - V'_{F2})\Delta S_a$$

The forces from segments **a** and **b** seen in figure 4.5 affecting a particular node are then added together and transformed back into the original coordinate system, with both x_1' and x_3' components now influencing each of the x_1 and x_3 components. The x_2 component is unaffected as it is the axis of rotation.

$$F_{ai} + F_{bi} = -A_{ij}(V_j - V_{Fj}) \tag{4.60}$$

The non-zero components of A_{ij} are listed below

$$A_{11} = \tfrac{1}{2}\left(\beta_{11}^{-1}v_s\beta_{11} + \beta_{13}^{-1}v_p\beta_{31}\right)_a \rho\Delta s_a + \tfrac{1}{2}\left(\beta_{11}^{-1}v_s\beta_{11} + \beta_{13}^{-1}v_p\beta_{31}\right)_b \rho\Delta s_b \tag{4.61}$$

$$A_{13} = \tfrac{1}{2}\left(\beta_{11}^{-1}v_s\beta_{13} + \beta_{13}^{-1}v_p\beta_{33}\right)_a \rho\Delta s_a + \tfrac{1}{2}\left(\beta_{11}^{-1}v_s\beta_{13} + \beta_{13}^{-1}v_p\beta_{33}\right)_b \rho\Delta s_b \tag{4.62}$$

$$A_{31} = \tfrac{1}{2}\left(\beta_{31}^{-1}v_s\beta_{11} + \beta_{33}^{-1}v_p\beta_{31}\right)_a \rho\Delta s_a + \tfrac{1}{2}\left(\beta_{31}^{-1}v_s\beta_{11} + \beta_{33}^{-1}v_p\beta_{31}\right)_b \rho\Delta s_b \tag{4.63}$$

$$A_{33} = \tfrac{1}{2}\left(\beta_{31}^{-1}v_s\beta_{13} + \beta_{33}^{-1}v_p\beta_{33}\right)_a \rho\Delta s_a + \tfrac{1}{2}\left(\beta_{31}^{-1}v_s\beta_{13} + \beta_{33}^{-1}v_p\beta_{33}\right)_b \rho\Delta s_b \tag{4.64}$$

$$A_{22} = \tfrac{1}{2}\rho v_s\left(\Delta s_a + \Delta s_b\right) \tag{4.65}$$

All the other forces acting at a particular node F_i are accounted for in the computational scheme

$$F_i + F_{ai} + F_{bi} = \tfrac{m}{\Delta t}(V_i - V_{Pi}) \tag{4.66}$$

where V_{Pi} is the value of V_i from the previous time step.
Re-arranging this

$$F_i = (A_{ij} + \delta_{ij}\tfrac{m}{\Delta t})(V_j - V_{Fj}) + (V_{Fi} - V_{Pi})\tfrac{m}{\Delta t} \tag{4.67}$$

therefore

$$V_i = V_{Fi} + N_{ij}\left(F_j + \left(V_{Pj} - V_{Fj}\right)\tfrac{m}{\Delta t}\right) \tag{4.68}$$

where N_{ij} is the inverse of the matrix $(A_{ij} + \delta_{ij}\ m/\Delta t)$ and δ_{ij} is again the Kronecker delta.

Therefore all nodes on the boundary between the soil and the bedrock are subject to forces in addition to those for an internal node as described above. Otherwise boundary nodes are treated as described earlier in section 4.2.1.

Accuracy

For each solution space to produce an accurate solution, the resolution of the two dimensional mesh has to be such that the smallest wavelength to be modelled is represented reliably. For both solutions the shear waves propagating throughout the mesh have the shortest wavelengths, so the resolution of the mesh is controlled by these waves. The shortest wavelength is

$$\lambda_{MIN} = \frac{v_{s_{MIN}}}{f_{MAX}} \tag{4.69}$$

where Vs_{MIN} is the lowest value of the shear velocity of the soil in the analysis and f_{MAX} is the highest frequency to be modelled. For the nonlinear analysis some estimate of Vs_{MIN} must be made, for example half the value of the low strain Vs_{MAX}. Once the shortest wavelength has been determined the maximum nodal spacing is set to ensure a fixed number of nodes per wavelength. Ten nodes per wavelength is a common criteria, but five may be acceptable. The final recommendation for the nodal spacing Δx is therefore

$$\Delta x_{MAX} = \frac{v_{s_{MIN}}}{10 \cdot f_{MAX}} \tag{4.70}$$

Stability

Once the nodal spacing has been determined the maximum time step used in the analysis is limited to ensure stability. If this condition is violated the solution will become unstable. For the PSV solution from Alterman and Lowenthal (1972) for square elements and the linear elastic case

$$\Delta t \leq \frac{\Delta x_{MIN}}{v_p\left(1 + \left(\frac{v_s}{v_p}\right)^2\right)^{\frac{1}{2}}} \qquad 4.71$$

These conditions are derived for the linear elastic case and do not guarantee stability in the nonlinear analysis. However from experience these elastic criteria are a good guideline, and if approximately half their value is used for the time step used in the analysis the solution has always been found to converge.

Joyner (1977) discusses the possible need to filter numerical noise generated at frequencies in the vicinity of 1/4 Δt. However with the time steps used in all the analyses presented in this study the frequencies of this noise are greater than 100 Hz, and therefore are beyond consideration. No filtering is applied for this reason.

4.3 ONE DIMENSIONAL SOLUTION

4.3.1 Basic Computational Scheme

The major component of earthquake motion influencing the response of soil deposits in one dimension is the vertical propagation of shear waves through the body of the soil, thus creating an alternate cyclic shearing stress condition. Shear wave propagation is assumed vertical due to the continued refraction of the waves as they travel from the usually deep source. Equations of motion may therefore be derived for vertical propagation of shear waves. Considering the element shown in figure 4.6, the deformation of this element may be described by

$$\frac{\partial u}{\partial z} = \gamma \qquad 4.72$$

where γ is the shear strain

u is the horizontal displacement of the particles

Taking the time derivative yields

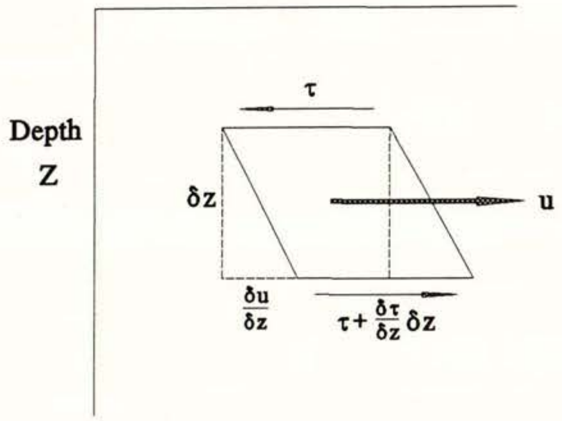

Fig. 4.6 A typical soil element

$$\frac{\partial}{\partial t}\left(\frac{\partial u}{\partial z}\right) = \frac{\partial \gamma}{\partial t}$$

$$\frac{\partial \dot{u}}{\partial z} = \frac{\partial \gamma}{\partial t} \qquad 4.73$$

which is a differential equation describing the changing shear strain throughout the soil layer.

From figure 4.6, the sum of forces in the horizontal direction is

$$(\tau + \frac{\partial \tau}{\partial z}dz) - \tau = 0 \qquad 4.74$$

where τ is the shear stress

From Newton's 2nd law

$$\frac{\partial \tau}{\partial z}dz = m\frac{\partial^2 u}{\partial t^2} \qquad 4.75$$

As a one dimensional case, the volume of the element may be given by dz and therefore Thus the two differential equations (4.73 and 4.76) fully describe vertical wave propagation in a one dimensional situation.

$$\frac{\partial \tau}{\partial z} = \rho \frac{\partial^2 u}{\partial t^2} \qquad 4.76$$

Solution of the Shear Wave Propagation Equations

The wave equations may be solved in coupled form numerically using an explicit finite difference representation. The equations are written in discrete form and a solution is computed at discrete points in time and space.

4.3.2 The Constitutive Relationship

For a non linear dynamic analysis an appropriate constitutive relationship is required. It has been shown by Martin et al. (1979) and Larkin and Donovan (1979) that the most important factor in the modelling of soils is the form of this relationship, therefore accurate modelling is important. The general three dimensional constitutive relationship detailed in section 4.2.2 may be simplified to one dimension, and is the form used here. This is outlined in some detail below.

The Elastoplastic Element

The basic component of the model is the linear elastoplastic element, which may be represented as a combination of a linear spring and Coulomb resistor, as shown in figure 4.7.

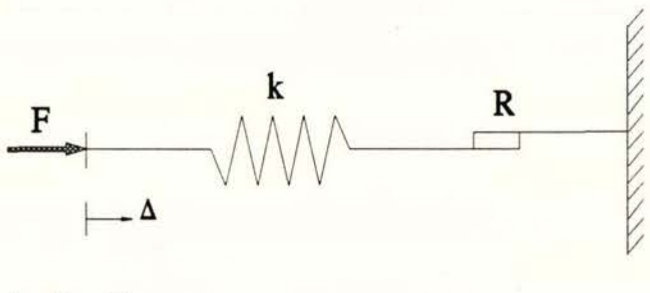

Fig. 4.7 Basic Elastoplastic Element

An element has two parameters describing its response: a spring stiffness k and a

Coulomb resistance R. An individual element has a linear response up to its Coulomb resistance (or yield limit) which is given by

$$F = k\Delta \tag{4.77}$$

where Δ = displacement of spring
and $F < R$

When the force on the element reaches the yield limit (R), it becomes fully plastic and remains at a constant state of stress.

There is no energy loss from the element until the yield stress is reached, as up until this point it is a totally elastic response. At the yield displacement and beyond however, the element responds plastically and strain energy absorbed is not recoverable, and hence lost to the system. This represents strain dependent damping known as hysteretic damping. Therefore the physical damping of a soil is inherently modelled by an element without the need for an extra damping term.

Modelling the Constitutive Relationship

As in the two dimensional program an array of these elastoplastic elements arranged in either series (Iwan) or parallel (Taylor and Larkin) may be used to model the initial loading curve, and from this the complete hysteresis loop. The parallel model gives stresses as a function of strain which is useful in dynamic analyses as deformations are normally taken as the independent variable. A parallel array is used in this study (figure 4.8) and shall be described in detail. Similar numbers of elements are used to describe an initial loading curve as in the two dimensional system.

Each element undergoes the same deformation but has a different stiffness and yield limit, thus each element yields at a different stress point in the loading. As the deformation increases and individual elements yield in turn, the combined stiffness of the system decreases as the yielded elements no longer contribute to the system and remain at constant stress. Hence there are less elements contributing to the overall stiffness of the system and the modulus correspondingly decreases. In this manner the initial loading

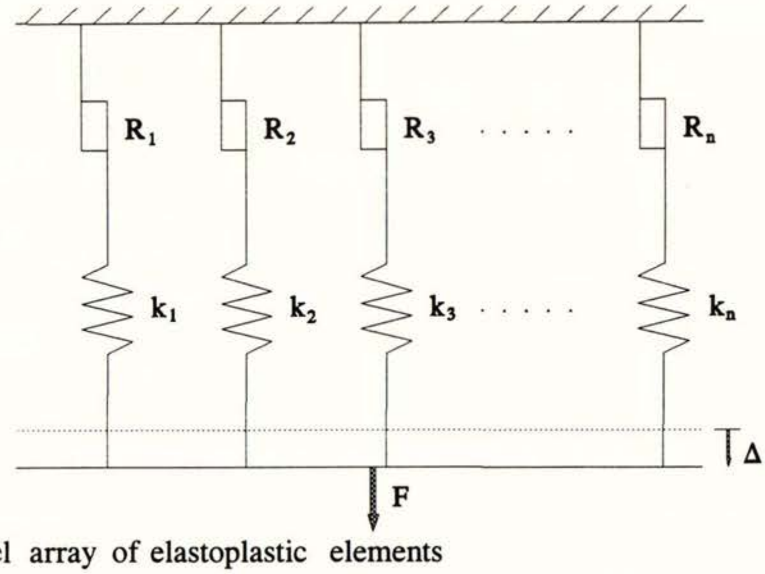

Fig. 4.8 Parallel array of elastoplastic elements

curve may be built up as a piecewise linear approximation by selecting the appropriate element parameters. Figure 4.9 shows this method of approximation to an initial loading curve (where $k_T = \Sigma k_n = G_{max}$).

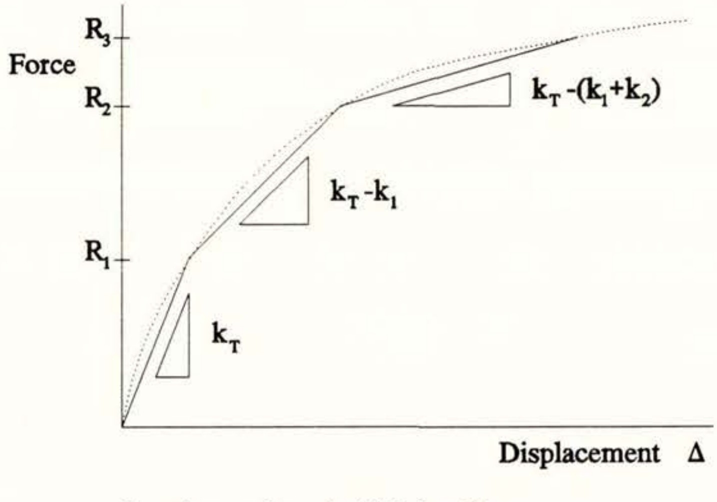

Fig. 4.9 Piecewise approximation of an initial loading curve

Initially the modulus is at a maximum as all n elements are in their elastic state. The response of the whole system at this point is

$$F = \sum_{j=1}^{n} k_j \Delta \tag{4.78}$$

where k_j is the individual stiffness of each element

Δ is the displacement of the overall system

This is valid until the first element reaches its yield stress (R_1), at which point the response of the system is made up of 2 separate quantities:

1) Sum of the forces in the unyielded elements
2) Sum of the constant forces in the yielded elements

The response of the system may then be given by

$$F = \sum_{j=1}^{m} R_j + \sum_{m+1}^{n} k_j \Delta \qquad 4.79$$

where m is the number of elements that have yielded

When the direction of deformation is reversed (caused by a load reversal), each element becomes fully elastic again and the modulus returns to its maximum value. This conforms to the first of Masing's criteria. The response of the system is then similar to that of the initial loading phase with the exception that it is scaled up by a factor of two in accordance with Masing's 2nd criteria.

Calculation of Element Parameters

Each individual element has two parameters, k and R that must be calculated to match the model to the properties of the soil under investigation. These properties are usually obtained experimentally. The parameters may be calculated directly from the initial loading curve or from the relationship between secant shear modulus G and shear strain amplitude γ. If experimental data is not available more general empirical relationships of the form shown in figures 4.10 and 4.11 may be used. Based on a wide range of experimental data, empirical normalized modulus versus shear strain curves have been developed for both cohesive and non cohesive soils. Originally developed by Seed and Idriss (1970), updated curves have been produced by Sun et al. (1988) for cohesive soils and Seed et al. (1984b) for cohesionless soils. These are shown in figures 4.10 and 4.11 respectively.

Vucetic and Dobry (1991) have also presented similar curves for cohesive soils. The

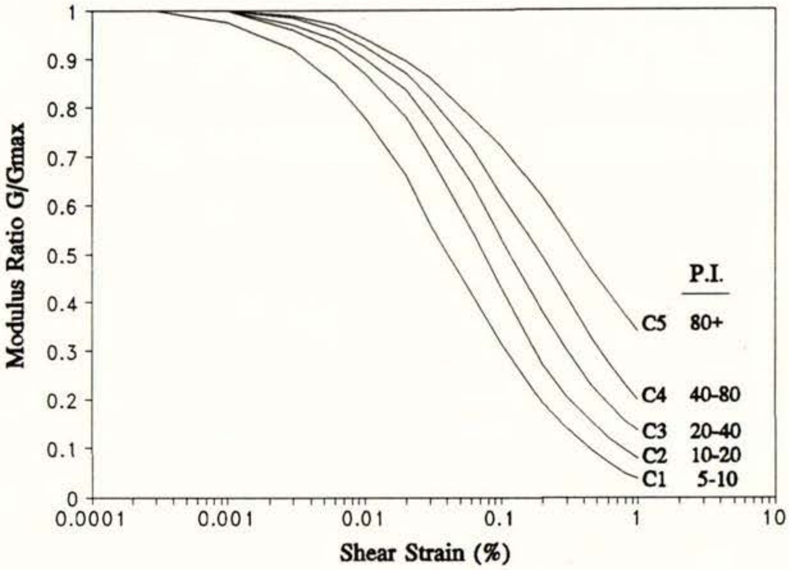

Fig 4.10 Normalized moduli curves for cohesive soils (from Sun et al. 1988)

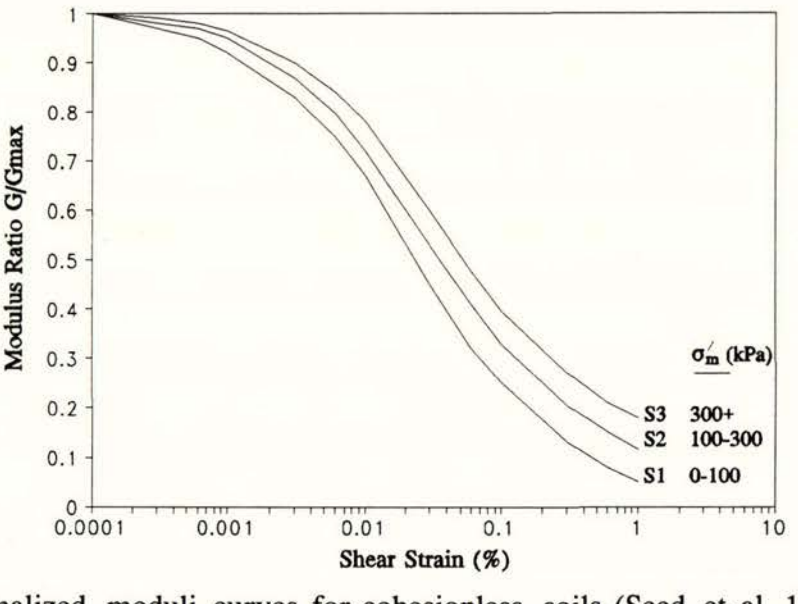

Fig 4.11 Normalized moduli curves for cohesionless soils (Seed et al. 1984b)

dynamic properties of cohesive soils have been found to be a function primarily of plasticity index, hence the different curves for different plasticity ranges. Dynamic properties of non cohesive soils have been found to be a function of the level of mean effective confining stress.

Such curves may be used to represent dynamic soil properties when experimentally determined data is not available. These may then be used to calculate the parameters of the multi linear model by the following method.

For a single element, the displacement at yield (δ_y) may be given by

$$\delta_y = \frac{R}{k} \tag{4.80}$$

where R is the yield limit

The effective secant modulus of the element (k_{eff}) for a displacement in the plastic state ($\delta > \delta_y$) is then

$$k_{eff} = \frac{R}{\delta} = \frac{\delta_y k}{\delta} \tag{4.81}$$

For n elastoplastic elements arranged in parallel, the effective stiffness is the summation of all the elemental stiffnesses. If δ_{yi} is the displacement of the ith element at the point of yield then

$$\begin{aligned} k_{eff} &= \sum_{j=1}^{i-1} \frac{R_j}{\delta} + \sum_{j=i}^{n} k_j \\ &= \frac{1}{\delta_{yi}} \sum_{j=1}^{i-1} \delta_{yj} k_j + \sum_{j=i}^{n} k_j \end{aligned} \tag{4.82}$$

Now for all n elements, a system of n linear simultaneous equations may be generated as follows

$$\begin{array}{cccccc} k_1 & + k_2 & + \dots & & + k_n & = \overline{G}_1 \\ \cdot & \cdot & & & \cdot & \cdot \\ \cdot & \cdot & & & \cdot & \cdot \\ \dfrac{\gamma_1}{\gamma_i} k_1 & + \dfrac{\gamma_2}{\gamma_i} k_2 & + \dots & & + k_n & = \overline{G}_i \end{array} \tag{4.83}$$

By substituting in values of G and γ from experimental or empirical results, the system can be put in the matrix form

$$[A][k] = [\overline{G}] \tag{4.84}$$

and solved for [k]

The coulomb resistances of each element R_i may then be found from

$$R_i = \gamma_{yi} k_i \qquad 4.85$$

thus defining all the parameters required.

The computer program MOGEN (Larkin 1978a) may be used to calculate the element parameters using the above procedure.

4.3.3 Loading History

The previous loading history of a soil influences its behaviour by either increasing or decreasing the shear modulus through hardening or softening. In dry soils (particularly sands) the cyclic shear loading leads to slip at grain contact points resulting in a volumetric compaction, the extent of which is dependent on the original density. This increase in density and creation of more stable grain to grain contact points increases the soil's resistance to shear deformations, and hence the modulus increases. This process is known as strain hardening. For an undrained saturated sand the same grain slip is assumed to occur but not the associated volume change. This potential volume change is counterbalanced by the expansion of the sand skeleton with reducing effective stress (chapter five).

It is difficult to apportion the hardening effect between grain slip and volume compaction, but Finn et. al (1975) suggests the creation of more stable grain contact points is the dominant factor. It is therefore concluded that as grain slip occurs in undrained shear, strain hardening must also occur.

Experimental studies of cyclic loading on sands have provided results in the form of figure 4.12, indicating hardening to be a function of shear strain magnitude and the previous volumetric strain (ϵ_{vd}). Volumetric strain may be considered as a representation of previous strain history.

It can be seen from figure 4.12 that the increase in modulus is proportional to the original modulus, and is a function of previous volumetric strain. Larkin (1977) proposed the expression

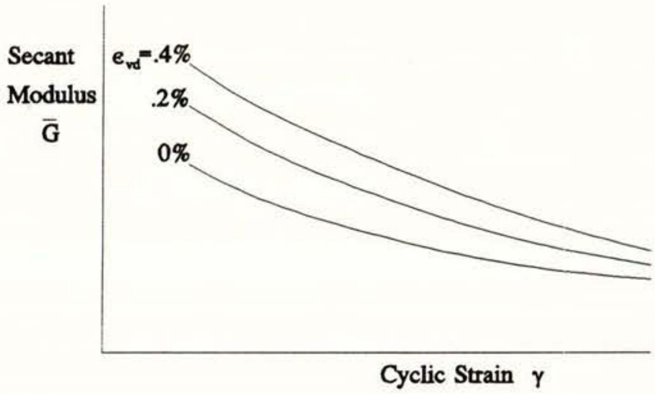

Fig. 4.12 Strain hardening influence on shear modulus for sands

$$G = G_o(1 + a\epsilon_{vd} + b\epsilon_{vd}^2) \tag{4.86}$$

where G_o is the original modulus

ϵ_{vd} is the volumetric strain

a,b are experimentally determined constants

to describe this behaviour. Finn et al. (1975) observed experimentally that the bulk of volume change for a dry sand (and hence grain slip and hardening) occurs on the unloading phases of the loading cycle. Therefore corrections to the constitutive relationship for these effects are made only on these phases of the loading cycle.

The extent of strain softening in clays (degradation) is less understood and has been less studied than for sands. The dynamic properties of clays under cyclic loading is of less concern with respect to liquefaction studies, and most research has been directed into other areas. No useable model has been developed to account for strain softening in clays, and is therefore ignored.

Chapter Five

Pore Pressure Models

5.1 INTRODUCTION

The second component of a non linear effective stress analysis is the calculation of the generation and dissipation of excess pore pressures during earthquake loading (effective stress). The extent to which excess pore pressure is generated depends on the characteristics of the soil and the severity of the cyclic loading. Saturated sands and silts are significantly more susceptible than clays or partially saturated sands.

The pore pressure generation model detailed in this chapter is based on the fundamental work of Martin et al. (1975), and the later advancement by Byrne (1991). From this point forward, the combined model shall be referred to as the "MB Model". It is incorporated into both the one and two dimensional analyses presented in this study. The stress controlled pore pressure model implemented by O'Halloran (1986) is also presented as it was incorporated into the two dimensional program by the author for use in the comparative studies presented in chapter eight.

5.2 PORE PRESSURE GENERATION IN SANDS- (MB MODEL)

Cyclic loading of dry sands tends to cause densification and leads to a vertical one dimensional volume change called the volumetric strain (ϵ_{vd}). This also occurs in drained tests on saturated sands where the sand is sufficiently permeable for the water to drain from the reduced void spaces. If the same loading was applied under undrained conditions it is reasonable to assume from experimental data that similar intergranular slip would occur, resulting in similar volumetric strains. As the water in the void spaces is unable to escape, this strain results in an increase in stress on the pore water. As the total stress is constant there is a reduction in the effective stress acting on the sand skeleton. This reduction in vertical effective stress causes the sand skeleton to expand elastically, and the associated recoverable volumetric expansion strain per load cycle is

$$\Delta\epsilon_{vr} = \frac{\Delta\sigma_v^{\prime}}{\bar{E}_r} \qquad 5.1$$

where $\Delta\sigma_v^{\prime}$ is the reduction in vertical effective stress per load cycle

$\Delta\epsilon_{vr}$ is the elastic recoverable volumetric strain increase per load cycle

E_r is the rebound modulus

As the pore water is assumed incompressible compared to the sand skeleton, there is no change in the total volume of the sand. The volume decrease of the voids due to loading must therefore equal the volume increase from the elastic rebound of the soil skeleton

$$\Delta\epsilon_{vd} = \Delta\epsilon_{vr} \qquad 5.2$$

The change in vertical effective stress required to maintain constant volume is therefore

$$\Delta\sigma_v^{\prime} = \bar{E}_r\Delta\epsilon_{vd} \qquad 5.3$$

where $\Delta\epsilon_{vd}$ is the volumetric strain increment per load cycle

With constant total stress, the decrease in effective stress must equal the increase in pore pressure and therefore equation 5.3 becomes

$$\Delta u = \bar{E}_r\Delta\epsilon_{vd} \qquad 5.4$$

where Δu is the increase in pore pressure per load cycle

This mechanism may be seen schematically in figure 5.1

The above explanation is the basis for the MB model for calculating pore pressure increases per load cycle, with an extended expression being given for an incompletely saturated case as well. The above theory is based on the case of a sand that densifies under cyclic loading. This is the case for most sands but very dense sands will tend to dilate which will cause a negative pore pressure and a resulting increase in effective stress. In this case the mechanism is the same except in the opposite sense and therefore has the opposite sign. The use of this model requires expressions for the calculation of the rebound modulus and volumetric strain per cycle for a specific sand.

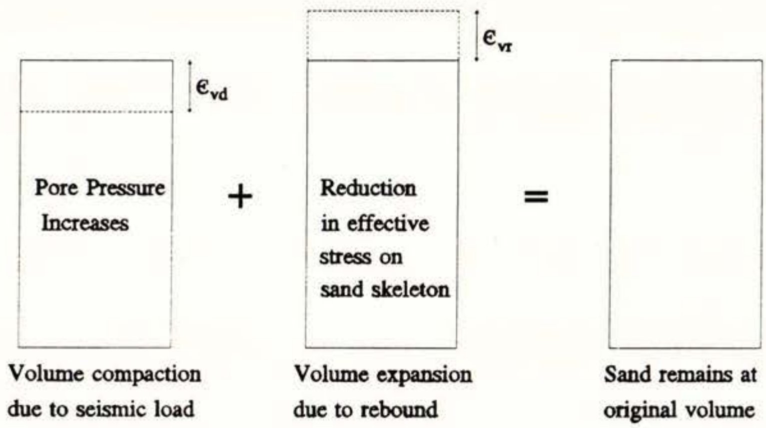

Fig. 5.1 Illustration of the mechanism of pore pressure generation

5.2.1 Rebound Modulus

The one dimensional tangent rebound modulus (E_r) defines the relationship between the change in vertical effective stress and the associated change in vertical elastic strain. Hendron (1963) studied the one dimensional loading and unloading of sands and concluded the vertical strain upon loading may be split into two types:

1) A non recoverable plastic strain that occurs because of slip at grain to grain contact points
2) A recoverable elastic strain that results from elastic deformations at grain contact points

Upon vertical unloading due to reducing effective stress levels, the elastic component of the vertical strain rebounds. This behaviour may be seen schematically in figure 5.2.

The pore pressure generation model requires a rebound modulus for a range of vertical effective stress values during unloading. Experimentally obtained unloading data has produced curves of the form shown in figure 5.3 for different initial unloading stresses. An experimental unloading curve may be approximated by the expression

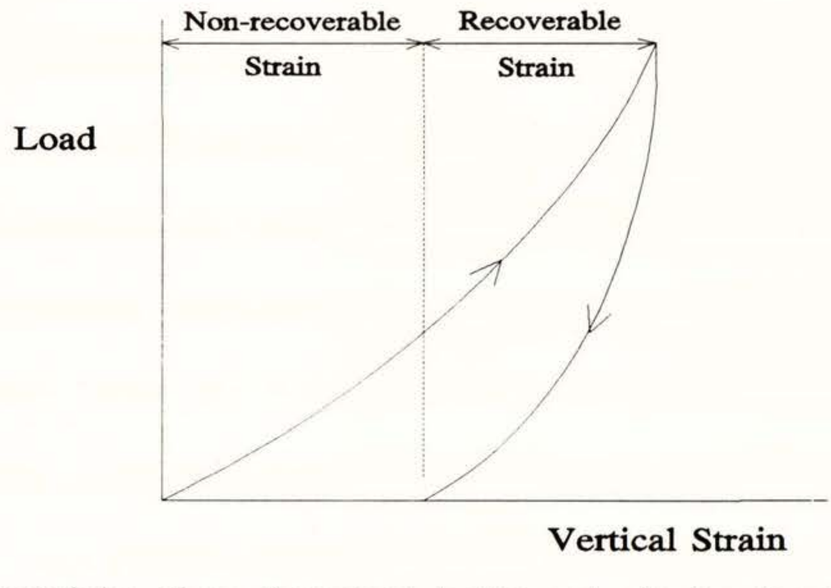

Fig. 5.2 Characteristics of one dimensional loading and unloading for sands

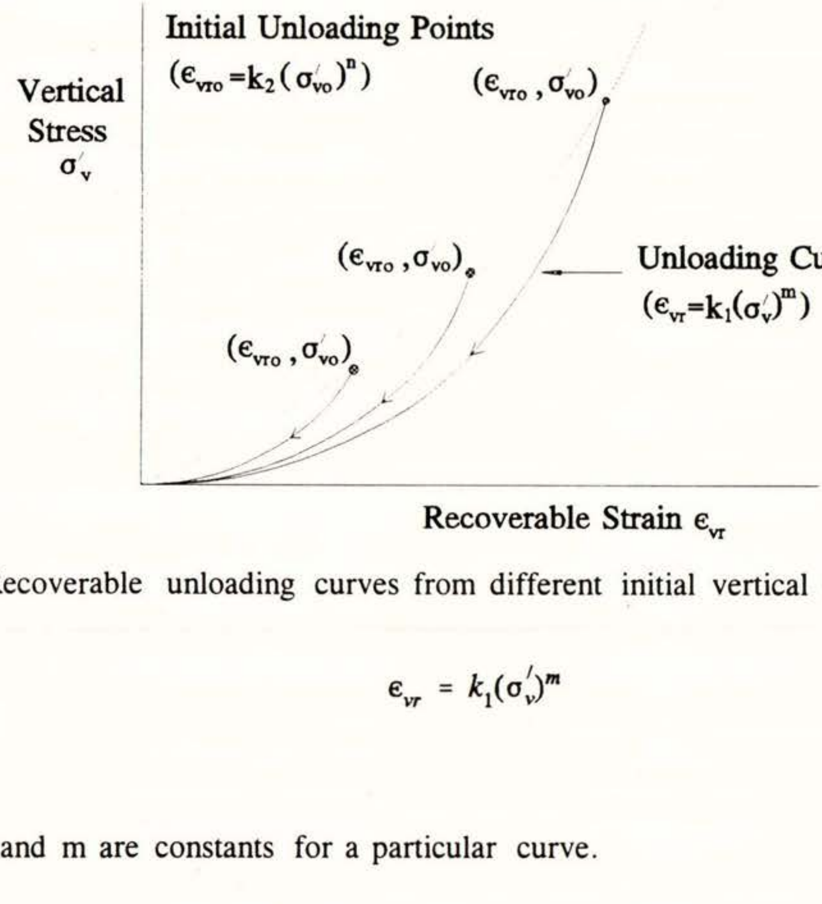

Fig. 5.3 Recoverable unloading curves from different initial vertical stresses

$$\epsilon_{vr} = k_1(\sigma'_v)^m \qquad 5.5$$

where k_1 and m are constants for a particular curve.

Unloading curves from various initial effective stresses σ_{vo} have been found to be geometrically similar and hence may be related by the expression

$$\frac{\epsilon_{vr}}{\epsilon_{vro}} = \left(\frac{\sigma_v'}{\sigma_{vo}'}\right)^m \tag{5.6}$$

where ϵ_{vro} is the recoverable strain at the initial effective stress σ_{vo}.

The initial recoverable strains may be related to the initial vertical stresses by the expression

$$\epsilon_{vro} = k_2(\sigma_{vo}')^n \tag{5.7}$$

Hence a general expression for all unloading curves may be written as

$$\begin{aligned} \epsilon_{vr} &= \epsilon_{vro}\left(\frac{\sigma_v'}{\sigma_{vo}'}\right)^m \\ &= k_2(\sigma_{vo}')^n\left(\frac{\sigma_v'}{\sigma_{vo}'}\right)^m \\ &= k_2(\sigma_{vo}')^{n-m}(\sigma_v')^m \end{aligned} \tag{5.8}$$

The tangent rebound/unloading modulus is the slope of the unloading line, given by

$$\begin{aligned} \bar{E}_r &= \frac{d\sigma_v'}{d\epsilon_{vr}} \\ &= \frac{(\sigma_v')^{1-m}}{mk_2(\sigma_{vo}')^{n-m}} \end{aligned} \tag{5.9}$$

where m,n,k_2 are experimentally determined constants for a specific sand

Equation 5.9 gives an analytical expression for the rebound modulus that is only a function of the vertical effective stress, and is the expression of Martin et al. (1975).

5.2.2 Volumetric Strain

The second component in the pore pressure model is the calculation of the one dimensional volumetric strain per load cycle ($\Delta \epsilon_{vd}$) for a sand under cyclic shear loading.

Experimental strain controlled cyclic loading tests on a dry sand of particular density has produced data of the form shown in figure 5.4.

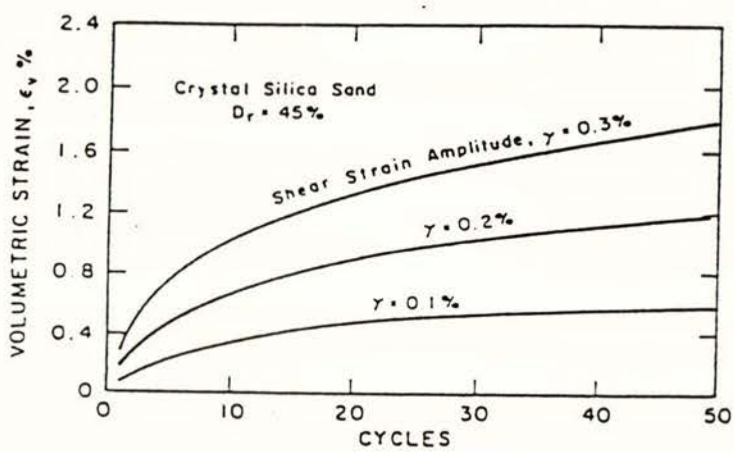

Fig. 5.4 Volumetric strains for constant strain amplitude tests (from Martin et al. 1975)

Experimentally it has been shown for a constant number of load cycles, the volumetric strain is proportional to the amplitude of the applied shear strain. The volumetric strain curves for different shear strain amplitudes may therefore be determined from the results of a single test.

Figure 5.4 shows that the volumetric strain increases with strain amplitude, but the rate of increase decreases with the number of loading cycles. Martin et al. (1975) replotted the data from figure 5.4 in the form shown in figure 5.5, thus determining the volumetric strain increment per load cycle ($\Delta\epsilon_{vd}$) to be a function of both the shear strain amplitude (γ) and the accumulated volumetric strain (ϵ_{vd}).

From the data in this form, the following expression was obtained

$$\Delta\epsilon_{vd} = C_1(\gamma - C_2\epsilon_{vd}) + \frac{C_3(\epsilon_{vd})^2}{\gamma + C_4\epsilon_{vd}} \qquad 5.10$$

where C_1-C_4 are experimentally determined constants for a specific sand

Byrne (1991) suggests this expression may not be stable for all situations, and has derived a different expression. Replotting the original data from figure 5.4 in the form of the

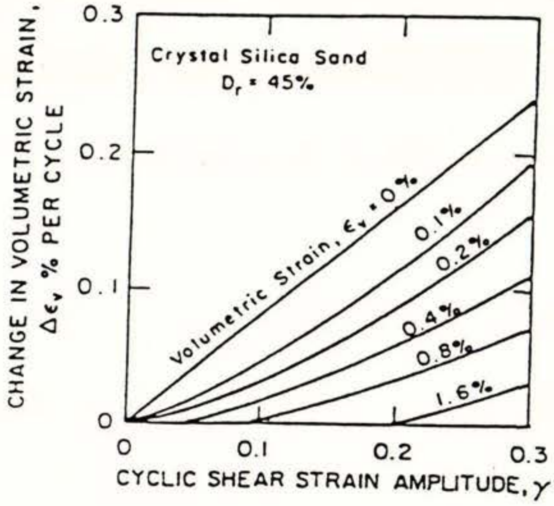

Fig. 5.5 Incremental volumetric strain curve from data in fig 5.4

incremental volume strain versus the accumulated volumetric strain produces curves shown in figure 5.6

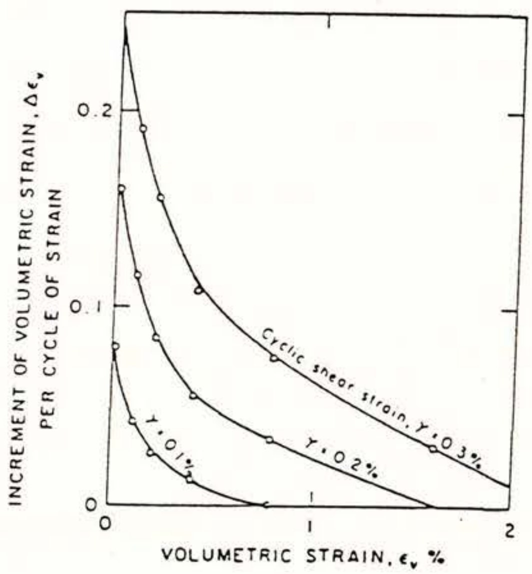

Fig. 5.6 Alternate volumetric strain curves for data from figure 5.4

If both axes are normalized by the shear strain, the data collapses to a single curve shown in figure 5.7, due to the result that ϵ_{vd} and hence $\Delta\epsilon_{vd}$ are proportional to the applied shear strain amplitude.

Byrne suggests the curve of figure 5.7 may be represented by the expression

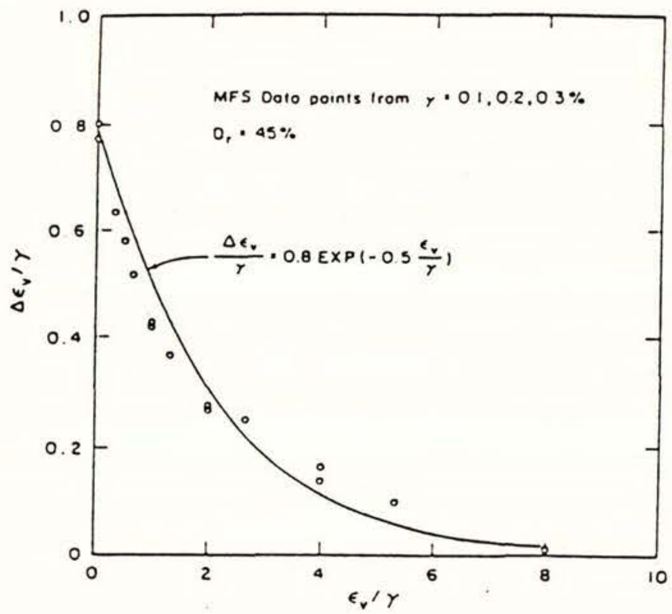

Fig. 5.7 Normalized volumetric strain curves (from Byrne 1991)

$$\frac{\Delta\epsilon_{vd}}{\gamma} = B_1 \ \exp(-B_2(\frac{\epsilon_{vd}}{\gamma})) \qquad 5.11$$

where B_1 and B_2 are constants for the sand

This expression has the advantage over the Martin et al. expression in that there are now only two constants that must be determined instead of four. The shape of the curve of figure 5.7 is also independent of the relative density of sand which is not the case for the alternative. Byrne has proposed simple correlations with normalized SPT values and relative density for the calculation of the two constants, thus not requiring experimental simple shear tests for their determination.

The above expressions completely define models for pore pressure generation.

5.3 PORE PRESSURE DISSIPATION IN SANDS

5.3.1 One Dimensional Analysis

Saturated sand layers dissipate excess pore pressures by drainage, or redistribution if drainage is not possible. This process occurs simultaneously and in opposition to pore pressure generation. The excess pore pressures are redistributed from areas of high to low pressure within the sand. Dissipation retards the rate of pore pressure generation within sands, particularly in the case of long duration motion and high permeability sands. An expression to describe this behaviour is therefore required.

Consider the element shown in figure 5.8.

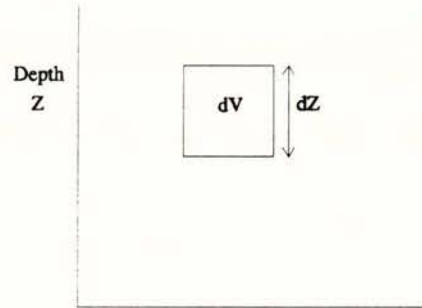

Fig. 5.8 Elemental Volume within a soil deposit

In a one dimensional situation it is assumed all water flow takes place vertically and obeys Darcy's law.

The volume change of the element in the time interval dt may be given by

$$\Delta V = \frac{\partial \epsilon}{\partial t} dtdz \qquad 5.12$$

where ϵ is the vertical strain (compression positive)

This volume change of the element can only occur by water entering or leaving the element in the same time interval dt. The net volume of water entering or leaving ΔQ may be given as

$$\Delta Q = \frac{\partial \dot{v}}{\partial z} dzdt \qquad 5.13$$

where v is the pore water velocity

From continuity, the net volume of water entering or leaving the element must equal the net volume change of the element, assuming the water to be incompressible. Therefore ΔV must equal ΔQ. Darcy's law states

$$\dot{v} = -K\frac{\partial H}{\partial z} \tag{5.14}$$

where k is the permeability, and

$$H = \frac{p}{\gamma_w}+z \tag{5.15}$$

where γ_w is the unit weight of water

p is the excess pore pressure

Therefore

$$\dot{v} = -(\frac{k}{\gamma_w}\frac{\partial p}{\partial z}) \tag{5.16}$$

From continuity (equating 5.14 and 5.15)

$$\frac{\partial \epsilon}{\partial t} = \frac{\partial \dot{v}}{\partial z} = -\frac{\partial}{\partial z}(\frac{k}{\gamma_w}\frac{\partial p}{\partial z}) \tag{5.17}$$

The net change in pore pressure is the difference between the generation from seismic loading and the reduction from diffusion. This may be given by

$$dp = dp_d + dp_s \tag{5.18}$$

where d_d is the reduction due to diffusion

d_s is the increase due to seismic loading

The theory for predicting increases in pore pressure is associated with conditions of constant volume. Vertical strains and associated volume changes are therefore only associated with the migration of pore water to or from the elemental volume. The change in effective stress due to volume change from diffusion may be given by

$$d\sigma_d^{/} = \bar{E}_r d\epsilon = -dp_d \tag{5.19}$$

where E_r is the Tangent Rebound Modulus

As the total volume remains constant, the recoverable deformation of the sand skeleton due to a change in effective stress must equal the volume change due to the net entering or leaving of the pore water. In the time interval dt and from the above equation

$$\frac{\partial \epsilon}{\partial t} = -\frac{1}{\bar{E}_r}\frac{\partial p_d}{\partial t} \tag{5.20}$$

As $\delta p_d = \delta p - \delta p_s$

$$\frac{\partial \epsilon}{\partial t} = -\frac{1}{\bar{E}_r}\left(\frac{\partial p}{\partial t} - \frac{\partial p_s}{\partial t}\right) \tag{5.21}$$

Equating equations 5.17 and 5.21 for $\delta\epsilon/\delta t$ gives

$$\frac{\partial p}{\partial t} = \bar{E}_r \frac{\partial}{\partial z}\left(\frac{k}{\gamma_w}\frac{\partial p}{\partial z}\right) + \frac{\partial p_s}{\partial t} \tag{5.22}$$

From previously, $\Delta u = E_r \Delta \epsilon_{vd}$ and therefore

$$\frac{\partial p}{\partial t} = \bar{E}_r \frac{\partial}{\partial z}\left(\frac{k}{\gamma_w}\frac{\partial p}{\partial z}\right) + \bar{E}_r \frac{\partial \epsilon_{vd}}{\partial t} \tag{5.23}$$

This equation is a one-dimensional parabolic diffusion equation incorporating pore pressure generation as a source term. Thus equation 5.23 fully describes the pore pressure generation and dissipation within the sand, and is used in this form in this study.

Solution of the One Dimensional Diffusion Equation

The diffusion equation may be solved numerically using an implicit finite difference scheme which allows solution as a system of linear equations in matrix form. The solution is therefore unconditionally stable.

5.3.2 Two Dimensional Analysis

The two dimensional pore pressure dissipation solution is not accounted for in this study, but is the subject future work. As a result the two dimensional effective stress analyses presented in this study may be considered as undrained behaviour.

5.4 SHEAR STRESS CONTROLLED PORE PRESSURE MODEL

The following passage outlines the theory of the stress controlled pore pressure model used by O'Halloran (1986) and implemented in the comparative study of chapter eight. Experimentally (section 3.4) it has been found that strain levels are the governing factor in the pore pressure response of sands, but shear stress control may be used as an alternative in a numerical analysis.

The octahedral shear stress is used to govern the level of pore pressure generation, which is stated in equation 5.24

$$\tau_{oct} = 1/3((S_{11}-S_{33})^2 + (S_{33}-S_{22})^2 + (S_{11}-S_{22})^2 + 6S_{13}^2)^{0.5} \qquad 5.24$$

where S is the value of deviatoric stress

The peak value of octahedral shear stress is recorded for every half cycle of loading, which is then used to calculate the increment in pore pressure for that particular half cycle. An alternative to using the octahedral stress is the horizontal shear stress (τ_{31}) induced at every half cycle. From previous sections it is clear that the permanent pore pressure generation is a function of the horizontal shear stress/strain, and transient pore pressures from volumetric/compressional loading are not permanent. As a result, for this study the horizontal shear stress was taken as the independent variable rather than the octahedral shear stress that O'Halloran used. This assumption allows a more direct comparison between the shear strain (section 5.2) and shear stress models. It also allows access to the database of shear stress ratio versus blow count data (figure 3.4) for numerical investigations of liquefaction potential.

From a liquefaction curve of the form shown in figure 5.9 (which may be determined experimentally or empirically), a value for the equivalent number of loading cycles to initiate liquefaction corresponding to the value of the peak shear stress may found.

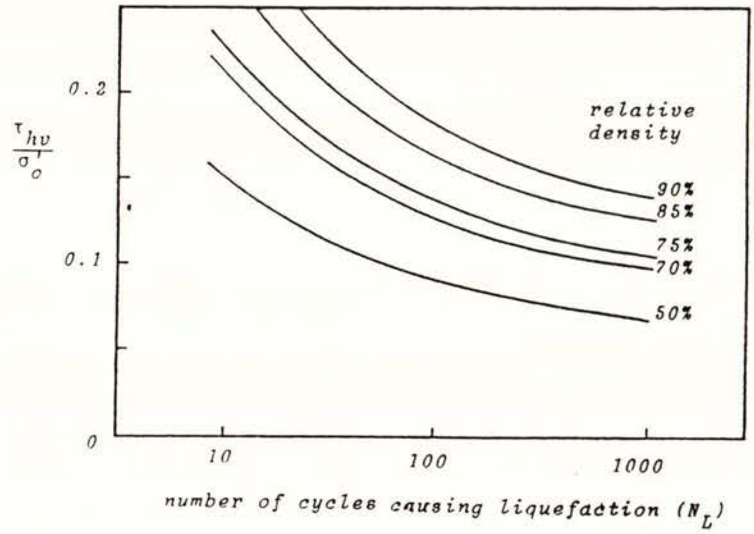

Fig. 5.9 Typical form of a liquefaction strength curve

The increment in cyclic ratio corresponding to that level of induced stress for the half cycle may be found from equation 5.25

$$\Delta R_N = \frac{1}{2}\frac{1}{N_L} \qquad 5.25$$

where $R_N = N/N_L$

The total level of cyclic ratio may then clearly be determined from

$$R_N = R_N + \Delta R_N \qquad 5.26$$

The magnitude of the pore pressure increment may be determined from the shape of the normalised pore pressure generation curve shown in figure 5.10. The shape of this curve is governed by the properties of the sand, although it has been found experimentally that most sands fall within a band width as also shown in figure 5.10. A numerical representation of this curve may be given by the simple equation

$$\frac{u}{\sigma_{vo}} = \frac{2}{\pi}\arcsin\left(\frac{N}{N_L}\right)^{\frac{1}{2\alpha}} \qquad 5.27$$

where α is an experimental constant

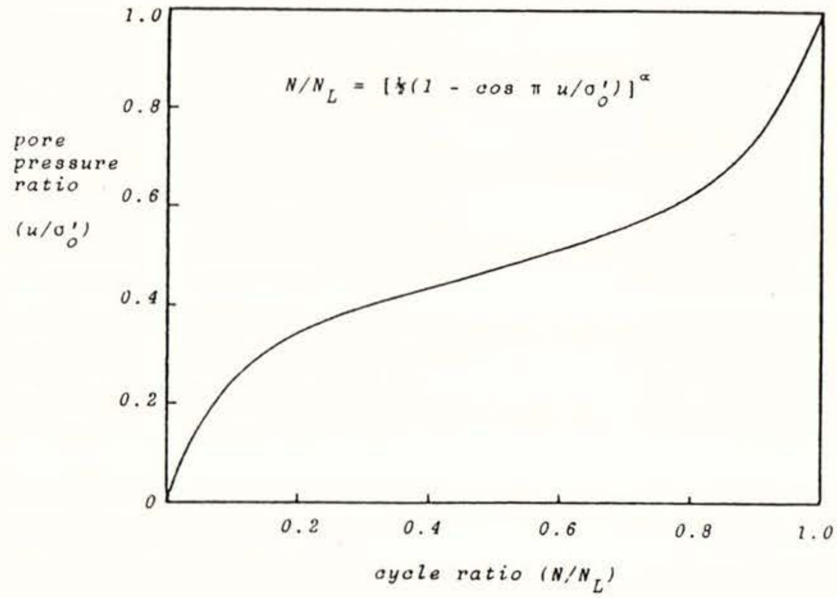

Fig. 5.10 Shape of pore pressure generation curves for sands

From the known cyclic ratio R_N, the value of pore pressure ratio may be determined using equation 5.27, and by inspection the value of excess pore pressure may be determined for each element using equation 5.28

$$u_{cyc} = R_u \sigma'_{mo} \tag{5.28}$$

The increment in pore pressure for this half cycle of loading for each element is then calculated from

$$u^{*} = u + u^{*}_{cyc} - u_{cyc} \tag{5.29}$$

5.5 IMPLEMENTATION OF PORE PRESSURE MODELS FOR EFFECTIVE STRESS ANALYSES

The MB pore pressure generation model outlined in section 5.2 is a shear strain dependent model. To achieve effective stress solutions, this model must be coupled with the total stress analyses of chapter four. The shear strains generated by the analysis are used in the pore pressure model to determine the levels of excess pore water pressure. It has been well established that the properties of cohesionless soils are dependent on the effective stress state. As a result, in the effective stress analysis the constitutive relationship must account for this changing state by altering the material properties. It has been shown experimentally that the majority of pore pressure generation (and hence material softening) occurs on the unloading portions of load cycle, and therefore the alterations to material properties of both the one and two dimensional analyses are only made on these portions of the loading cycles.

5.5.1 One Dimensional Analysis

The one dimensional analysis generates a horizontal shear strain which is used as an input to the pore pressure model. The one dimensional form of the multi linear (Iwan type) model has both stiffness and yielding elements. To represent the soil properties at a particular effective stress state, these elements are altered in accordance with equation 5.30

$$G = G_o \left(\frac{\sigma_v^{/}}{\sigma_{vo}^{/}} \right)^{1/2} \qquad 5.30$$

where G_o is the initial modulus

$\sigma_v^{/}$ is the current level of effective stress

σ_{vo} is the initial effective stress

This modulus value is updated at every time step for the changing effective stress state.

5.5.2 Two Dimensional Analysis

The two dimensional in-plane analysis generates one horizontal shear strain and two dynamic principal strains. These principal strains are cyclic in nature and tend to generate pore pressures due to the volumetric increase and decrease they cause. This type of pore pressure change is termed the dynamic component. It is possible to model these fluctuating pore pressures but they are not of great significance. Therefore the implementation of the MB model is purely based on the magnitude of induced horizontal shear strains, and this steadily increasing pore pressure is termed the residual component.

The two dimensional constitutive relationship requires parameters for both the nested yield surface radii and the kinematic hardening constants. As the size of the outer most yield surface is governed by the shear strength of the soil, a relationship between the effective stress state and the shear strength of the soil is also required. The relationship used in this study is given by equation 5.31

$$\tau = f(\sigma_m^{\prime})^b \qquad 5.31$$

where τ is the shear strength of the soil

b is an experimental constant (assumed to be unity for most soils)

Assuming that all nested yield surfaces remain proportional to each other, kinematic hardening (or softening as is the case for a reducing effective stress state) of the yield surfaces for each element may be given by

$$k_n = \frac{\tau}{\tau_o} k_{no} \qquad 5.32$$

where n is the nested yield surface number

τ_0 is the initial value of shear strength

k_{no} is the initial yield radius of each yield surface (n)

The relationship for shear modulus given in equation 5.30 is also valid for the two dimensional case. The yield surface hardening constants govern the representation of shear modulus, and are altered for a changing stress state in accordance with equation 5.33

$$C_n = \frac{G}{G_o} C_{no} \qquad 5.33$$

where G_0 is the initial value of low strain modulus

C_{no} is the initial value of the kinematic hardening constant of each yield surface

Figure 5.11 illustrates the alterations of the yield surfaces (looking down the space diagonal) for a changing effective stress state.

The bulk modulus is also influenced by the effective stress state of the sand and must

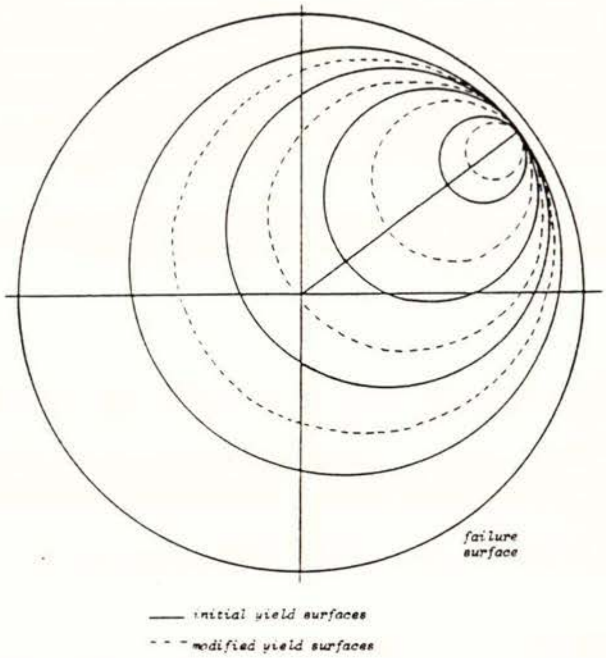

Fig. 5.11 Typical kinematic and isotropic hardening of a nested yield surfaces subjected to a changing effective stress state

altered in accordance with equation 5.34 at each time step

$$K = K_o \left(\frac{\sigma_v^{/}}{\sigma_{vo}^{/}} \right)^a \qquad 5.34$$

where K_o is the initial modulus

$\sigma_v^{/}$ is the current level of effective stress

σ_{vo} is the initial effective stress

a is a constant of the material

Chapter Six

Dynamic Properties of Volcanic Soils

6.1 INTRODUCTION

The geologically active past of New Zealand has lead to widespread deposits of volcanically derived soils throughout the country. The central region of the North Island, known as the Taupo Volcanic Zone (TVZ), extends 250 km across the Island and contains extensive deposits of volcanic ash, clays and pumiceous sands. This region includes the central plateau and extends through to the Bay of Plenty and White Island on the East coast. The Auckland region contains large deposits of predominantly ash and Tuff deposited from the many small volcanic cones in the area. Worldwide these soils occur abundantly in countries such as Japan, Indonesia, many Pacific Islands, Africa, Central America and the northwest of the United States. The dynamic properties of these soils, and indeed the static properties, have not been extensively studied to date.

Problems with volcanic sands have been encountered in the past in large geotechnical projects. The main difference to quartzitic sands is the softness of the grains, low in situ densities and high void ratios in natural deposits. The Edgecumbe earthquake of 1987 exhibited widespread liquefaction of these sands, and a number of geotechnical failures have also been witnessed in recent years, particularly in the area of hydro development and their associated canal structures. Clean quartzitic sand deposits are not generally at risk from significant site amplifications due to their inherent high damping properties. Very little work has been carried out to investigate if the same is true for sands of volcanic origin. It is therefore of interest to investigate the dynamic properties of these sands in comparison to the well studied properties of their quartzitic counterparts.

Volcanic ash and the clays derived from weathering are also widely encountered in geotechnical practice. As ash and clay soils are not particularly susceptible to liquefaction, the main dynamic interest is in their shear modulus and damping response over various strain levels. The modulus and hysteretic damping strongly influences the earthquake amplification characteristics of the site. Larkin and Donovan (1979) showed that for non liquefied soils, the shear modulus degradation curve, and hence induced shear strain levels, is the major governing factor in computer modelling. The earthquake that devastated Mexico City in 1985 graphically confirmed this finding. For volcanic soil deposits it is therefore important to gain information as to the form of the shear modulus versus shear strain curve, and compare this to the widely used empirical curves that are available in the literature (Vucetic and Dobry 1991), that have generally been collated from work on sedimentary soils.

This chapter shall present both a brief literature review of the existing data on volcanic soils, and present experimental work undertaken during the course of this study. Due to the limited experimental scope, the main focus of testing was the dynamic properties of volcanic sands, and in particular the undrained liquefaction properties. These liquefaction tests were performed using a cyclic triaxial testing apparatus, and some use of bender elements was also made. One type of volcanic sand was tested, which was river sand taken from the Puni river the Waikato, and is known as Puni pumice sand. The experimental results of this testing are then used in the numerical work presented in other chapters.

6.2 REVIEW OF EXISTING DYNAMIC VOLCANIC SOIL PROPERTIES

As stated above, the experimental and empirical data in the literature on volcanic soils is very limited. Static properties of andisol ash soils have been investigated in the United States by Thrall (1981) who found significant deviations in the properties of these soils when compared to commonly used soil correlations. Pranjoto and Larkin (1995) investigated the Puni river sand that is investigated further in this study, and determined the basic physical and strength properties of the sand. Some of their data is used in this study and shall be detailed in a later section.

Chan (1990) investigated the dynamic soil properties of two volcanic ash soils from the Rotorua region using the free vibration torsion test. This work produced shear modulus versus shear strain curves for those soils and are also made use of in this study. Pender et al. (1992) investigated the cyclic response of a volcanic ash from Tauranga. This study found that the volcanic ash had a greater sensitivity to pore water pressure increase than a typical Auckland clay exhibiting similar basic soil classification data. This pore water pressure increase would however be most likely insufficient to lead to liquefaction for the particular ash soil. Further investigation found that the ash soil had a sensitive structure that is degraded by repeated cyclic loading, and that the response of the ash is more complex than the typical Auckland clay. The shear modulus curves were found to be within the boundaries of the empirical curves for clays. Unfortunately little other dynamic data on volcanic soils was available, which necessitated the experimental program that is described in the following sections.

6.3 INTRODUCTION TO EXPERIMENTAL DYNAMIC TESTING PROGRAMME AND PROCEDURE

In order to gain some understanding of the dynamic properties of a volcanic sand, a number of dynamic triaxial tests on the Puni river sand were undertaken. As indicated above, no information was available as to the dynamic behaviour of volcanic sands. For this study, the more difficult stress controlled tests were used, as these were considered most appropriate at this stage. From these tests the undrained liquefaction strength of the volcanic sand could be determined. These results also provided information on the shear modulus characteristics of the sand at various levels of shear strain. Both loose and dense sand samples were investigated, although the main focus was directed at the loose samples where liquefaction is more prevalent. Use was also made of bender elements to investigate the low strain shear wave velocity characteristics of the sand.

6.3.1 Testing Equipment

The stress controlled cyclic loading tests were performed under load control on an MTS (materials testing system) closed loop electro hydraulic testing machine. This unit incorporates a feedback system to ensure the load is in agreement with the control signal. The feedback load cell was an MTS 3 kN cell, with a gain setting of 5. The MTS control panel and inbuilt function generated were used to generate the loading signal, which was a sine wave of 0.1Hz.

Samples were contained in a triaxial cell, which allowed samples of up to 100 mm in diameter and 200 mm in length. Two drainage connection points from the sample were used, one for pore pressure measurement and one for consolidation purposes. An external burette was connected to the drainage tap which allowed measurement of volume change during the consolidation phase. The load ram passed into the triaxial cell through a bearing system that rendered a relatively frictionless system, which was confirmed by experimental calibration. This load ram was then threaded into the top platen to provide a solid connection with the top of the sample. All recording instruments (as outlined below) were external to the triaxial cell, and hence it was important to achieve a relatively frictionless path for the load ram.

The response of the samples, and hence the results presented in this study were recorded on a completely independent system from the MTS. This system consisted of a 5kN load cell, an LVDT displacement transducer and a single base mounted pore water pressure transducer. These three transducers were connected to a Daytronics signal conditioning unit. A National Instruments 16 bit data acquisition card (AT-MIO-16X) was used in a 486 computer to record the output from the Daytronics unit. Data acquisition software was written for this system using the National Instruments LABVIEW development environment package. This software recorded the three input channels at a sampling rate of 50 points pre load cycle, plotted the results to the computer screen in real time, and saved the data to disk for later analysis.

6.3.2 Testing Procedure

Sample Preparation

The initial difficulty with the testing of sands is in the formation of the samples. It has been widely established that the relative density has a strong influence on the cyclic response of the sample, which makes sample preparation very important (Seed 1979, Ishihara 1993). Pranjoto and Larkin (1995) investigated a number of sample preparation techniques and concluded that a dry deposition method gave reliable and repeatable results. This method used a small glass funnel to carefully place the sand at the centre of a 3 piece split mould, whilst slowly lifting the funnel opening to maintain a constant fall height. This method produces samples of relatively constant density in a loose state, with average relative density values of 35% being obtained. Dense samples were made in the same way, except a vibrating table was used to compact the samples to near their maximum density.

Once in the triaxial cell, the samples were flooded with pressurised carbon dioxide (CO_2) to expel the air from the voids and then flooded with de-aired water. With the back pressure raised to 700 kPa and the cell pressure a little higher to maintain a positive effective stress, the samples were left overnight to allow sufficient time for all of the carbon dioxide and remaining air pockets to dissolve into the pore water. This amount of 'soakage time' was required due to the nature of the pumiceous sand particles. Once the complete saturation of the sample was confirmed the next day with the B test, sample testing could begin. B test values of 1.0 were consistently achieved, indicating complete saturation of the samples.

In all tests the effective confining pressure of the sample was set to 100 kPa, which was set during the consolidation phase of the testing. To maintain a 700 kPa back pressure the cell pressure was set at 800 kPa. The volume of pore water expelled during consolidation was measured in the burette, along with the change in length of the sample. From these two measurements the consolidated cross sectional area of the sample could be determined.

Cyclic Load Controlled Testing

The MTS testing system and function generator were programmed to cycle the sample between a positive and negative load ($\pm P_c$). A sine wave was used as the form of the driving control signal, scaled to $\pm P_c$ at a frequency of 0.1 Hz. The first cycle of sinusoidal loading was a compression phase. The cyclic loads were in the range of 10% of the capacity of the MTS control load cell, which was considered to be of acceptable accuracy. In all tests the upthrust load from the cell pressure was balanced out of the load readings, hence the loads displayed below are net loads on the sample. The ASTM (1991) standard on cyclic testing was closely followed during this testing program where applicable. In accordance with the accepted practice in geomechanics, compression forces and displacements are considered positive.

6.4 GENERAL SOIL PROPERTIES OF PUNI SAND

As stated before, Pranjoto and Larkin (1995) have investigated the static soil properties of the Puni River sand, and this sand was chosen for dynamic testing because this earlier work had already been done. In addition to this data, some more general soil properties were investigated that have direct relevance to the earthquake field of study and these shall also be given below. For this study the sand was not altered in composition from its natural state as the size of the samples diminished the influence of larger particles. This is a deviation from Pranjoto and Larkin who graded out particles above 1.18mm and below 300 μm for their investigation. The liquefaction response of the natural sand was therefore determined in these tests.

Particle Size Distribution

The natural particle size distribution of the sand was determined and is shown in figure 6.1. From this grading curve the sand may be classified as a well graded medium to coarse sand. Also shown are the particle size range curves for liquefaction that have been determined from field observations, from Tsuchida and Hayashi (1971) for well graded sands. The Puni sand falls within the readily liquefied zone of the graph and is hence a good choice of sand for dynamic liquefaction testing.

Density and Void Ratio

Table 6.1 summarises the basic soil property test results as determined by the author for the and, except for the solid density value which was taken from Pranjoto and Larkin (1995) These results are used throughout this study.

The specific gravity value (G_s) of 1.7 is an overall result for the sand, but Pranjoto and Larkin found this parameter to be a function of grain size. This is not surprising as pumiceous particles tend to be porous and have pockets of air trapped within them, which gives a lower solid density for the larger particles, hence the nature of pumice.

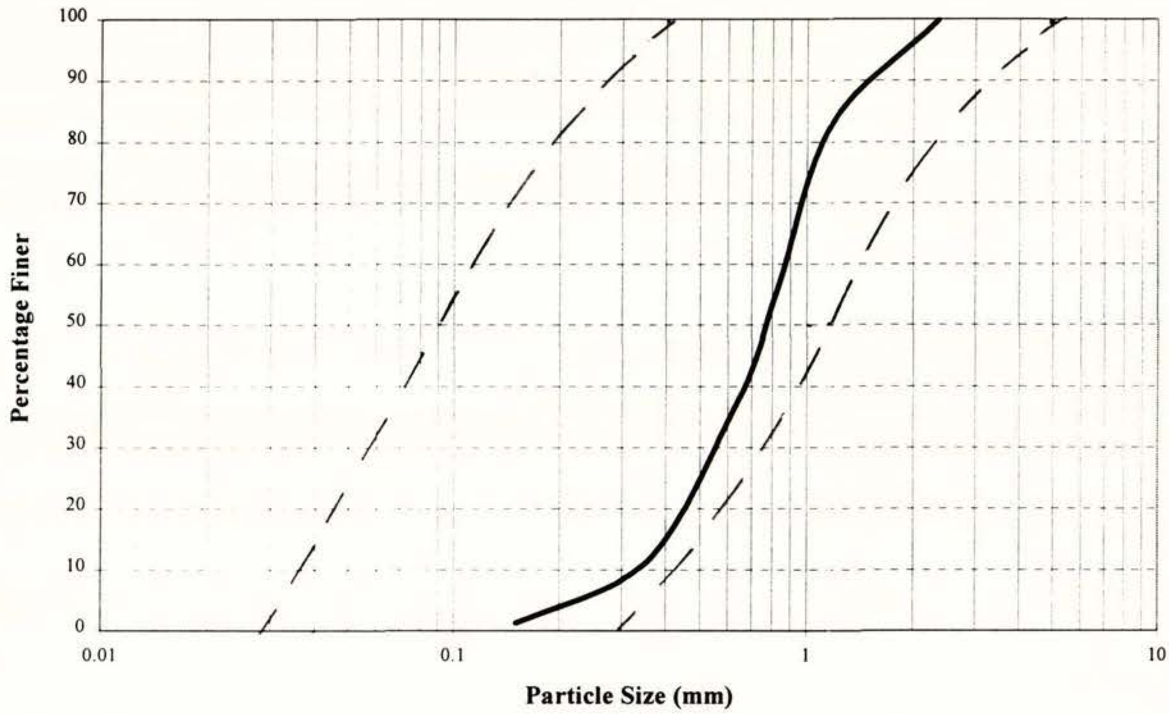

Fig. 6.1 Particle grading curve for natural Puni River sand, with liquefaction grading ranges

Table 6.1 Basic properties of the Puni river sand

Soil Property	Value
Dry density$_{max}$ (kg/m^3)	896.3
Dry density$_{min}$ (kg/m^3)	729.9
Void ratio$_{max}$	1.7
Void ratio$_{min}$	1.1
G_s (t/m^3)	1.7-1.8
d_{50} (mm)	0.76

Permeability

The permeability of the Puni sand was investigated, as this can have a significant influence on the liquefaction response of the sand deposit (Marks 1992). A constant head permeameter test was used to evaluate the permeability of the sand for five different relative densities, and from this the coefficient of permeability (k) was determined. Figure 6.2 shows the results of the constant head permeameter test for a sample with a relative density of 54%.

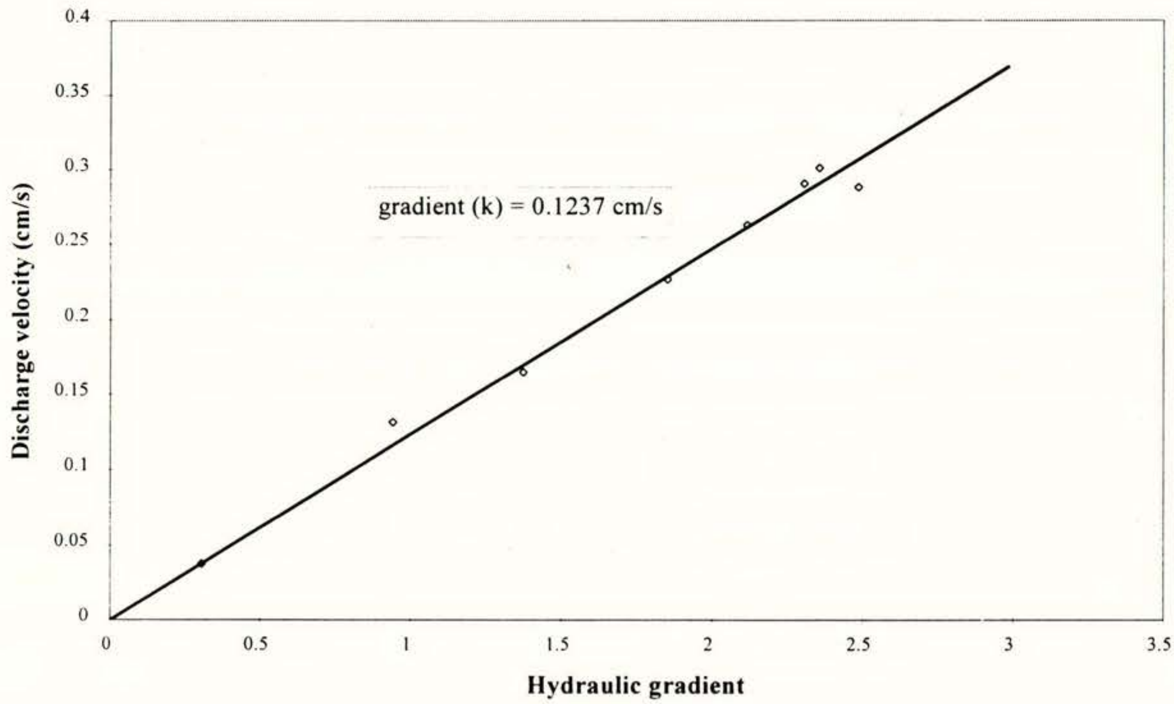

Fig. 6.2 Constant head permeability result for sand sample of 54% relative density

Similar results were gained for other relative densities, and are summarised in figure 6.3.

An exponential interpolation function was used to gain a general expression for the permeability of the natural river sand as a function of relative density, and takes the form

$$k=0.4e^{-0.02\,DR} \qquad 6.1$$

where k=permeability (in cm/s)

DR is the relative density (%)

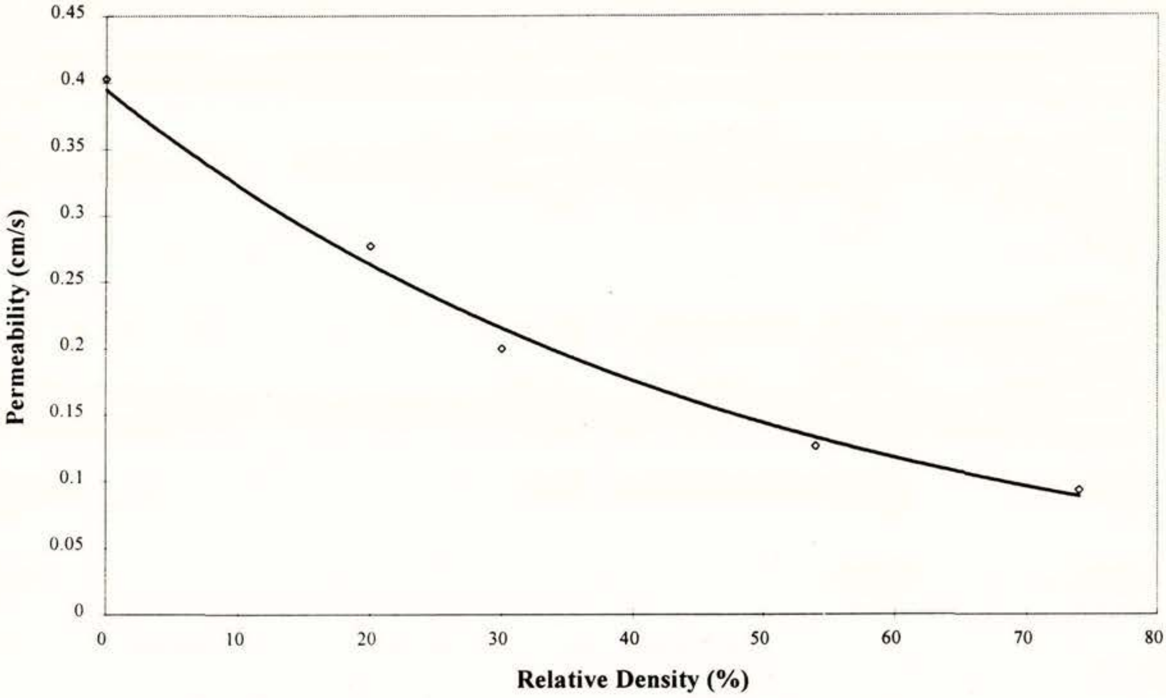

Fig. 6.3 Permeability versus relative density for natural Puni River sand

From figure 6.3 it can be seen that the permeability of the Puni sand falls within the range of 0.08 to 0.4 cm/s. General classification charts for permeability (Freeze and Cherry 1979) consider this as a high permeability, and term the sand as relatively coarse, a similar classification to the particle grading curves.

6.5 DYNAMIC SOIL PROPERTIES OF PUNI SAND

The dynamic properties investigated of the Puni sand include the liquefaction response, the low strain shear modulus and the shear modulus versus shear strain curve, and the shape of the pore pressure buildup curves. This data was required to investigate the liquefaction properties of the volcanic sand and to compare to the widespread empirical data available for quartzitic sands.. As most of the experimental interest was directed towards loose sands, the results of these shall be presented first, and a small section on the dense sand sample shall follow.

6.5.1 Loose Volcanic Sand

Load controlled dynamic triaxial tests were performed on a number of loose samples during the course of this testing programme. Initially however the repeatability of the sample preparation and testing procedure was investigated

Repeatability of Load Controlled Testing

The repeatability of the sample preparation method (dry pluviation) and testing procedure was investigated by testing two different loose samples (labelled D and E for convenience here) at the same cyclic load and comparing the results. The two sample dimensions and properties are shown in table 6.2. All samples are nominally 100 mm in diameter and 200 mm in length.

Table 6.2 Repeatability of sample preparation (dry pluviation) technique

Soil Property	Sample D	Sample E
Volume (m^3)	$1.604e^{-3}$	$1.592e^{-3}$
Mass of sand (kg)	1.271	1.250
Dry density (kg/m^3)	792.0	785.0
Bulk Density (kg/m^3)	1443.0	1439.0
Relative Density (%)	37.0	33.0

Table 6.2 indicates the dry pluviation method generates a loose sample of similar dry and bulk density (when flooded with water), thus demonstrating that the loose sample are all of a relatively similar nature.

The repeatability of the testing procedure was then investigated. The two samples (D and E) were set up in the triaxial cell and tested at the same cyclic load (and hence cyclic stress ratio). The resulting axial load vs axial strain hysteresis loops are shown in figures 6.4 and

6.5.

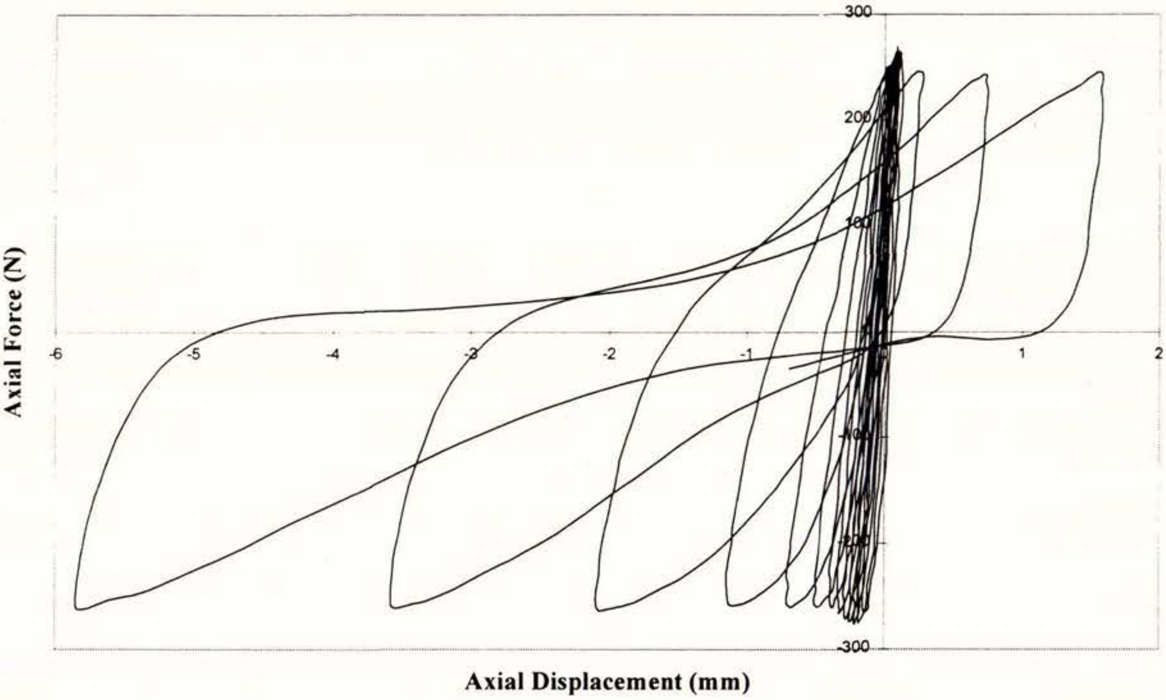

Fig. 6.4 Axial load displacement plot for (loose) sample D

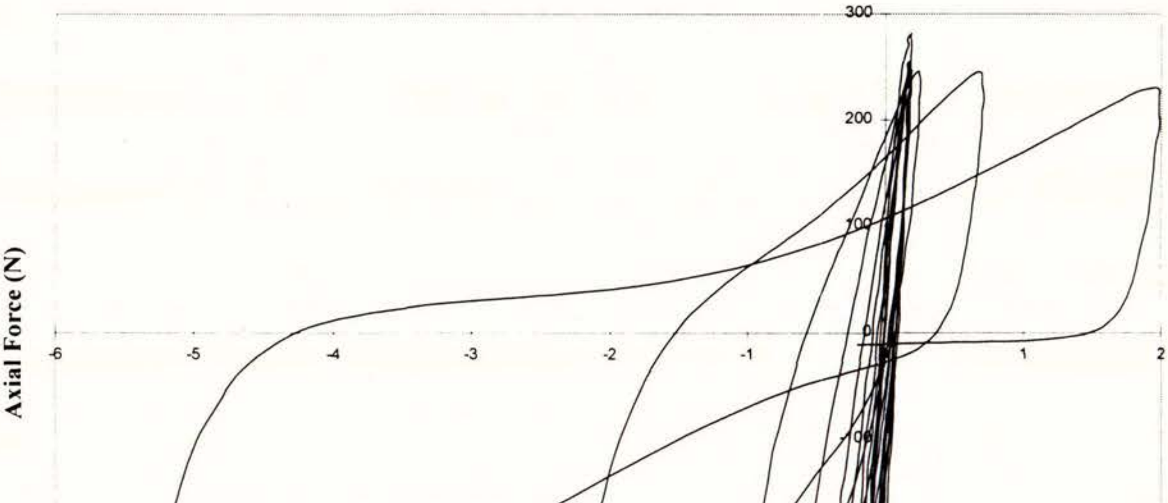

Fig. 6.5 Axial load displacement plot for (loose) sample E

These figures show a similar response of the two samples, sample D experienced liquefaction in 13.5 cycles, and sample E in 14.5 cycles of loading. Both failed in the extension phase of the loading cycle, hence the extra ½ cycle.

Figures 6.6 and 6.7 show the generation of excess pore pressure against the normalised number of cycles to liquefaction (N/Nl). These essentially show the time history of the generation of pore pressure and are also in good agreement with each other. The results of these comparison tests give confidence as to the repeatability of the testing procedure, particularly as load control liquefaction testing is more difficult to duplicate than the displacement control test (chapter two).

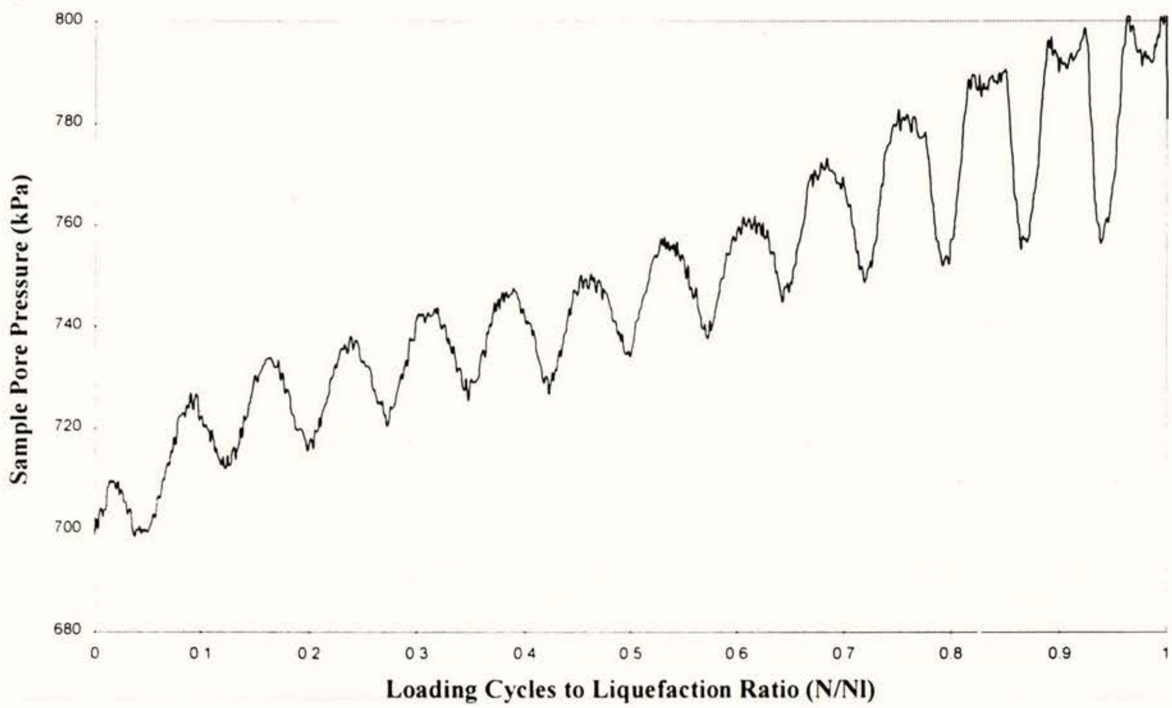

Fig. 6.6 Pore pressure buildup curve for sample D

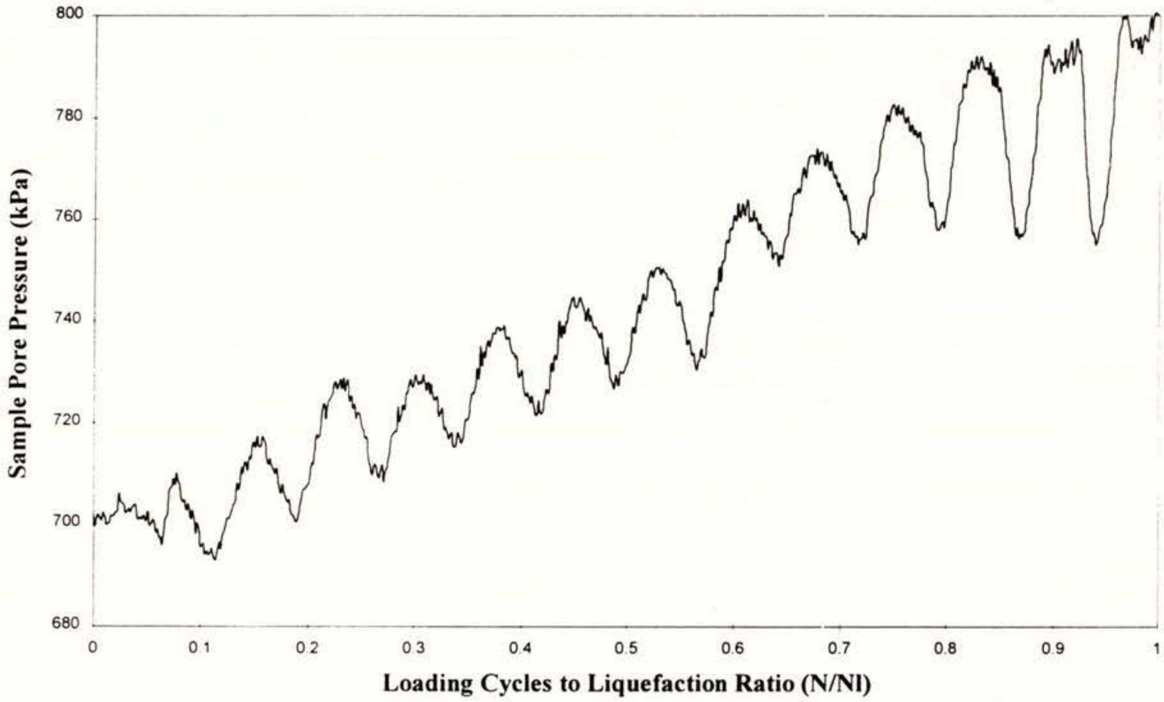

Fig. 6.7 Pore pressure buildup curve for sample E

Observations and Limitations of the Testing Procedure

Some limitations of the testing were discovered as the work proceeded and they shall be briefly described here before continuing with the presentation of the results. The first was the limitation of the MTS being unable continue past the point of liquefaction without overloading the hydraulic system. When the soil loses strength, to try and maintain the loads at the required testing frequency, the loading arm is required to move too quickly for the system. At this point the hydraulic system starts to noisily vibrate and it is not possible to maintain the cyclic loading past the point of strength loss (liquefaction). As a result this testing programme was unable to gain data concerning the post liquefaction behaviour of the sand.

There was also some difficulty in maintaining the value of load reversal in the compression (+ve) and extension (-ve) phases for some of the tests. This problem appeared in two forms. The first was termed load 'fall off' which occurs when the displacements became large, but before complete failure took place. Again this is a limitation of the MTS testing equipment to maintain load control throughout relatively large sweeping displacements. The second was the inability of the system in many tests to cycle about a constant ± axial load (P_c), even at very small displacements. For all of the tests that exhibited this behaviour, the extension load of the cycle was in the order of 10% larger than the compression load. It was not clear as to the reasons for this load imbalance and efforts were made to correct this problem. It was not possible to find the reason within the MTS system for this imbalance however, and in these tests the cyclic axial load was taken as the mean of the two loading phases.

Liquefaction Response of Load Control Testing

A number of load control tests at a variety stress ratios were performed to generate a liquefaction strength curve for the loose sand state. In addition to the two tests described in the repeatability section above, another five loose samples were tested at different stress ratios. Table 6.3 lists the sample data for all of the seven loose samples tested.

Table 6.3 Relative density of the loose Puni sand samples tested

Sample Number	Relative Density (%)	Stress Ratio ($\sigma_d/2\sigma_3$)
A	40.0	0.23
B	34.0	0.20
C	35.0	0.18
D	37.0	0.16
E	33.0	0.16
F	40.0	0.15
G	29.0	0.14

It is clear from table 6.3 that most of the samples are of relatively similar density, and therefore the liquefaction properties of these samples were able to be compared for different stress ratios of loading. Figure 6.8 shows the liquefaction resistance curve for the seven loose sand samples (as diamond points) and a line of best fit through those experimental data points. This graph displays the well established shape of the liquefaction resistance curve for sands and indicates that the general form of the volcanic sand's liquefaction properties are similar to the database of these other sands.

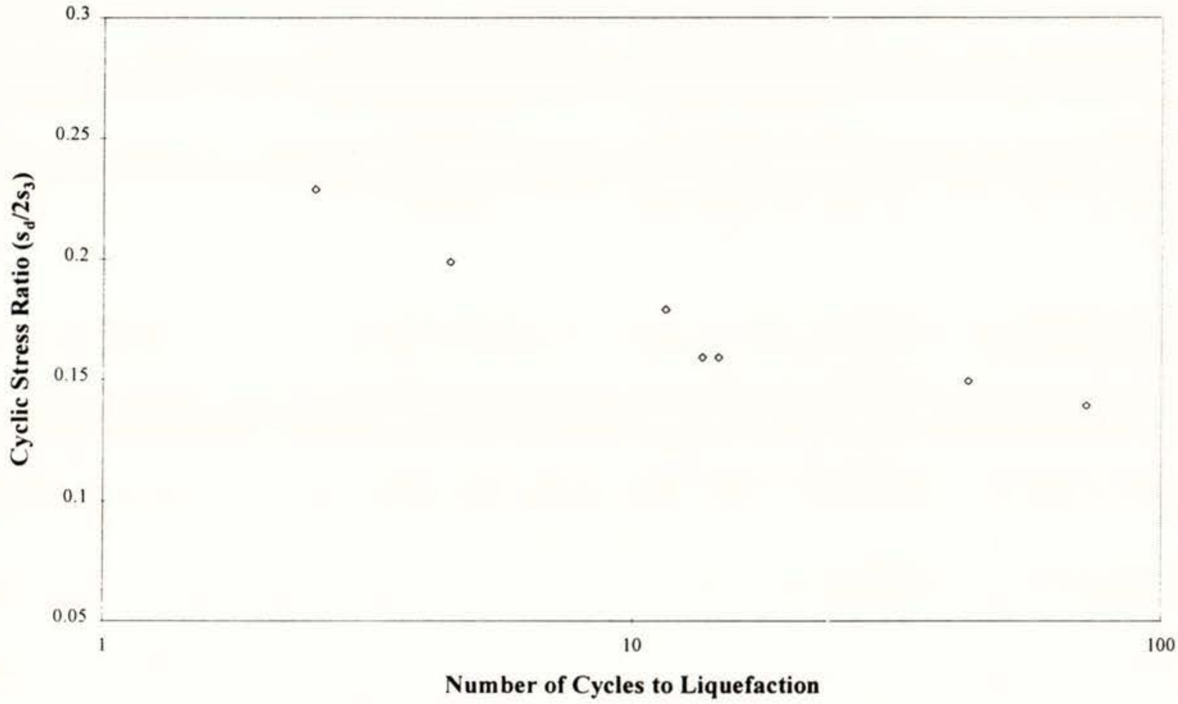

Fig. 6.8 Liquefaction resistance curve for loose Puni sand samples

The pore pressure generation behaviour of the seven sand samples for the different loading stress ratios is shown in figure 6.9. These originally took the form of the two curves shown in figures 6.6 and 6.7, but for graphing purposes the dynamic component of the pore pressure response that is in-phase with the deviator stress has been omitted. This leaves the steadily increasing residual pore pressure component that is a result of the shearing stress acting within the sample. The residual component of the pore pressure for each test is taken at the centre of the loading cycle, which is the point where there is no dynamic component present.

These pore pressure generation curves show similar behaviour for all of the loose tests, and all fall within the boundaries of cyclic triaxial test results reported by Seed et al. (1975b) for quartzitic sands. This indicates that the volcanic sand behaves in a similar way to other sands when generating pore pressure. The expressions used in the stress controlled pore pressure model (chapter five) should therefore be valid for these sands.

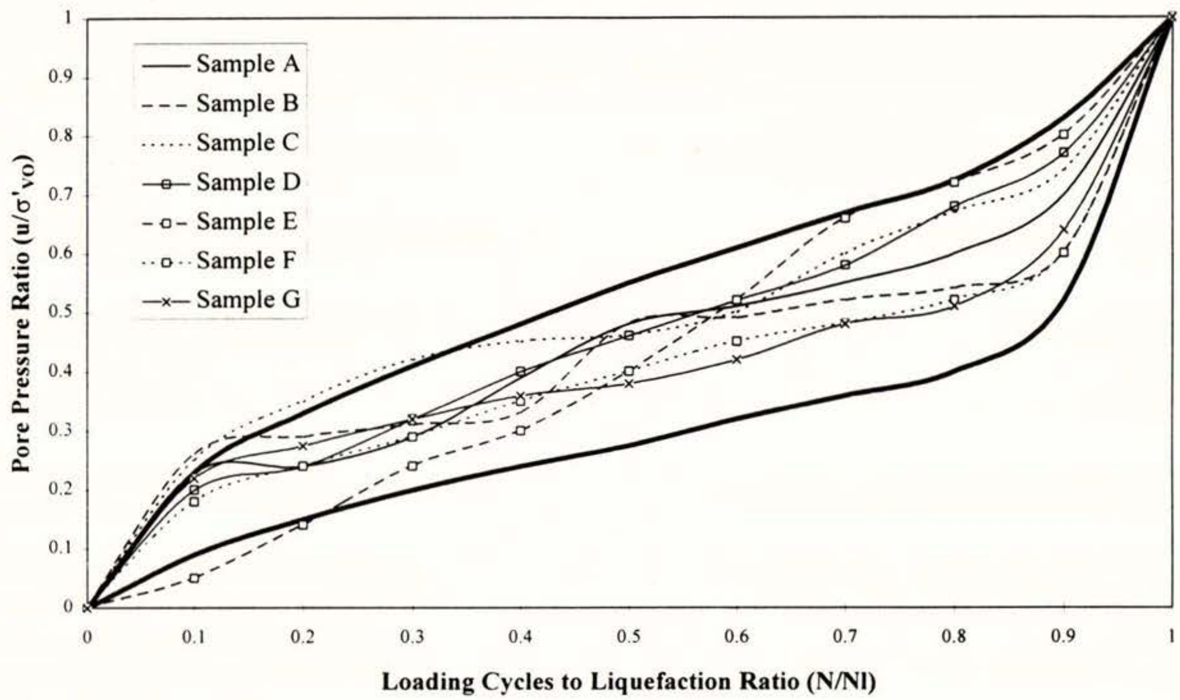

Fig. 6.9 Normalised pore pressure generation curves for Puni sand, with quartzitic boundary limits shown in dark lines (from Seed et al. 1975b)

Influence of Loading History on Liquefaction Response

The influence of loading history on the response of the loose sand samples was investigated by cycling a loose sample initially at a small stress ratio (0.10) for 50 cycles. The sample was then reconsolidated and tested at the same stress ratio as sample D and E from above (stress ratio=0.16).

The reconsolidation produced a volume decrease in the sample volume of 0.3%, which is a small volume change and indicated essentially no excess pore pressure generation. When retested at the stress ratio of 0.16, the number of cycles of loading to liquefaction increased from 13.5 or 14.5 (sample D and E respectively) to 23.5 cycles.

This is a significant increase in the liquefaction resistance strength of the sample, and indicates any stress history may be significant in the determination of liquefaction properties of this volcanic sand, independent of the relative density. An explanation of this may be the influence of the grain shape, softer grains and grain contact points. Even cyclic loading of low magnitudes may promote some grain to grain motion and more stable contact points, which are increased by the softer grains. This promotes a more stable sand that is therefore more resistant to liquefaction.

6.5.2 Dense Volcanic Sand

Some investigation of the properties of the Puni sand in dense form was also undertaken. Dense sands are generally not susceptible to liquefaction and the associated serious strength loss. As a result, a reduced testing programme was undertaken.

Liquefaction Response of Load Controlled Testing

A dense sample (sample H) of Puni sand was tested in the cyclic load control apparatus for the liquefaction response. The cyclic stress ratio for this test was 0.32. This very high level of load was chosen because several trials at loadings of the order of the loose sand (table 6.3) had shown very little response of the sand.

The dense samples in this section were constructed using the dry pluviation method detailed above, but were vibro-compacted on a vibration table during the sample preparation. Construction of a number of dense samples confirmed the repeatability of this procedure. Table 6.4 lists the material properties of the dense sample for liquefaction testing..

Table 6.4 Material properties of dense Puni sand sample

Property	Value
Volume (m^3)	1.60e-3
Mass of sand (kg)	1.385
Dry Density (kg/m^3)	865.0
Bulk Density (kg/m^3)	1484.0
Relative Density (%)	75.0

The response of the dense sample to a stress ratio of 0.32 is shown in figure 6.10 to a limit of 35 loading cycles, at which point the test was stopped.

This plot clearly illustrates the concept of limited strain potential that dense sands tend to exhibit, rather than the more marked and sudden failure of loose samples. This can be explained with the aid of figure 6.11, which shows the excess pore pressure generation within the sample. It can be seen here that there is significantly higher dilatancy component than in the loose tests (figure 6.6, 6.7) which tends to retard the excess pore pressure for a large component of the loading cycle and limits the induced strains. There is therefore no sudden failure as in the loose sand case because high pore pressures only develop for a short phase in each loading cycle, after which they reduce due to the dilatancy.

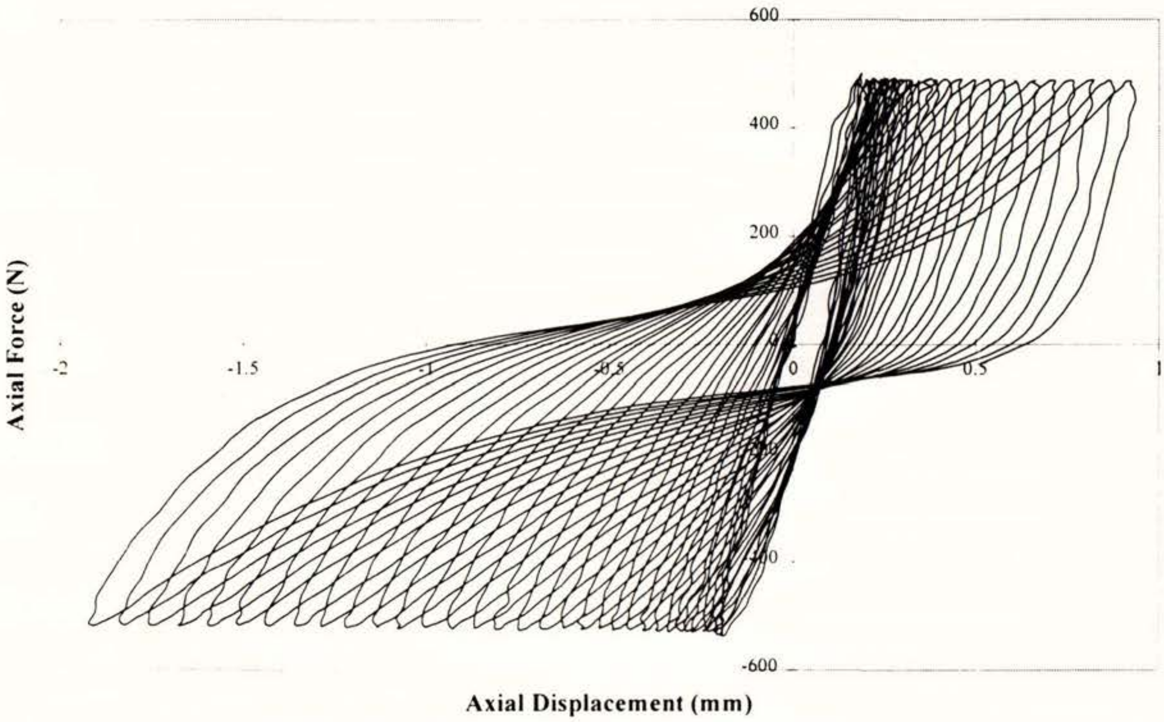

Fig. 6.10 Axial load displacement plot for (dense) sample H

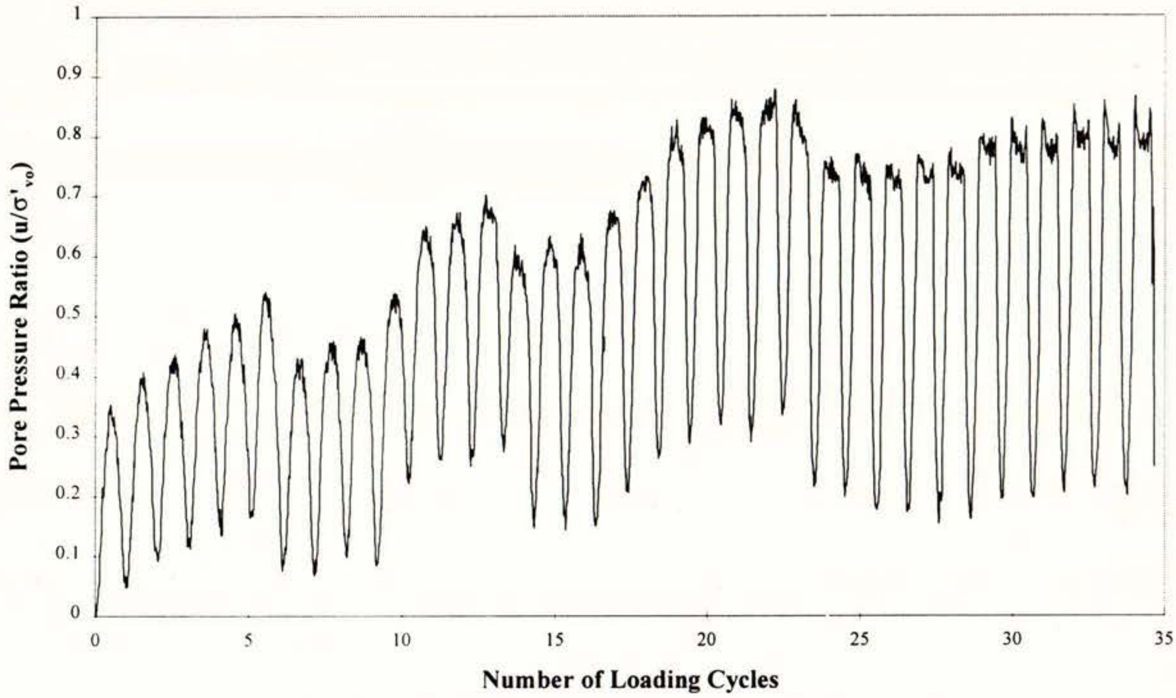

Fig. 6.11 Pore pressure generation curve for (dense) sample H

Evidence of Grain Crushing in Dense Samples

The softness of volcanic sand grains in comparison to those of quartzitic origin is a significant difference between the two types of sand, and therefore the possibility of any grain crushing during liquefaction testing was investigated. Pranjoto and Larkin (1995) found significant grain crushing for their triaxial critical state testing, although the deviator stresses applied to those sand tests were in the range of 500 to 2000 kPa whereas the deviator stresses for the liquefaction tests was in the range of 20 to 50 kPa.

Two dense samples (sample K and L) were tested at a varying range of stress ratios and numbers of loading cycles to investigate grain crushing. Sample K was subjected to a stress ratio of 0.3 for 30 cycles of loading (similar to sample H above), and then a particle grain size test was made. The results of this are shown in figure 6.12. A second dense sample (sample L) was subjected to a total of 6 separate tests at a variety of medium and very high stress ratios. The sample was reconsolidated between each test. Figure 6.12 also shows this plot.

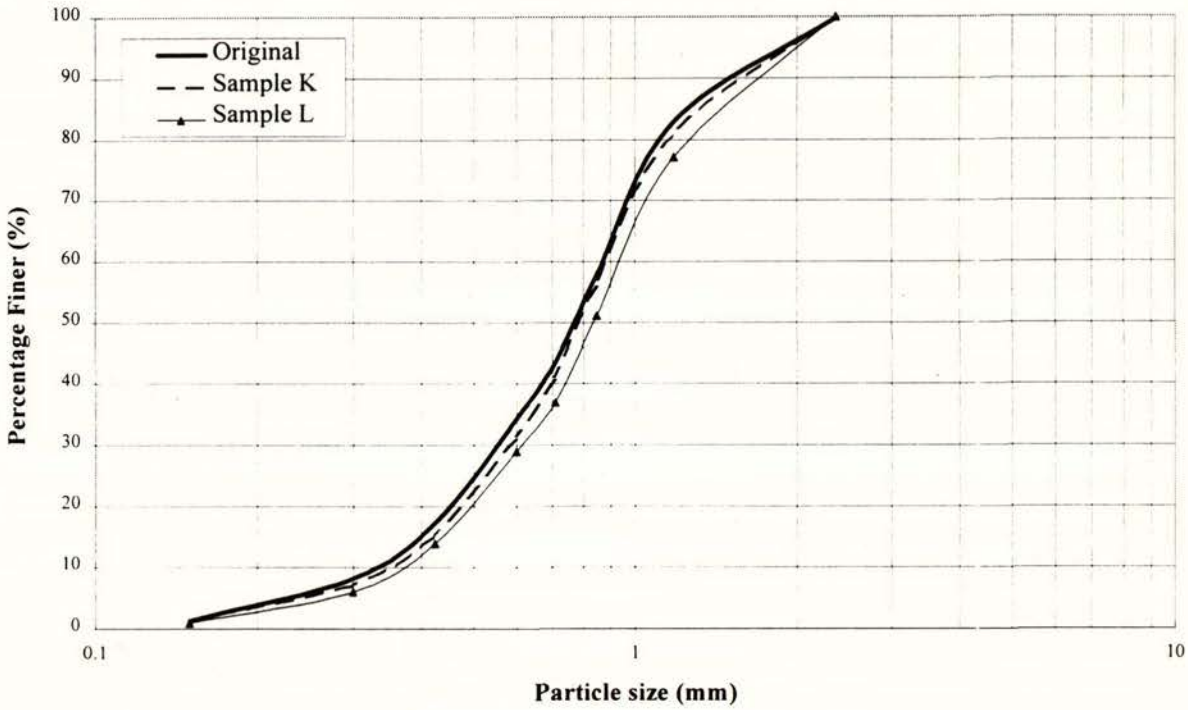

Fig. 6.12 Particle size distribution curves for dense sands subjected to cyclic testing

The above figure actually shows a slight increase in the grain sizes of the two samples after the testing has occurred, but within a very small tolerance. It was not considered possible for the grains to combine into larger grains during the testing, so the explanation for this behaviour is therefore the natural variation of the soil distribution between different samples. The samples used were in their 'natural' state when tested and some variation if grain size distribution would be expected.

What figure 6.12 clearly shows is the lack of grain crushing in the samples, even when the loadings were very much higher and of longer duration than would likely be experienced by the sand during an earthquake (sample L). From this data it was concluded that grain crushing for the Puni sand would not be a factor in the liquefaction performance. Loose sand grain crushing was not investigated as it was deduced from the dense results that such testing was not required. This was based on the thought that loose sands sustain lower shear loads and hence lower grain to grain forces, which would tend to limit grain crushing. One aspect of loose sand loading however is that larger deformations tend to be induced which may tend to promote some extra crushing, but this was not investigated at this stage.

Low Strain Shear Modulus (G_{max})

The low strain shear modulus for the dense sand was investigated using the bender elements that have been developed and used at Auckland University over recent years. Two bender elements, one at each end of the sample were used. The basic principle is that one element emits a shear wave which is received by the second bender element at the other end of the sample, as detailed below. The time delay between the sending and receiving signals may be measured and the shear wave velocity, and hence low strain shear modulus, may be determined.

Each bender element is a small transducer comprised of two thin piezoceramic plates rigidly bound together in a sandwich type arrangement. The configuration of the ceramic material is such that it enables the bender element to convert electrical energy into mechanical energy and vice versa. Hence an applied voltage will cause the bender element to deflect a small amount (which generates the shear wave), and conversely the bender element generates a voltage when it is bend (upon receiving the shear wave). These tests measure the elastic shear modulus of the soil and are non destructive. The applied voltage and measurement of the receiving signal were controlled by a Yokogawa oscilloscope and function generator. The oscilloscope has a maximum sample rate of 100 MHz, which gave a sufficient discretizing interval for the bender element signals.

For this experimental programme a dry dense sand sample (sample J), whose properties are listed in table 6.5, was tested using the bender elements at a variety of confining pressures.

Table 6.5 Properties of the dense sand (sample J) used for bender element testing

Property	**Value**
Length (mm)	138.5
Volume (m^3)	6.283e-4
Mass of sand (kg)	546.0
Dry/ bulk density (kg/m^3)	870.0
Relative density (%)	78.0

Bender element traces were taken for a range of confining stresses from 25 to 900 kPa at regular intervals. Figure 6.13 shows a trace of the bender element output taken from the oscilloscope showing the trigger time and 1st arrival time for a confining stress of 125 kPa. The ΔT reading in the top left corner of the trace is the time recorded for the arrival of the shear wave, and when divided by the distance between the two bender elements the shear wave was calculated. The shear modulus may be then calculated from the elastic equation 6.2.

$$G_{max}=\rho V_s^2 \qquad 6.2$$

where ρ is the density of the sample

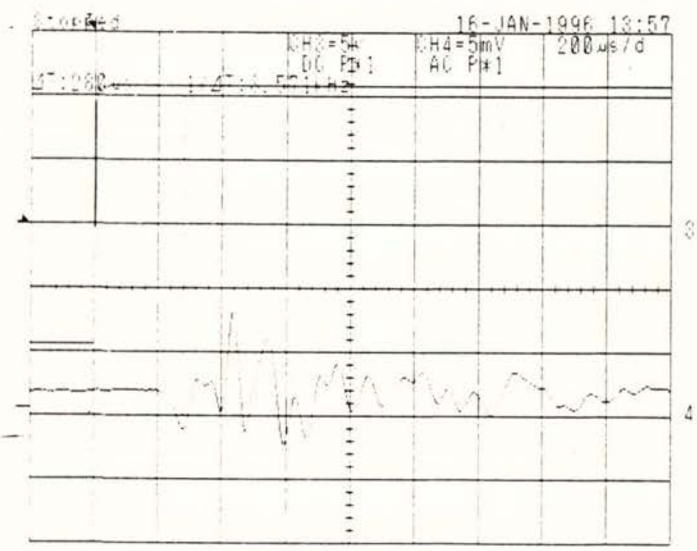

Fig. 6.13 Sample bender element trace for dense sand at 500 kPa confining stress

Figures 6.14 and 6.15 show the shear wave and low strain modulus profile versus confining stress respectively for all of the tests on the dense Puni sand.

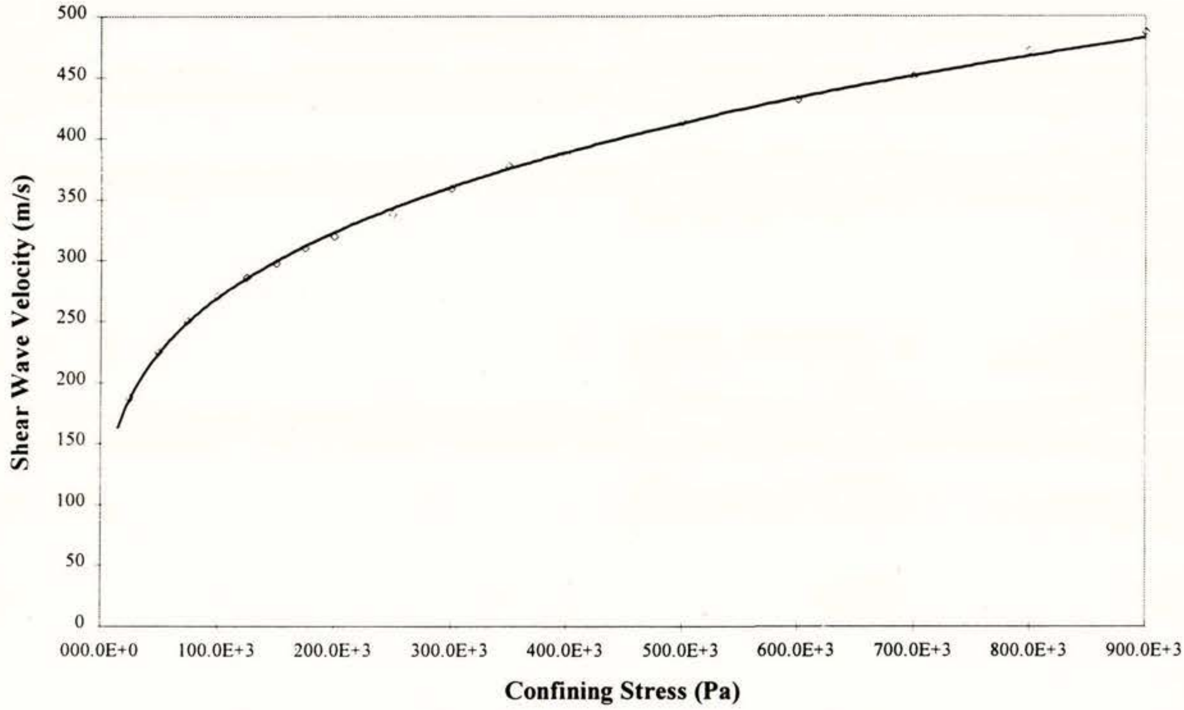

Fig. 6.14 Shear wave velocity versus confining stress profile for dense sand

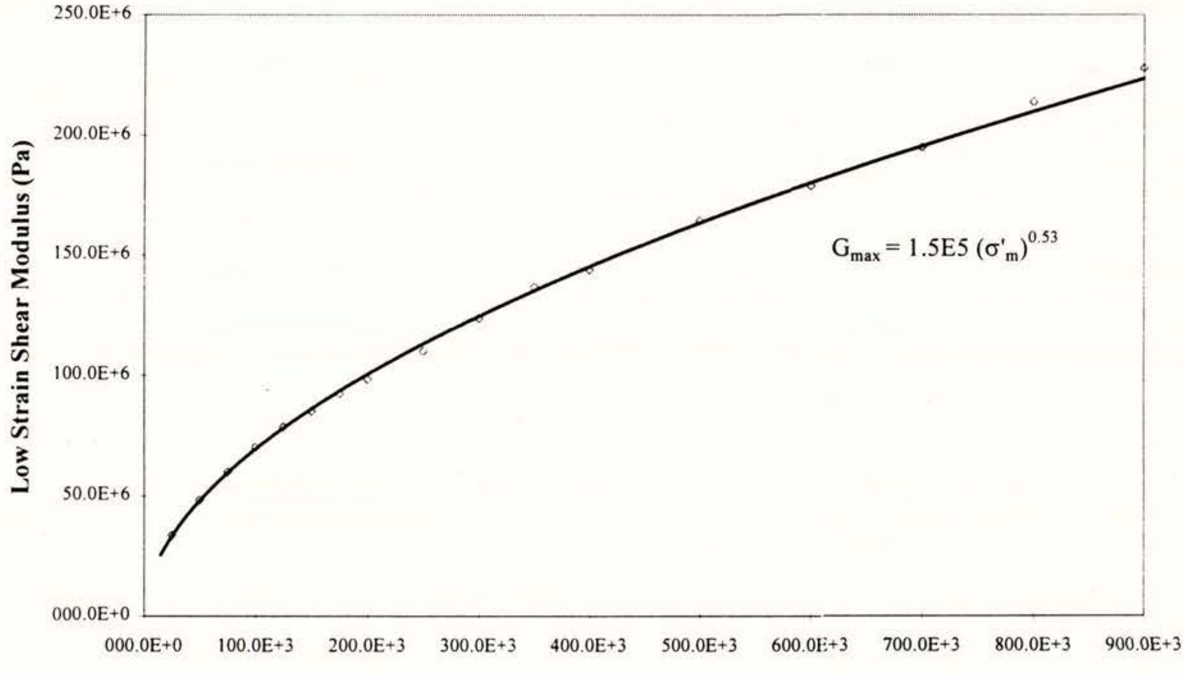

Fig. 6.15 Low strain shear modulus versus confining stress profile for dense sand

Both the above figures indicate that the volcanic sand follows the same shape of curve as the well investigated quartzitic sand. The best fit line through the shear modulus data of figure 15 has the equation

$$G_{max}=1.5e5\ (\sigma'_m)^{0.53} \tag{6.3}$$

The power value of 0.53 conforms to the widely accepted value of ½ for sands, which does suggest that, once again, grain crushing has limited impact on the properties of the sand in the range of loads of interest. Seed et al. (1984b) give the empirical expression (in SI units)

$$G_{max}=6945\ k_2\ (\sigma'_m)^{0.5} \tag{6.4}$$

where σ'_m is the mean effective stress

k_2 is a constant dependent on SPT blow count

From 6.3

$$G_{max}=1.5e5\ (\sigma'_m)^{0.5}\ (\sigma'_m)^{0.03} \tag{6.5}$$

Dividing 6.4 by 6.5 gives

$$k_2=21.6\ (\sigma'_m)^{0.03} \tag{6.6}$$

For the confining stresses likely to be encountered in practice, the $(\sigma'_m)^{0.03}$ term is in the range of 1.4 to 1.5 and can not be ignored. It is clear from this that only a small deviation in the power term of 0.5 can lead to a marked difference in the value of k_2 and by extension shear modulus. By assuming an average value of $(\sigma'_m)^{0.03}$ as 1.45, the value of the equivalent k_2 for the dense Puni sand is 32.0. From Seed et al. (1984b)

$$k_2=20\ ((N_1)_{60})^{1/3} \tag{6.7}$$

For k_2=32, the equivalent dense sand blow count is calculated (from equation 6.7) as 4 blows/ft. for a dense sand. This equivalent blow count is a result that is lower than would be expected. Even for the pumiceous sand that exhibits a higher void ratio and grain crushing potential the expectation would be of a higher blow count for the dense state than 4 blows/ft.

An explanation perhaps lies in a combination of factors. The first is the fact that the Seed et al. equations are empirically based on a database of primarily quartz sands, and there is a margin of scatter in the results that they are derived from. The influence of the pumiceous nature of the sand must also not be overlooked, as particularly higher void ratios would likely lead to lower blow counts that for the equivalent dense quartzitic sands. Investigation of the SPT response of the Puni sand was outside of the scope of this present study, and it remains an important area of further research to quantify this influence. The main conclusion that can be taken from the above results is that the empirical equations are only an indication and may not apply to all sands. If possible insitu or perhaps laboratory experimentation should be used to confirm or reject the empirical results.

Investigation of the Nonlinear Behaviour of the Puni Sand

The form of the constitutive relationship of the dense Puni sand was investigated from results of the cyclic triaxial testing programme fro dense sands. This relationship generally takes the form of secant shear modulus versus induced shear strain, and is generally nonlinear. From the axial load-displacement results of the initial undrained loading curves of the dense samples, the associated shear stress and shear strain may be determined. The shear stresses were determined in the usual way, and the shear strains (γ) were determined from equation 6.8, which is derived from the observation that Poisson's ratio=0.5 for undrained loading.

$$\gamma=1.5\varepsilon \qquad 6.8$$

where ε is the axial strain

The values of shear modulus may then be calculated by shear stress divided by the shear strain. These shear modulus values may then be normalised by the low strain shear modulus determined above from the bender element tests and an overall relationship for the Puni sand may be developed, which is shown in figure 6.16.

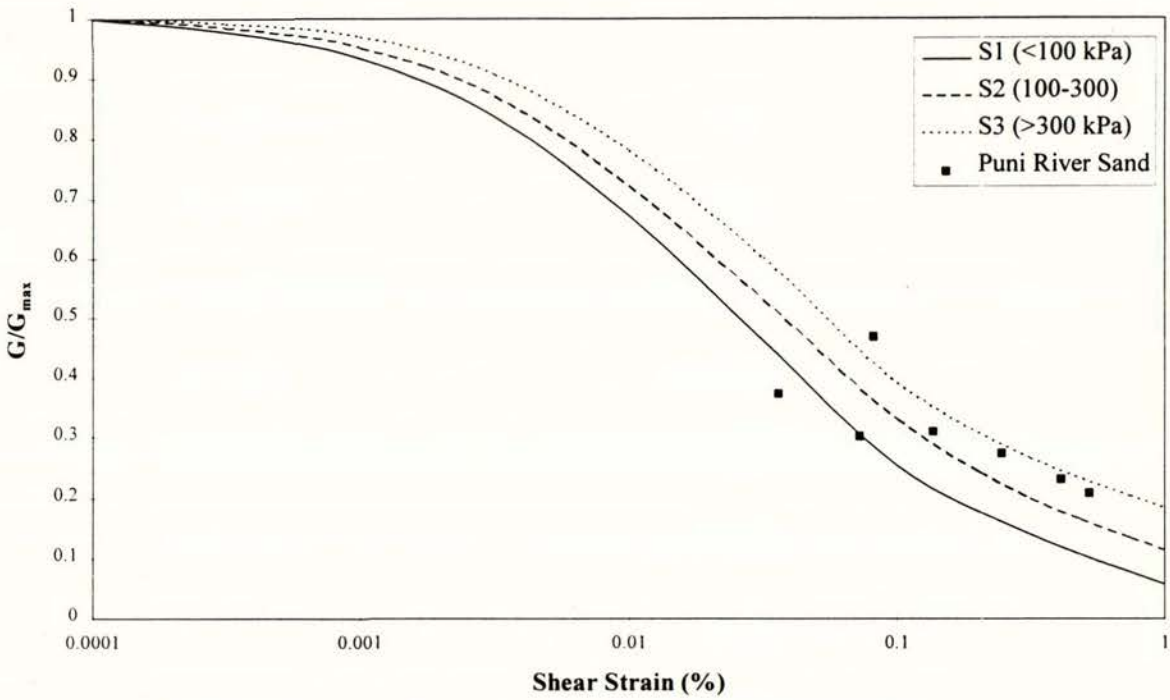

Fig. 6.16 Normalised modulus vs strain relationships (from Seed et al. 1984b) with the Puni sand results overlayed

From the above figure it can be seen that the Puni sand lies generally between the S2 and S3 empirical sand curves. The cyclic triaxial samples were tested at a confining pressure of 100 kPa. The trend of these results is to suggest that the volcanic sand has a less damped, less nonlinear relationship than the general data base, From the cyclic triaxial results, it is not possible to investigate the lower shear strain zone of the curve with accuracy as the induced strains of the triaxial test are too large, and there is a greater margin for compliance errors in the system. The wider scatter of the Puni results seen in figure 6.16 as the shear strains reduce tends to indicate this. Further investigation of the shear modulus behaviour at the lower strain levels is outside the scope of this study, as the resonant column or torsional column tests are more suited to this task. The results presented here do however provide a tentative trend for the higher strain response of the sand.

6.6 SUMMARY

From the literature review it was clear that there is limited data available on both the static and dynamic behaviour of volcanically derived soils. These soils can be characterised as cohesive and non cohesive. The limited work on cohesive soils indicated that their dynamic behaviour is similar to the international empirical data base of soil properties. As no data was available on the non cohesive dynamic soil properties of these soils, a testing programme was undertaken on the pumiceous Puni river sand. An extensive static soil property testing programme had already been done on this sand, so it was an ideal choice for dynamic testing.

Initially the repeatability of the dynamic triaxial test and sample preparation techniques was investigated. The results from this were favourable and the next step was a loose sand dynamic testing programme at a number of stress ratios. The results of this testing conform to the expected shape for both the liquefaction curves and the pore pressure response curves, indicating the pumiceous sand behaves in a similar manner to other sands. Dense sand results also indicated this and showed no grain crushing during liquefaction testing. Permeability and soil classification tests indicated very high void ratios were a feature of this sand, and as a result the permeabilities were high (chapter 9 investigates this further). The shear modulus and non linear behaviour of the dense sand was investigated and some interesting results were found. The nonlinear behaviour of the sand closely followed the accepted results for the given confining pressure, but the widely used empirical low strain shear modulus expressions were found to be questionable when applied to the dense sand.. Standard or Cone penetration testing is required to quantify this difference and was outside the scope of the study.

As a result of the testing programme, it is possible to use some of the experimental results in the numerical section of this study for the response of some volcanically derived soil deposits. This work is presented in the following chapters.

Chapter Seven

The Two Dimensional Response of Cohesive Volcanic Deposits

7.1 INTRODUCTION

The seismic response of cohesive volcanic soil deposits was investigated to determine the influence of the site geometry on the overall response of a two dimensional valley. As most site response studies in New Zealand and overseas are one dimensional, the lateral geometry of the site is assumed to have no influence on the response of the soil deposit to vertically incident seismic waves. It is important to investigate this assumption further, particularly for sites such as narrow valleys where the aspect ratio is low. This chapter presents studies of a number of valley geometries to determine the influence of the lateral dimension.

The influence of non linear soil behaviour is also investigated, especially for large magnitude events. The influence of varying magnitude events on the response of the varying geometries is also presented. Higher magnitude events induce large strains which tend to push the soil deposit response into the strongly non linear range. Both a stiff and relatively soft soil deposit were investigated to gain a greater understanding of the results. In order to isolate the influence of the valley geometry, single frequency harmonic inputs were used for much of the results reported here. These responses are compared to continuum expressions for linear soil behaviour, and deviations from this linear behaviour due to the non linear nature of the soils are investigated. The results of the analyses are presented with the aid of Fourier amplitude spectra, response spectra and a variety of time history plots.

7.2 ALLUVIAL BASIN CONFIGURATIONS

The selection of two dimensional valley shapes was kept simple to isolate the geometrical influence as much as possible. The valley geometries were therefore symmetrical about the central vertical axis, the sides of the basin were 45° and a constant depth was maintained for all of the analyses. Figure 7.1 shows a typical valley geometry, with the depth (D) and width (W) measurements shown.

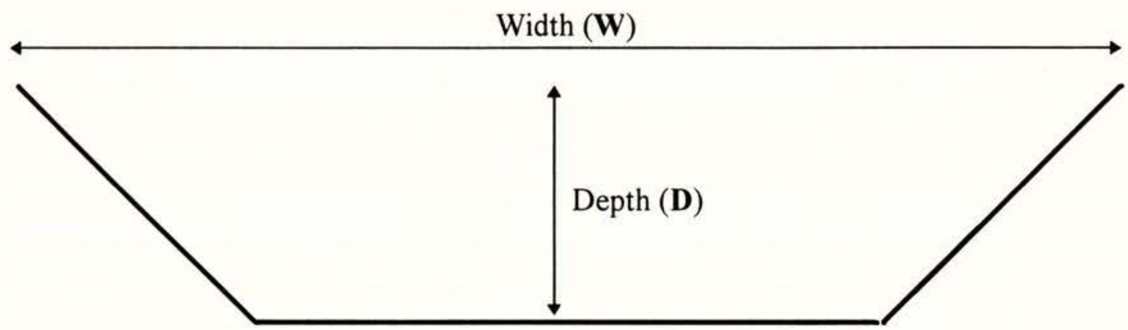

Fig. 7.1 Typical soil basin configuration used in this study

A constant depth of 100m was maintained for all of the analyses, which corresponds to a medium to shallow valley. This figure was chosen as volcanic soil deposits are typically not excessively deep due to the method of their formation. The non linear soil medium filters and scatters the shear waves throughout the valley, and therefore the distance the waves travel through the soil is an important factor in numerical site response analyses. By maintaining a constant and typical depth for each geometry this, variable is eliminated and the geometrical influences may be isolated.

Five different valley geometries were investigated with different width to depth ratios (W/D from figure 7.1). These were W/D ratios of 16, 8, 6, 4 and 2 which correspond to the range of wide to narrow valleys. This wide range of valley widths is important as volcanic deposits tend to be of the infill type, which fill existing structures of a variety of widths. By maintaining a constant depth of 100m the width of each valley geometry was 1600m, 800m, 600m, 400m and 200m respectively. Similarly geometries were used in the effective stress liquefaction studies presented in chapter eight for consistency between the cohesive and noncohesive volcanic soil studies.

7.3 MATERIAL PROPERTIES

From the review of section 6.2, the limited data for cohesive soils of volcanic origin indicated that the dynamic properties followed similar trends to the existing data base of properties in the literature, but unexpected pore pressure generation within these soils due to a sensitive fabric was a feature of both studies. These observations result from only two limited studies at the University of Auckland of a Tauranga ash and ash silts from a site in the Whakarewarewa State Forest. Unfortunately no experimental testing of silts or cohesive volcanic soils was able to be included in this study so the data base is very limited indeed.

As a result of the indications from the available experimental data and the lack of any other evidence, the volcanic soil properties used in this chapter are derived using typical New Zealand soil properties rather than any specific volcanic soil properties. The assumption is therefore that volcanic soils will act under dynamic conditions in a similar manner to other New Zealand soils. The need for this assumption highlights the requirement for more specific investigations of New Zealand volcanic cohesive soils in the future.

For the results presented in this chapter two soil types were investigated. The first corresponded to a stiff cohesive soil, whilst the second was a softer soil. These shall be referred to in the text as the stiff and the soft soil from now on. It was assumed that these soils overlayed a Greywacke bedrock, which is typical in volcanic areas. The soils properties are listed below

Cohesive Soils

The stiff soil was assumed to have a mass density (ρ) of 1700 kg/m^3, and an undrained shear strength (Su) of 100 kPa. The soft soil was assumed to have a similar mass density and half of the undrained shear strength of the stiff soil (50 kPa). From published data (Seed 1979) the low strain shear modulus may be found from the empirical relationship

$$G_{max} = 3000\ S_u \qquad 7.1$$

Therefore

$$v_s = \sqrt{\frac{G_{max}}{\rho}} \qquad 7.2$$

where v_s is the low strain shear wave velocity

Assuming a value of 0.48 for Poisson's ratio, the compressional wave velocity (v_p) of the soils was calculated.

Greywacke Bedrock

A mass density of 2700 kg/m^3 was assumed for the underlying bedrock. A typical value of 3300 m/s was assumed for the shear wave velocity, with the low strain shear modulus being calculated from the rearrangement of equation 7.2

$$G_{max} = \rho V_s^2 \qquad 7.3$$

By assuming a Poisson's ratio of 0.3 for the rock, the compressional wave velocity was again calculated for the rock. A summary of the material properties used in this chapter are given in table 7.1

Table 7.1 Summary of the material properties used in the analyses

Material Property	Stiff Soil	Soft Soil	Bedrock
S_u (kPa)	100.0	50.0	N/A
ρ (kg/m^3)	1700.0	1700.0	2600.0
v_s (m/s)	400.0	200.0	3300.0
v_p (m/s)	2080.0	1040.0	6900.0

For simplicity these soil properties were assumed to be constant throughout the soil deposit, which isolates the influence of the basin geometry. The form of the non linear soil relationship was taken to be the C1 curve of the family of curves for cohesive soils (Sun et al. 1988) which corresponds to a relatively low plasticity soil. This C1 curve was modelled by using a modified hyperbolic expression within the computer program. Both soils were modelled with the same C1 curve to allow an exact comparison, although in reality the softer soil would most likely have a higher plasticity index and hence a slightly less pronounced non linear response.

7.4 INPUT MOTIONS

Most of the analyses presented in this chapter involved vertically incident harmonic motions of constant frequency and peak amplitude throughout the 20 second excitation period. This was done to isolate the response of the soil deposit to each frequency individually. A general understanding could then be built up for the response of the deposit geometry to a wide range of input frequencies. Each source motion time history was calculated from the equation

$$a(t)=A \sin(\omega t) \tag{7.4}$$

and

$$\omega = \frac{2\pi}{T} \tag{7.5}$$

where T is the period of the input motion

A is the peak acceleration amplitude of the motion

A constant peak acceleration was used for each frequency mainly for clarity of the results as many analyses in engineering practise relate to acceleration and force magnitudes rather than velocity magnitudes. From the mean value theorem and integrating the acceleration time history expression (7.4), the peak acceleration value A corresponds to an average or mean acceleration magnitude of 0.637A. A constant peak acceleration for each frequency does not imply constant peak velocity however as may be seen from the following.

$$\begin{aligned} v(t) &= \int a(t)dt \\ v(t) &= \int A\sin(\omega t)dt \\ v(t) &= -\frac{A}{\omega}\cos(\omega t) \end{aligned} \tag{7.6}$$

It can be seen from equation 7.6 that as the angular frequency of the input motion decreases (increasing period) the peak velocity (and mean velocity) will also increase.

The second component of the studies presented in this chapter is the influence of the non linear soil properties. This was investigated by increasing the peak acceleration magnitude of the harmonic input motions in careful steps to induce larger strains in the soils and hence push the response further into the non linear range. Finally a brief investigation of the response of each geometry subjected to the Old Castaic Ridge Route Station motion (recorded during the 1971 San Fernando earthquake) was carried out illustrate the earlier findings when applied to a real earthquake motion.

7.5 DETAILED RESPONSE OF THE WIDE VALLEY GEOMETRY

Marsh and Larkin (1991) showed that the centre of an 8:1 valley responds in a similar manner to a one dimensional solution using the same properties, the inference being that the lateral boundaries are not influential for this and greater aspect ratio valleys. This valley geometry was therefore analysed in detail to ascertain the characteristics of the computer program and the non linear soil behaviour before investigating the other narrower geometries. Both the stiff and soft soils were investigated. An extension of these non linear studies was a brief investigation of the reliability of using small tremor and even micro tremor data for the calculation of the natural periods of a site, and then using those same results for calculating the large magnitude response.

7.5.1 Response of the Volcanic Soil Deposit to Small Harmonic Source Motions

The smallest harmonic source motion used was a sine wave with a peak acceleration amplitude of 0.05 m/s^2 ($\approx$0.005g). This value was considered to be reasonable for the simulation of small motions and a relatively elastic response. The range of frequency inputs for the source motions was from frequencies of 10 Hz to 0.2 Hz (periods of 0.1 to 5.0 seconds) at 0.1 second period intervals

Stiff Soil Deposit

The stiff soil deposit was subjected to each single frequency harmonic source motion in turn for a duration of 20 seconds, and the combined response of the 8:1 valley was computed. The results of the peak acceleration ratios at the center and at the 1/4 and 3/4 points of the valley surface are shown in figure 7.2. The peak acceleration ratio was calculated by normalising the peak accelerations at the half and quarter points on the valley surface by the magnitude of the peak input acceleration (0.05 m/s^2 in this case). Thus the vertical axis gives an amplification ratio for the valley at each input frequency.

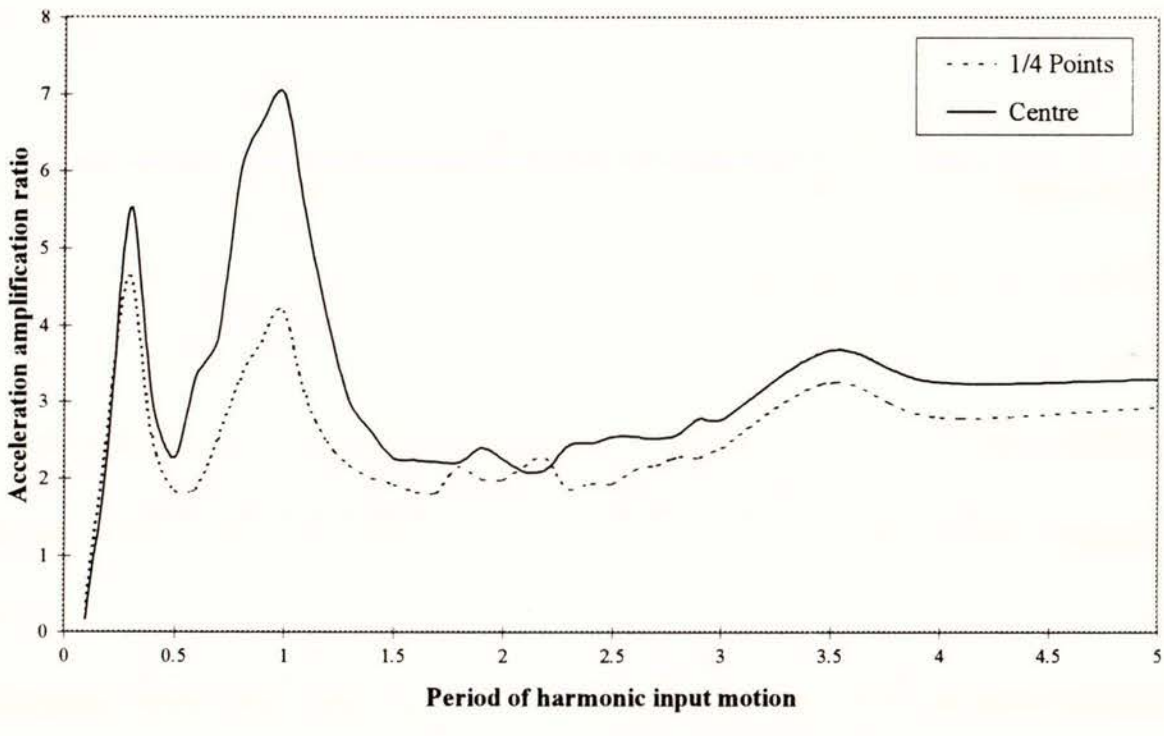

Fig. 7.2 Numerical response of the 8:1 stiff valley to different frequency source motions

It is clear from figure 7.2 that the first two natural modes of vibration of the stiff soil valley at centres about 1 second and 0.3-0.4 seconds. These periods show acceleration amplification factors in the range of 5-7, which are not unexpected for the small magnitude of the input acceleration. The soil deposit is behaving relatively elastically (but not totally so) at these motions and therefore the damping is not high. Haskell (1960) developed the following expression for an elastic system to calculate the amplification factor of surface displacements in one dimension.

$$A = \frac{2}{\sqrt{\cos^2\left(\frac{\omega H}{v_s}\right) + \left(\frac{G v_s^{/}}{G^{/} v_s}\right)^2 \sin^2\left(\frac{\omega H}{v_s}\right)}} \qquad 7.7$$

where the primed quantities denote bedrock

The displacement amplification factors from this equation for the same range of source motion periods of figure 7.2 are shown in figure 7.3

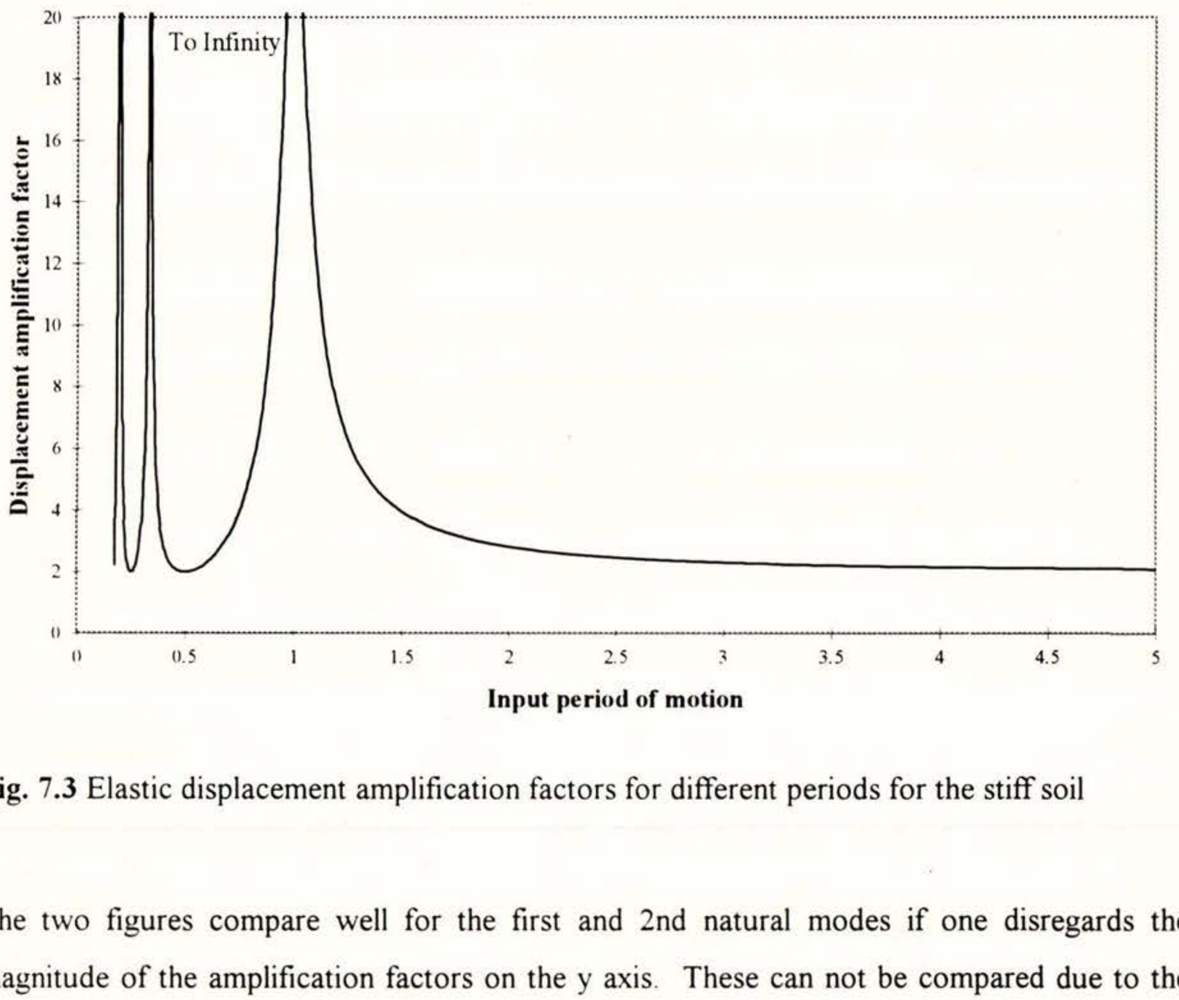

Fig. 7.3 Elastic displacement amplification factors for different periods for the stiff soil

The two figures compare well for the first and 2nd natural modes if one disregards the magnitude of the amplification factors on the y axis. These can not be compared due to the fact that the Haskell expression contains not material damping, and therefore there is an infinite displacement amplification response at the natural periods. The most interesting conclusion from the comparison of the two figures is that it indicates the computer program is giving correct answers when compared to continuum expressions for small magnitudes. The comparison between the one dimensional continuum and the two dimensional numerical solutions are valid as the high (8:1) geometry allows the valley to respond as essentially an one dimensional system at the centre. The model is unable to pick up the natural periods beyond the second due to the relatively large size of the spatial discretisation of the and soil deposit.

The maxima of Haskell's expression correspond to the natural periods of that elastic system. Differentiating 7.7 and setting the differential to zero, the following expression was gained for the natural periods of a one dimensional system.

$$T = \frac{1}{(2n-1)} \frac{4H}{v_s} \qquad 7.8$$

where n is the period number; n=1..∞

For the stiff soil the following table shows the periods calculated for the 100m deep deposit from equation 7.8 and the periods of peak response from figure 7.2

Table 7.2 Natural periods for the stiff soil from theoretical and numerical results

Mode number (n)	Theoretical period (s)	Numerical period (s)
1	1.0	1.0
2	0.3333	0.3
3	0 2	N/A

Figure 7.2 shows higher amplification factors in the longer period range than the elastic expression. This is due to the fact that induced strains are a function of velocity magnitudes calculated at the internal nodes, so by assuming a constant peak acceleration input motion the magnitude of the velocity input increases for these longer period motions. As the magnitude of the velocity input is higher the peak surface acceleration are also higher. The amplification factors show in figure 7.2 are normalised by the peak acceleration, hence the results show a higher value in the long periods.

Figure 7.2 also shows the peak surface acceleration response of the valley at the 1/4 and 3/4 points. There is only one quarter point line drawn on the graph as the results were the same for each side. These quarter points show the same natural period response as the central point, although the magnitudes of the response are less. This indicates that the wide two dimensional geometry has little effect for relatively elastic motions on the characteristics of the site, but tends to more highly damp the motion. This may be due to the closer proximity of the quarter points to the edges of the valley system where the transmitting boundary allows the lateral transmission of some energy back into the surrounding bedrock. Further investigation of the overall surface response of the valley to the small magnitude harmonic event are shown below.

Further investigation of the 8:1 valley geometry was then undertaken once it was established that reliable results were being obtained for the small magnitude event. The main area of interest was the surface motions and the lateral spatial response of the valley to the input motions. The wide valley was therefore subjected to a 20 second harmonic input motion of 1 Hz, which corresponded to the 1st mode low strain frequency. This input frequency was chosen so as to initiate a characteristic resonant type response. Surface acceleration Fourier and response spectra for the surface node points were calculated and are given below.

Both of the following spectra show a large excitation across the valley at a period of 1 second, which corresponds to the period of the input motion and the natural period of the site. For the small 0.05 m/s^2 peak input acceleration, the peak spectral acceleration (figure 7.4) at the 1 second period is 2.5 m/s^2 which is a very large magnification at that period. Even though the results of Larkin and Marsh (1991) clearly showed that the centre of the 8:1 valley is equivalent to a one dimensional analysis, the above figures indicate that the central valley response may be different, particularly in magnitude, that that at other points on the valley surface. This attenuation of the magnitudes of the spectral response closer to the valley boundaries is because of the lateral loss of energy into the surrounding bedrock (through radiation), which is the most dominant form of damping in the soil system at these long period small magnitude motions the shear strain magnitudes through the deposit are a result of the imposition of zero shear strain at the surface boundary condition.

Soft Soil Deposit

A similar investigation was carried out on the equivalent soft soil deposit, which was a softer volcanic soil with an average shear wave velocity of 200 m/s throughout. Single frequency low magnitude harmonic input motions were again used to investigate the peak responses of the wide valley to each separate frequency. This was done to confirm the trends shown in the section above for a different soil condition. Figure 7.7 shows the peak surface acceleration ratios for the soft valley, clearly showing the periods of peak response.

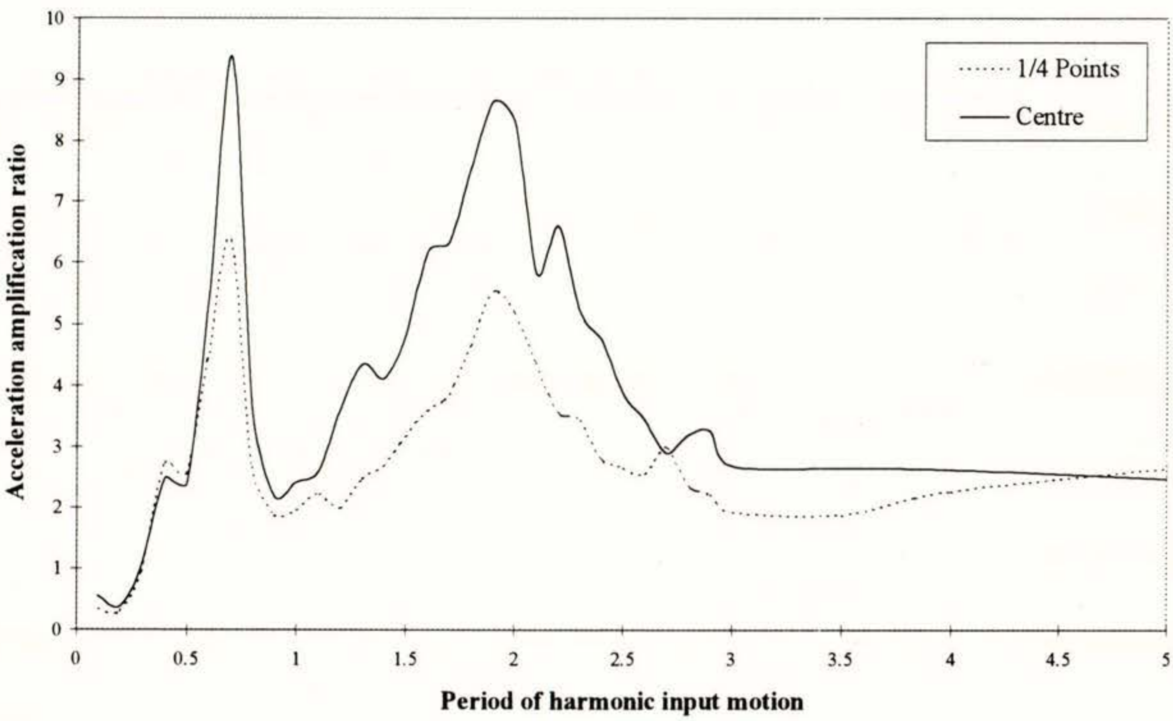

Fig. 7.7 Numerical response of the 8:1 soft valley to different frequency source motions

When compared to the closed form solution of Haskell (figure 7.8), it is clear that the results for the softer valley follow the same trends. A halving of the shear wave velocity produces a doubling of the natural periods of the site. This trend is followed in the numerical results shown in figure 7.7. Table 7.3 compares the closed form and numerical solutions and shows very good agreement for the wide two dimensional valley. Once again the magnitude of the response at the 1/4 and 3/4 points across the valley surface is less than at the centre, with the percentage reduction very similar to that of the stiff deposit (figure 7.2).

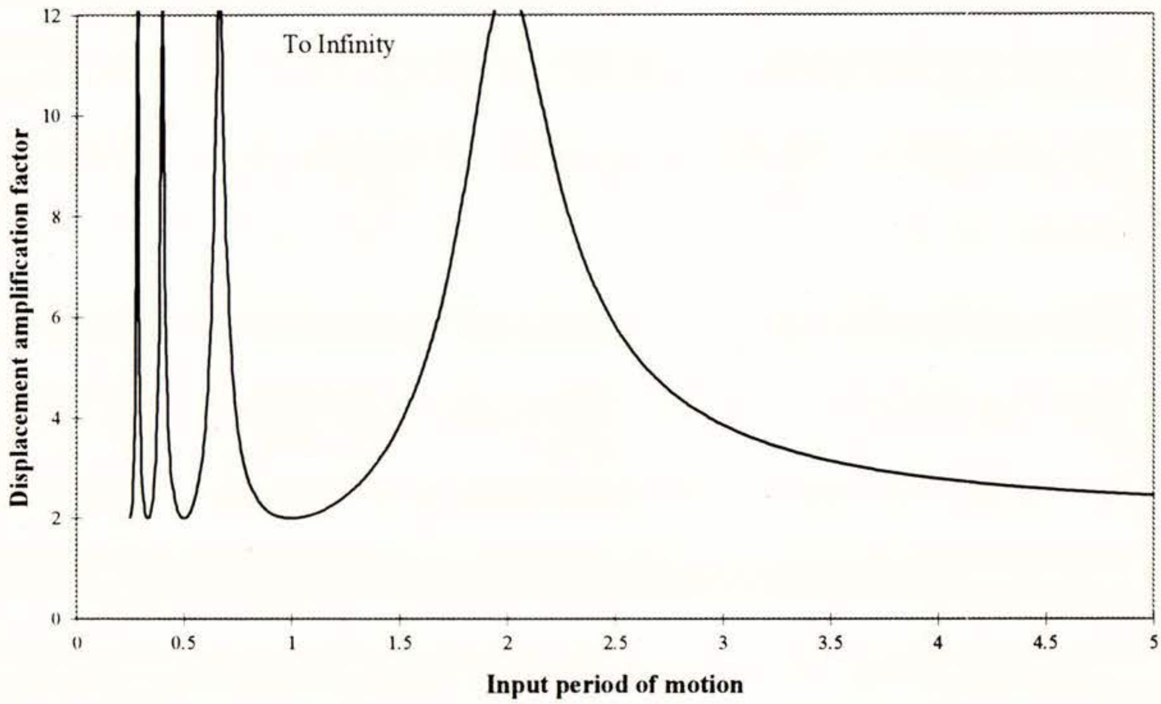

Fig. 7.8 Haskell's expression for the response of the soft cohesive deposit

Table 7.3 First three natural modes for the soft soil

Mode number (n)	Theoretical period (s)	Numerical period (s)
1	2.0	2.0
2	0.666	0.6-0.7
3	0 4	N/A

The soft site was then investigated further by subjecting it to single frequency harmonic motions and analysing in detail the response. Initially the source motion was a 1 Hz sine wave of 20 seconds duration, the surface spectra for which may be seen in figure 7.9. As expected there was very little amplification of the source motion, with only a small response in the spectra at 1 second. This contrasts sharply with the stiff deposit result of figure 7.4 for the same input motion. It is clear that input motions that do not generally correspond to the natural periods of the site are not amplified to any extent.

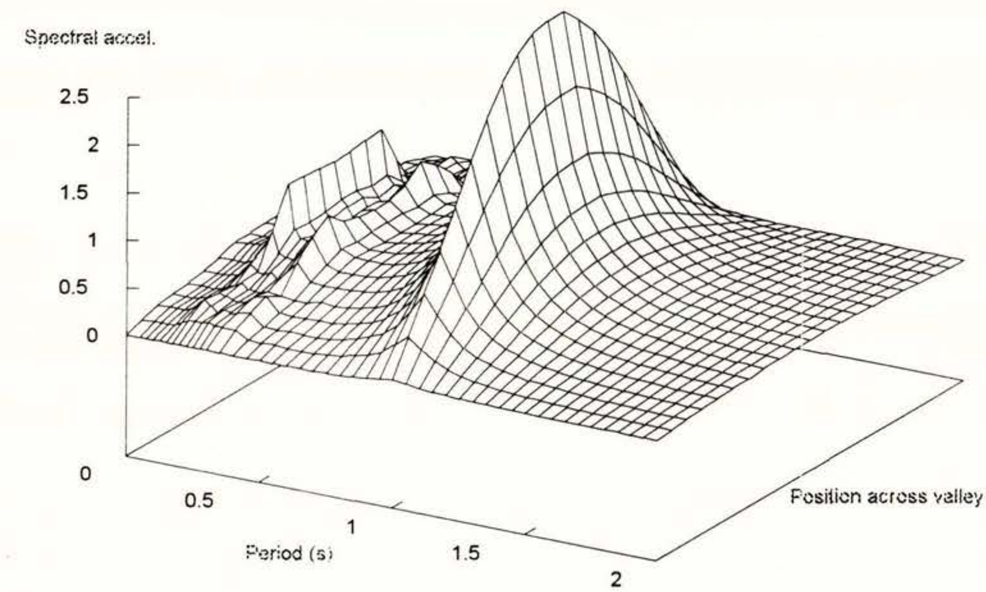

Fig. 7.4 Response spectra across the valley for the 1 second period harmonic input

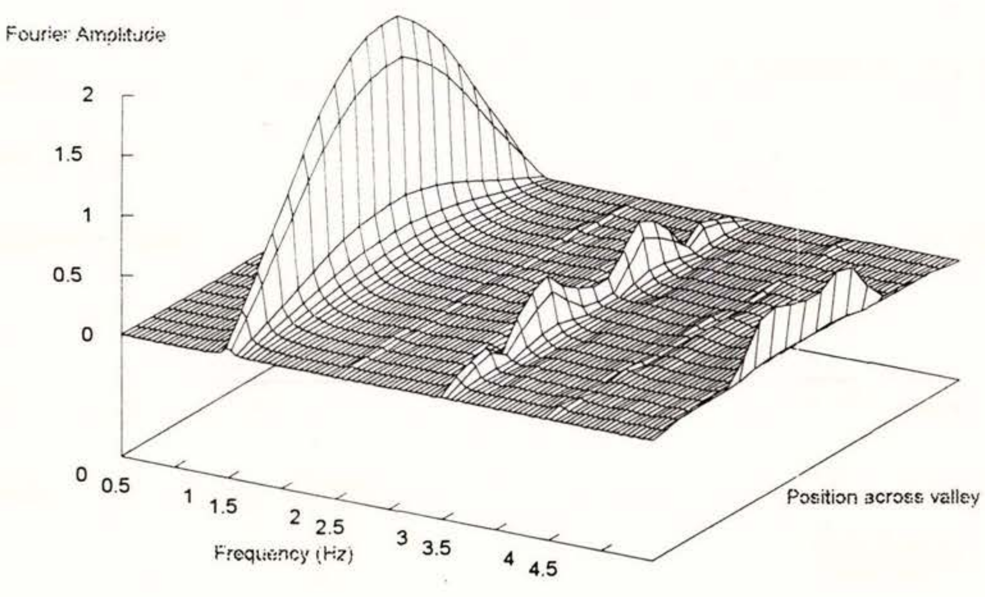

Fig. 7.5 Fourier amplitude spectra across the valley for the 1 second period harmonic input

The minimal material damping within the soil deposit can be quantified by investigating the levels of induced shear strain at the centre of the valley, which are shown in figure 7.6. The centre of the valley was selected as this is the region that the radiation damping will be at a minimum, and therefore the damping is material and hysteretic.

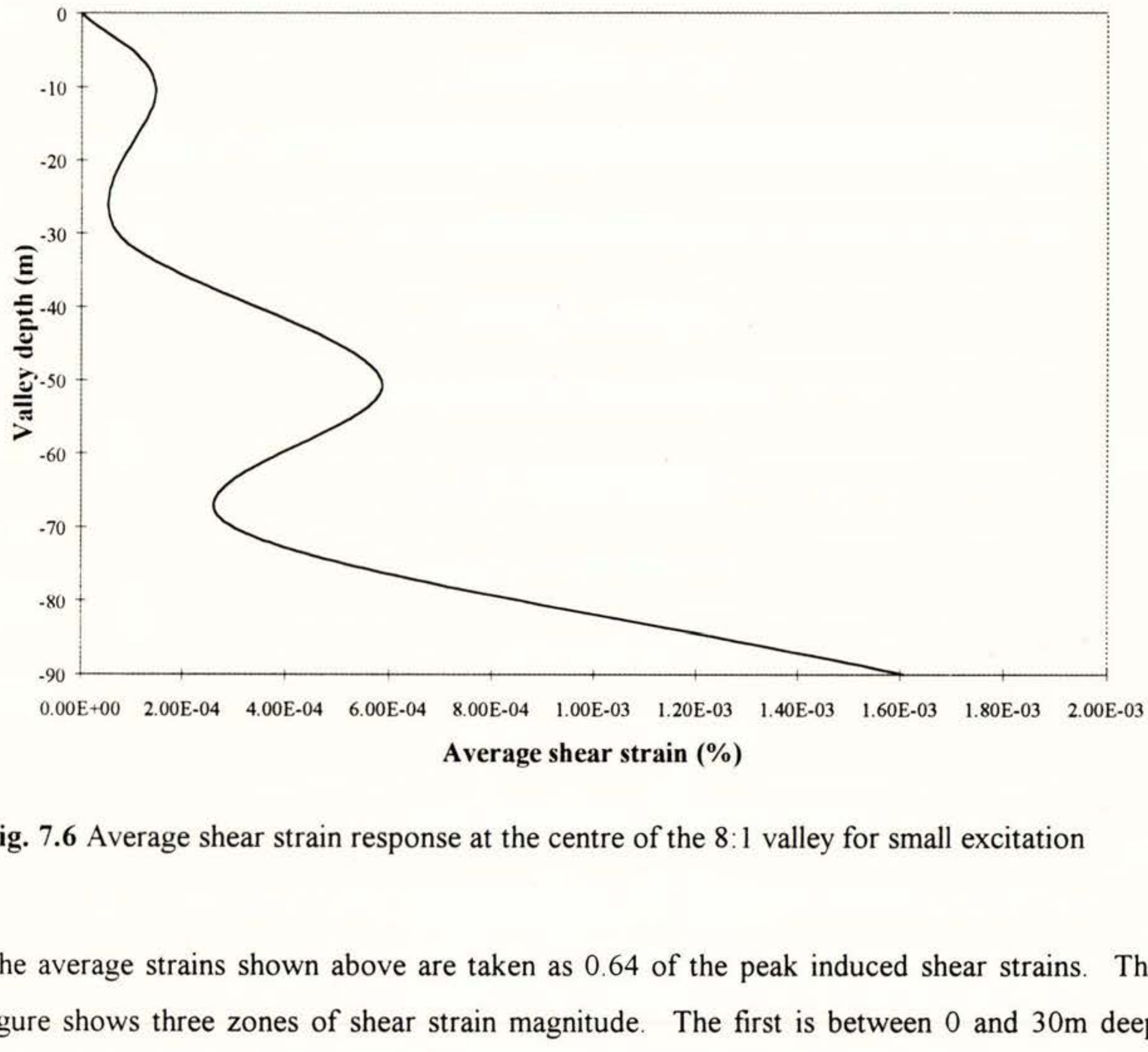

Fig. 7.6 Average shear strain response at the centre of the 8:1 valley for small excitation

The average strains shown above are taken as 0.64 of the peak induced shear strains. This figure shows three zones of shear strain magnitude. The first is between 0 and 30m deep, where the strains are small ($1*10^{-4}$ %) and relatively constant.. The second zone is between 40 and 70m ($4*10^{-4}$ %), and the third is between 70 and 100m deep, where there is a large shear strain gradient. For the C1 non linear curve used in these analysis, induced shear strains in the first zone correspond to a G/G_{max} ratio of 1.0 which is linear for that strain range. The second zone experiences some material damping (G/G_{max}=0.98) and the final zone has the highest level of damping (G/G_{max}=0.95). These correspond to equivalent viscous damping factors in the range of 0-2%. The effect of these damping levels are very minimal and therefore the analysis can be considered as elastic for these small levels of input motion. The attenuation of

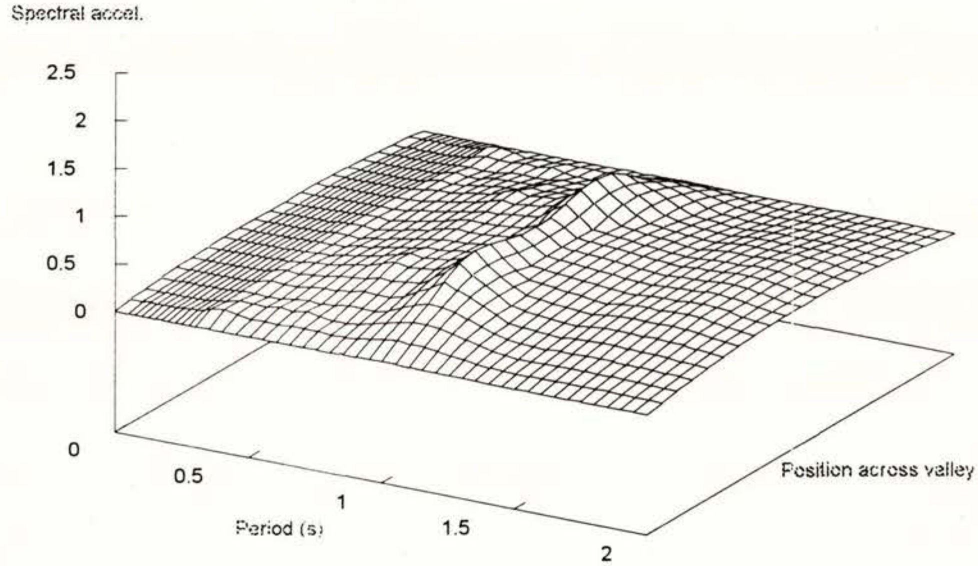

Fig. 7.9 Response of the soft site to the same 1 Hz input motion as figure 7.4

Figures 7.10 and 7.11 show both surface acceleration and Fourier response spectra for a 0.5 Hz (2 second period) input harmonic, which corresponds to the first natural period of the soft soil deposit. Once again there is a very strong response at this period in the surface spectra. There is also an excitation of the higher modes, which was also evident in the stiff site but to a lesser extent. This is due to the difficulty of accurately representing the high frequency motion with the relatively large numerical spatial discretisation of the soil deposit. The frequencies of the higher modes of the stiff site are double in value those of the soft site and tend to fall within the high frequency zone. Once again the strongest response of the valley is at the centre, with the same decreasing response near the edges of the valley as was seen before.

The results presented above allowed an insight into the response of a typically wide volcanic soil deposit to very small motions.. The use of single frequency harmonic input motions allowed the response of the valley to each frequency to be isolated in turn. These results showed that the generally accepted analytical expressions (equation 7.8) of determining the natural response frequencies of one dimensional systems could be applied to the wide two dimensional valley.

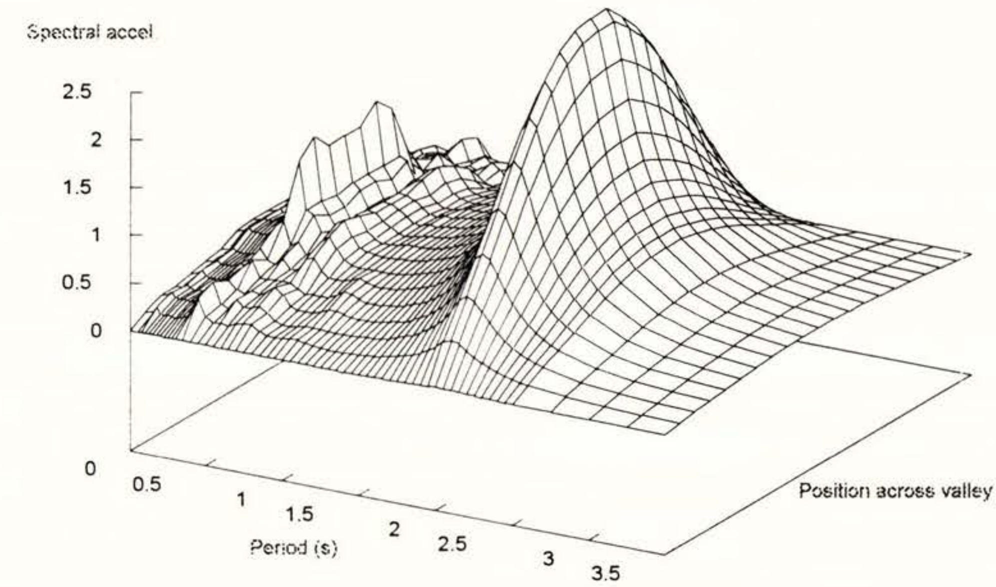

Fig. 7.10 Acceleration response spectra of the soft site to the 2 second period harmonic input

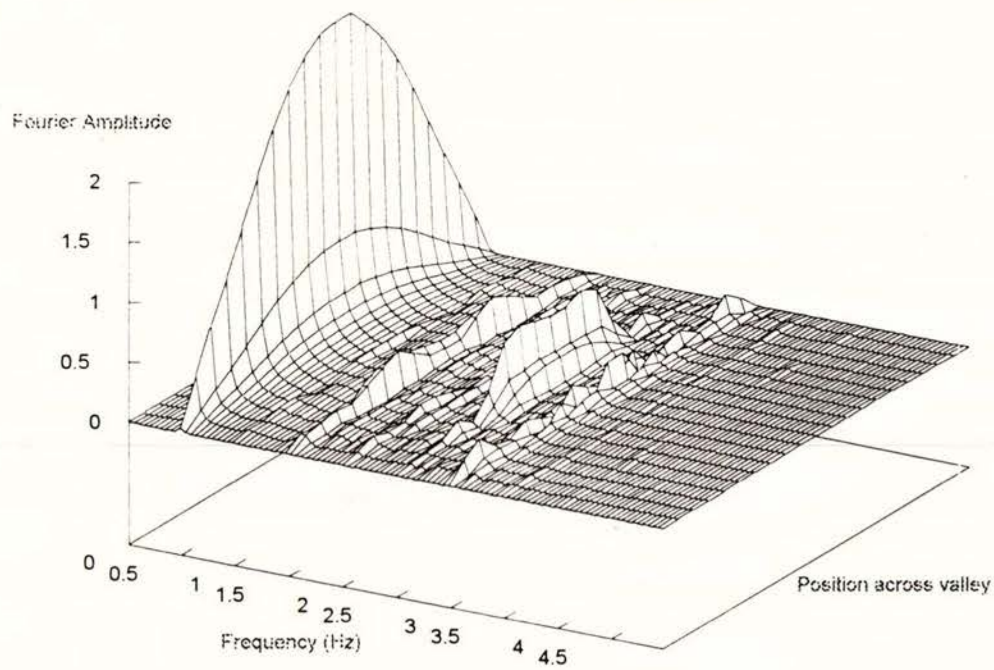

Fig. 7.11 Fourier amplitude response of the soft site to the 2 second period harmonic input

One thing to note in the results is that the natural periods are not just distinct point values, but may be considered as a period bandwidth in which there is an elevated response. The magnitude of this response peaks at a certain period, which is the value quoted in the text as the natural period, but in all of the results seen above there is a definite bandwidth of periods surrounding the peak value. The bandwidth was noticeably larger for the softer longer period site than the stiff site, but in all cases the peak response period corresponded to the traditional expression (7.8). The results also highlighted how dominant the natural frequencies are in the resulting surface response.

Once these characteristics of the wide valley response had been established, the influence of the geometry of the seismic response of the soil basin was investigated, The results of this are given in the following sections.

7.6 INFLUENCE OF BASIN GEOMETRY ON THE RESPONSE

The basin geometry of a two dimensional valley can be an important factor in seismic response studies. The main factor in the two dimensional geometry is the lateral boundaries, which tend to both reflect and dissipate (through the transmitting boundary) the internal wave energy of the soil deposit. This reflection and dissipation can alter the fundamental seismic response of the valley. Simple valley geometries were used in this investigation, and the influence of non linear soil properties were minimised in an attempt to isolate the geometrical influence.

The response of four different basin geometries was investigated using the same depth and soil properties as for the indepth 8:1 valley study above. The four different geometries were the narrower 6:1, 4:1 and 2:1 basins, and one larger 16:1 aspect ratio basin. The sides of the valley were again modelled at 45°. Each basin was investigated for both the stiff and soft soil deposits as explained in section 7.5, and the source input motion was the same low magnitude harmonic previously described. Once again the valleys were subjected to each single frequency harmonic motion for a duration of 20 seconds. This system of input motions isolates the frequencies of peak response of the soil deposit, and hence it is clearly seen how these responses change with different basin geometries. A summary of the important results for each valley geometry shall be presented below, with conclusions drawn as to the influence of the lateral boundaries in the overall response of the valley for small magnitude events.

7.6.1 Results for Various Basin Geometries

Medium Aspect Ratio (6:1) Basin

Figures 7.12 and 7.13 show the peak acceleration amplification ratios for the stiff and soft sites respectively. These figures clearly indicate the periods of peak response, and indicate a reduction in the peak response natural period from the 8:1 basin for both soil types. The peak response periods for this geometry are summarised in table 7.3.

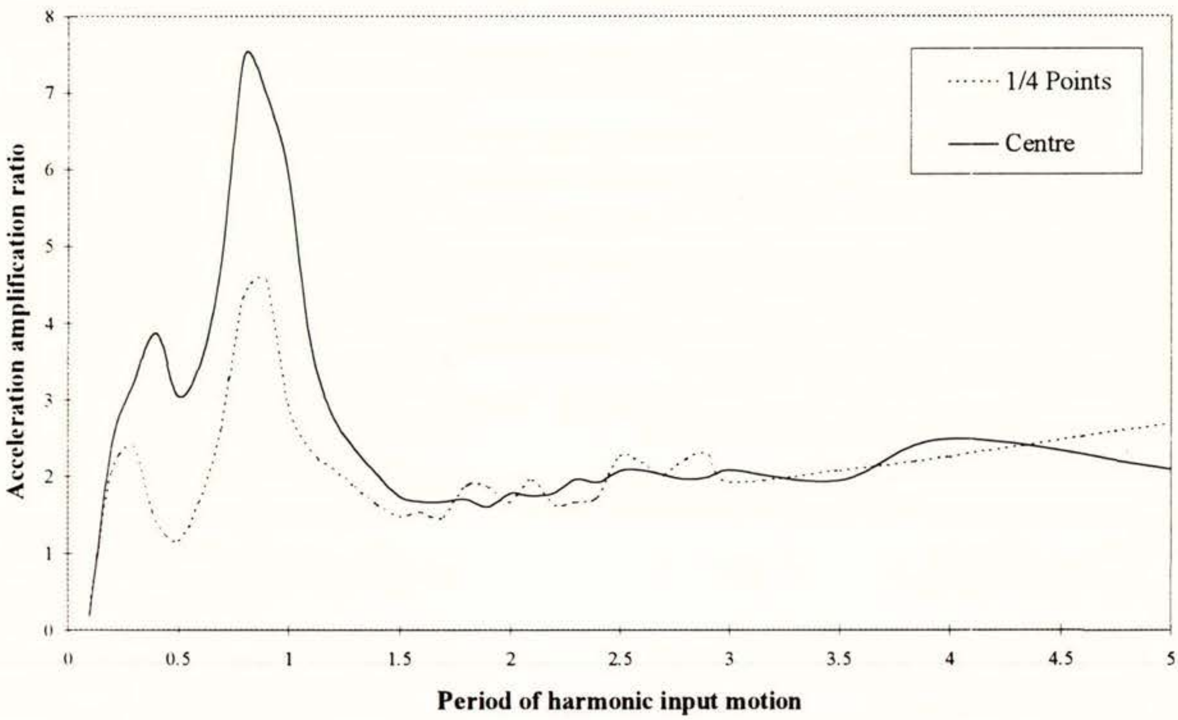

Fig. 7.12 Numerical response of the 6:1 stiff valley to different frequency harmonic motions

Table 7.3 Peak response periods for the stiff and soft 6:1 geometry

Mode number	Stiff Site	Soft Site
1	0.8 seconds	1.75 seconds
2	0.4 seconds	0.7 seconds

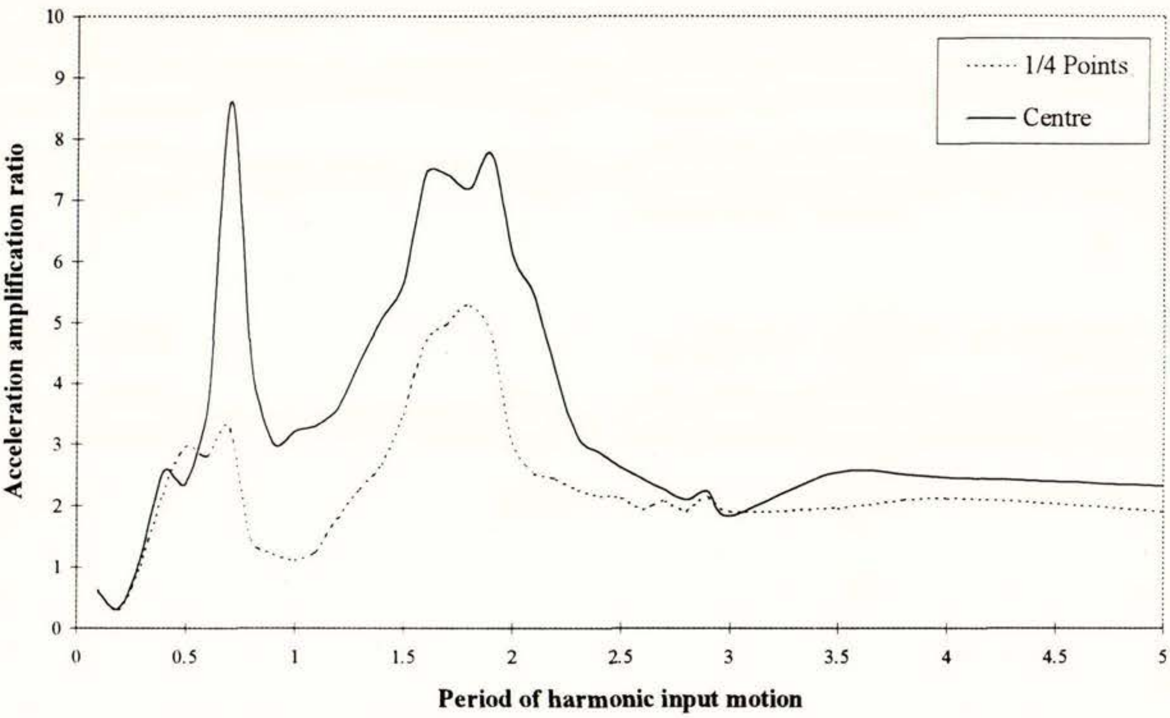

Fig. 7.13 Numerical response of the 6:1 soft valley to different frequency harmonic motions

Narrow Aspect Ratio (4:1) Basin

The results for a relatively narrow aspect ratio valley for both soil types are shown in figures 7.14 and 7.15. They show a further reduction in the peak response periods from the 6:1 valley

Very Narrow Aspect Ratio (2:1) Basin

This aspect ratio represents a very narrow basin geometry, which is the shape of an inverted triangle shape. The peak acceleration ratio results shown in figures 7.16 and 7.17 are only plotted at the centre of this valley.

These results again show a further reduction in the natural periods of the site due to the increased confining influence of the lateral boundaries. The higher modes of the stiff site are not visible in figure 7.17 due to the loss of high frequency motion from the spatial discretisation.

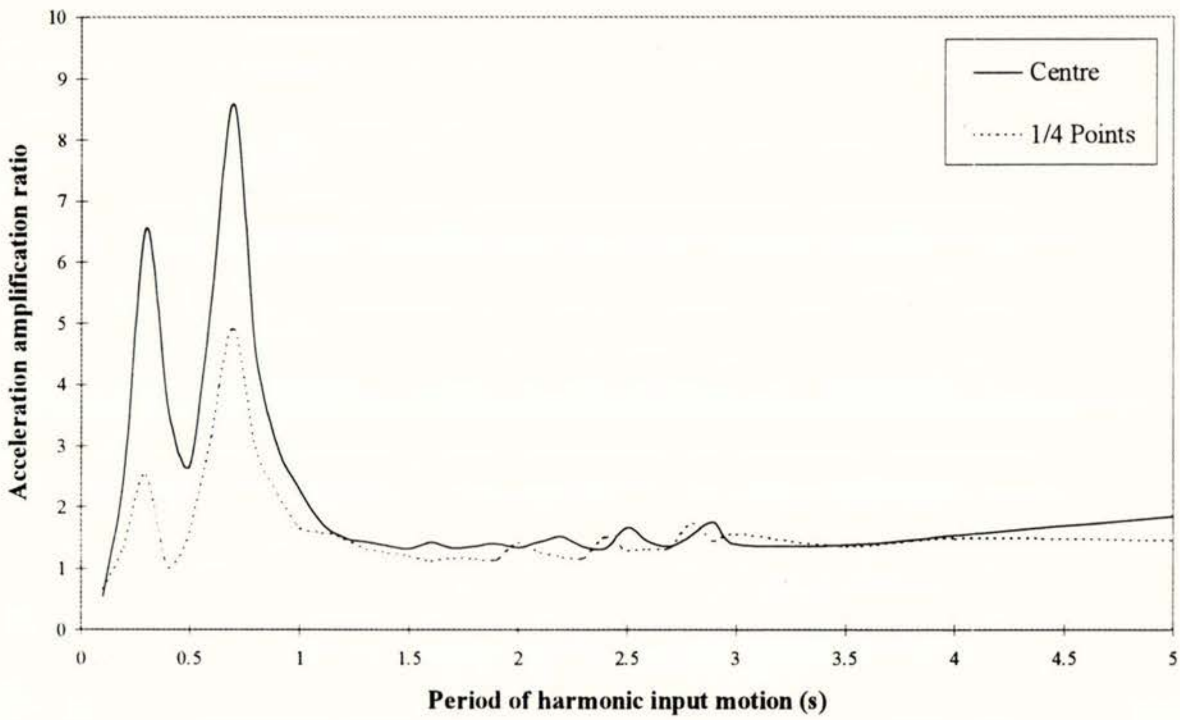

Fig. 7.14 Numerical response of the 4:1 stiff valley to different frequency harmonic motions

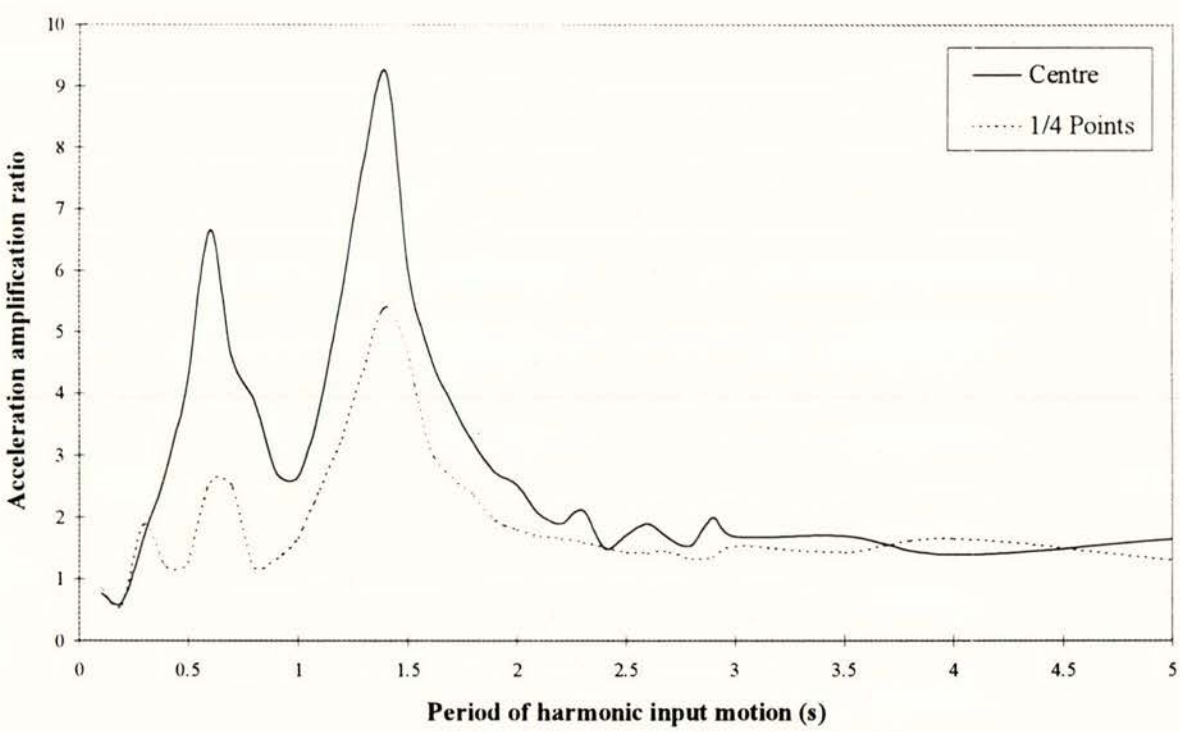

Fig. 7.15 Numerical response of the 4:1 soft valley to different frequency harmonic motions

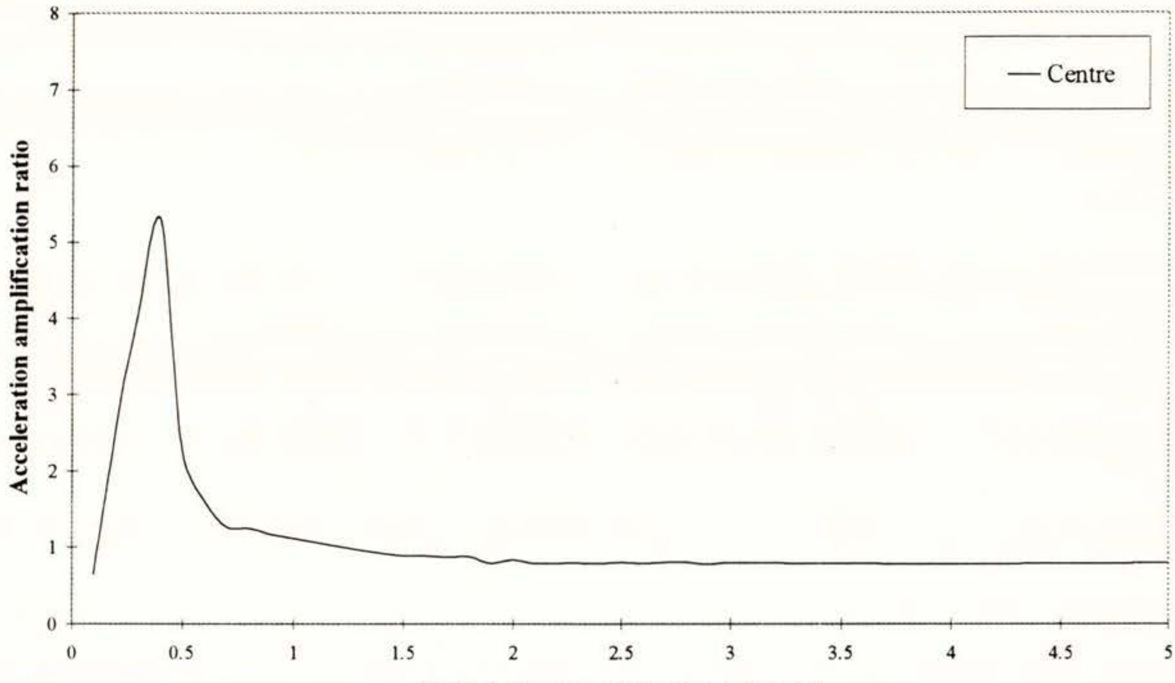

Fig. 7.16 Numerical response of the 2:1 stiff valley to different frequency harmonic motions

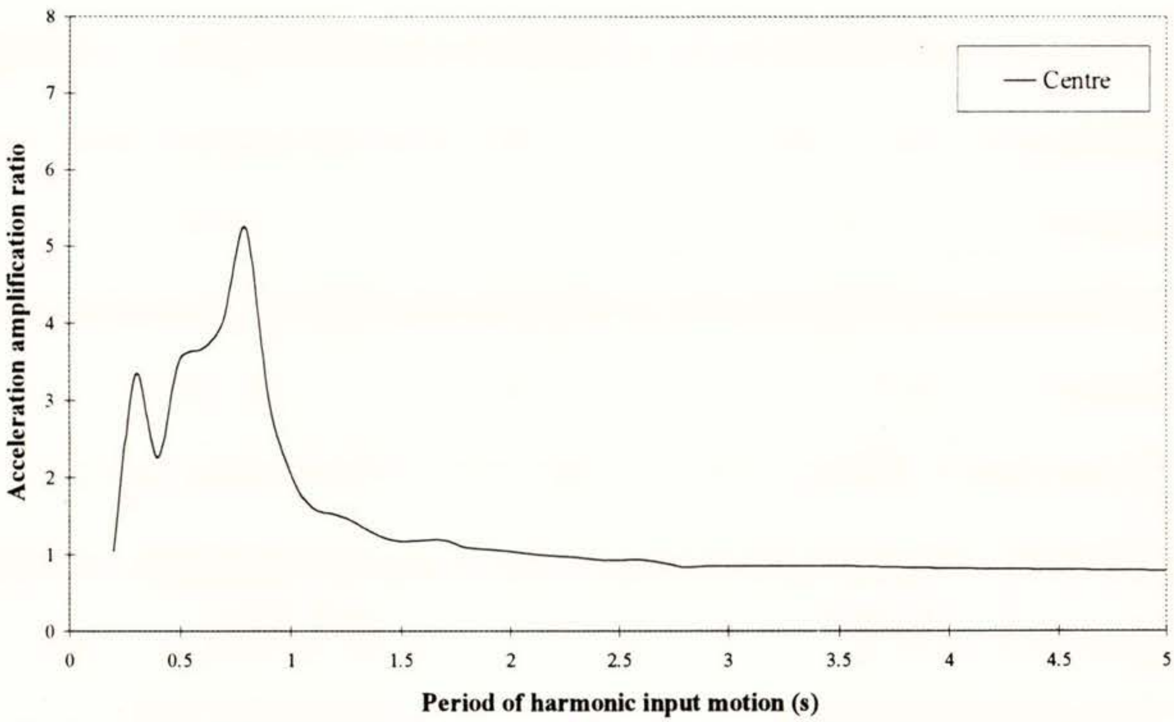

Fig. 7.17 Numerical response of the 2:1 soft valley to different frequency harmonic motions

Very Wide Aspect Ratio (16:1) Basin

Finally a very wide valley was analysed, with the results shown in figures 7.18 and 7.19 for the stiff and soft site respectively.

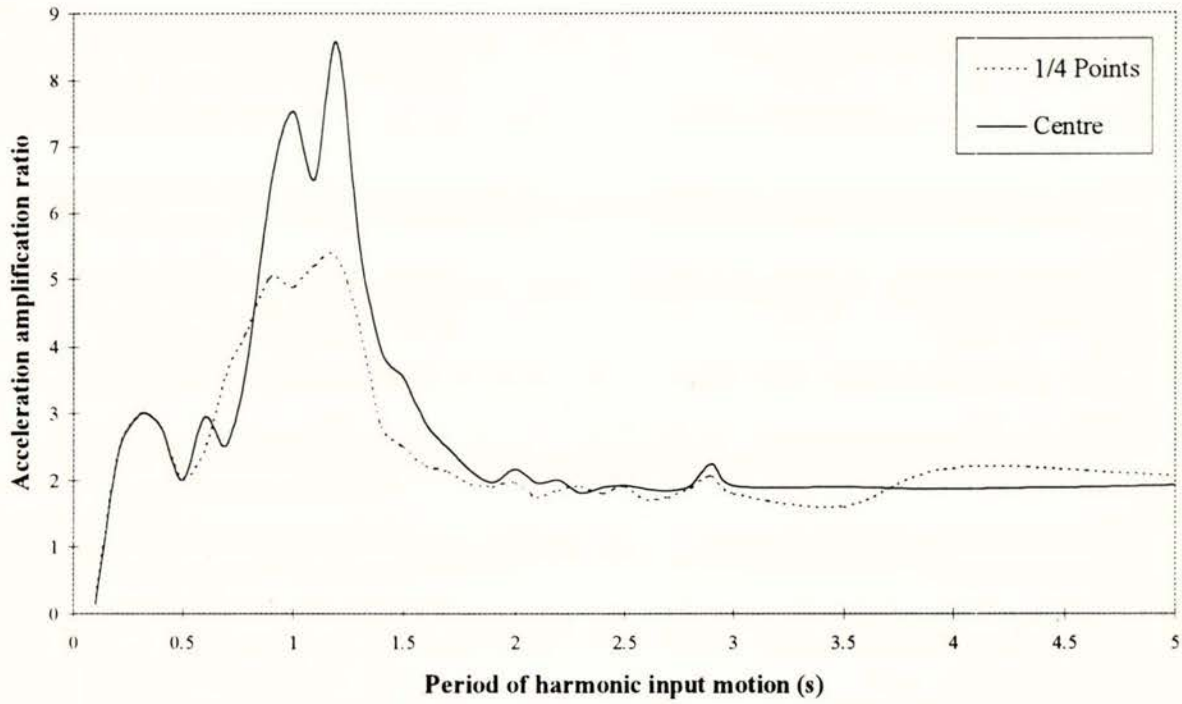

Fig. 7.18 Numerical response of the 16:1 stiff valley to different frequency harmonic motions

Both of these results indicate a slight lengthening of the peak response periods. This suggests that the 8:1 valley may not be quite sufficiently wide to totally ignore the influence of the lateral boundaries, even though most of the results of closed form solutions and one and two dimensional comparisons (Larkin and Marsh 1991, Marks and Larkin 1995) indicate this to be the case. This is a minor point however as the lengthening of the natural periods in the very wide valley are relatively small.

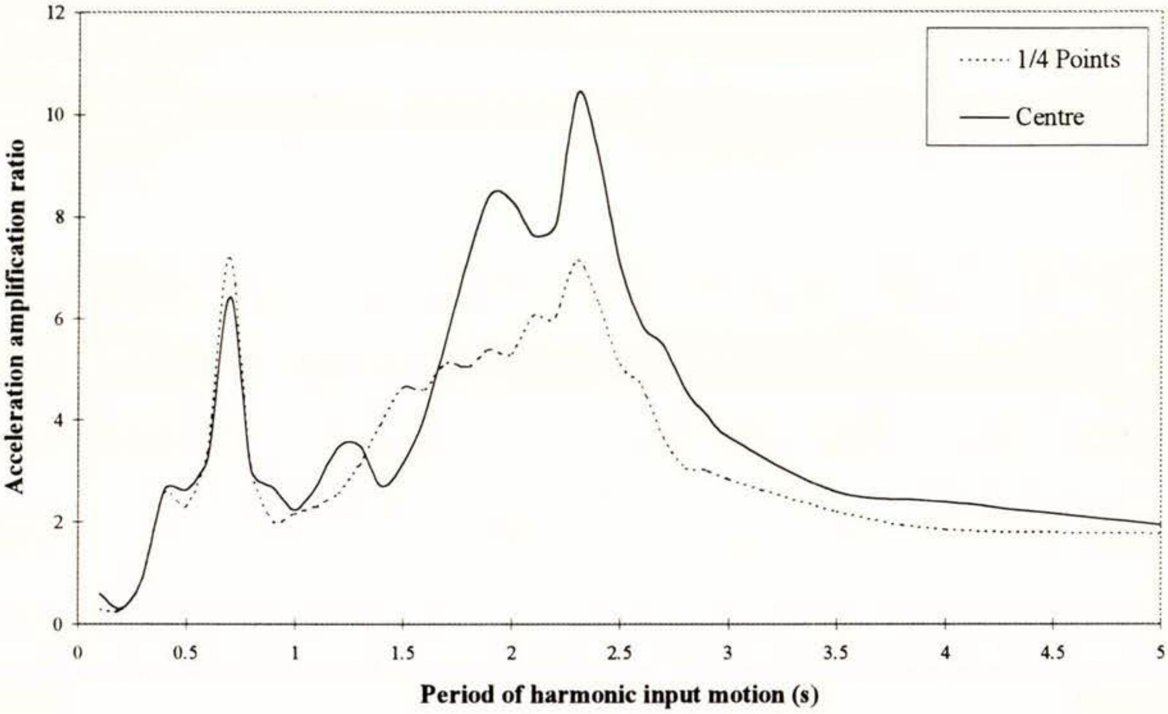

Fig. 7.19 Numerical response of the 16:1 soft valley to different frequency harmonic motions

7.6.2 Summary of the Influence of Valley Geometry

In summary, it is clear from the above results that the main influence of a changing geometry is that it alters the peak response natural periods of the soil deposit. For the simple geometries studied, there is a clearly defined trend that has the natural periods of each site decreasing with decreasing aspect ratio. As the depth for each case was kept constant at 100 metres the changes observed can only be from the closing in of the lateral boundaries. This trend was evident for both the stiff and soft soil, as is evident in figures 7.20 and 7.21 respectively.

The trends of both the stiff and soft soils are similar, with a marked plateau at aspect ratios higher than 8:1. A relatively smooth relationship exists between the 8:1 and 2:1 ratios, which graphically shows the influence of the narrowing lateral boundaries. The results were interpolated past the smallest 2:1 aspect ratio to add completeness to both graphs, although the second modes of the stiff soil (figure 7.20) were not due to the lack of a result for the 2:1 aspect ratio.

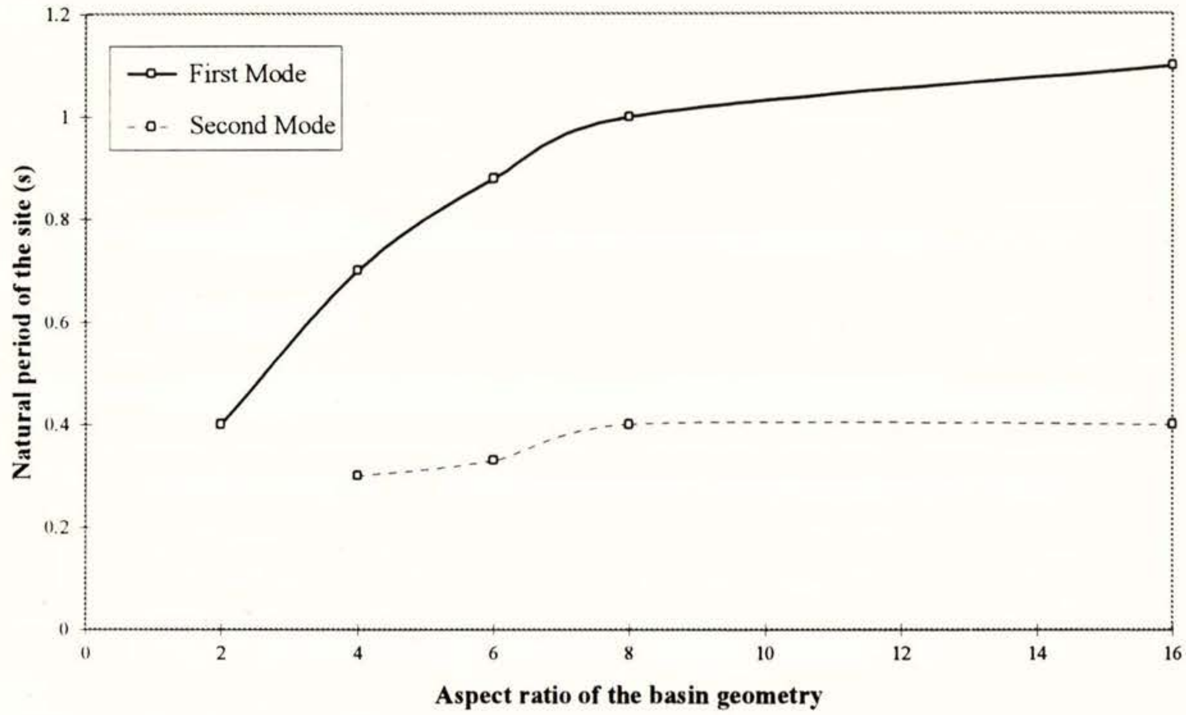

Fig. 7.20 Relationship between basin geometry and natural periods for the stiff soil deposits

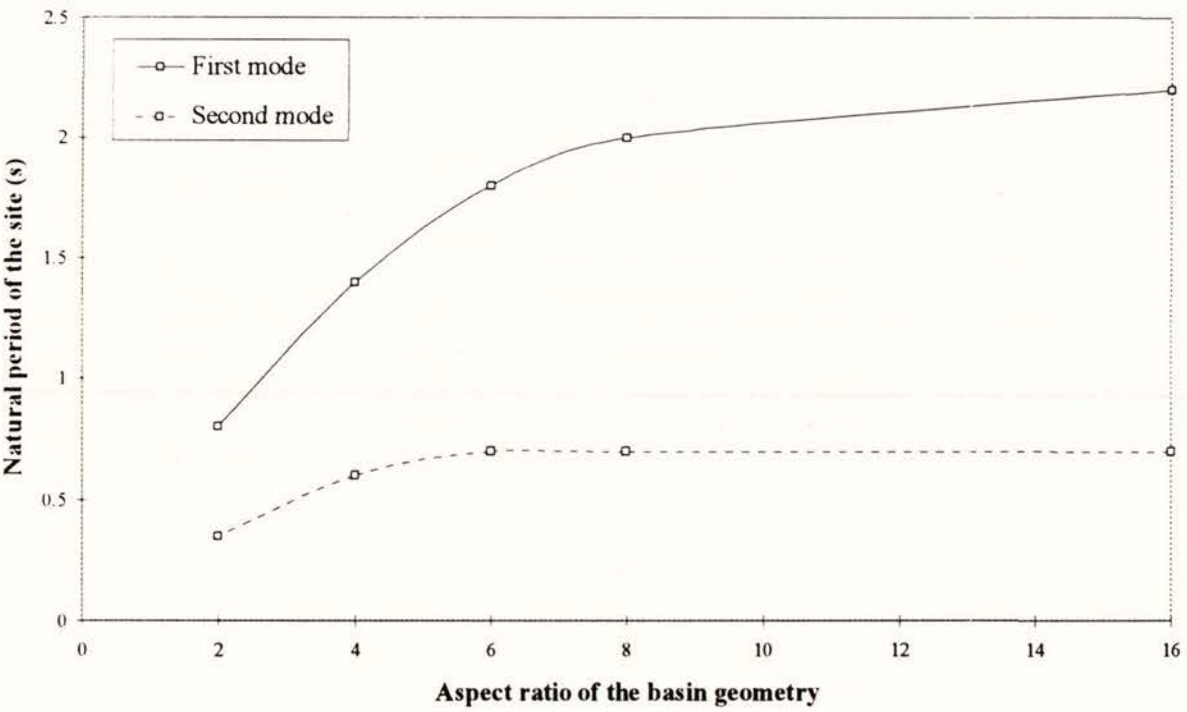

Fig. 7.21 Relationship between basin geometry and natural periods for the soft soil deposits

Influence of Valley Geometry when Subjected to a Small Magnitude Earthquake

A clear indication of the influence of the valley geometry may be seen when the 8:1 wide stiff soil valley and the 2:1 stiff soil narrow valley are subjected to the same source motion. The source motion used was the Old Castaic Ridge Route Station motion recorded during the 1971 San Fernando earthquake scaled down to represent a small motion event. This event was scaled to a peak acceleration of $0.05 m/s^2$, which is the same as the harmonic inputs described previously. A Fourier amplitude spectrum of this source motion is shown in figure 7.22, which shows that the earthquake motion has a relatively wide bandwidth. There is a peak amplitude response at around 3 Hz (0.33 seconds) with a larger concentration of energy in the region of 1.8 Hz to 3.2 Hz (0.3 to 0.6 seconds). This is clearly shown in the response spectra of figure 7.23, where the lower period area dominates the motion. As would be expected, both figures show the same characteristics of the motion.

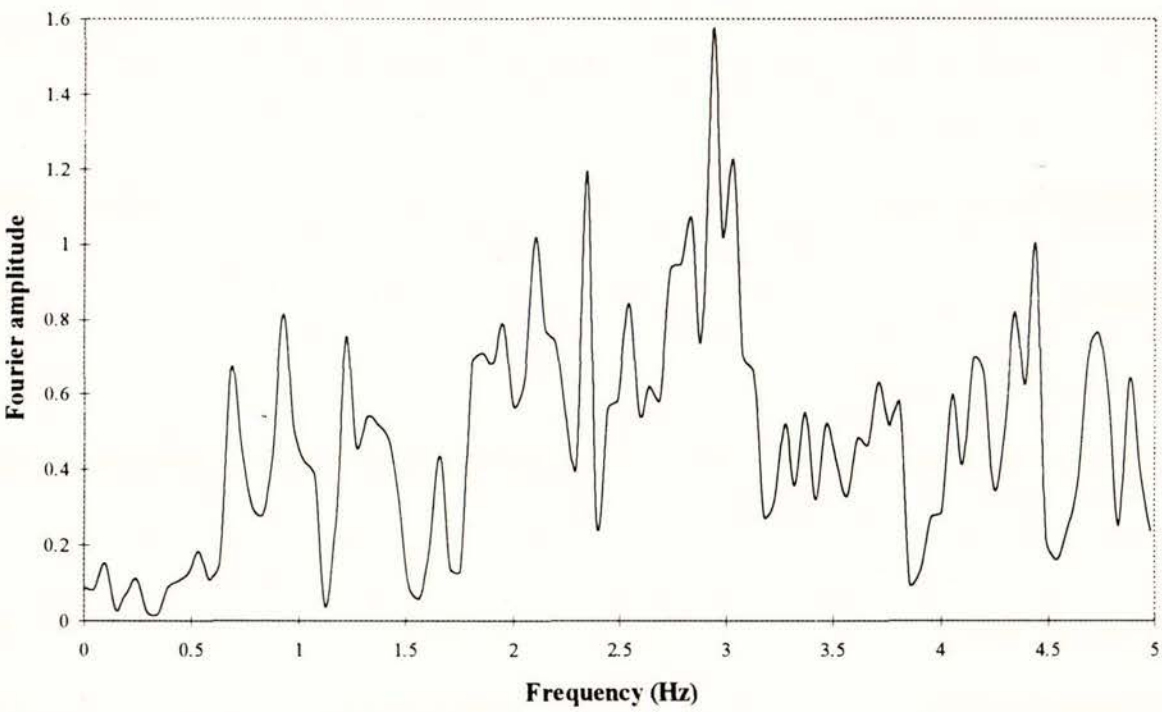

Fig. 7.22 Fourier amplitude spectra for the Old Castaic Ridge Route Station input motion

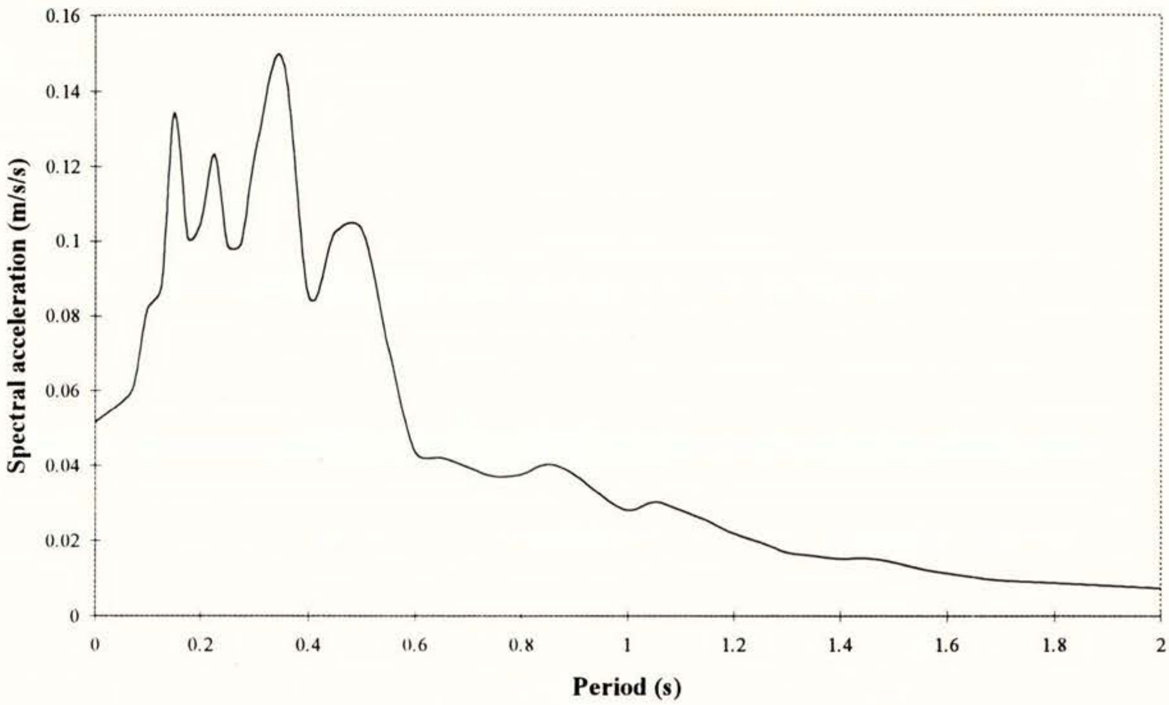

Fig. 7.23 Acceleration response spectra for the input motion (5% damping)

The wide valley (8:1) surface response spectra is show in figure 7.24 when this basin is subjected to the input motion described above. This figure shows a relatively high magnitude uniform level of surface motion across the basin, particularly in the lower period (higher frequency) range of 0.3 to 0.6 seconds. This corresponds to the maximum energy region of the input motion, and therefore a large response of the valley in this area is expected. It also corresponds to the second mode of the soil deposit. There is a noticeable rise in response of the surface spectra in the period region of 1 second, which is the natural period of the stiff soil site (see section 7.5). This longer period response is less uniform over the width of the valley, as it is more concentrated near the centre.

The very narrow valley (2:1) exhibits a very different surface response when subjected to the same input motion as can be seen in figure 7.24. There is no noticeable response in the 1 second region, and there is more solid low period response. This means that the range of periods over which there are significant surface amplifications is larger for the very narrow valley. than for the wide one, even though the wide valley tended to show slightly higher response magnitudes.

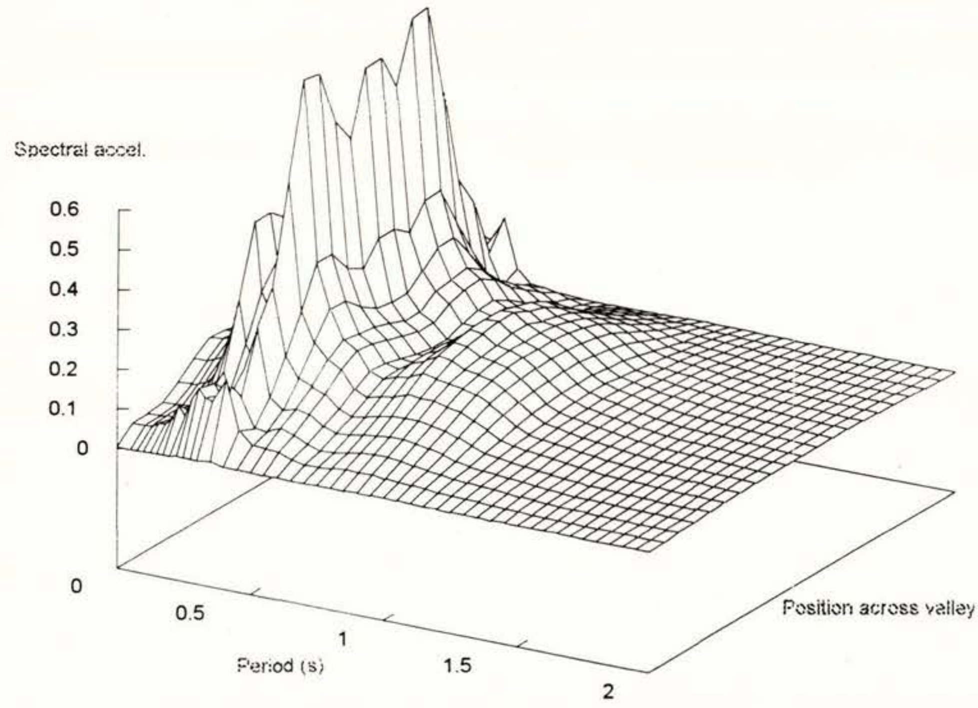

Fig. 7.24 Response spectra for the 8:1 valley subjected to actual earthquake input record

The larger peak responses in the wide valley can be explained by the fact that the lateral boundaries are further away from the central area, and as a result there is less energy radiated into the lateral bedrock from this area than in the narrow valley where the boundaries are much closer.

This is particularly relevant when studying small motions as the loss of energy into the surrounding bedrock is a significant damping component in the system. The wider period response zone can be explained by the results seen in section 7.6, where the first modes had a relatively wide bandwidth surrounding the peak response, whilst the higher modes were rather more peaky values.

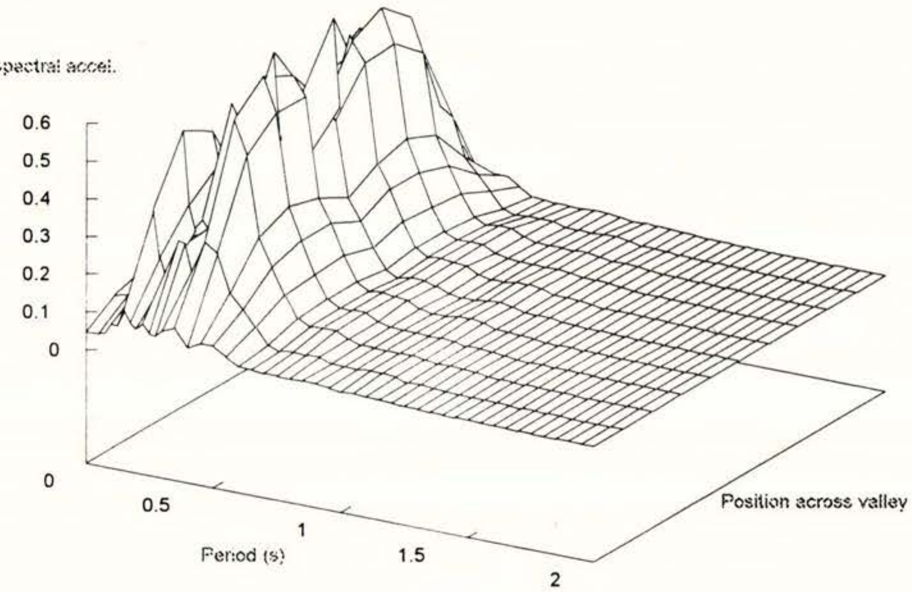

Fig. 7.25 Response spectra for the 2:1 valley subjected to actual earthquake input record

7.7 INFLUENCE OF THE SOURCE MOTION MAGNITUDE ON THE RESPONSE OF THE VALLEY SOIL DEPOSITS

The response of a soil deposit to a source excitation is strongly dependent on the non linear constitutive relationship of the soil (Larkin and Donovan 1979). The constitutive relationship of a soil is a function of the soil properties, and the levels of this non linear behaviour is a function of the induced strain levels. The induced strain levels are a function of the magnitude of the input seismic motion. In summary therefore, it is clear that the response of a soil deposit is a strong function of the magnitude of the input motion.

To investigate how strong this relationship is for a non linear soil deposit, all of the aspect ratio valleys detailed above were subjected to a series of 20 second single frequency harmonic input motion (as before) of differing magnitudes. The magnitudes of the input motions were governed by the value of peak acceleration of the sine wave. Only a limited number of these results shall be shown in this section due to space limitations, but conclusions as to the influence of the earthquake magnitude are made based on the entire set of results.

8:1 Valley Geometry

Both the stiff and soft 8:1 basins (constant geometry) were subjected to a range of magnitude harmonic source motions. Figure 7.26 and 7.27 show the results for each period of the harmonic input motion for a range of magnitudes.

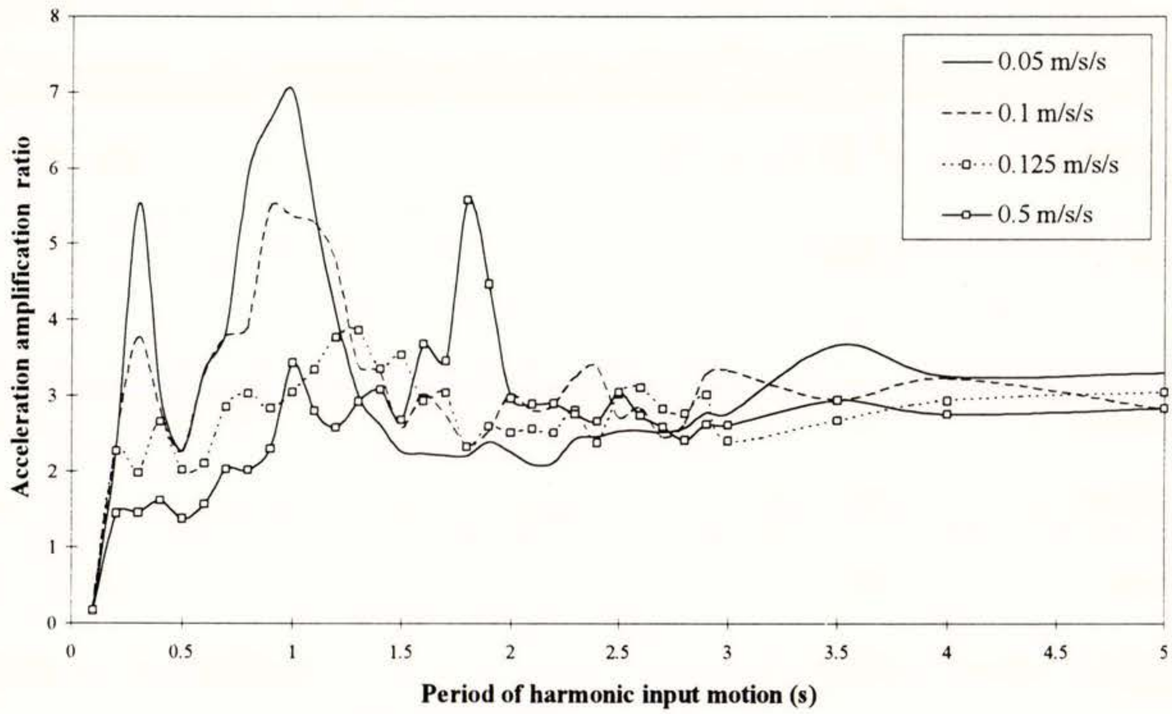

Fig. 7.26 Centre response of the 8:1 stiff valley subjected to varying amplitude harmonics

It can be seen from both of the figures that the periods of peak response of the central surface node tend to increase as the magnitude of the source motion increases up to a point. At relatively higher magnitudes the results tend to become a bit unclear as the soil damping tends to dominate. This lengthening period for larger motions is due to the larger magnitudes of induced strain within the soil deposit. Larger induced strains introduce more non linearity into the solution, which leads to a change in the value of shear modulus at each time step. As a result, there is an "average" change in shear modulus for the soil deposit as a whole over the duration of the event (this is the concept behind the equivalent linear method of approximating non linear soil behaviour).

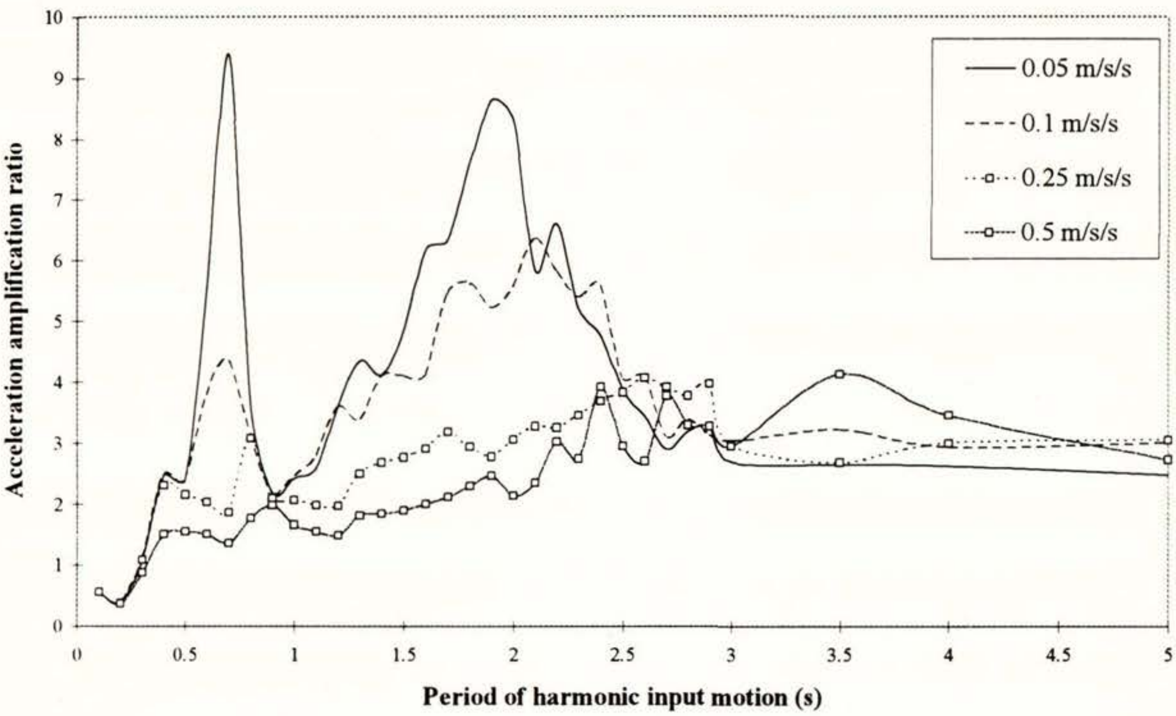

Fig. 7.27 Centre response of the 8:1 soft valley subjected to varying amplitude harmonics

The corresponding average shear modulus for the soil deposit is reflected in an average shear wave velocity, which will always be lower than the initial low strain value. From equation 7.8 is can be seen that the natural periods of a site are a function of the reciprocal of the shear wave velocity, so that any reduction in the average shear wave velocity will lead to a lengthening of the natural periods.

It is difficult to quantify the magnitude of this lengthening of the average natural periods, but from the results of the numerical studies some generalisations can be made. For small input motions up to a magnitude of around 0.1 to 0.2 m/s^2 the period of the site tends to increase by around 10 to 15% above that for micro tremors, but for large motion events there seems to be no clear trend that can be detailed. This means care should be taken when attempting to scale up the characteristic response properties of a site that have been determined from microtremor studies when predicting large motion responses.

The influence of the non linear hysteretic damping can be clearly seen in figures 7.26 and 7.27. As the magnitude of the input motion increases the surface peak acceleration ratio decreases. This is because hysteretic damping is again a function of induced strain levels. The reduction in the acceleration amplification ratios is quite marked for relatively small increases in magnitude until a limiting magnitude was reached when the higher motions had a lower impact on the surface response amplification ratios, and the high damping tends to flatten these out across the period spectrum. From the two figures above it can be seen that the 0.25 m/s^2 and 0.5 m/s^2 amplification responses are relatively similar, and this is consistent with other results for different basin geometries.

7.8 SUMMARY

This chapter investigated a number of aspects of the response of two dimensional cohesive volcanic soil deposits subjected to a range of input motions. Any numerical study on the properties of soils starts with the properties of the soils themselves. This provided a great difficulty in this study as the literature contained little information on either the static or dynamic properties of volcanic ashes or other cohesive forms. The two limited data sets that were available indicated that a volcanic ash or silty soil tends to have a sensitive structure, and testing on these soils lead to a breakdown of this structure which manifested itself in an elevated pore pressure response. Neither result suggested any danger of liquefaction but it is an indication of a different response to dynamic loading. In other aspects of the data however the volcanic soils tended to follow well established empirical trends, particularly in the form of the shear modulus versus shear strain relationships. As a result it was considered reasonable to use the empirical results available and ignore any pore pressure effects for these soils.

An indepth study on the response of the wide (8:1) valley for small motions produced results that were comparable with closed form solutions. It also showed that the closed form solution for estimation of the natural period of a site was valid for this level of motion. It was also found that the natural periods of a site dominate the response of that site, and therefore the frequency content of any input motion is an important factor in the characteristics of the resulting surface motion.

The two dimensional influence on the response of a valley structure was extensively investigated using a range of single frequency harmonic input motions. The influence of the lateral boundaries was found to primarily stiffen the valley, which lead to an decrease in the overall natural period of the soil deposit. This study tended to confirm that the wide 8:1 valley essentially behaves as a one dimensional solution at the centre, but there was some indication that there was still a small influence of the lateral boundaries at this central point. Other positions across the valley surface did not follow the one dimensional solution, even for the wide valley.

The influence of non linear soil properties was investigated by studying the response of the wide valley to a range of earthquake magnitudes. This showed that non linear soil properties started to significantly influence the response of the soil at earthquake motions in excess of 0.1 m/s^2. The result of this non linear response was to increase the average natural period of the site. For larger magnitudes the non-linearity dominated the response of the soil, which clearly indicates that micro tremor data or elastic solutions are unlikely to accurately represent the response of the soil during a large magnitude event.

Chapter Eight

Analyses of Liquefaction Potential

8.1 INTRODUCTION

The liquefaction response of volcanic sand deposits is described in this chapter using the numerical models developed for this work. Also included are some additional analyses of the experimental results presented in chapter six, particularly in the area of the liquefaction characteristics and response.

Most of the results presented use the strain dependent model developed for this report and described in chapter 5. Some verification and comparative studies using the one dimensional version and the two dimensional empirical stress controlled model are also included. The experimentally determined sand properties reported in chapter six are extensively used in the numerical investigations presented. Finally the influence of the high permeabilities of pumiceous sands on the overall liquefaction response of a typical site are investigated. As the two dimensional model assumes undrained loading, the one dimensional version was used for this aspect of the study.

8.2 LIQUEFACTION CHARACTERISTICS OF VOLCANIC SANDS

The liquefaction results for the Puni sand are compared to the empirical trends for sands that have been described in the literature over a number of years. This is to assess if the liquefaction properties of the volcanic sand deviated from other empirical results, and if so the magnitude of these variations. Most empirical liquefaction potential evaluation methods make heavy use of insitu SPT or CPT results. This penetration data is then used to determine if a site is susceptible to liquefaction through the empirical relationships that were detailed in chapter three. How the properties of the Puni sand relate to penetration resistance data is therefore a very important factor to investigate. The results presented below relate the relative density and liquefaction resistance properties of the sand to SPT values using empirical relationships. Unfortunately no field or laboratory data on penetration resistance for the specific Puni sand was available to confirm the derived SPT values. The shape of the full experimental liquefaction curve is also investigated.

Relative Density

The void ratios of the Puni sand were found to be in the range of 1.45 to 2.1 (section 6.4), which are high when compared to similar quartzitic sands. As the relative densities are related to aspects of the void ratio and figure prominently in empirical correlations, the volcanic sand was compared to the literature to check for agreement. Seed (1979) reports studies of comparisons between insitu blow count data, and laboratory determined relative densities for high quality quartz sand samples. Figure 8.1 shows the data values of their results

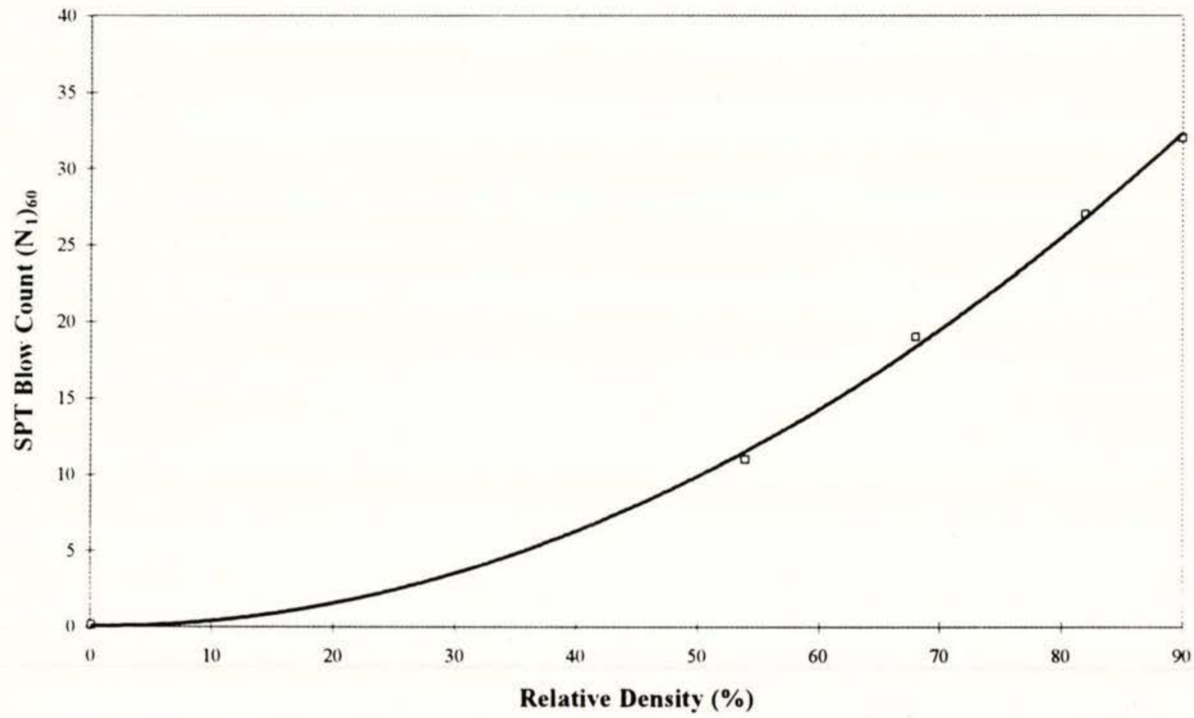

Fig. 8.1 Relative density versus SPT blow count for quartzitic sands (from Seed 1979)

This graph shows actual data points, with a best fit curve overlayed. Tokimatsu and Seed (1987) have determined an analytical expression that fits the above and more recent data, which is given by

$$(N_1)_{60} = \left(\frac{DR}{15}\right)^2 \qquad 8.1$$

where DR is the relative density (%)

The relative density of the loose Puni samples that were tested for liquefaction was in the range of 30-40%. From equation 8.1, this corresponds to a normalised blow count of 4 to 6.5 blows/ft for the quartzitic sand.

Liquefaction Potential and Blow Count Relationships

Seed (1979) reports the experimental values of K_O for normally consolidated quartzitic sands to be around 0.4. Pranjoto and Larkin (1995) found similar average values to this for the Puni sand when tested in a large scale K_O cell.

As stated in chapter three, the cyclic triaxial test induces different stress ratio conditions than the simple shear tests, and therefore a correlation factor is required to relate the two tests. This correction must be made as the empirical data is based on level ground stress ratios, which corresponds to the simple shear conditions. The general form of the correlation is given in equation 8.2.

$$\frac{\tau}{\sigma'_{vo}} = C_r \frac{\sigma_{dc}}{2\sigma_a} \qquad 8.2$$

where C_r is the correlation factor

A number of expressions for the correlation factor C_r exist in the literature, with most finding that it is essentially a function of the K_O value. For a K_O value of 0.4, Seed (1979) gives the value of C_r as 0.57, which is the value used for the calculations below.

With the value of C_r and the experimental liquefaction curve from the loose cyclic triaxial testing results (figure 6.8), it is possible to generate the equivalent horizontal stress ratio liquefaction curve. This curve is shown in figure 8.2

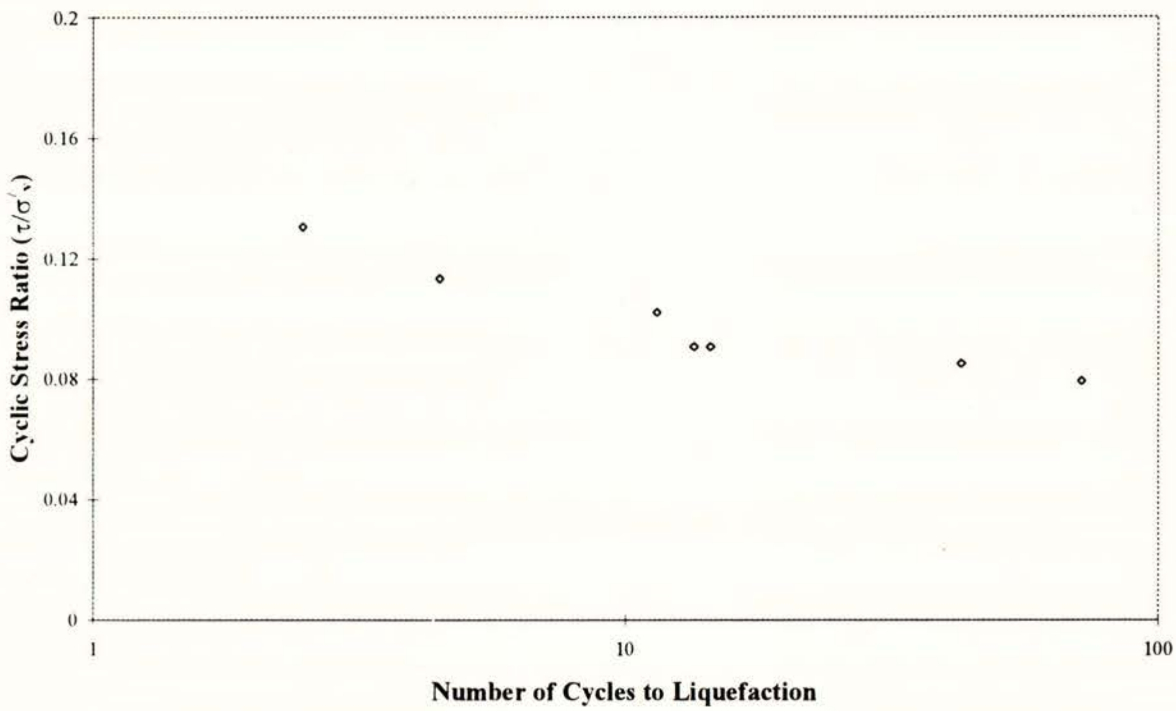

Fig. 8.2 Experimental loose Puni sand liquefaction curve for simple shear stress conditions

The standard empirical technique for determining the shear stress ratio in liquefaction design procedures is to use the curves of Seed et al. (1984, figure 3.4) which relate SPT blow counts to the stress ratio required to initiate liquefaction in 15 equivalent cycles. It is considered that the 15 loading cycles corresponds to a magnitude 7.5 earthquake. For the loose Puni sand, the stress ratio at 15 loading cycles is known from figure 8.2, and it is therefore possible to work backwards and determine the equivalent SPT blow count from the relationship of figure 3.4. At 15 cycles of loading, the stress ratio from figure 8.2 was taken as 0.095. This corresponds to an $(N_1)_{60}$ SPT value of 7 blows/ft from the empirical curves of figure 3.4, which is similar to the blow count derived from relative density values earlier.

As stated earlier there is no insitu experimental blow count data available for the sand to gauge if these answers are in the correct region, but it would be expected that a loose sand would have relatively low blow counts that are comparable with the above results. The real difficulty in this assumption is that the volcanic sand has a higher void ratio and softer particles, both of which would indicate that a penetration test should yield lower results than for an equivalent quartzitic sand. The extent to which these factors would influence the SPT results is very difficult to quantify and assess without experimental verification.

The derivation of the blow count from the empirical liquefaction relationship is a particularly interesting result. Assuming that 7 blows/ft is a reasonable SPT value for the loose sand, it suggests that the liquefaction testing programme has produced reliable results. It may also suggest that the empirical relationships which have been derived from historical field observations are relatively accurate when compared to experimental results. From the literature, the empirical relationship between shear stress ratio to initiate liquefaction and SPT blow count of Seed et al. (1984) does not appear to have been confirmed by laboratory testing. An combined experimental investigation of liquefaction potential and blow count is required to investigate this area further, particularly with reference to New Zealand soils. Such a testing programme could confirm and further improve the form of the empirical relationship. The single result from this study indicates that the empirical field relationship may be valid for the Puni sand.

Form of Liquefaction Curves

The third area of comparison between the Puni sand results and general empirical trends is the form (or shape) of the liquefaction curve. Based on the experimental data of De Alba et al. (1976), the shape of the liquefaction curve is relatively constant for any density of sand (section 3.3.1 and figure 3.4), and a shape function has been derived to describe this. All of the empirical methods of determining the liquefaction resistance curve from penetration data usually require this shape function. It is therefore useful to investigate how the shape of the Puni sand liquefaction curve in figure 8.2 compares to the general shape of empirical data. Figure 8.3. shows the two results

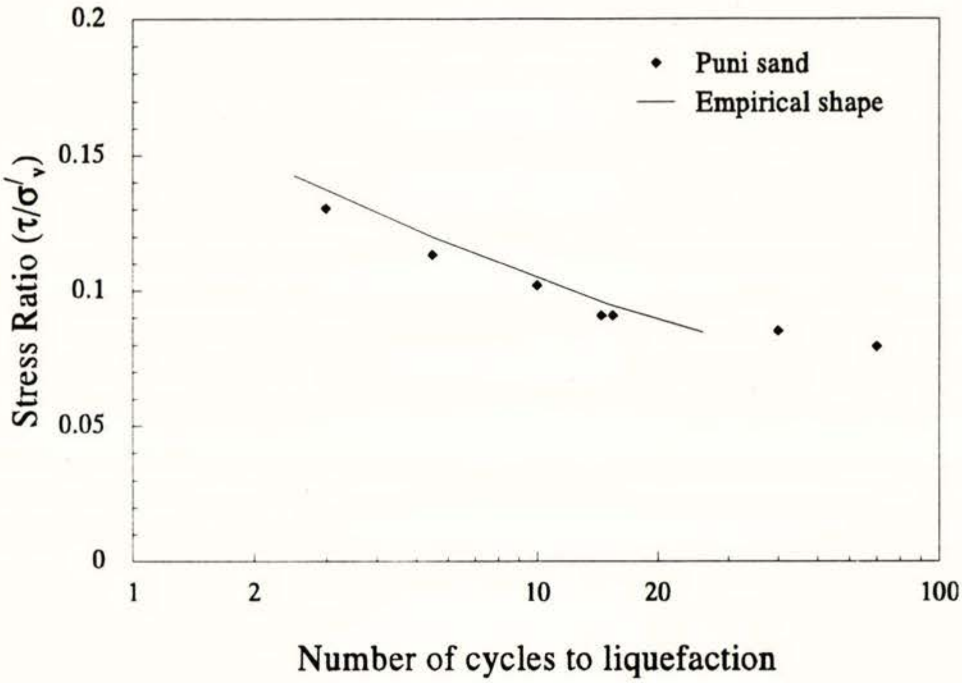

Fig. 8.3 Comparison of loose Puni sand liquefaction and empirical data

It is clear from this graph that the results of the Puni sand follow the same general shape as the empirical data. The empirical data only ranges from 3 to 26 cycles, but this is the most important zone for liquefaction studies.

The general conclusion of the results presented above indicate that the volcanic sand tends to follow similar trends to other sands as far as liquefaction behaviour is concerned. As the induced stresses from cyclic loading are not excessively high, there appears little influence of the softer particles on the response of the sand as a whole. These are only preliminary findings however and more research is required into the subject, particularly in the areas of blow count response where the larger void ratios and softer particles may have a larger influence.

8.3 NUMERICAL MODELLING OF EXPERIMENTAL LIQUEFACTION RESULTS

To numerically model the liquefaction behaviour of the volcanic sand, a number of constants relating to the sand must be derived first. This has traditionally been the problem with numerical liquefaction studies because these constants have been difficult to determine without expensive testing. This type of testing, which involves volumetric strain and elastic rebound testing of the sandy soil, has inherent problems as well, particularly in the area of sample disturbance and preparation. A satisfactory solution to the problem of determining all of these constants was found by Larkin and Marks (1994), using some simplified results from Byrne (1991).

The required constants could be found with the aid of a numerical simple cyclic shear analysis program (Larkin 1977). This program models the simple cyclic shear test, and uses the same pore pressure model that is incorporated into the larger site response programs. When cyclic liquefaction data is not available the liquefaction curve can be derived from blow count data, which tends to be the case in practice. This highlights the very important relationship between blow count and liquefaction performance for volcanic sands. As outlined above, the experimental relative density and liquefaction results for the loose sand correlate to an $(N_1)_{60}$ blow count of 5-7 blows/ft using standard empirical correlations. Such a value of blow count would be expected for a loose sand, but there is no data available as to the behaviour of a loose volcanic sand. The softer particles and higher void ratios may have a significant influence on the blow count that is not as significant in the sand's liquefaction response behaviour. As a result it is very inadvisable to rely heavily on blow count data when investigating the liquefaction response of volcanic soils. This relationship therefore requires a significant future research effort if credible liquefaction potential analyses are to made.

For this study the equivalent cyclic simple shear liquefaction strength curve was available from the transformed cyclic triaxial test data. The influence of the penetration resistance relationships is therefore reduced, but unfortunately not eliminated. The procedure to evaluate the required liquefaction constants is then to calculate the volumetric strain constants from approximate correlations to blow count, and the rebound constants are then determined by a backfitting procedure. Briefly this involves matching the output of the numerical simulation to the known liquefaction curve and backfitting the required three constants. It was found that using different values of these three constants had minimal effect on the pore pressure model provided the liquefaction curve was accurately matched. The difficulties of this procedure are that the transformation from the cyclic triaxial test to the cyclic simple shear test results (C_r constant) has again been developed from quartzitic sand tests in the United States. One can speculate that because the lateral K_O value of the volcanic sand (Pranjoto and Larkin 1995) was found to be similar to the quarztitic equivalent in the literature, that the correlation factor

C_r between the two cyclic tests would also be similar. The other problem is the relationship between volumetric strain and blow count which is used in determining the volumetric strain constants. As stated previously this is a continuing problem.

With the above factors in mind, the numerical constants were determined for the analytical equivalent of the experimental liquefaction curve. All of the experimental liquefaction testing data was obtained at a confining stress of 100 kPa, and therefore the same confining stress was used to evaluate the numerical constants. The matched cyclic simple shear liquefaction curves are shown in figure 8.4

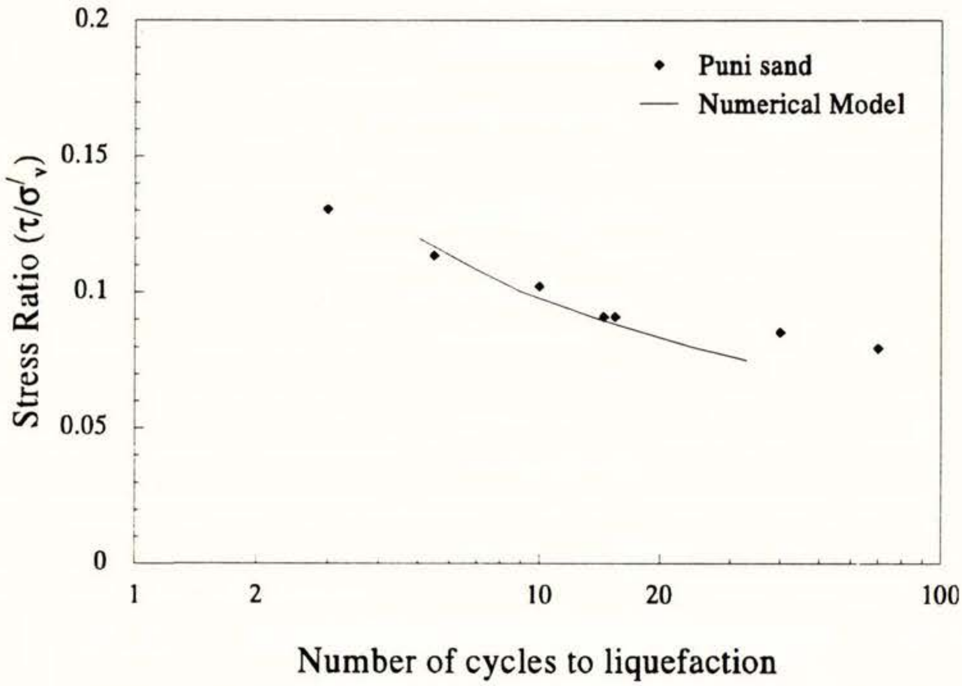

Fig. 8.4 Numerical cyclic simple shear model compared to transposed experimental data

As the liquefaction curve of the loose Puni sand is similar in form to other sands, the numerical model simulated this curve well, particularly in the range of 5 to 25 cycles which is the most important zone for seismic liquefaction studies. Large numbers of low stress cycles are more applicable to machine vibrational loading, and low numbers of cycles of large stress are applicable to blast loading rather than seismic actions. The numerical model was therefore applicable to this type of volcanic sand, and could be used in site response studies presented later in the chapter. The 5 pore pressure constants determined by the backfitting procedure are given in table 8.1

Table 8.1 Liquefaction constants for the Puni sand at 100 kPa confining stress

Constant	Value
B_1	1.05
B_2	0.382
m	0.466
n	0.635
k_2	0.0044

The pore pressure model was calibrated to the liquefaction strength curve over a wide range of stress ratios and numbers of loading cycles. The simple shear model could be compared to the results of one of the transformed cyclic triaxial tests to investigate further the applicability of the model to a single cyclic shear test. Clearly it would be preferable to compare the simulation of the cyclic simple shear test with actual cyclic simple shear test results, but as only the triaxial apparatus was available, applying the transformation constant (C_r) to the triaxial results was the only option. Sample E from the testing programme (section 6.5.1) was taken as the test to simulate, which reached liquefaction in 14.5 cycles. This test was used as 15 cycles empirically corresponds to a magnitude 7-7½ earthquake, which is a magnitude that has initiated liquefaction in past events. The shear stress-shear strain response (hysteresis loops) of the numerical liquefaction model is shown in figure 8.5. Liquefaction is reached in this numerical simulation at 14.5 cycles.

The experimental test result for sample E is shown in figure 8.6, which is a reprint of figure 6.5. This load displacement history was converted to an equivalent hysteretic graph by using the appropriate conversion factors. The first is from axial load to shear stress ratio, which is performed by converting the axial load to a deviator stress ratio, and then multiplying this deviator stress ratio by the C_r factor to convert it to an equivalent cyclic simple shear stress ratio. The equivalent shear strain was found by assuming a Poisson's ratio of 0.5 (due to the undrained testing), and converting the axial strain.

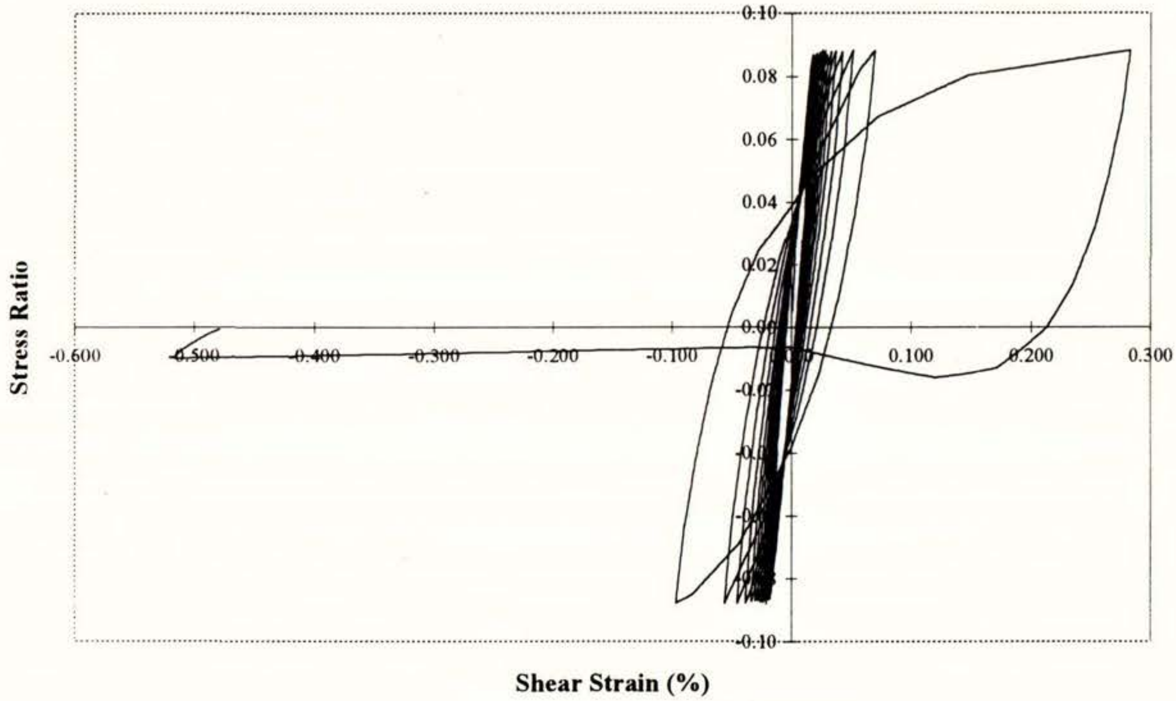

Fig. 8.5 Numerical cyclic simple shear stress/strain results for the Puni sand.

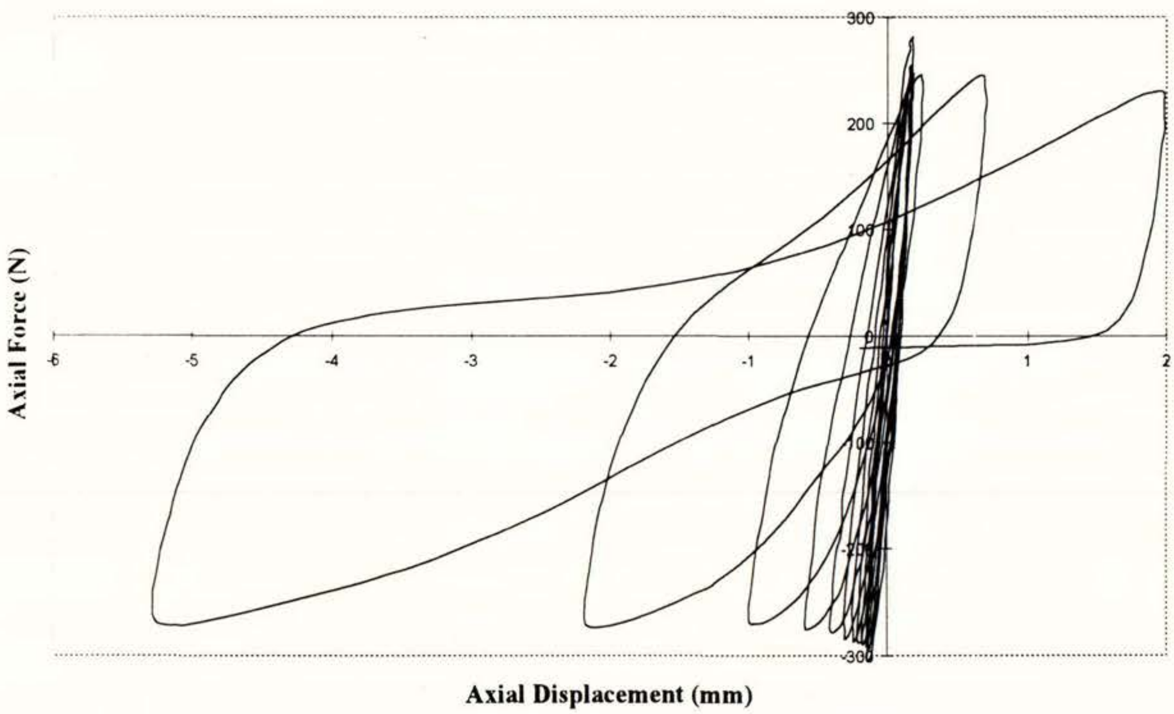

Fig. 8.6 Load displacement results for experimental loose Puni test result (sample E)

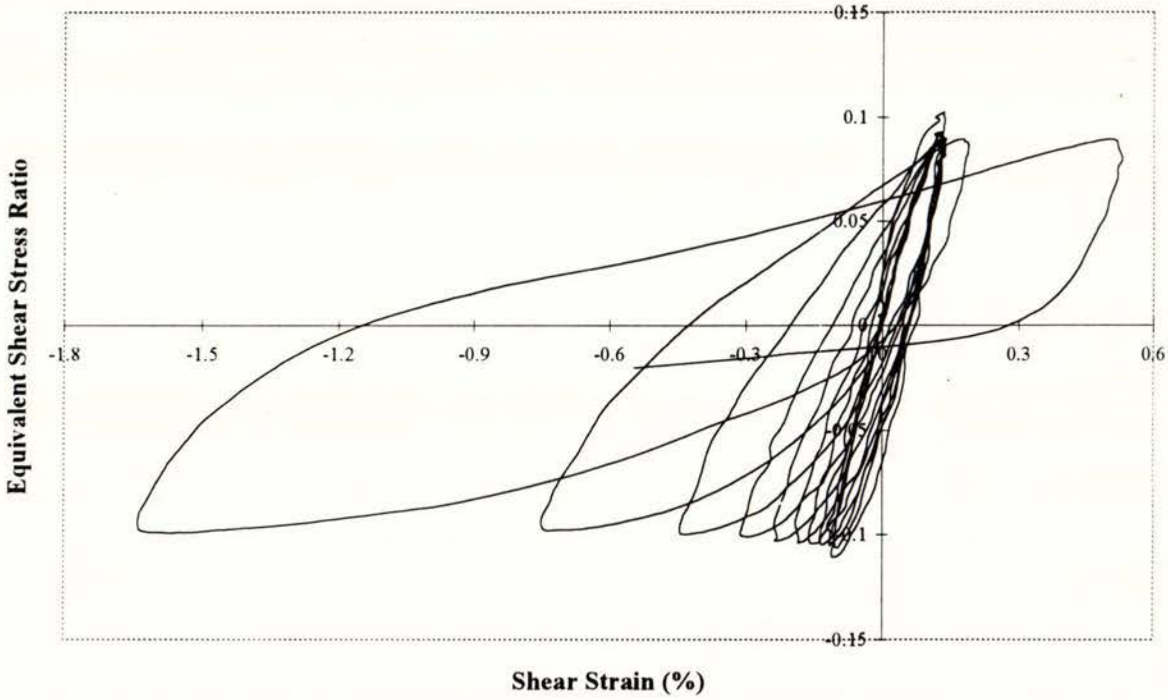

Fig. 8.7 Equivalent shear stress ratio vs shear strain converted from figure 8.6

The agreement between the two results is reasonable, although the experimental results indicates higher strains than the numerical results do. One reason for this is that the numerical model dose not take into account the dynamic components of the pore pressure loading, but only allows for the steadily increasing residual component. The result of the dynamic component of pore pressure is to momentarily decrease the level of effective stress at some points during the loading cycle, which tends to aid the development of larger strains. Another reason for the larger magnitude of shear strains is that the cyclic triaxial machine is load controlled rather than stress controlled. The larger strain migration occurred in the extensional phase of the loading cycle (taken as negative), which is to be expected because this phase of loading reduces the cross sectional area of the sample and hence increases the local shear stress. This problem is exacerbated due to the application of the slightly higher extensional loads (as described in chapter 6).

Perhaps the most important explanation for the differences in results is the fact they are two separate types of tests with entirely different stress conditions. The correlation factor C_r focuses on converting the triaxial results to simple shear results. The resulting strains will be sensitive to boundary effects. In spite of these and other factors, the agreement is reasonable.

The generation of the residual excess pore pressure ratio from the numerical model is shown in figure 8.8

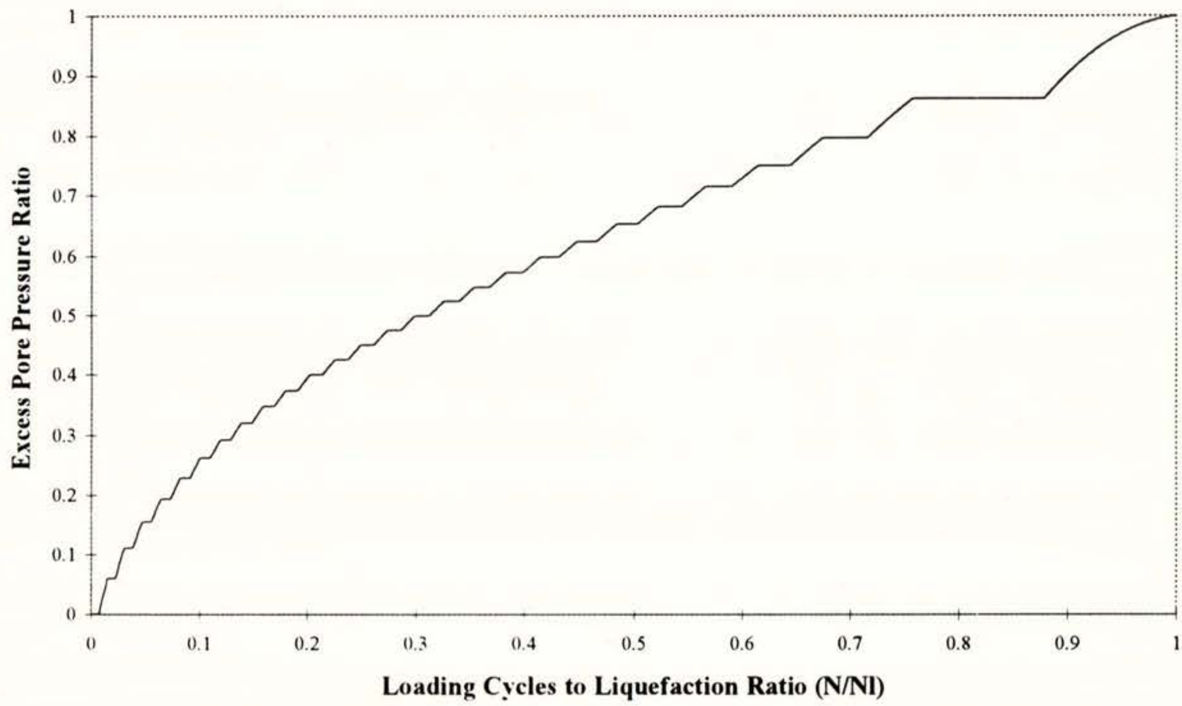

Fig. 8.8 Numerical excess pore pressure generation ratio curve

The equivalent experimental results from sample E are shown in figure 8.9, which is a reprint of figure 6.7.

Both the dynamic and residual pore pressure responses are shown in figure 8.9, whereas the numerical results do not attempt to include the dynamic component. The experimental curve shows more linearity than the numerical simulation. However, if the dynamic component is ignored there is again reasonable agreement between the two.

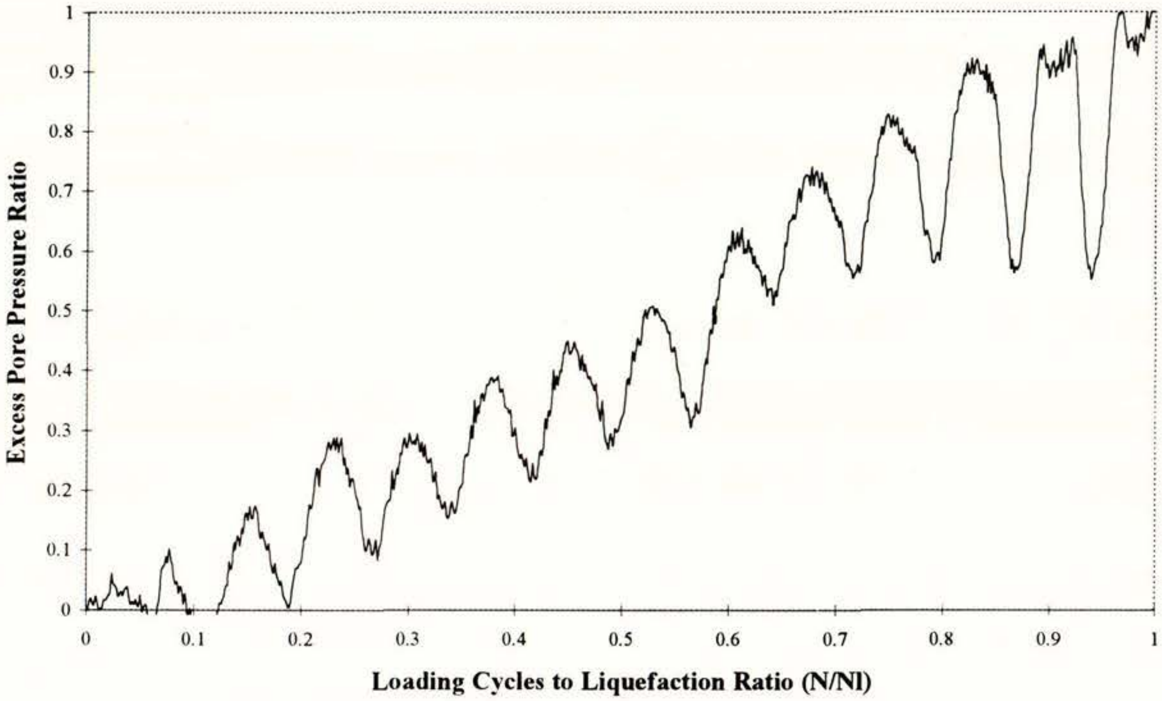

Fig. 8.9 Experimental excess pore pressure generation ratio curve for sample E

In summary the above results indicate that the numerical pore pressure model may be reasonably applicable to the Puni volcanic sand, not withstanding the number of correlations that are involved. The pore pressure model and derived liquefaction constants can then be used in site response analyses to investigate the characteristic behaviour of these volcanic sands in more depth. This work is presented in the following sections.

8.4 SITE RESPONSE ANALYSES OF VOLCANIC SANDY SITES

The results presented below involve basins with the same geometry as those discussed in chapter seven, but the soil deposits within these valleys are assumed to be loose volcanic sands. All of the material properties used to model these sands have been derived from the experimental work carried out from this project. This includes the low strain shear modulus/wave velocity profiles from the bender element tests, densities and the liquefaction model constants derived above. This section of results is intended to provide an overview of the two dimensional effective stress computer model and how volcanic sands may be incorporated into it.

8.4.1 Comparison Between One and Two Dimensional Solutions

Initially the two dimensional strain controlled effective stress program was compared to the existing one dimensional effective stress program (NESSA) to ascertain any significant differences in the results. The wide (8:1) two dimensional valley was used for this comparison, and the results were taken at the centre of this valley. The source motion used for this aspect of the results was that recorded at the Castaic Old Ridge Route Station in 1971. For the purposes of this study the motion was scaled down to 0.15g, as the full magnitude motion initiated widespread liquefaction in the sand deposits. The rational for reducing the motion to 0.15g was the wish to compare accurately the one and two dimensional solutions. Widespread liquefaction in both analyses would not make a basis for a very good comparison. The motion was therefore scaled so as to induce a medium to high excess pore pressure response in each analysis. Both analyses were also undrained. Figure 8.10 shows the peak excess pore pressure comparison between the one and two dimensional analyses.

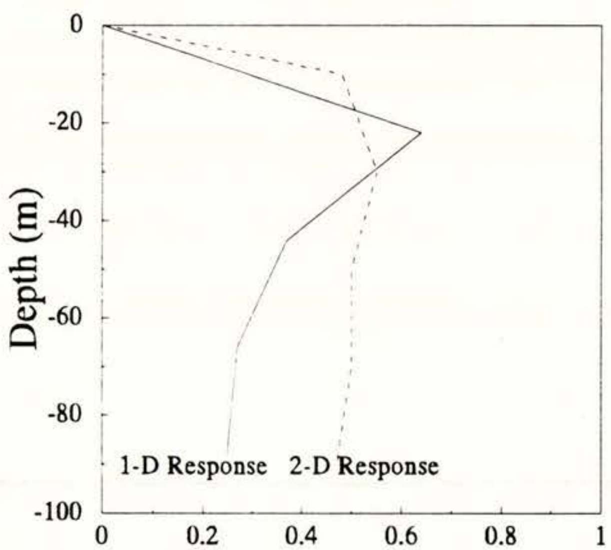

Fig. 8.10 Comparison of central peak pore pressure between 1-D and 2-D analyses

Both analyses show reasonable agreement to a depth of 40 metres, below which the two dimensional analysis gives pore pressures twice that of the one dimensional model. To some extent this behaviour is reflected in the induced shear strains in the two solutions, which are shown in figure 8.11. In the deep part of the soil profile the two dimensional response shows higher strains, and the one dimensional response shows higher strains in the upper section of the profile. From the peak shear strain profile one may expect a higher pore pressure response where higher peak shear strains are induced but this is not always the case. The complex nature of the two dimensional non linear constitutive relationship is different from the non linear one dimensional relationship, and therefore the comparisons of peak strain alone can not be taken as a direct relationship to the levels of induced pore pressures. The two dimensional analysis also shows some oscillations about a non zero mean (not shown) which also affects the magnitudes of the pore pressures.

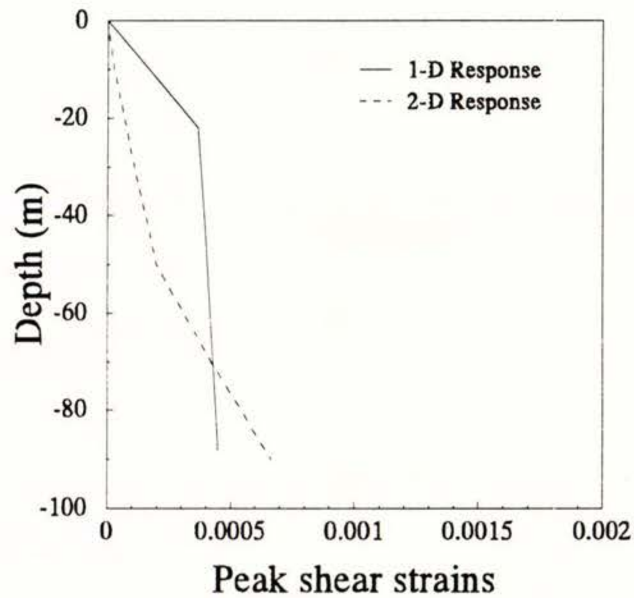

Fig. 8.11 Comparison of central peak shear strains between 1-D and 2-D analyses

From figure 8.11 it is clear that the shear strain-pore pressure relationship is not a linear one. Further investigation of the comparison between the two solutions is shown in figure 8.12, where the surface response spectra (5% damping) for both are shown.

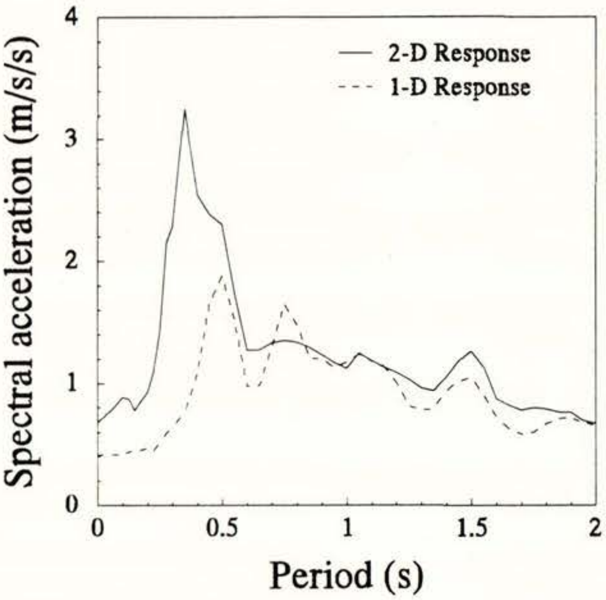

Fig. 8.12 Comparison between central surface response spectra for 1-D and 2-D analyses

This figure shows very good agreement between the two spectra at periods greater than 0.5 seconds. The low period range shows less agreement with the two dimensional solution producing a significantly larger response in this region. In general however it is clear that there is reasonable agreement between the one and two dimensional solutions for a wide two dimensional valley. This result gives confidence that the two dimensional program is producing reliable results, and can therefore be used in further analyses.

8.4.2 Comparison of Stress and Strain Controlled Liquefaction models

Comparative studies between the two dimensional stress controlled and strain controlled pore pressure models were undertaken to investigate the agreement between the two models when evaluating the liquefaction potential of a site. The stress controlled model (section 5.4) is an empirical model that calculates the magnitudes of excess pore pressure from the induced level of the stress ratio. If no experimental data is available, the stress controlled approach generally uses the empirical relationships. As experimental testing data is available for this study, the relationships required for this model could be determined with some accuracy. The shape of the pore pressure generation curve may be given by the numerical relationship (Seed 1979)

$$\frac{u}{\sigma'_{vo}} = \frac{2}{\pi}\arcsin\left(\frac{N}{N_L}\right)^{\frac{1}{2\alpha}} \qquad 8.3$$

where α is a shape constant.

The value of the α constant could be determined by matching the numerical expression to the set of experimental results. A value of α=1.3 gave the result shown in figure 8.13 for the Puni sand.

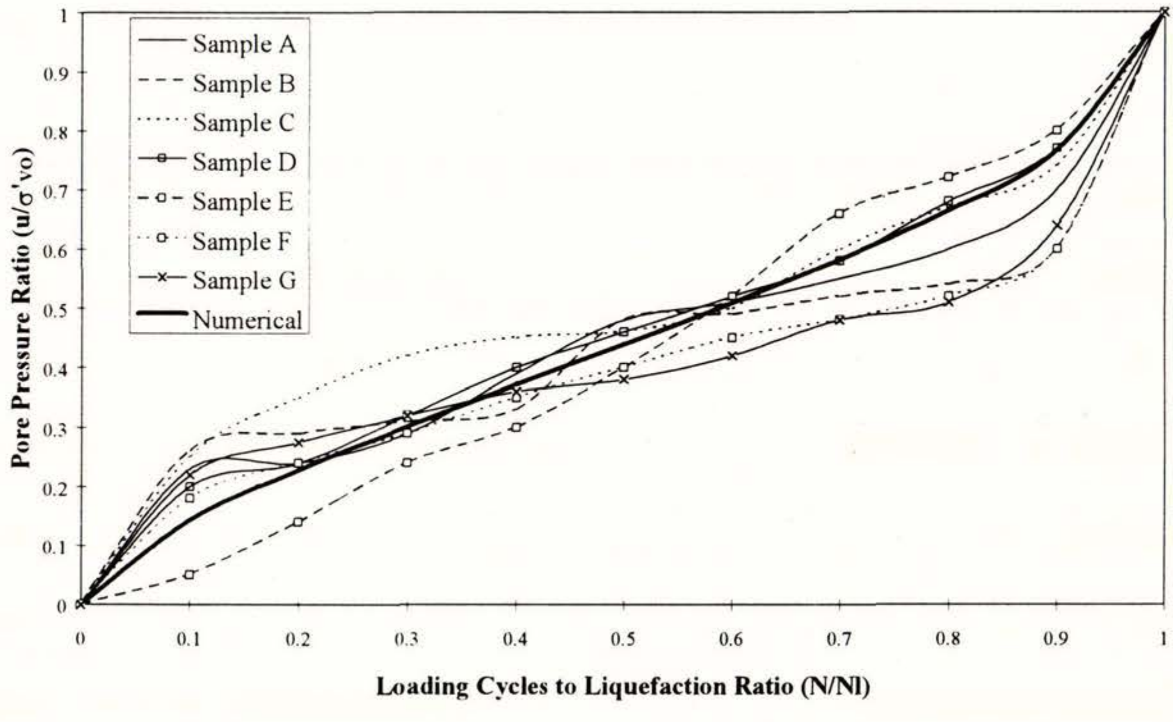

Fig. 8.13 Pore pressure generation curves showing the numerical relationship superimposed

The shape of the liquefaction strength curve used in the stress controlled model was taken from the known experimental results shown in figure 8.2. The cubic spline interpolation was then used to interpolate between the known values of stress ratio and number of cycles to liquefaction (detailed in chapter five).

Both two dimensional effective stress models were subjected to the same seismic motion (as previously) to investigate their behaviour. Figures 8.14 and 8.15 show the peak excess pore pressure contours for the stress controlled and strain controlled results.

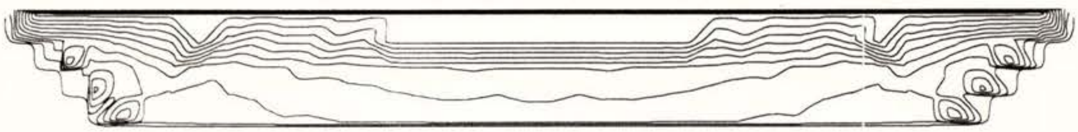

Fig. 8.14 Peak excess pore pressure contours from stress controlled model

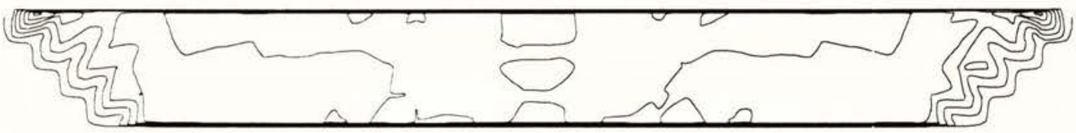

Fig. 8.15 Peak excess pore pressure contours from strain controlled model

Each contour line represents a pore pressure ratio of 0.1. It is clear from figure 8.14 that the stress model produces a stronger liquefaction response than the strain model. There is a more uniform liquefaction response over the depth of the strain model than the stress model. This can be clearly seen in figure 8.16, which shows the peak pore pressure response profile of each model at the centre of the valley.

The reason for the larger liquefaction response of the stress controlled model is that the stress model is a function of stress ratios rather than just stress. Figure 8.17 shows the maximum shear stress contours throughout the two dimensional basin, and figure 8.18 shows the corresponding peak stress ratio contours. Considering the fundamental difference between the two methods, these results show a moderate degree of difference, which would be expected.

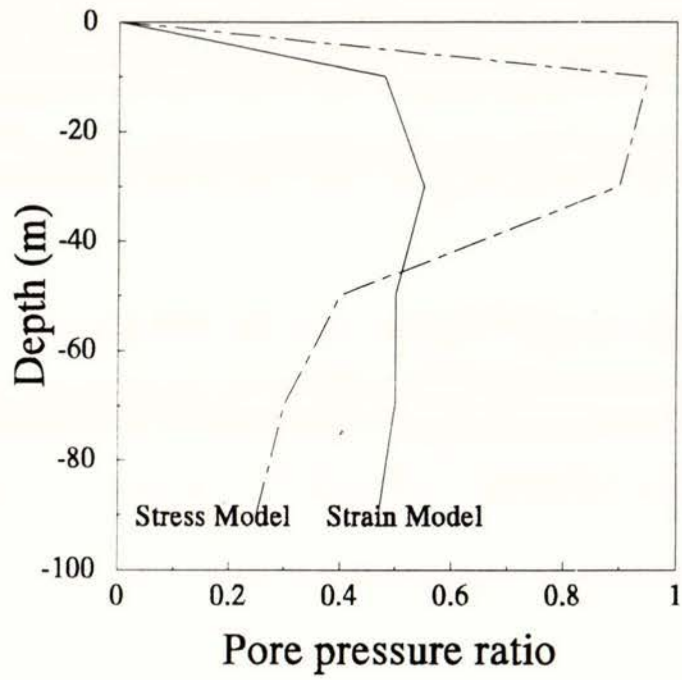

Fig. 8.16 Comparison between stress and strain controlled models at centre of wide valley

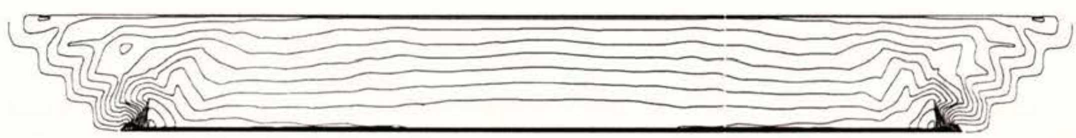

Fig. 8.17 Induced maximum shear stress contour plot for the wide valley

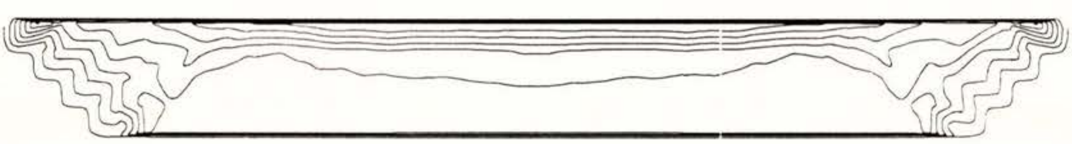

Fig. 8.18 Induced maximum stress ratio plot for the wide valley

These figure clearly show the difference between the induced stresses and the induced stress ratios. The induced shear stresses are greatest near the bottom of the basin as one would expect. The stress ratios however are very large near the surface of the soil profile where the overburden pressures are low. The stress ratio peaks at a value of 0.23, which is very high. When compared to the liquefaction strength curve of figure 8.4 for the Puni sand, this induced stress ratio is extremely high, which is why these near surface layers showed a strong liquefaction response. The stress controlled model uses the induced stress ratios of each cycle of loading to calculate an equivalent number of cycles to liquefaction, hence the results are very sensitive to the value of induced stress ratio.

One reason for such a large stress ratio being induced in the near surface areas of the analysis (for a medium level of input motions) is that the bulk density of the volcanic sands is low, in the region of 1400 kg/m^3 (chapter six). Therefore the effective overburden stresses will also tend to be low which leads to high stress ratios. These results show that the stress controlled model is very sensitive to the induced stress ratio, and therefore care should be taken when using the results. Both the stress and strain controlled analyses induce essentially the same levels of shear stress, but the stress model is significantly more sensitive to the induced stress ratios, hence the importance of the overburden stress. The results of the strain controlled model are also dependent on the levels of overburden stress, but the sensitivity of the analysis to this parameter is not as great.

8.4.3 Liquefaction Response of Two Dimensional Basins

This section investigates the seismic response of a number of valleys containing volcanic sands. These have also been subjected to the same source motion as described previously. The strain controlled model was used for all of these analyses. The deposits were modelled as a homogeneous volcanic sand layer so as to isolate the influence of the valley geometry on the liquefaction response of the soils. The material properties of these sands were taken to correspond with the properties of the Puni sand. All of the two dimensional analyses in this section are undrained effective stress analyses. Once again the source motion was taken as 0.15g, which allowed comparisons of the extent of liquefaction in each valley geometry without widespread liquefaction being induced.

Figure 8.19 shows the excess pore pressure contours for each valley geometry, with the peak pore pressure ration also shown. Each contour was taken as a pore pressure ratio of 0.08.

These excess pore pressure contour plots show a number of interesting features. There are very high pore pressure gradients around the sloping boundaries of each result. This is because there are very high strain gradients in this region as the low strain high stress motion in the surrounding bedrock propagates into the valley where the lower stiffness of the sand induces larger shear strains. All of the contours show a relatively symmetrical liquefaction response, which is to be expected as the seismic motion was applied to all boundary nodes simultaneously.

As the strain controlled model is undrained, no account of pore pressure redistribution throughout the deposit is taken. This would most likely make the liquefaction response more uniform over the entire deposit, and this aspect is discussed in the next section. All of the results show a higher excess pore pressure response in the near surface layers which is to be expected as the effective overburden pressure are less.

The corresponding response spectra for each valley are shown in figures 8.20 to 8.24. All of the vertical abissca in these plots are of spectral acceleration in m/s^2.

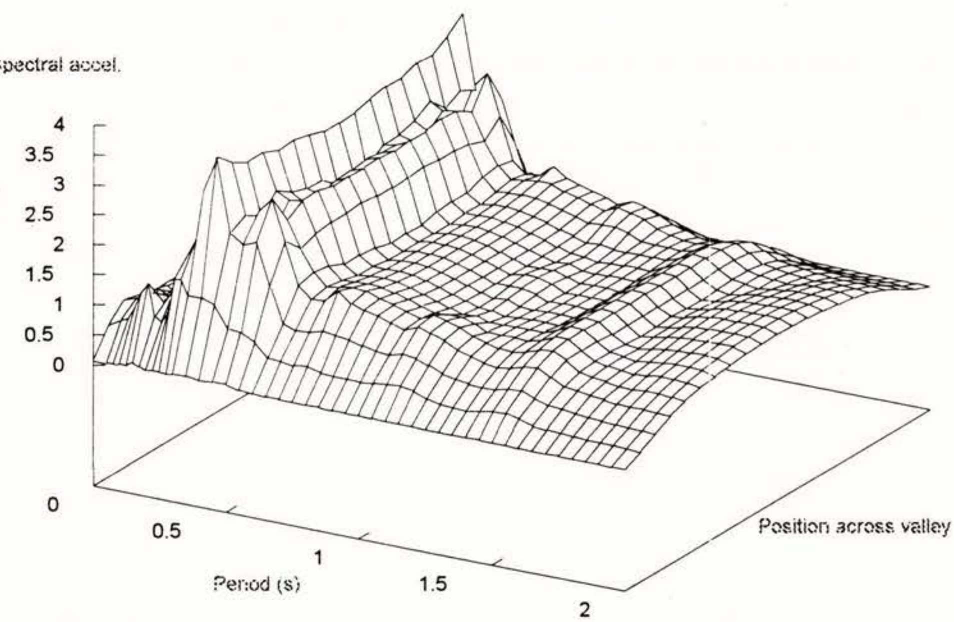

Fig. 8.20 Surface response spectra for the 16:1 aspect ratio valley

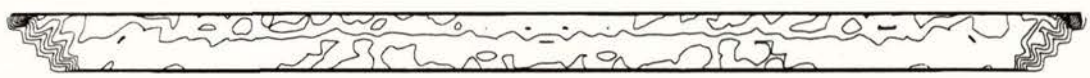

(a) 16:1 aspect ratio (peak pore pressure ratio=0.63)

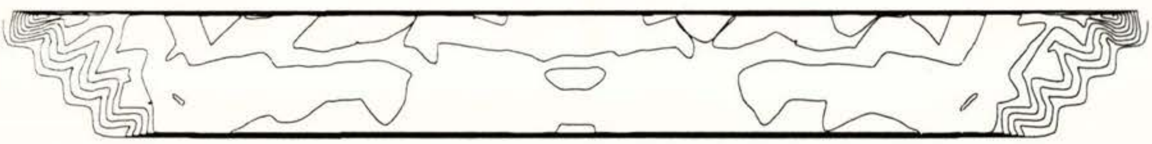

(b) 8:1 aspect ratio (peak pore pressure ratio=0.64)

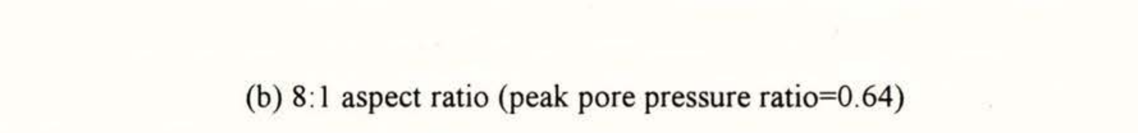

(c) 6:1 aspect ratio (peak pore pressure ratio=0.78)

(d) 4:1 aspect ratio (peak pore pressure ratio=0.9)

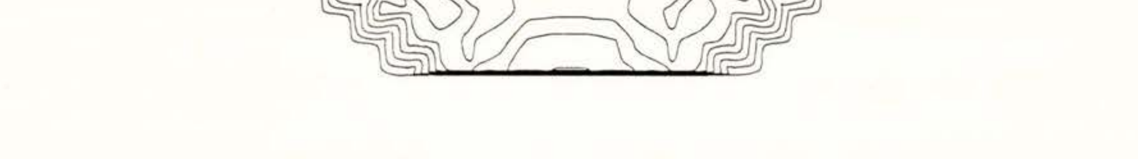

(e) 2:1 aspect ratio (peak pore pressure ratio= 0.91)

Fig. 8.19 Excess pore pressure ratios for different aspect ratio valleys

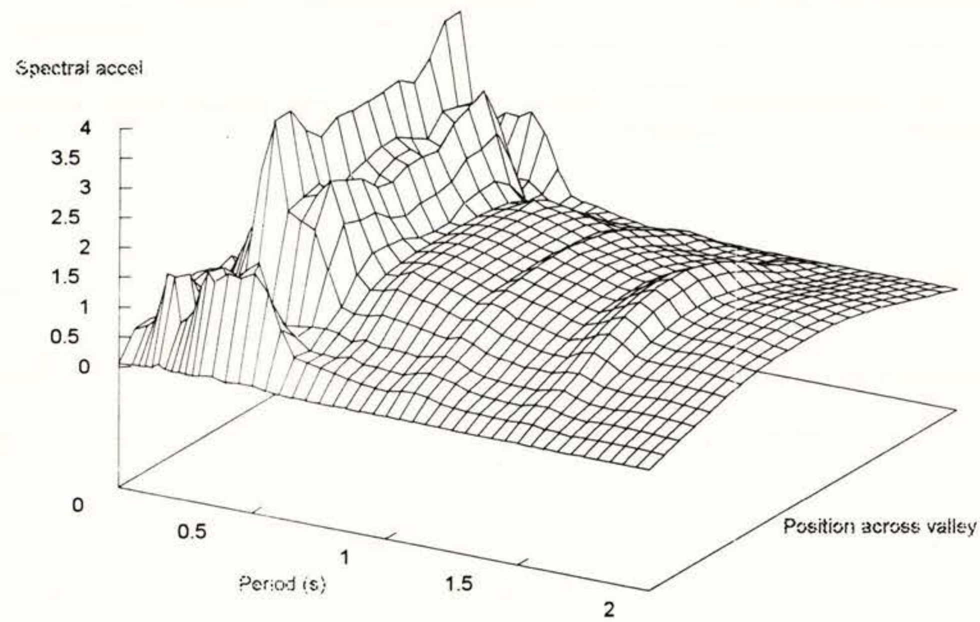

Fig. 8.21 Surface response spectra for the 8:1 aspect ratio valley

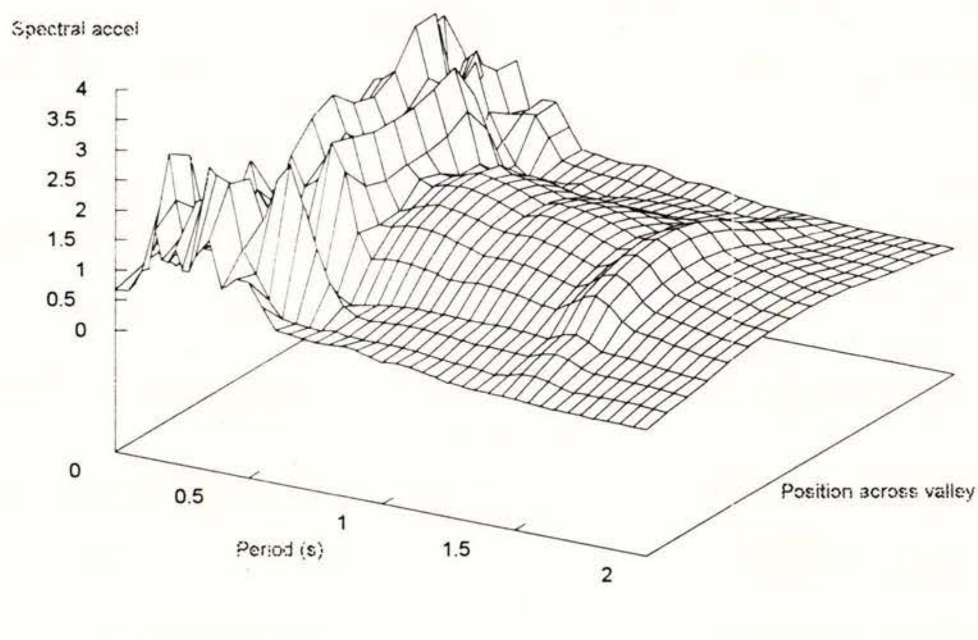

Fig. 8.22 Surface response spectra for the 6:1 aspect ratio valley

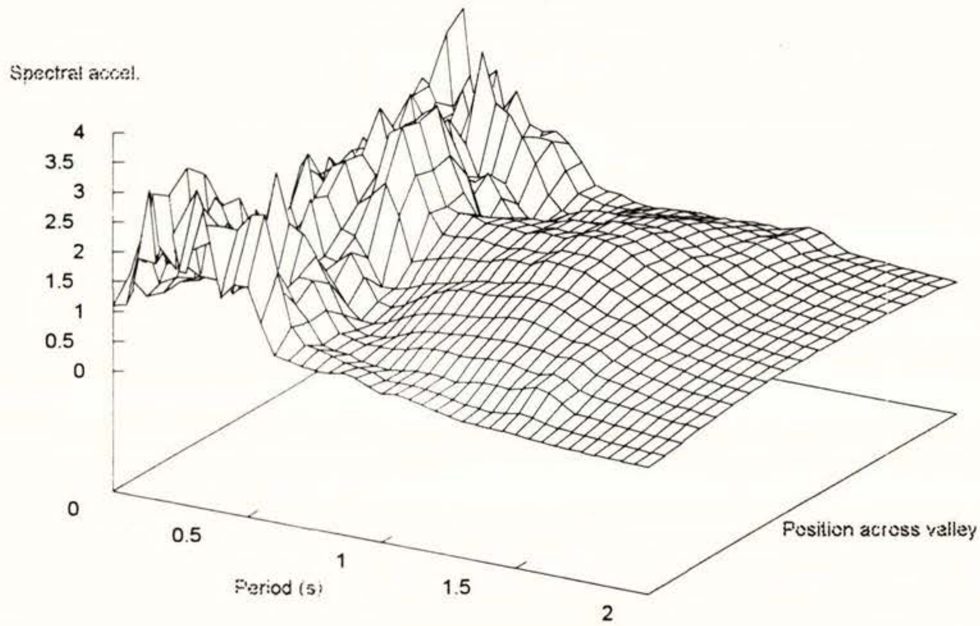

Fig. 8.23 Surface response spectra for the 4:1 aspect ratio valley

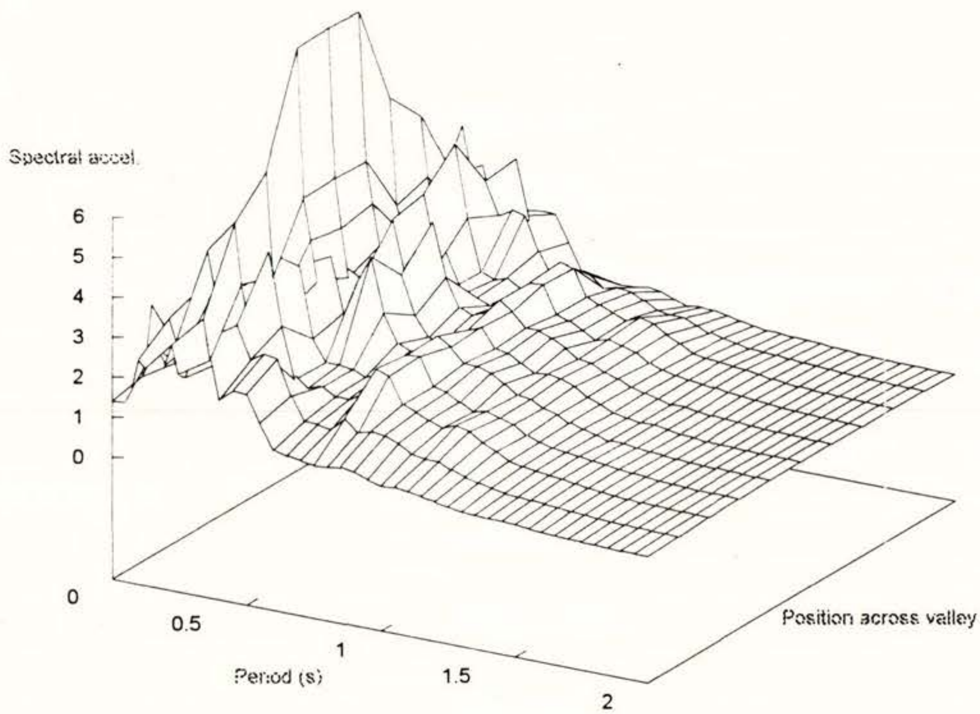

Fig. 8.24 Surface response spectra for the 2:1 aspect ratio valley

The lateral boundaries have a marked influence on the surface response spectra as the aspect ratio decreases. This feature was also seen in chapter seven for cohesive volcanic soil deposits. The magnitude of the induced pore pressures are also significantly affected by the geometry of the basin. There is little difference between the response of the very wide 16:1 and the wide 8:1 valley. This is the case for both the surface response spectra and the peak pore pressure response. As the aspect ratio decreases, the lateral boundaries stiffen the soil deposit. For the source motion used in these results, this lead to a higher liquefaction response in the valley which increased the magnitude of the induced excess pore pressures by as much as 50% for the narrow basins.

These results again show that the geometry of the soil basin is an important factor to be accounted for when evaluating the liquefaction potential of a site. The results of the one dimensional effective stress analysis have been found to be accurate for the wide valleys, but as the aspect ratio decreases, the divergence between the two analyses increases. The magnitude of the divergence between the two solutions is dependent on both the material properties and the characteristics of the source motion.

8.5 INFLUENCE OF PERMEABILITY ON SITE RESPONSE CHARACTERISTICS

The experimental results of chapter 6 showed that the Puni sand exhibits high permeabilities when compared to similar quartzitic sands. The liquefaction response of soils depends on two opposing factors: the first is the generation of excess pore water pressure from the potential for induced volumetric strains, and the second is the reduction in this excess pore water pressure due to the drainage and pressure redistribution within the soil deposit. If the permeabilities are high the pore pressure will drain before significant levels are attained, which is one of the reasons gravels rarely experience liquefaction. Previous studies (Marks 1992) showed that values of the coefficient of permeability greater than 10^{-4} m/s can influence the liquefaction response of a soil. The experimentally determined values of permeability for the Puni sand may be expressed by the equation

$$k=0.004e^{-0.02DR} \qquad 8.4$$

where k is the coefficient of permeability in m/s

DR is the relative density in %.

For the loose and dense states of the Puni sand, this formula gives permeability values of $2*10^{-3}$ and $7*10^{-4}$ m/s respectively. As these are higher than to 10^{-4} m/s value, the influence of permeability in site response analyses of volcanic sands was investigated. As the two dimensional effective stress program does not include a numerical pore pressure redistribution scheme, the one dimensional program was used for this aspect of the study.

A number of analyses in the form of case studies were performed to investigate various aspects of pore pressure redistribution, and the results of these studies are given below. The influence of pore pressure redistribution within highly stratified deposits is also investigated. The general sand and liquefaction properties used in these analyses are the same as for the Puni sand results presented above in the two dimensional work unless otherwise stated.

8.5.1 Source Motion

The source motion used in these analyses was from the 1987 Edgecumbe earthquake, recorded as a free field motion adjacent to the base of the Matahina earth Dam. This motion was used as during the 1987 event, widespread liquefaction of volcanically derived sands was observed. The recorded time history of the major component of this motion (labelled N07W) is shown in figure 8.25.

It is clear that main concentration of earthquake motion occurs between 10 and 15 seconds, and tails off after that. This motion was extended by a further 100 seconds in the following analyses to allow for a reasonable degree of pore pressure redistribution after the motion had stopped.

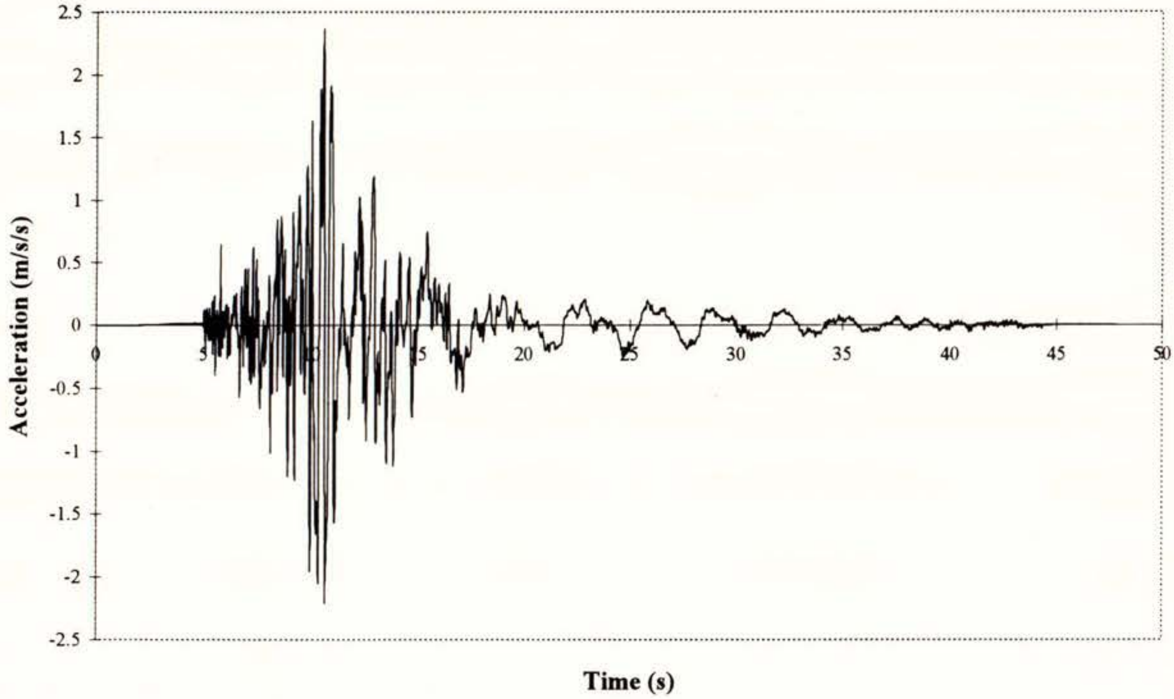

Fig. 8.25 Recorded time history of the Matahina earthquake motion in 1987

It is clear that main concentration of earthquake motion occurs between 10 and 15 seconds, and tails off after that. This motion was extended by a further 100 seconds in the following analyses to allow for a reasonable degree of pore pressure redistribution after the motion had stopped.

8.5.2 Case Study One: Homogeneous Sand Deposit

This first case study analyses a 24 metre deep deposit of loose Puni sand. This was chosen as an initial study as it was simple and would isolated many of the factors that were of interest. The input earthquake motion was scaled down to a peak acceleration of 0.1g from the recorded 0.22g. This was required as widespread liquefaction of the loose sand was observed when the full magnitude of the motion occurred. Initially an undrained liquefaction analysis was performed, which yielded a relatively wide band of liquefaction at depths of between 3 and 7 metres. This result corresponds to the observed results of liquefaction occurring in relatively surface zones. This soil deposit was then reanalysed, this time including the effects of drainage. The value of the coefficient of permeability of the loose Puni sand was taken as the value quoted above ($2*^{10-3}$). Figure 8.26 shows the difference between the peak levels of pore pressure for the undrained and drained analyses.

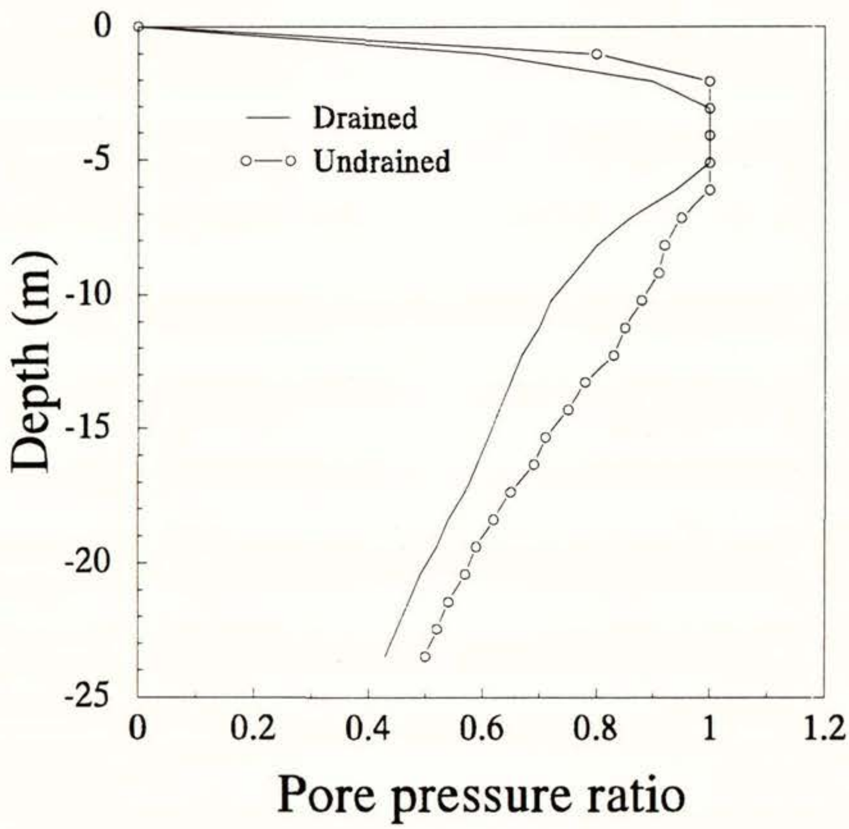

Fig. 8.26 Excess peak pore pressure response for drained and undrained analyses

It can be seen that although both display liquefaction, in the undrained case liquefaction is more widespread, as the drained case shows some reduction in pore pressure due to drainage. The influence of drainage may be more clearly seen in the time history plots of pore pressure. Theses are shown in figure 8.27 and 8.28 for the undrained and drained analyses respectively.

The drained time history analysis clearly shows the inhibited liquefaction response from the effects of drainage. A gradual reduction in the levels of pore pressure can be seen, particularly in the lower area which drains towards the surface, thus keeping the near surface pore pressures high.

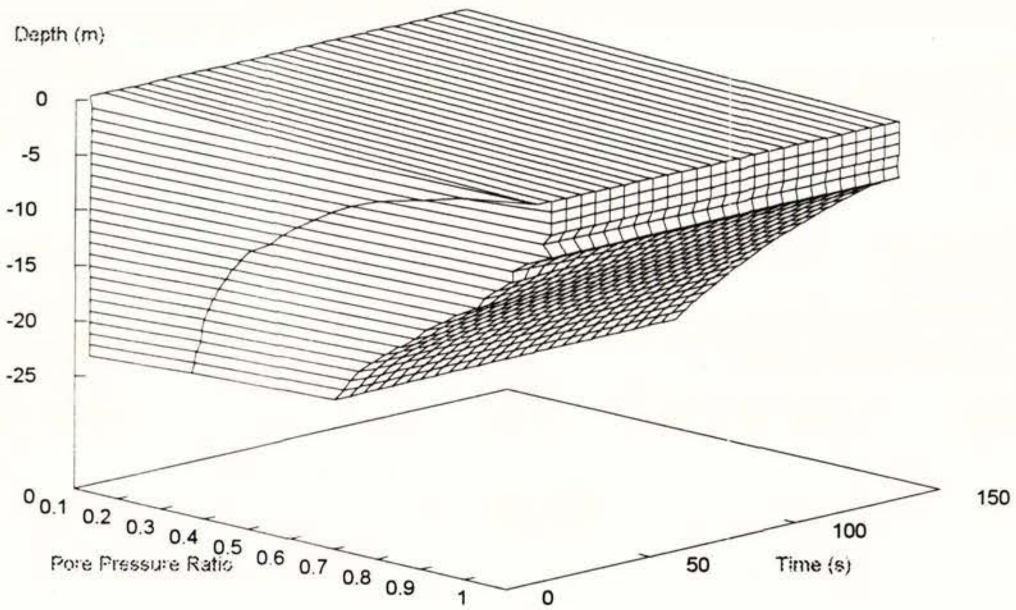

Fig. 8.27 Undrained pore pressure time history response for singe sand layer

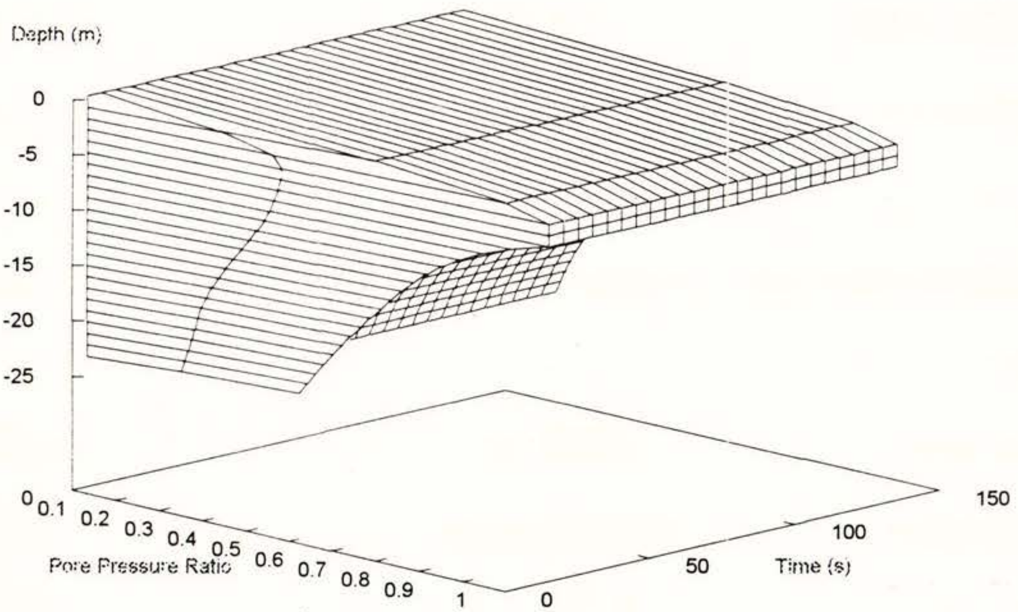

Fig. 8.28 Drained pore pressure time history response for singe sand layer

8.5.3 Case Study Two: Loose and Dense Sand Combination

The second case study involves a simple profile of one dense and one loose layer of pumice sand. The dense surface layer is underlain by a loose sand layer, each of 12 metres thick. This maintains the overall thickness of 24 metres used in case study one. The dense sand layer is assumed to generate no excess pore pressure, which allows the drainage paths to be clearly shown. The experimental testing showed that the dense Puni sand did develop some excess pore pressures under cyclic loading, but for these analyses this was ignored.

Figure 8.29 shows the peak excess pore pressure response for the undrained and drained analyses. The values of the coefficient of permeability for the both the loose and dense Puni sand used are those stated earlier.

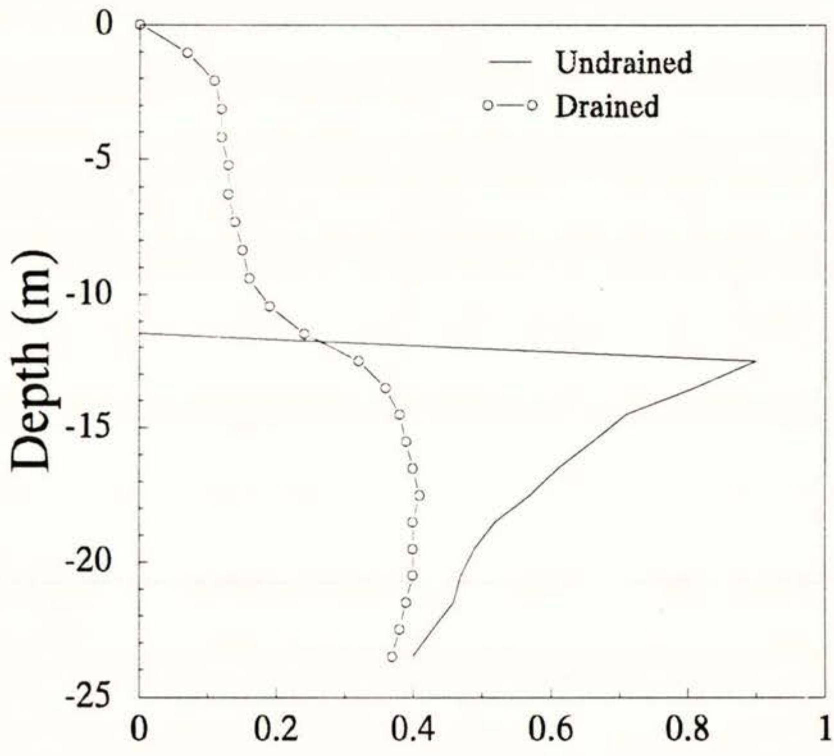

Fig. 8.29 Excess peak pore pressure response for drained and undrained analyses

This figure shows the difference in peak pore pressure response between the drained and undrained analyses. Due to the increased depth and corresponding increase in confining pressure of the loose sand layer, there is no liquefaction in the undrained case. The peak excess pore pressure value of 0.9, at a depth of 13 metres is similar to the full depth undrained analysis of case one. There is no excess pore pressure in the top layer for the undrained analysis as no pore pressure is generated in this region. The influence of drainage is very clear from this figure, decreasing the excess pore pressure from 0.9 to 0.4, which is a substantial reduction. The pore pressure time history shown in figure 8.30 clearly illustrates the influence of pore pressure drainage.

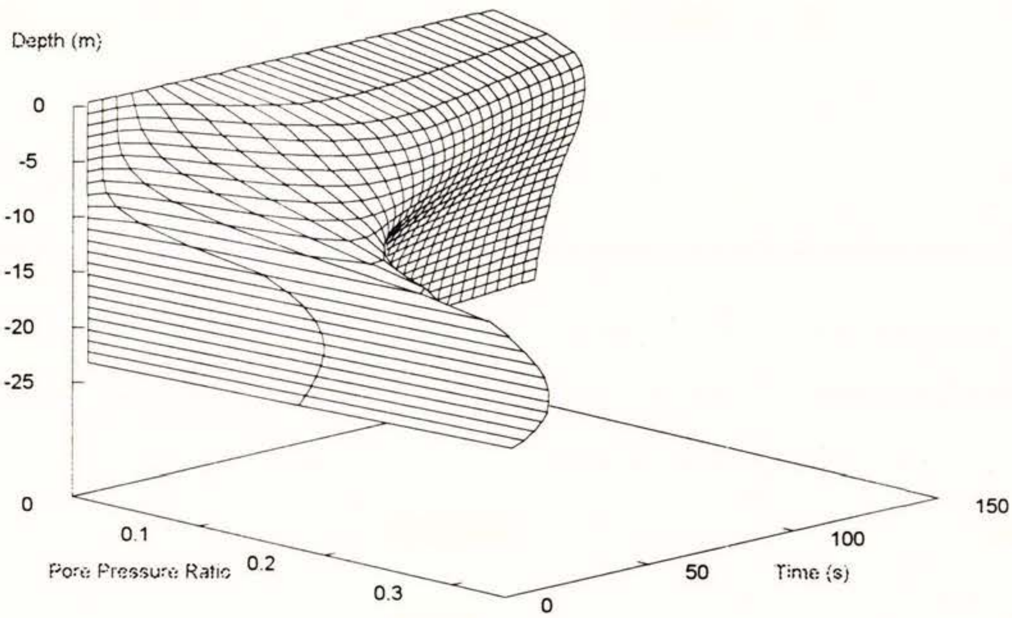

Fig. 8.30 Drained pore pressure time history response for the two layer sand deposit

This figure shows the generation of pore pressures in the lower layers initially due to the seismic motion. Later in the time history the drainage becomes significant as the pore water flows towards the surface through the dense sand. This effect can also be seen in figure 8.31, which shows the pore pressure profile at two different times during the analysis. The first is at 15 seconds when the pore pressure generation is dominant, and the second is at 50 second when drainage dominates the response. This example suggests that the increase in liquefaction resistance that volcanic sands may display when compared to quartzitic sands is due to their higher permeabilities.

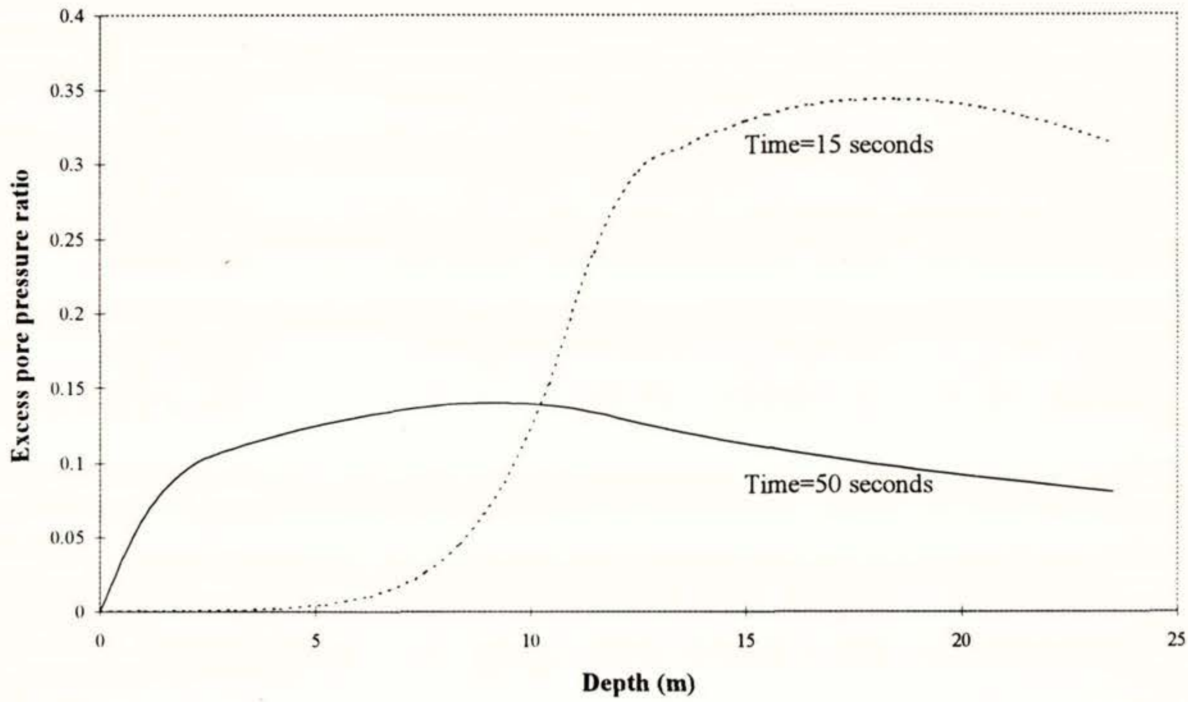

Fig. 8.31 Excess pore pressure response at two different times showing drainage influence

8.5.4 Case Study Three: Complex Stratified Deposits

Most sand deposits are not uniform in nature, but may in fact be a complex combination of interbedded layers of loose and dense sands, and possibly silts and clays. These different layers may alter the liquefaction response of a site considerably, but are often ignored in traditional liquefaction analyses. Dense sand layers, depending on their properties, tend to "soak up" excess pore pressures generated during seismic loading by adjacent loose layers. This can have the effect of reducing the potential for liquefaction within a sand deposit. Thin silt or clay layers act as impermeable boundaries to the flux of dissipating pore water, inhibiting this dissipation and leading to an increased liquefaction response in some cases.

The liquefaction response of a complex sand deposit was investigated to determine the characteristics of these soil deposits. The 24 metre deep complex stratified profile of loose and dense sand layers is shown in figure 8.32. This profile was chosen as it was considered typical of some sites in the Bay of Plenty area (Pender 1994). Table 8.2 shows the SPT blow count profile that was assumed for this case study.

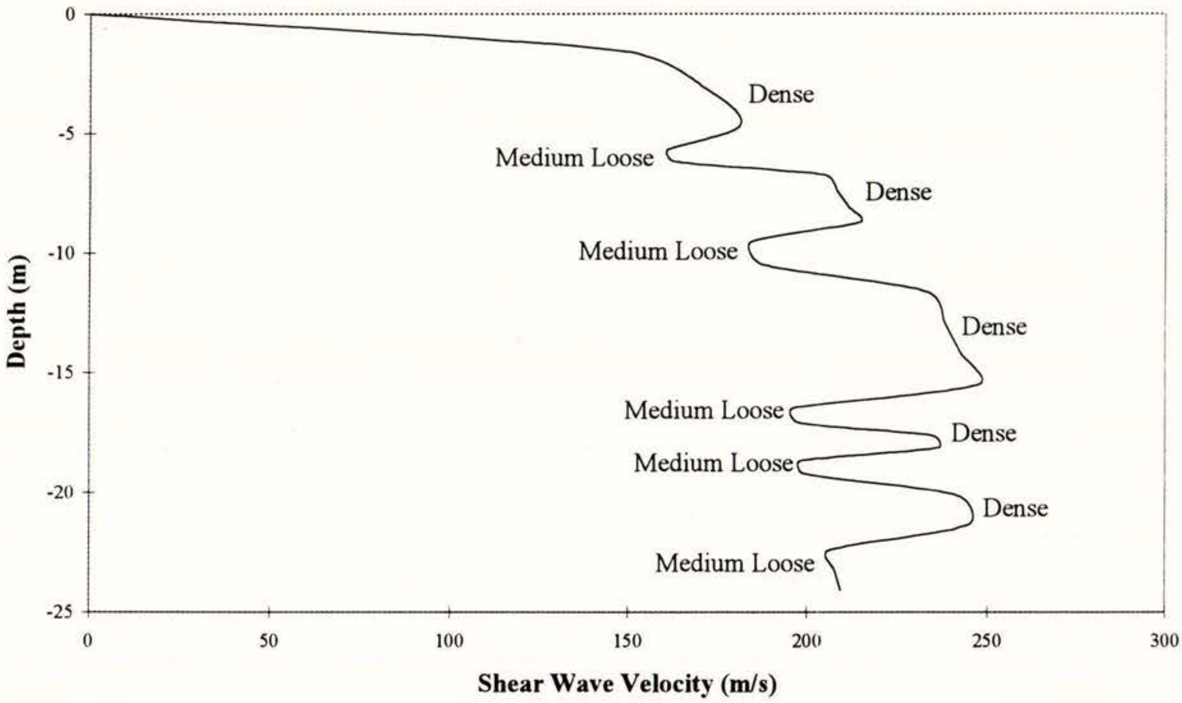

Fig. 8.32 Shear wave velocity profile of the complex stratified deposit

Table 8.2 $(N_1)_{60}$ blow count data for each layer of the complex stratified deposit

Layer Number	$(N_1)_{60}$ (blows/ft)
1	30
2	9
3	33
4	12
5	40
6	11
7	30
8	10
9	30
10	10

As with the other case studies both a drained and undrained analysis were performed. The input motion was however scaled up to a 0.3g peak input acceleration to approach what was considered as a reasonable design earthquake. Figure 8.33 shows the undrained response of the stratified deposit, again with zero pore pressure generation in the dense layers.

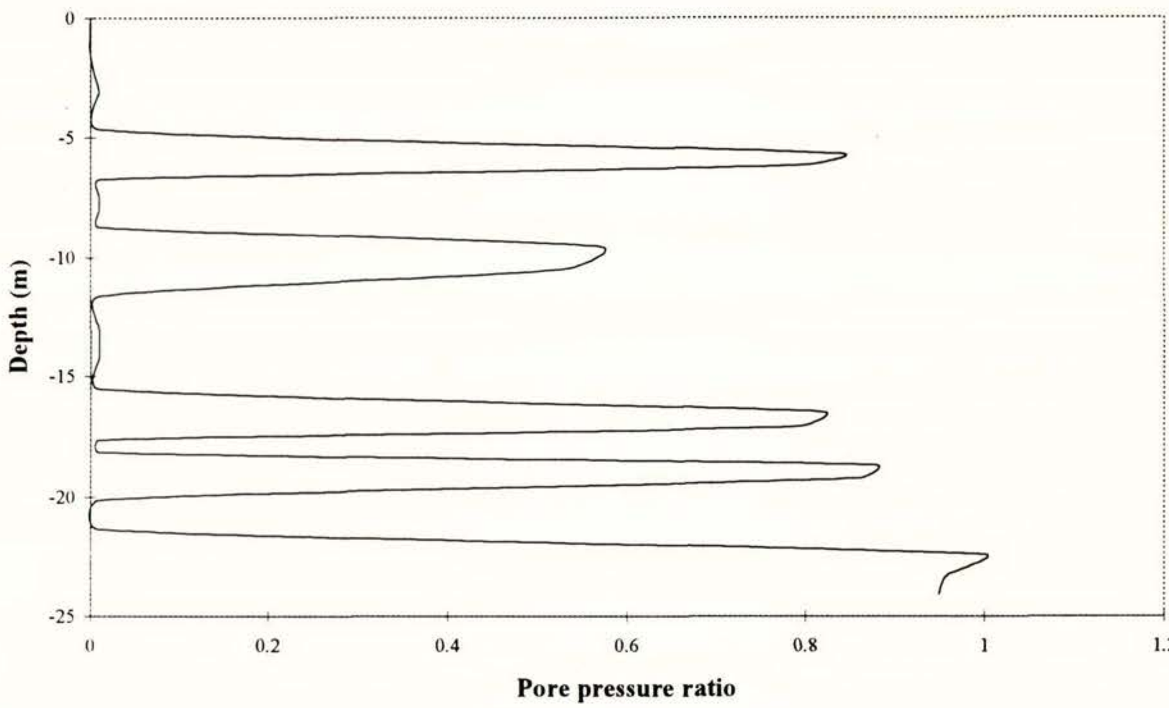

Fig. 8.33 Excess pore pressure response for the undrained stratified deposit

It can be seen that high pore pressures are developed in all of the loose layers, which one would expect when considering the level of input motion. The drained time history response of these stratified layers is shown in figure 8.34, which shows a marked reduction in the levels of excess pore pressure.

There are two reasons for this very marked reduction in the liquefaction response. As with the other case studies the general redistribution throughout the deposit limits the pore pressure rise. The level of excess pore water pressure reduction from drainage is larger for this case study than the others, and this lower liquefaction response may be explained by the other factor

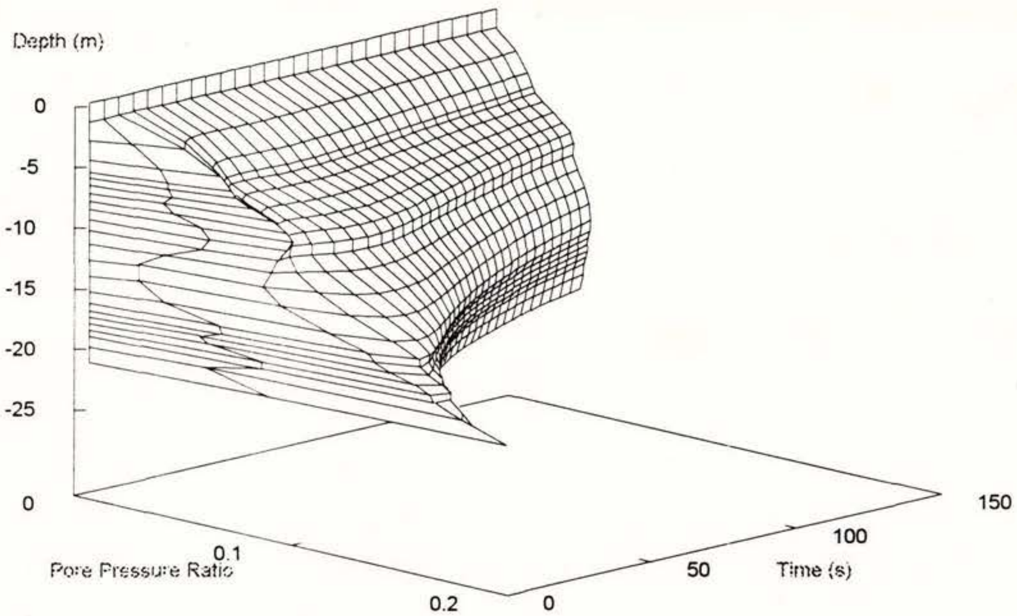

Fig. 8.34 Pore pressure time history response for drained stratified profile

The second reason is that the volume of pore water that must flow to allow redistribution is small due to the limited thickness of each loose layer. This pore water therefore easily flows into the adjacent low pressure dense sand layers which are large enough to accommodate this drained pore water. The net result of these two factors is that stratified deposits may be significantly more resistant to liquefaction as a whole, even though some of the individual layers may be considered susceptible by themselves.

Influence of Impermeable Layers

Stratified deposits often contain thin silt or clay lenses that are relatively impermeable which may severely restrict the flow of pore water with the soil. To investigate this, one of the dense sand layers near the centre of the complex stratification profile was assumed to contain such lenses, which rendered this layer impermeable. Figure 8.35 shows the time history of the pore pressure response of this case.

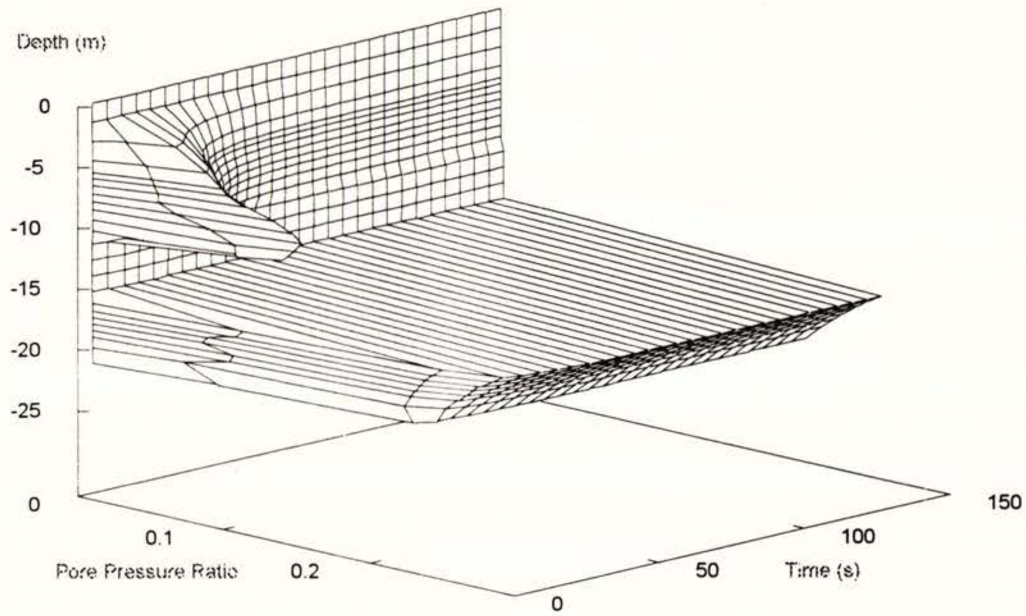

Fig. 8.35 Pore pressure time history with impermeable silt layer

The influence of the impermeable layer can be clearly seen in the above plot. The flow of pore water is severely restricted in the bottom of the soil deposit, and the pore pressures in this zone rise accordingly. They do not however rise to the very high levels seen in the undrained case however, because the three loose and two dense layers in this region redistribute the pore water pressure. The levels of excess pore pressure in the top zone of the soil profile remain essentially unaltered as they drain to the surface. The thin impermeable layers can have an important influence on the liquefaction behaviour of a soil deposit. If adjacent dense layers are not present, the liquefaction response of adjacent loose layers can be essentially undrained, leading to the higher pore pressures seen in the undrained case.

Pore pressure tend to redistribute laterally as well as vertically, and therefore the pore water would not remain trapped in the lower layers. As the impermeable layer is unlikely to be complete throughout a two or three dimensional profile, vertical drainage would occur at some location and the excess pore pressures would eventually dissipate. The one dimensional analysis can not account for such factors, but it is likely that this form of redistribution would take some time, leaving the effect of the impermeable layer evident.

For stratified deposits such as the one analysed above it appears to be conservative to assume undrained conditions in a liquefaction analysis. This may be particularly so when considering volcanic sands that exhibit higher permeabilities. The very important rider to this statement is that any impermeable layers present may significantly decrease the ability of adjacent dense sand layers to redistribute the large excess pore pressure developed in the loose layers. As most site investigations are unlikely to be thorough enough to find all of the thin impermeable layers that may be present, care should be taken in assuming that adjacent dense sand layers will have a significant retarding influence on the liquefaction of that deposit.

8.6 SUMMARY

The focus of this chapter was to evaluate the ability of the numerical models to reflect the behaviour of the volcanic Puni sand. Initially the numerical simple shear program was used to evaluate the relevant liquefaction constants by backfitting the model to the known experimental results. This procedure involved transforming the cyclic triaxial results to an equivalent simple shear result with the widely used empirical conversion factors. It was not possible to evaluate if the transformation constant would vary for the volcanic soils, but K_o testing helped in defining this factor. The numerical simulation of the experimental results agreed relatively well when considering the number of unknowns in the system. The largest area of disagreement was the extensional phases of the cyclic triaxial tests. From these results it was clear that the strain controlled pore pressure model was capable of simulating the seismic response of the Puni sand.

A number of two dimensional valleys were then investigated. Initially however, comparisons between the wide two dimensional valley and the one dimensional analysis were made. This provided encouraging results as the two solution agreed relatively well. This result gave some confidence in the results of the two dimensional solution. The two dimensional shear stress and shear strain controlled models were then compared to ascertain the differences between these two approaches. It is widely accepted that pore pressure generation is a function of induced strain rather than induced stress levels (chapter three), so it was important to investigate the differences. The results clearly showed that in the relatively near surface zone the stress controlled model showed a significantly larger liquefaction response than the strain model. The stress controlled model is very sensitive to the magnitude of the induced stress ratio, and for low overburden pressures in the near surface zone, very high stress ratios were induced. As a result, liquefaction was predicted in these areas by the stress controlled model, whereas the strain model only predicted pore pressure ratios in the region of 60%.

Two dimensional strain controlled analyses showed that the geometry of the valley can be a significant factor when considering the liquefaction response of a site. It was found that decreasing the aspect ratio of the valley induced a larger liquefaction response for the volcanic sand. Decreasing the width of the valley tends to stiffen the peak natural response of the system. The relationship for larger strain non linear behaviour between aspect ratio and peak response periods is not as clear as for the small strain elastic responses shown in chapter seven, but the overall effect is similar. The influence of the geometry on the liquefaction response is therefore a function of the aspect ratio, material properties and the periods of higher energy in the source motion. It is therefore not possible to make the general assumption that narrower valleys induce higher pore pressures, as the results of this study have shown.

The high levels of permeability of the Puni sand found in the experimental phase of this study can have a significant influence on the liquefaction response of that sand. Larger sand permeabilities then to reduce the liquefaction response of a sand, particularly when the loose sands are surrounded by denser ones (although the dense sand permeabilities must be larger than 10^{-4} m/s as was the case for the dense Puni sand). The one factor that must be considered however is the influence of this silt or clay layers within the soil deposit that can act as an impermeable layer. In some cases this may force the sand to respond in an undrained condition for much of the analysis.

Chapter Nine

Conclusions

9.1 CONCLUSION

The aim of the research presented in this study was to investigate the seismic site response characteristics of typical New Zealand volcanic soils, and to draw some conclusions as to their behaviour under seismic loading conditions. Very little research had been done in this area to date, and it was therefore an important area to consider. The lack of data on both the static and dynamic properties of New Zealand volcanic sands lead to a static and dynamic testing programme on a volcanic sand from the upper central North Island. This programme provided valuable data that was then used in the numerical studies presented in this report.

The computer programs developed allowed the investigation of liquefaction potential in a two dimensional soil deposit, which is an important advancement on total stress analyses. Many past earthquakes have graphically illustrated the disastrous results of liquefaction and therefore it is an important factor to consider in the analyses of ground motions. Two effective stress models were implemented into the two dimensional code. Both a stress controlled and strain controlled model were used, which allowed comparisons and validations of the models to be done. The equivalent one dimensional model was also used in this investigation.

Volcanic soils can be classed as either cohesive or noncohesive. From the literature there was only two studies on cohesive soils and no data at all on noncohesive soils. The available data on cohesive volcanic ash and silts indicated that their dynamic behaviour was similar to other cohesive soils, although they did exhibit a very sensitive structure. As a result of no data being found on volcanic sands, a testing programme on a volcanically derived sand was undertaken at the University of Auckland. This testing programme included permeability and general classification tests, cyclic triaxial testing and investigations of the low strain shear modulus and non linear behaviour.

The static Puni sand properties were characterised by crushable grains, low bulk density, and relatively high permeability and void ratio. The pumice grains could be crushed by hand, but under cyclic triaxial shear loading (liquefaction testing) no crushing was detected. Other triaxial shear testing on this material at the University of Auckland found significant grain crushing, but the magnitude of the stresses under cyclic liquefaction testing were found to be insufficient for grain crushing. This means one of the characteristic properties of this pumiceous sand can perhaps be disregarded when considering its liquefaction response. Whether this is the case for other volcanic sands is not clear.

The reliability and repeatability of the cyclic triaxial liquefaction testing procedure was investigated and found to be accurate. The dry pluviation technique was used to construct the loose sand samples, and a dry vibration method was used to construct the dense sand samples. Repeatability tests of the loose samples subjected to liquefaction testing produced agreement of the results to within 7% . Data aquisistion software was written for the experimental testing programme. Once the testing procedure was established a series of loose samples were tested at different stress ratios, and a liquefaction strength curve was produced. This curve took a similar form to quartzitic sands, as did the pore pressure generation curves. These results indicated that the Puni sand behaved in a similar manner under liquefaction testing conditions to quartzitic sands.

Investigation of the low strain and non linear behaviour of the Puni sand was then undertaken. It was found that the non linear properties of this sand followed similar trends to the empirical data base in the literature. The low strain shear wave velocity, and hence shear modulus, was investigated using bender elements. These results showed that the shear modulus was proportional to $(\sigma_m^{/})^{0.53}$ which is different from the usual power term which is taken as 0.5. Although a small difference, this can lead to significant variations in shear modulus and wave velocity for confining stresses likely to be encountered in deep seismic valley analyses.

The main unknown factor in the behaviour of this pumiceous sand is its response to penetration testing. As the bulk of liquefaction analyses rely on either SPT or CPT penetration test results this is a very important area to investigate in the future, but was outside the scope of this present report. The experimental programme did however indicate that many of the dynamic and liquefaction properties of the Puni sand are similar to the quartzitic sand properties that dominate the literature. Based on the results of this one sand it is not possible to generalise as to the dynamic behaviour of other volcanically derived noncohesive soils.

An indepth study of the response of in-plane two dimensional cohesive valley deposits to seismic motions was then carried. Since the limited data on noncohesive volcanic soils mentioned earlier indicated similar behaviour to other cohesive soils, generalised soil properties were used to model the volcanic soil properties. The sensitive structure of cohesive volcanic soils could not be modelled in terms of effective stress as a reliable excess pore pressure model is not available or cohesive volcanic soils. Past studies of pore water pressure in sands has shown that limited excess pore pressure generation is relatively insignificant in the response of the soil deposit as a whole.

The response of a wide two dimensional valley subjected to small motions was investigated using a range of single frequency harmonic inputs. The levels of the input harmonic motions were set to model small earthquakes and micro tremors. This was found to initiate an essentially elastic response in the numerical analysis. The range of input frequencies allowed the natural periods of a range of soil deposits to be isolated and compared with an existing one dimensional elastic closed form solution. It was found that the wide valley agreed with the closed form solution, giving confidence in the numerical program. The influence of the lateral boundaries of the two dimensional valley was found to be significant at aspect ratios of less than 8:1. The lateral boundaries stiffened the response of the soil deposit which decreased the natural period of the soil deposit. A larger than 50% decrease in the natural period was observed for very narrow valleys. This is an important finding as the natural periods of a system dominate the linear response of that system, which is the basis for the elastic modal superposition analysis method. Seismic motions tend to have concentrations of energy at various frequencies, and an understanding of the natural periods of a soil valley under is very important.

For larger input motion the behaviour of the soil is dominated by the non linear constitutive relationship. It was found that input motions as low as $0.1 m/s^2$ begin to initiate a non linear response. The non linear behaviour tends to reduce the average value of the shear wave velocity and shear modulus of the soil, which leads to a lengthening of the periods of peak response. Motions in excess of $0.3 m/s^2$ for the soil deposits investigated induced large non linear behaviour, and the response of the valley became dominated by this non linear behaviour. The peak response frequencies clearly evident for the small motion elastic analyses were no longer evident as the response became smeared over the frequency range. From these results it can be concluded that the response of a soil deposit to small motions can not just be scaled up to represent the response during a large motion event. This particularly relates to the data gained from field micro tremor studies.

Finally numerical modelling of the high strain earthquake response of volcanic sand deposits was undertaken. The liquefaction constants for the Puni sand were evaluated by the backfitting procedure that has been developed by the authors for effective stress analyses. The cyclic triaxial results gained in the experimental testing had to be transformed to equivalent cyclic simple shear results for the numerical model. The conversion factor was taken from the literature as no other data was available, but K_O testing at the University of Auckland by other researchers helped in defining the factor. The numerical simulation of the simple cyclic shear test agreed relatively well with the transformed triaxial data once the relative constants had been determined. The numerical pore pressure generation curves and hysteresis loops both showed similar features to the experimental data. From these results it was clear that the existing pore pressure model was capable of simulating the excess pore water pressure response of the Puni sand, and could therefore be used in site response analyses.

Initially the two dimensional strain controlled effective stress solution was compared to the equivalent one dimensional solution. This showed reasonable agreement when all of the relevant factors were considered. The peak pore pressures at the centre of the wide valley agreed very well in the near surface zone with the one dimensional results, but there was some divergence at depth. Comparisons were then made between the two dimensional stress controlled and strain controlled effective stress solutions. The stress controlled model may be considered as more empirical than the strain controlled model. It is generally accepted that pore pressure generation is a function of shear strain rather than shear stress. The results showed good agreement between the two solutions at depth, but significantly diverged at the near surface zone. This was because the stress controlled model was very sensitive to the induced stress ratios, and large stress ratios were observed in the near surface zones. Although the stress distribution of the two analyses was similar, the particularly low overburden pressure from the volcanic overlying sand meant that the stress ratios were high in this area, thus leading to high induced stress ratios. From these results it was concluded that care must be taken when evaluating the results of analysis methods that are very sensitive to a particular parameter. The strain model was found to be less sensitive to these low overburden pressures.

Site response analyses were carried out on a variety of two dimensional volcanic sand deposits to investigate the influence of basin geometry on the liquefaction response. It was found that the valley geometry had a significant effect on the liquefaction response of the deposit, with up to 50% higher responses being shown in the narrow valleys. The main reason for the elevated response seen in the narrow valleys was a combination of the material properties of the sand, the influence of the lateral geometries and the concentration of energy in the source motion.

Low magnitude studies in chapter seven showed that the lateral boundaries tended to stiffen the overall response properties of the site. When higher magnitude source motions are applied to the deposit, non linear behaviour starts to dominate and the boundary influence becomes much harder to accurately quantify. It is reasonable to assume however that a similar general stiffening effect occurs to some extent in high motion events as the aspect ratio decreases. This can be seen in the fact that the liquefaction response is elevated for the narrower valleys in these analyses. This general stiffening induced a higher site response in the valley for the narrow basins which is reflected in the elevated pore pressures. As the site response is a strong function of the peak response periods of a site, when the source motion has a significant component of energy in these frequencies, the site response will increase. The induced liquefaction results could be reversed if the stiffening effect induced a lower site response in the narrow valleys, which is possible if the source motion was different or the material properties were different. Therefore the liquefaction response of different aspect ratio valleys is a function of the general site response of that valley. It must be stressed that the non linear behaviour of the soil during large motion events makes these factors very difficult to quantify, and therefore only trends can be observed and concluded upon.

The high levels of permeability found during the experimental phase of the testing programme had a significant influence on the computed liquefaction response. The one dimensional effective stress site response program was used in these analyses as it contained an excess pore water pressure redistribution model. These analyses showed that the high permeabilities significantly retard the development of excess pore water pressure under seismic loading. The results showed reductions of up to 60% in the liquefaction response when compared to undrained loading. Adjacent dense layers tended to "soak up" much of the excess pore water, leading to an overall reduction in the liquefaction potential of many sites. A highly stratified deposit was also investigated which showed similar trends. The one apprehension when considering the influence of excess pore water redistribution is that many stratified deposits may contain thin lenses of silts and clays that may significantly retard the flux of pore water, thus negating the positive influence of drainage. As many site investigations may not be detailed enough to pick up all of the thin layers, care should be exercised when the designer is relying on drainage to inhibit the liquefaction potential of a site, particularly when considering volcanic sites with their high permeabilities.

9.2 RECOMMENDATIONS FOR FURTHER WORK

A number of areas requiring further research in the area of volcanic soil site response have been unearthed during the course of this study. These extend to both the numerical and the experimental area. The numerical models presented have inherent simplifications that should be addressed at a later date. The first simplification is the fact that the analysis program is two dimensional, with the second lateral dimension assumed to be infinite. Ideally a three dimensional model could be developed that would fully account for all of the motions from a seismic source.

A finite element model as opposed to the current finite difference formulation would allow more complex site geometries and surface structures to be modelled, although the constant recalculation of the stiffness matrix make this method slow for non linear soil properties. It would however allow complex soil structure interaction to be taken into account, with the most likely applications being the earthquake response of earth and rockfill dams in conjunction with the dam foundations, abutments and the surrounding canyons. The yielding criterion for the non linear soil model is the Von Mises yield criterion at present, and this may be updated to a more accurate soil model. This could be extended further to allow for a number of different yield criteria, depending on the type of soil or rock being modelled.

The effective stress pore pressure model has possible limitations also. One concern is that it is based on experimental data that was derived from quartzitic sands tested in the United States. As a result it is unclear if the model is as accurate for other types of sands, particularly New Zealand volcanic sands. The in-plane two dimensional analysis only allows for one horizontal direction of shear loading, whereas in reality there are two components. Experimental data has shown that multi directional loading can have a strong influence on the liquefaction response of sands, and therefore a three dimensional site response and pore pressure model would more accurately account for the influence of these out of plane motions. The large permeabilities of the volcanic sands indicate that a two dimensional pore pressure redistribution model is required to be coupled to the current site response and pore pressure generation program. This would allow the influence of drainage systems and other characteristics to be investigated. The main retardant to the above recommendations is the large increase in complexity and computational requirements that accompanies such advancements. The increasing power of today's computers however makes a number of these advancements a distinct possibility.

The experimental testing programme also indicated a number of areas where further research is required. The data available on New Zealand volcanic soils was found to be very limited indeed, with most practitioners relying on overseas derived relationships. This was particularly the case for the dynamic properties of residual volcanic soils. As many geotechnical designs are strongly based on insitu penetration data the most pressing need is for research into this area. In particular the influence of the lighter pumiceous particles of cohesionless soils and the more sensitive clay and ash structures of cohesive soils must be investigated, particularly in relationship to their penetration response. Other properties of volcanic soils that could be investigated include the pore pressure response of ash, comparisons of soil properties to quartzitic based sands and a more rigorous investigation of the non linear constitutive behaviour. Such data would provide a higher level of confidence in the design of structures involving New Zealand volcanic soils.

References

Aki K. (1988), 'Local Site Effects on Strong Ground Motion', in *Earthquake Engineering and Soil Dynamics II- Recent Advances in Ground Motion Evaluation*, Geotechnical Special Publication No. 20, ASCE, pp. 103-155.

Aki K. and Larner K.L. (1970), 'Surface Motion of a Layered Medium Having an Irregular Interface Due to Incident Plane SH Waves', *Journal of Geophysical Research*, Volume 75, pp. 933-

Alterman Z. and Lowenthal D. (1972), 'Computer Generated Seismograms', in *Methods in Computational Physics, Volume 12: Seismology, Body Waves and Sources*, ed. Bolt B.A., Academic Press.

Ansal A.M. and Erken A. (1989), 'Undrained Behaviour of Clay Under Cyclic Stresses', *Journal of the Geotechnical Division, Proc. ASCE*, Volume 115, pp. 968-983.

ASTM (1991), 'Standard Test Methods for the Determination of the Modulus and Damping Properties of Soils Using the Cyclic Triaxial Apparatus", Designation D 3999-91.

Bard P.Y. and Bouchon M. (1980), 'The Seismic Response of Sediment Filled Valleys, Part I', *Bulletin of the Seismological Society of America*, Volume 70, pp. 1263-1286

Bard P.Y. and Bouchon M. (1985), 'Two Dimensional Resonance of Sediment Filled Valleys', *Bulletin of the Seismological Society of America*, Volume 75, pp. 519-541.

Bazant Z.P., Ansal A.M. and Krizek R.J. (1982), 'Endochronic Models for Soils', in *Soil Mechanics- Transient and Cyclic Loads*, ed. Pande G.N. and Zienkiwicz O.C., John Wiley and Sons, Ltd., pp. 419-438.

Bazant Z.P., Kriezek R.J. and Shieh C.L. (1983), 'Hysteretic Endochronic Theory for Sand', *Journal of the Engineering Mechanics Division, Proc. ASCE*, Volume 109, No. EM4, pp. 1073-1083.

Benites R. and Haines A.J. (1991), 'The Ricatti-Matrix Equation- Boundary Integral Method to Compute Seismic Wavefield in Heterogeneous Media', *EOS*, Volume 72, No. 44, 532D-1, 332.

Berrill J.H. (1995), 'Seismic Liquefaction of Cohesionless Soils', *New Zealand Geomechanics News*, No. 49, pp. 1-21.

Bhatia S.K. and Nanthikesan S. (1987), 'The Development of Constitutive Relationship for Seismic Pore Pressure', in *Soil Dynamics and Liquefaction,* Developments in Geotechnical Engineering, ed. Cakmak A.S., Volume 42, pp. 19-30.

Biot M.A. (1962), 'Mechanics of Deformation and Acoustic Propagation in Porous Media', *Journal of Applied Physics*, Volume 33, No. 4, pp. 1482-1498.

Boore D.M., Larner K.L. and Aki K. (1971), 'Comparison of Two Independent Methods for the Solution of Wave Scattering Problems: Response of a Sedimentary Basin to Vertically Incident SH Waves', *Journal of Geophysical Research*, Volume 76, pp. 558-

Bouchon M. (1973), 'Effect of Topography on Surface Motion', *Bulletin of the Seismological Society of America*, Volume 63, pp. 615-632.

Byrne P.M. (1991), 'A Cyclic Shear-Volume Coupling and Pore Pressure Model for Sand', *Proceedings of the 2nd International Conference on Recent Advances in Geotechnical Engineering and Soil Dynamics*, St Louis, Missouri.

Byrne P.M. and Yan, L. (1990), '1D-LIQ: A Computer Code for Predicting the Effective Stress One-Dimensional Response of Soil Layers to Seismic Loading', *Soil Mechanics Series*, No. 146, Dept. Civil Engineering, University of British Columbia.

Carter D.P. and Seed H.B. (1988), *Liquefaction of Sand Deposits Under Low Levels of Excitation*. Report No. EERC 88-11, Earthquake Engineering Research Centre, University of California, Berkeley.

Castro C. (1987), 'On the Behaviour of Soils During Earthquakes', in *Soil Dynamics and Liquefaction,* Developments in Geotechnical Engineering, ed. Cakmak A.S., Volume 42, pp. 169-204.

Chan S.Y. (1990), *Measurement of dynamic Properties of Some Volcanic Ash Soils*, M.E. Thesis, University of Auckland

Cole D.M., Kosloff P.P. and Minister J.B. (1988), 'A Numerical Boundary Integral Equation for Elastodynamics I', *Bulletin of the Seismological Society of America*, Volume 68, pp. 1331-1357.

De Alba P., Seed H.B. and Chan C.K. (1976), 'Sand Liquefaction is Large Scale Simple Shear Tests, *Journal of the Geotechnical Division, Proc. ASCE,* Volume 102, No. GT9, pp. 909-927

Dikmen S.U. and Ghaboussi J. (1984), 'Effective Stress Analysis of Seismic Response and Liquefaction, Theory', *Journal of the Geotechnical Division, Proc. ASCE*, Volume 110, No. 5, pp. 628-644.

Dobry R., Stokoe K.H., Ladd R.S. and Youd T.L. (1981a), 'In Situ Shear Wave Velocity Measurements to Evaluate Susceptibility', *ASCE National Convention*, St. Louis, Missouri.

Dobry R., Yokel F.Y. and Ladd R.S. (1981b), 'Liquefaction Potential of Overconsolidated Sands in Areas with Moderate Seismicity', *Proceedings of Conference on Earthquake and Earthquake Engineering in the Eastern U.S.*, Knoxville, Volume 2, pp. 643-664.

Finn W.D.L. (1985), 'Dynamic Effective Stress Response of Soil Structures; Theory and Centrifugal Model Studies', *Proceedings of the 5th International Conference on Numerical Methods is Geomechanics*, Nagoya, Japan, Volume 1, pp. 35-36

Finn W.D.L. (1988), 'Dynamic Analysis in Geotechnical Engineering', in *Earthquake Engineering and Soil Dynamics II- Recent Advances in Ground Motion Evaluation*, Geotechnical Special Publication No. 20, ASCE, pp. 523-591.

Finn W.D.L. and Bhatia S.K. (1981), 'Prediction of Seismic Porewater Pressures', *Proceedings 10th International Conference on Soil Mechanics and Foundation Engineering*, Stockholm, Sweden

Finn W.D.L., Lee K.W. and Martin G.R. (1977), 'An Effective Stress Model for Liquefaction', *Journal of the Geotechnical Division, Proc. ASCE*, Volume 103, No. GT6, pp. 517-533

Finn W.D.L., Yogendrakumar M., Yoshida N. and Yoshida H. (1986), *TARA-3: A Program to Compute the Response of 2-D Embankments and Soil Structure Interaction Schemes to Seismic Loading*, Department of Civil Engineering, University of British olumbia, Vancouver, Canada.

Finn W.D.L. and Vaid Y.P. (1977), 'Liquefaction Potential from Drained Constant Volume Cyclic Simple Shear Tests', *Preprints of the Sixth World Conference on Earthquake Engineering*, New Delhi, Volume 6, pp. 7-12.

Fishman K.L. and Ahmad S. (1995), 'Seismic Response for Alluvial Valleys Subjected to SH, and SV Waves, *Soil Dynamics and Earthquake Engineering*, Volume 14, pp. 249-258.

Frankel A. and Vidale J. (1992), 'A Three Dimensional Simulation of Seismic Waves in Santa Clara Valley, California, from a Loma Prieta Aftershock', *Bulletin of the Seismological Society of America*, Volume 82, pp. 2031-2045.

Freeze R.A. and Cherry J.A. (1979), *Groundwater*, Prentice Hill.

Harder L.F. (1988), *The Use of Penetration Tests to Determine the Liquefaction Resistance of Sands During Earthquake*, PhD Thesis, University of California, Berkeley.

Haskell N.A. (1960) 'Crustal Reflection of Plans SH Waves', *Journal of Geophysical Research*, Volume 65, p. 4147.

Hendron A.J. Jr. (1963), *The Behaviour of Sand in One Dimensional Compression*, PhD Thesis, University of Illinios.

Holzer T.L. (1994), 'Loma Prieta Damage Largely Attributed to Enhanced Ground Shaking', EOS, Volume 75, No. 26, pp. 299-301.

Hong T.L. and Helmberger D.V. (1977), 'Glorified Optics and Wave Propagation in Non Planar Structures', *Bulletin of the Seismological Society of America*, Volume 68, pp. 1313-1330.

Hudson M., Idriss I.M. and Beikae M. (1994), *QUAD4M*, Center for Geotechnical Modelling, Department of Civil and Environmental Engineering, University of California, Davis, California

Idriss I.M. and Seed H.B. (1974), 'Seismic Response by Variable Damping Finite Elements', *Journal of the Geotechnical Division, Proc. ASCE*, Volume 100, pp. 1-13.

Idriss I.M. and Seed H.B. (1968), 'Seismic Response of Horizontal Soil Layers', *Soil Mechanics and Foundations Division, Proc. ASCE*, Volume 94, p. 1003.

Ishihara K. (1985), 'Stability of Natural Deposits During Earthquakes', P*roceedings of the 11th International Conference on soil Mechanics and Foundation Engineering*, Volume 1, San Francisco, California, pp. 321-376.

Ishihara K. (1993), 'Liquefaction and Flow Failure during Earthquakes', *Geotechnique*, Volume 43, No. 3, pp. 351-415.

Ishihara K. and Towhata I. (1982), 'Dynamics Response Analysis of Level Ground Based on the Effective Stress Method', in *Soil Mechanics- Transient and Cyclic Loads*, ed. Pande G.N. and Zienkiwicz O.C., John Wiley and Sons, Ltd., pp. 133-172.

Iwan W.D. (1967), 'On a Class of Models for the Yielding Behaviour of Continuous and Composite Systems', *Journal of Applied Mechanics*, Volume 34, p. 612.

Joyner W.B. (1975), 'A Method for Calculating Non Linear Seismic Response in Two Dimensions', *Bulletin of the Seismological Society of America*, Volume 65, pp. 1337-1357.

Joyner W.B. and Chen A.T.F. (1975), 'Calculation of Non Linear Ground Response in Earthquakes', *Bulletin of the Seismological Society of America*, Volume 65, pp. 1315-1336.

Kanai K. (1950), 'The Effect of Solid Viscosity of Surface Layer on the Earthquake Movements', *Bulletin of the Earthquake Research Institute*, Tokyo University, Volume 28, p. 31.

Ladd R.S., Dobry R., Dutko P., Yokel F.Y. and Chung R.M. (1989), 'Pore-Water Pressure Buildup in Clean Sands Because of Cyclic Straining', *Geotechnical Testing Journal, ASTM*, Volume 12, No.1, pp. 77-86.

Larkin T.J. (1976), *The Propagation of Seismic Waves Through Non Linear Soil Media*, PhD Thesis, University of Auckland

Larkin T.J. (1977), *The Liquefaction of Sands Under Cyclic Loading*, Internal Report 515086, Norwegian Geotechnical Institute.

Larkin T.J. (1978a), *DENSOR, A Computer Program for Seismic Response Analysis of Non Linear Horizontal Soil Layers*, Internal Report 51508-7, Norwegian Geotechnical Institute.

Larkin T.J. (1978b), *Non Linear Effective Stress Dependent Seismic Site Response of Horizontal Media*, Internal Report 51508-7, Norwegian Geotechnical Institute.

Larkin T.J. (1985), 'Dynamic Torsion Tests and Two Dimensional Constitutive Modelling', Unpublished Manuscript, University of Auckland.

Larkin T.J. and Donovan N.C. (1979), 'Sensitivity of Computed Nonlinear Effective Stress Soill Response to Shear Modulus Relationships', *Proceedings of the Second US National Conference on Earthquake Engineering,* Stanford, pp. 573-582.

Lee V.W. (1978), *Displacement Near A Three Dimensional Hemispherical Canyon Subjected to Incident Plane Waves*, Report No. 78-16, Department of Civil Engineering, University of California, San Diego.

Lee V.W. (1984), 'Three Dimensional Diffraction of Plane P, SV and SH Waves by a Hemispherical Alluvial Valley', *Journal of Soil Dynamics and Earthquake Engineering,* Volume 3, No. 3, pp. 133-144.

Lee J.J. and Lanston C.A. (1983), 'Wave Propagation in a Three Dimensional Circular Basin', *Bulletin of the Seismological Society of America*, Volume 73, pp. 1937-1953.

Liou C.P., Streeter V.L. and Richart F.E. (1977), 'Numerical Model for Liquefaction' *Journal of the Geotechnical Division, Proc. ASCE*, Volume 103, No. GT6, pp. 589-606.

Luco J.E., Wong H.L. and De Barros F.C.P. (1990), 'Three Dimensional Response of a Cylindrical Canyon in a Layered Half Space', *Earthquake Engineering and Structural Dynamics*, Volume 19, pp. 799-817.

Lysmer J., Udaka, Tsai C.F., Seed H.B. (1974), *LUSH: A Computer Program for Complex Response Analysis of Soil Structure Systems*, Report EERC 74-4, Earthquake Engineering Research Centre, University of California, Berkeley.

Marks S. (1992), *The Seismic Response of Sandy Sites*, Masters Thesis, University of Auckland.

Marks S. and Larkin T.J. (1995), 'The Influence of Dimension and Earthquake Magnitude in Numerical Site Response Studies', *NZNSEE Annual Conference*, Rotorua, pp. 149-153.

Marks S., Pender M.J. and Larkin T.J. (1995), 'The Liquefaction Response of Stratified Sand Deposits', *Proceedings of the Pacific Conference ion Earthquake Engineering*, Melbourne, Australia.

Marsh E.J. (1992), *Two Dimensional Non Linear Ground Response Studies*, PhD Thesis, University of Auckland.

Marsh E.J., Larkin T.J., Haines A.J. and Benites R.A. (1995), 'Comparison of Linear and Non Linear Seismic Responses Of Two Dimensional Alluvial Basins', *Bulletin of the Seismological Society of America,* Volume 85, No. 5, pp. 874-889

Martin G.R., Finn W.D.L., and Seed H.B. (1975), 'Fundamentals of Liquefaction Under Cyclic Loading', *Journal of the Geotechnical Division, Proc. ASCE*, Volume 101, No. GT5, pp. 423-438.

Martin G.R., Tsai C.F. and Arulmoli K. (1991), 'A Practical Assessment of Site Liquefaction Effects and Remediation Needs', *Proceedings of the Second International Conference on Recent Advances in Geotechnical Earthquake Engineering and Soil Dynamics*, St Louis, Missouri.

Martin P.P. (1975), *Non Linear Methods for Dynamic Analysis of Ground Response*, PhD Thesis, University of California.

Martin P.P. and Seed H.B. (1979), 'Simplified Procedure for Effective Stress Analysis of Ground Response', *Journal of the Geotechnical Division, Proc. ASCE*, Volume 105, No. GT6, pp. 739-758.

Miura S., Toki S. and Tatsuoka F. (1994), 'Cyclic Undrained Triaxial Behaviour of a Sand by a Cooperative Test Program in Japan', in *Dynamic Geotechnical Testing II*, STP 1213, American Society for Testing and Materials, pp. 305-329.

Mossessian T.K. and Dravinski M. (1989), 'Amplification of Elastic Waves by a Three Dimensional Valley, Part I: Steady State Response', *Earthquake Engineering and Structural Dynamics*, Volume 19, pp. 667-680.

Mossessian T.K. and Dravinski M. (1990), 'Scattering of Elastic Waves By Three Dimensional Surface Topographies', *Wave Motion*, Volume 11, pp. 579-592.

Mulilis J.P., Seed H.B., Chan C.K., Mitchell J.K. and Arulanandan K. (1977), 'Effects of Sample Preparation on Sand Liquefaction', *Journal of the Geotechnical Division, Proc. ASCE*, Volume 103, No. GT2, pp. 91-108.

Muraleetharan K.K., Mish K.D. and Arulanandan K. (1994), 'A Fully Coupled Non Linear Dynamic Analysis Procedure and its Verification Using Centrifuge Test Results', *International Journal for Numerical and Analytical Methods in Geomechanics*, Volume 18, pp. 305-325.

Nowack R. and Aki K. (1984),' The Two Dimensional Gaussian Beam Synthetic Method: Testing and Applications', *Journal of Geophysical Research*, Volume 89, pp. 7797-7819.

O'Halloran M. (1986), *The Earthquake Stability of Earth Structures*, PhD Thesis, University of Auckland.

Ohtsuki A. and Itoh T. (1987), 'Two Dimensional Effective Stress Analysis of Liquefaction of Irregular Ground Including Soil-Structure Interaction', E*arthquake Engineering and Structural Dynamics*, Volume 15, pp. 345-366.

Peacock W.H. and Seed H.B. (1968), 'Sand Liquefaction Under Cyclic Loading Simple Shear Conditions', *Journal of the Soil Mechanics and Foundations Division, Proc. ASCE*, Volume 94, No. SM3, pp. 689-708.

Papageorgiou A. (1994), 'Two and Three Dimensional Effects on Ground Motion', *Research Accomplishments: 1986-1994,* NCEER Report, Univerisity of New York State, Buffalo, pp. 163-171.

Pedersen H.A., Campillo M. and Sanchez-Sesma F.J. (1995), 'Azimuth Dependent Wave Amplification in Alluvial Valleys, *Soil Dynamics and Earthquake Engineering*, Volume 14, pp. 289-300.

Pender M.J. (1994), Personal Communication

Pender M.J., Duske G.C. and Peploe R.J. (1992), 'Cyclic Undrained Stiffness of Stiff Clay and a Volcanic Ash', *Proceedings of the 6th Australia New Zealand Conference on Geomechanics*, Christchurch, New Zealand.

Pranjoto S. and Larkin T.J., (1995), 'Some Engineering Properties of a Volcanic Sand', *Proceedings of the Second Australia-New Zealand Young Geotechnical Professionals Conference, IPENZ Technical Group*, Volume 21, Issue 3, pp. 157-162

Prevost J.H. (1988), *DYNA1D: A Computer Program for Non Linear Seismic Site Response Analysis*, Report No. NCEER-89-0025, Department of Civil Engineering and Operations Research, Princeton University.

Robertson P.K. and Campanella M. (1985), 'Liquefaction Potential of Sands Using the CPT', *Journal of the Geotechnical Division, Proc. ASCE*, Volume 111, No. 3, pp. 384-403.

Rollins K.M. and Seed H.B. (1990), 'Influence of Buildings on Potential Liquefaction Damage', *Journal of the Geotechnical Division, Proc. ASCE,* Volume 116, No. 2, pp. 165-185.

Sanchez-Sesma F.J. (1993), 'Diffraction of Elastic Waves by Three Dimensional Surface Irregularities', *Bulletin of the Seismological Society of America,* Volume 73, pp. 1621-1636.

Sanchez-Sesma F.J., Chavez-Perez-Sergio and Aviles-Javier (1984), 'Scattering of Elastic Waves by Three Dimensional Topographies', *Proceedings of the 8th World Conference on Earthquake Engineering,* San Francisco, pp. 639-646.

Sanchez-Sesma F.J. and Esquviel J.A. (1979), 'Ground Motion on Alluvial Valleys Under Incident Plane SH Waves', *Bulletin of the Seismological Society of America,* Volume 69, pp. 1107-1120.

Schnabel P.B., Lysmer J. and Seed H.B. (1972), *SHAKE: A Computer Program for Earthquake Response Analysis of Horizontally Layered Sites,* Report No. EERC 72-12, Earthquake Engineering Research Centre, University of California, Berkeley.

Scott R.F. (1994), 'Review of Progress in Dynamic Geotechnical Centrifuge Research', in *Dynamic Geotechnical Testing II,* STP 1213, American Society for Testing and Materials, pp. 305-329.

Scott R.F. and Zuckerman K.A. (1973), 'Sand Blows and Liquefaction', *The Great Alaskan Earthquake of 1964-Engineering Volume,* Committee on the Alaska Earthquake, Division of Earth Sciences, NRC, Washington D.C., pp. 179-189.

Seed H.B. (1979), 'Soil Liquefaction and Cyclic Mobility Evaluation for Level Ground During Earthquakes', *Journal of the Geotechnical Engineering Division, Proc. ASCE,* Volume 105, No. GT2, pp. 201-255.

Seed H.B. and Idriss I.M. (1971), 'Simplified Procedures for Evaluating Soil Liquefaction Procedures', *Journal of the Soil Mechanics and Foundations Division, Proc. ASCE,* Volume 97, pp. 1249-1273.

Seed H.B. and Lee K.L. (1966), 'Liquefaction of Saturated Sands During Cyclic Loading', *Journal of the Soil Mechanics and Foundations Division, Proc. ASCE,* Volume 92, No. SM6, pp. 105-134.

Seed H.B., Idriss I.M., Makdisi F. and Benerjee N. (1975), *Representation of Irregular Stress Time Histories by Equivalent Uniform Stress Series in Liquefaction Analyses,* Report No. EERC 75-29, Earthquake Engineering Research Centre, University of California, Berkeley.

Seed H.B., Martin P.P. and Lysmer J. (1975b), *The Generation and Dissipation of Pore Water Pressures During Soil Liquefaction,* Earthquake Engineering Research Centre, University of California, Berkeley.

Seed H.B., Tokimatsu K., Harder L.F. and Chung R.M. (1984), *The Influence of SPT Procedures in Soil Liquefaction Resistance Evaluations,* Report No. EERC 84-15, Earthquake Engineering Research Centre, University of California, Berkeley.

Seed H.B., Wong R.T., Idriss I.M. and Tokimatsu K. (1984b), *Moduli and Damping Factors for Dynamic Analyses of Cohesionless Soils,* Report No. EERC 84-14, Earthquake Engineering Research Centre, University of California. Berkeley.

Shah A.H., Wong K.C. and Datta S.K. (1982), 'Diffraction of Plane SH Waves in a Half Space', *Earthquake Engineering and Structural Dynamics,* Volume 10, pp. 519-528.

Siddharthan R. and Finn W.D.L. (1982), *TARA-2, Two Dimensional Non Linear Static and Dynamic Response Analyses,* Soil Dynamics Group, University of British Columbia, Vancouver, Canada.

Silver M.L., Chan C.K., Ladd R.S., Lee K.L., Tiedemann D.A., Townsend F.C., Valera J.E. and Wilson J.H. (1976), 'Cyclic Triaxial Strength of Standard Test Sand', *Journal of the Geotechnical Division, Proc. ASCE*, Volume 102, No. GT5, pp. 511-523.

Streeter V.L., Wylie E.B. and Richart F.E. (1974), 'Soil Motion Computations by Characteristic Method', *Journal of the Geotechnical Division, Proc. ASCE*, Volume 100, pp. 247-263.

Sun J.I., Golesorkhi R and Seed H.B. (1988), *Dynamic Moduli and Damping Ratios for Cohesive Soils*, Report No. EERC 88-15, Earthquake Engineering Research Centre, University of California, Berkeley.

Thrall F.G. (1981), *Geotechnical Significance of Poorly Crystalline Soils Derived from Volcanic Ash*, PhD Thesis, Oregon State University, Oregon, USA.

Toki S., Tatsuoka F., Miura S., Yoshimi Y., Yasuda S. and Makihara Y. (1986), 'Cyclic Undrained Triaxial Strength of Sand by a Cooperative Test Program', *Soils and Foundations, JSSMFE*, Volume 26, No, 3, pp. 117-128.

Tokimatsu K. and Seed H.B. (1987), 'Evaluation of Settlements in Sands Due to Earthquake Shaking', *Journal of the Geotechnical Division, Proc. ASCE*, Volume 113, No. 8, pp. 861-878.

Trifunac M.D. (1971), 'Surface Motion of a Semi-Cylndrical Alluvial Valley for Incident Plane SH Waves', *Bulletin of the Seismological Society of America*, Volume 61, pp. 1755-1770.

Tsuchida H. and Hayashi S. (1971), 'Estimation of Liquefaction Potential of Sandy Soil', *Proceedings of 3rd Meeting, U.S. Panel on Wind and Seismic Effects*, Tokyo.

Yu W., Anderson J.G. and Siddharthan R. (1993), 'On the Characteristics of Non Linear Soil Response', *Bulletin of the Seismological Society of America*, Volume 83, pp. 218-244.

Valanis K.C. (1971), 'A Theory of viscoplasticity Without Yield Surface, Part II', *Archive of Mechanics*, Volume 23, pp. 517-535.

Vucetic M. and Dobry R. (1991), 'Effect of Soil Plasticity on Cyclic Response', *Journal of the Geotechnical Division, Proc. ASCE*, Volume 117, pp. 89-107.

Whitman R.V. and Arulanandan K. (1985), 'Centrifuge Model Testing with Dynamic and Cyclic Loads', in *Advances in the Art of Testing Soils Under Cyclic Conditions, Proc ASCE*, ed. Khosla V., Detroit, pp. 255-285.

Wong H.L. and Jennings P.C. (1975), 'Effects of Canyon Topography on Strong Ground Motion', *Bulletin of the Seismological Society of America*, Volume 65, pp. 1239-1257.

Wong H.L. and Trifunac M.D. (1974), 'Surface Motion of a Semi-Elliptical Alluvial Valley or Incident Plane SH Waves', *Bulletin of the Seismological Society of America*, Volume 64, pp. 1389-1408.